Structural and stratigraphic trapping mechanisms in CO2 storage capacity and security

Pourmalek, Azadeh

Award date:
2023

Awarding institution:
Coventry University

Structural and stratigraphic trapping mechanisms in CO_2 storage capacity and security

By

Azadeh Pourmalek

PhD

Date

May 2021

Structural and stratigraphic trapping mechanisms in co_2 storage capacity and security

By

Azadeh Pourmalek

A thesis submitted in partial fulfilment of the University's requirements for the Degree of Doctor of Philosophy

Date

May 2021

Certificate of Ethical Approval

Applicant:	Azadeh Pourmalek
Project Title:	Structural and stratigraphic trapping mechanisms in CO2 storage capacity and security.

This is to certify that the above named applicant has completed the Coventry University Ethical Approval process and their project has been confirmed and approved as Low Risk

Date of approval:	17 Nov 2020
Project Reference Number:	P114355

Abstract

Carbon capture and storage (CCS) has been identified as an important option that can be applied to stabilise CO_2 concentrations in the atmosphere and limiting climate change. Structural or stratigraphic traps are the primary means by which injected CO_2, as one component of the CCS system, is stored in geological formations until other trapping mechanisms influence the storage process. This thesis investigates this mode of trapping mechanism by constructing 3D static models based on different geological outcrops and then performing flow simulations. To reduce the reliance on a single seal, it seems desirable to utilise primary and secondary stratigraphic traps or small-scale structural features. In Chapter 3, three different outcrops are selected, each representing a shallow-marine system with varying heterogeneity provided by siliciclastic-carbonate mixing that may form a small or large stratigraphic trap and contribute to secure CO_2 geological storage. It is demonstrated that facies interplay and associated sediment heterogeneity have a varying effect on fluid flow, storage capacity and security. Exhumed bleached palaeo-reservoirs provide a means of understanding fluid flow processes in geological media because the former movement of fluids is preserved as visible geochemical changes. In Chapter 4, a bleached palaeo-reservoir outcrop is used to test the importance of geological heterogeneity on fluid flow and identify possible pathways for fluids using flow modelling. Despite the permeability contrasts, the bleaching shows a remarkably uniform distribution within the palaeo-reservoir that crosses lithofacies boundaries that could be replicated by flow modelling, validating the Flora's rule. In Chapters 5 and 6, small-scale deformation bands are used for CO_2 flow simulation, to assess the extent to which these features act as effective mini-traps and contribute to long-term, secure CO_2 geological storage. A comprehensive set of simulation scenarios is applied to a single set of conjugate bands and also on clusters of deformation bands to evaluate the effects of the: i) deformation band density; ii) contrast in host rock/deformation band permeability; and iii) deformation band geometry, orientation and distribution on fluid movement. The findings of this study show the significance of the geometrical architecture of the bands, permeability contrast and the permeability of the host rock. Furthermore, it is shown that the highest number of bands observed and modelled for Penrith Sandstone outcrop, with three orders of magnitude permeability contrast, is a configuration that can contribute to the secure storage of CO_2 without causing an injectivity issue.

Dedicated to my beloved late Ali Pourmalek

Acknowledgment

This acknowledgment is my way to thank all the people, who helped me through this incredible journey.

I would like to express my sincerest gratitude to my director of studies, Dr Adrian Wood, for his great support and motivation.

I would like to express my deepest appreciation to my supervisor Dr. Seyed Shariatipour for offering me the opportunity to work with him. He has truly been an inspiration to me and I am very grateful for his continuous guidance, valuable advice, and constant support over the past eight years. Without his morals, his mentorship, and his passion for science, this journey would not have been as fascinating.

I would also thank Dr Andrew Newell for his fabulous insight and stimulating discussions.

I am very thankful to Dr Philip Costen for his valuable comments and for taking the time to proofread my manuscripts and this thesis and Dr Lorna Everall for her great support throughout my entire research.

I greatly appreciate the invaluable comments from my examiners, which significantly improved the quality of my work.

I appreciate Coventry University, Fluid and Complex Systems Research Centre, and the Doctoral College for offering me a PhD scholarship and providing all the required resources necessary for completing my research project.

Lastly, I want to acknowledge my family: my father who passed on six years ago. Without his human values, extensive knowledge, passion for education, and inspirational personality, I would not be the person that I am today; my mother for her unending and unconditional love and support; and finally, Amirhossein. I need a whole thesis to thank him, especially for his approach to life, which helped me stay positive during difficult moments. I am sure that you know how lucky I am to have you.

Nomenclature

Symbols:

P	Pressure
∇P	Pressure gradient
T	Temperature
φ	Porosity
K	Permeability
K_v	Vertical permeability
K_h	Horizontal Permeability
K_r	Relative permeability
S_w	Wetting phase saturation
S_{nW}	Wetting phase saturation
S_{wir}	Irreducible water saturation
P_C	Capillary pressure
r	Size of the pore throats
θ	Contact angle
σ	Interfacial tension
P_e	Capillary entry pressure
C	Capillary number
T_s	Interfacial tension
Γ	Gravity number
M	Mobility ratio
λ	Mobility
μ	Viscosity
u	Fluid velocity
ρ	Density
Δρ	Density difference
g	Gravitational acceleration
A	Reservoir area
H	Reservoir thickness
R_f	Recovery factor
B_f	Formation volume factor
Z	Gas compressibility factors
C_e	Capacity coefficient
C_c	Capacity coefficient
E	Effective storage factor

Subscripts

aq	Aqueous phase
Sc	Supercritical phase
w	Wetting phase
nw	Non-wetting phase
m	Mobility
b	Buoyancy
h	Heterogeneity
w	Water saturation

a	Aquifer strength

Abbreviation

CCS	Carbon Capture and Storage
EOR	Enhanced Oil Recovery
OGIP	INITIAL GAS IN PLACE
OOIP	INITIAL OIL IN PLACE
NFRs	NATURALLY FRACTURED RESERVOIRS
DFN	DISCRETE FRACTURE NETWORK MODELLING
E300	ECLIPSE COMPOSITIONAL SIMULATOR

Table of Contents

Abstract ..... *vi*

Acknowledgment ..... *viii*

Nomenclature ..... *ix*

Table of Contents ..... *xi*

List of Figures ..... *xiv*

List of Tables ..... *xix*

Chapter 1 20

Introduction 20

1.1 Climate change and greenhouse gases *20*

1.2 Carbon capture and storage *22*

1.2.1 Depleted oil and gas reservoirs 23

1.2.2 Deep saline aquifers 24

1.3 Thesis overview *25*

1.3.1 Motivation 25

1.3.2 Aim and objectives 26

1.3.3 Methodology 27

1.3.4 Thesis outline 28

Chapter 2 30

Background 30

2.1 CO_2 physical properties and subsurface pressure and temperature *30*

2.2 Driving forces *33*

2.3 CO_2 Trapping Mechanisms *34*

2.3.1 Structural and stratigraphic trapping mechanism 35

2.3.2 Hydrodynamic trapping mechanism 43

2.3.3 Residual trapping mechanism 45

2.3.4 Dissolution trapping 46

2.3.5 Mineral trapping 48

2.4 Depositional environment *48*

2.4.1 Fluvial reservoirs 49

2.4.2 Aeolian reservoirs 50

2.4.3 Deltaic reservoirs 50

2.4.4 Shallow-marine reservoirs 50

2.4.5 Deep-marine reservoirs 51

2.4.6 Carbonate reservoirs 51

2.5 Heterogeneity *53*

2.6 Storage capacity *54*

2.6.1 Oil and gas reservoirs 55

2.6.2 Deep saline aquifers 56

2.7 Storage security *59*

2.7.1 Faults, fractures and deformation bands 61

2.8 Outcrop *62*

2.9 CO_2 storage simulations in subsurface geological formation *63*

2.10 Summary *64*

Chapter 3 65

The impact of heterogeneous mixed siliciclastic-carbonate systems on CO_2 geological storage 65

3.1 Introduction *65*

3.2 Mixed siliciclastic-carbonate systems *66*

3.3 Introduction to the case studies *67*

3.3.1 Grayburg Formation – Siliciclastic-Carbonate Cyclical Interbedding 67

3.3.2 Lorca Basin – Steep Marine Margin Setting 68

3.3.3 Bridport Sand Formation – Mixing by Storm Processes 68

3.1 Methodology *68*

3.1.1 Flow Modelling 70

3.1.2 Reservoir models 73

3.2 Results *77*

3.2.1 Section 1 – Grayburg Formation 77

3.2.2 Section 2 – Lorca Basin 82

3.2.3 Section 3 – Bridport Sand Formation 83

3.3 Discussion *86*

3.4 Conclusion *89*

Chapter 4 90

Modelling of bleached palaeo-reservoir in the Salt Wash Graben, Utah 90

4.1 Introduction *90*

4.2 Geological setting *92*

4.2.1 Location 92

4.2.2 Entrada Sandstone Formation 92

4.2.3 Structure 92

4.2.4 Burial history 95

4.2.5 Field and laboratory methods 95

4.2.6 Lithofacies of the Entrada Sandstone Formation 95

4.2.7 Reducing agents 99

4.2.8 Regional fluid pathways 99

4.2.9 Distribution of the bleaching 100

4.3 Methodology *101*

4.3.1 Justification for numerical modelling 101

4.3.2 Reservoir model 102

4.3.3 Flow modelling 102

4.4 Results *106*

4.5 Discussion *112*

4.6 Conclusions *114*

Chapter 5 116

Application of X-shaped conjugate deformation bands as structural traps 116

5.1 Introduction 116

5.2 Origin and characteristics of deformation bands 117

5.3 Petrophysical properties of deformation bands and their effect on fluid flow 118

5.4 Deformation bands: an outcrop analogue 120

5.4.1 Penrith Sandstone of NW England 120

5.4.2 Deformation bands in Penrith Sandstone 120

5.5 Methodology 123

5.5.1 Reservoir model 124

5.5.2 Flow simulation 125

5.5.3 Sensitivity design 127

5.6 Results and discussion 129

5.6.1 The effects of bands intersection angle on CO_2 storage security and flow distribution 129

5.6.2 The effects of contrasting host rock-deformation band permeability on CO_2 distribution 131

5.6.3 The effect of permeability heterogeneity along the deformation bands 132

5.7 Conclusion 135

Chapter 6 136

The Impact of deformation bands clusters on CO_2 injection and storage 136

6.1 Introduction 136

6.2 Effects of deformation bands on fluid flow 137

6.3 Methodology 139

6.4 Reservoir Model 140

6.5 Flow simulation 141

6.6 The effects of clustered deformation bands on CO_2 storage 141

6.6.1 Sensitivity design 142

6.7 Result and discussion 147

6.7.1 Investigating the effects of deformation band density on CO_2 storage 149

6.7.2 The effects of host rock and deformation band permeability contrast on CO_2 storage 152

6.7.3 The effects of deformation bands geometry and their location against high transmissibility fault 154

6.7.4 Combined effects of deformation bands and fractures on CO_2 storage security 156

6.7.5 The effects of injection rate and well location on CO_2 storage security in a deformed reservoir 158

6.8 Conclusion 159

Chapter 7 161

Conclusion and recommendation 161

7.1 Conclusions 161

7.2 Future work 165

References 166

List of Figures

Figure 1.1: The Keeling Curve shows the full record of global CO_2 concentrations in the Earth's atmosphere. The latest figure on 10 January 2022 is 416.71 ppm (2.45 ppm higher from January 2021) (NOAA/ESRL 2020). 21
Figure 1.2: 0.84 °C increase in temperature, above the twentieth-century average, has occurred (NOAA 2020). 21
Figure 1.3: CO_2 concentrations based on different emission scenarios range between 400 – 900 ppm (Vuuren et al. 2011). 22
Figure 2.1: CO_2 phase diagram (ChemicaLogic Corporation 2018). 32
Figure 2.2: Variation of density with depth, assuming hydrostatic pressure, a geothermal gradient of 25 °C/km and surface temperature of 15 °C (IPCC 2005). 32
Figure 2.3: Density and viscosity of the CO_2 as a function of temperature and pressure (Nordbotten, Celia and Bachu 2005). 32
Figure 2.4: Structural traps. Blue is CO_2 accumulation. Red is the fault (after Biddle and Wielchowsky 1994). ...36
Figure 2.5: Fault-related folds and fault-free folds (after Biddle and Wielchowsky 1994). 37
Figure 2.6: Fault traps (after Biddle and Wielchowsky 1994). 38
Figure 2.7: Primary stratigraphic traps (after Biddle and Wielchowsky 1994). 39
Figure 2.8: Sleipner storage reservoir with inter-formational shale layers (Cavanagh and Haszeldine 2014). 40
Figure 2.9: (A) Residual trapping and (B) Dissolution trapping (after Zulczewski et al. 2012; Dong and Blunt 2009). 47
Figure 2.10: Depositional environments (USDOE 2010). 1) Alluvial, 2) Basalt, 3) Swamp, 4) Deltaic, 5) Deep marine, 6) Aeolian, 7) Fluvial, 8) Lacustrine, 9) Reef, 10) Shelf, 11) Slope, 12) Beach and barrier Island, 13) Beach, 14) Tidal flat, 15) Turbidite. 49
Figure 2.11: Dual porosity modelling. Two simulation cells are associated with each block, one for high porosity-low permeability matrix and one for low porosity-high permeability fractures. 52
Figure 2.12: Different CO_2 storage capacity classifications are proposed. They are shown in one table for comparison. Red is Goercki et al. (2009), blue is CO2CRC (2008), Purple is SPE (2017), Green is CSLF (2007) and yellow is USDOE (2010). 55
Figure 2.13: Leakage mechanisms: A) CO_2 escapes through a thin caprock or gap in the caprock; B) CO_2 Leaks due to higher CO_2 pressure than capillary entry pressure; C) CO_2 escapes through faults and fracture networks; D) CO_2 escapes via poorly completed injection wells; E) CO_2 escapes via abandoned wells; F) CO_2 is transported out of the storage unit by natural flow; G) CO_2 migrates beyond the regional caprock (IEAGHG 2011). 60
Figure 3.1: Stratigraphic cross-section from promontory G showing major facies in Grayburg Formation (Parker 2013). 69
Figure 3.2: Outcrop photo and stratigraphic of the Miocene-age Lorca Basin (Thrana and Talbot 2006). 69
Figure 3.3: Bridport Sand Formation: (a) Outcrop gamma-ray profile; (b) mean grain size data; (c) lithology and interpreted facies (cemented bands is in teal); (d) and outcrop photo of Bridport Sand Formation showing Inferior Oolite, closely spaced carbonate-cemented beds and widely spaced, discontinuous carbonate-cemented beds (modified after Hampson et al. 2014). 70
Figure 3.4: Relative permeability curves used throughout this study: a) Wabamun carbonate; b) Nisku carbonate; c) Redwater Leduc carbonate; and d) Viking Sandstone. K_r is relative permeability (K_{rw} relative permeability for water and K_{rg} relative permeability for gas) and S_g is gas saturation. 72
Figure 3.5: Capillary pressure curves used throughout this study: a) Wabamun carbonate.; b) Nisku carbonate; c) Redwater Leduc carbonate; and d) Viking Sandstone. 72
Figure 3.6: Comparing all endpoint relative permeability [$K_{rCO2max}$]to CO_2 at irreducible water saturation [S_{wir}]. 72
Figure 3.7: (a) Static reservoir models (1000 m × 1000 m × 100 m) from pure sandstone (GF-PS), varying ratio of sandstone to carbonate, and pure carbonate (GF-PC). C refers to carbonate and S refers to sandstone. (b) The percentage of each facies in each model is denoted by a number. For example, the case GF-10S-90C is a model with 10 percent sandstone and 90 percent carbonate (Pourmalek et al. 2022). 75
Figure 3.8: Static model (1000 m × 1000 m × 40m) of the mixed clastic-carbonate system of the Lorca Basin (Pourmalek et al. 2022). 75

Figure 3.9: Static models (2100m×2100m×60m) of Bridport Sand Formation were constructed based on the laser-scanned image. Towards the top of this sequence, the frequency of cemented horizons increases and their thickness decreases. The 3D extent of cemented layers was 90%, 70%, 50% and 10% of the model. Here only the model BPS-2 with 70% cemented layers is shown (Pourmalek et al. 2022). 76
Figure 3.10: Dissolved and mobile CO_2 in the reservoir and Mobile CO_2 beneath the caprock in all models investigated in Section 1. L, M and H refer to low, medium and high permeability carbonate facies and GF refers to Grayburg Formation. For properties see Table 3.1.....79
Figure 3.11: A low permeability layer developed across the entire model, from GF-C20-S80. This layer hindered the upward migration of CO_2 and allowed the lateral migration. 80
Figure 3.12: Flow distribution in models with different sandstone-carbonate ratios. The properties of low permeability carbonate (L) were used for the carbonate facies in Model 1 (Table 3.1). CO_2 migration towards the caprock is completely restricted in models with decreasing sandstone-carbonate ratios. Flow models with injectivity problems are not shown. GF refers to Grayburg Formation, C to carbonate, and S to sandstone. 81
Figure 3.13: Average field pressure, cumulative CO_2 injection and amount of dissolved CO_2 in the water phase in the pure sandstone model (GF-PS) and pure low carbonate model (GF-PC-L). GF refers to Grayburg Formation, C to carbonate, and S to sandstone.....81
Figure 3.14: Flow distribution in models with different sandstone-carbonate ratios. The properties of medium permeability Nisku carbonate were used for carbonate facies in Model 2 (Table 3.1). GF refers to Grayburg Formation, C to carbonate, and S to sandstone.....82
Figure 3.15: Flow distribution in models with different sandstone-carbonate ratios. The properties of high permeability carbonate were used for the carbonate facies in Model 3 (Table 3.1). 82
Figure 3.16: CO_2 mole fraction in the model with a) Low permeability carbonate (LB-CL-S); b) Medium permeability carbonate (LB-CM-S); c) High permeability carbonate (LB-CH-S); and d) Homogeneous model (LB-PS). The properties of the sandstone facies properties remained constant throughout the simulation. LB refers to Lorca Basin. For properties see Table 3.1. 83
Figure 3.17: Dissolved and mobile CO_2 in the reservoir and beneath the caprock. For the properties see Table 3.1. LB refers to Lorca Basin. 84
Figure 3.18: CO_2 mole fraction in the model BPS-2 with 70% cemented layers. CO_2 was injected through perforations: (a) into the bottommost sand layer (PbS); and (b) through all sand layers (PaS). (c) Homogeneous model (BPS-PS). (d) Results of the Eclipse dynamic-flow simulation shown on the vertical plane of the laser-scanned digital outcrop of the Bridport Sand Formation that was used to build the static models. The sandstone facies properties remained constant throughout the simulation. BPS, Bridport Sand Formation. For properties, see Table 3.2. 85
Figure 3.19: Dissolve CO_2 in the reservoir and mobile CO_2 in the high permeability layer (Inferior Oolite) in models with 20,000 Sm^3 (LI) and 30,000 Sm^3 injection rates (HI). In these models, CO_2 was injected through perforations into the bottom-most sand layer (PbS) or through all sand layers (PaS). BPS refers to Bridport Sand Formation. BPS refers to Bridport sand Formation. PS-HI and PS-LI are homogeneous sandstone models with high and low injection rates, respectively. 85
Figure 3.20: CO_2 and the pressure in the sands. The x-axis shows the layers where the well is open to CO_2 injection. 86
Figure 3.21: Percentage of the free gas beneath the caprock in all cases. GF: Grayburg Formation, LB: Lorca Basin, and PBS Bridport Sand Formation. 86
Figure 4.1: (A) Study area (black rectangle) is adjacent to the Salt Wash graben. NNW plunging Green River anticline is truncated by two major faults of the Salt Wash graben and Little Grand Wash fault (Allis et al. 2001; Doelling 2001). Faults are shown in red, anticlinal axes in black and selected geological formations are coloured and labelled from the Utah Geological Survey Map 180 (Newell et al. 2019). (B) Aerial photograph of the study area. Red line is the bleached area and the blue line is the Slick Rock Member (palaeo-reservoir). Red stars indicate the location of the two logged sections in Figure 4.4. 93
Figure 4.2: The Entrada Sandstone comprises the Slick Rock Member, which is the high permeability sandstone to silty sandstone palaeo-reservoir and the Earthy Member, which is a low permeability muddy sandstone topseal (courtesy of Andrew Newell and Andrew Butcher). 94

Figure 4.3: The abrupt truncation of the Slick Member and Earthy Member of the Entrada Sandstone Formation against the Cedar Mountain Formation (lower Cretaceous). The bleaching also extends into the Earthy Member (topseal) (courtesy of Andrew Newell and Andrew Butcher). 96
Figure 4.4: Sedimentology log of the upper Slick Rock Member and lower Earthy Member of the Entrada Sandstone Formation. The location of these sections is shown as red stars in Figure 4.1 (measured by Andrew Newell and Andrew Butcher). 97
Figure 4.5: Four main sandstone lithofacies within the Slick Rock Member: (A) High angle cross-bedded dune sandstones; (B) Low-angle wind-ripple laminated sandstone; (C) Wavy and convolute laminated sandstone damp interdune deposits; and (D) Massive and muddy wet interdune sandstones. Permeability generally decreases from A to D (courtesy of Andrew Newell and Andrew Butcher). 98
Figure 4.6: Two possible pathways for the migration of reducing fluids from depth into the Entrada Sandstone palaeo-reservoir at Salt Wash graben. Pathway 1 is via northern fault of Salt Wash graben. Pathway 2 is via Little Grand Wash fault. 100
Figure 4.7: (A) East and (B) West of the palaeo-reservoir showing uniform bleaching of the Slick Rock Member. The bleached zone extends c. 4 m into the Earthy Member. Features associated with numerous fractures were formed where reducing fluids escape vertically through the fracture cluster (courtesy of Andrew Newell and Andrew Butcher). 101
Figure 4.8: Reservoir model showing the distribution of lithofacies (Table 4.3) used for flow simulations. Little Grand Wash (LGW) fault is placed at the right-end of the model and the northern fault of the Salt Wash graben (SWG) is placed to the left-hand side of the model. Facies 1 permeability is 1000 mD, Facies 2 is 100 mD, Facies 3 is 10 mD and Facies 4 is 0.01 mD. 104
Figure 4.9: (a) Drainage relative permeability curve and; (b) Drainage capillary pressure curve for facies 1 (sandstone), facies 2 (silty sandstone), facies 3 (muddy sandstone) and facies 4 (sandy siltstone) (Onoja and Shariatipour 2018; Onoja et al. 2019). 104
Figure 4.10: a) CO_2 mole fraction at the end of the 20 years injection period and (b) At the end of the 1000 years post-injection period. CO_2 pathway is northern fault of the Salt Wash graben. INJ = Injection points. 108
Figure 4.11: a) Front view and (b) Top view of the CO_2 mole fraction at the end of the simulation. CO_2 pathway is northern fault of the Salt Wash graben. INJ = Injection points. 108
Figure 4.12: a) CO_2 mole fraction at the end of the 20 years injection period and (b) At the end of the 1000 year post injection period. CO_2 pathway is the Little Grand Wash fault. INJ = Injection points. 109
Figure 4.13: a) Front view and (b) Top view of CO_2 mole fraction when CO_2. Injected from the right-hand side of the model. CO_2 pathway is the Little Grand Wash fault. INJ = Injection points. 109
Figure 4.14: CO_2 mole fraction in Model 3. CO_2 pathways is both the Little Grand Wash fault and Salt Wash graben. 110
Figure 4.15: CO_2 mole fraction at the base of the imperfect seal (left) and tight seal (right). 110
Figure 4.16: Amount of CO_2 dissolved in the base of the topseal in Model 1 and Model 2. 111
Figure 4.17: Amount of pressure increase in the base of the topseal in Model 1 and Model 2. 111
Figure 4.18: (a) Distribution of CO_2 in the model with a permeability range of four orders of magnitude (see Table 4.5 Model A). (b) Distribution of CO_2 in the model with a permeability range of six orders of magnitude (see Table 4.5 Model B). Both scenarios result in a relatively uniform distribution of CO_2 across the boundaries of layered lithofacies. 112
Figure 4.19: Total amount of CO_2 dissolution in the brine in Model A and Model B. 112
Figure 5.1: (a) Map showing the location of the Eden field site in north-west England. (b) Geological map of the Vale of Eden Basin and distribution of the Penrith Sandstone, Eden Shale and St Bees Sandstone (Lafare, Peach and Hughes et al. 2016). 122
Figure 5.2: Outcrops of the Penrith Sandstone are within the Eden Gorge overlain by Eden Shale and St Bees Sandstone formations. NE-SW trending faults, which form in association with the deformation bands, are also presented (Pourmalek et al. 2021). 122
Figure 5.3: Variations in deformation band development from (a) Millimetre-wide bands showing conjugate cross-cutting arrangement; (b) Multiple anastomosing bands forming a zone several centimetres across; and (c) Thick zone composed of multiple bands with slip surface on the hanging wall (right hand) side (courtesy of Andrew Newell). 123

Figure 5.4: Typical arrangement of deformation bands in conjugate sets with a dihedral angle of c. 45 degrees [shown in the figure]. This value is used for the acute angle of intersection between two cross-cutting deformation bands throughout the flow modelling (courtesy of Andrew Newell).....123
Figure 5.5: Porosity and permeability measurements from samples of the Penrith Sandstone Formation outcrop. Blue dots are core plugs measurements based on liquid re-saturation (porosity) and nitrogen gas permeability tests. Red dots are porosity estimated by the image analysis and a predicted Carman-Kozeny permeability calculated from the total porosity and specific surface area. Both types of measurements demonstrate that host rock has a porosity of 10-30%, while the sandstone with deformation bands has a porosity <10%. Permeability decreases by several orders of magnitude in rocks with bands (courtesy of Andrew Newell and Antoni Mildowski).....126
Figure 5.6: A scenario of a single conjugate set of bands. A sandbox model with a spatial dimension of 20 m × 20 m × 20 m with a total of one million active cells [ni=100, nj=100, nk=100] was constructed. Two inclined planes (conjugate deformation bands) in opposite directions which were mutually cross-cutting were included in the model (shown in dark green). Three structures with varying hinge-line plunge were considered in the sensitivity study of Section 4.1: a) Intersection angle with the horizon is zero; b) Intersection axis is at an angle of 5^o; and c) Intersection axis is at an angle of 10^o. The angles are shown in red.....128
Figure 5.7: The effects of variation in hinge-line plunge on CO_2 distribution. The deformation band filled with CO_2 up to its spill point then the gas escaped in the X direction and ascended towards the upper layers. In CASE A the CO_2 plume shows a symmetrical distribution along the intersection axis. In CASE B and CASE C, the CO_2 plumes are asymmetrical along the axis. The homogenous model (CASE D) showed a symmetrical CO_2 plume around the injectors. 130
Figure 5.8: a) Plan view of the CO_2 mole fraction in the model with an acute angle of 45 degrees; and b) Model with an acute angle of 90 degrees. At the end of the post-injection period the CO_2 plume developed outside the enclosed volume in the model where bands had an acute angle of 45 degrees, while CO_2 has not yet left the enclosed volume in the model with an acute angle of 90 degrees. The dihedral angles used here are within the range reported by Fossen et al. (2017).....131
Figure 5.9: A) The effect of deformation band-host rock permeability contrast on CO_2 distribution. B) CO_2 distribution across the deformation bands plane. 133
Figure 5.10: Dissolved CO_2 and mobile CO_2 in the reservoir and the deformation band plane at the end of the simulation period. See Figure 5.9 for associated models and Table 5.6 for the porosity and permeability values.....134
Figure 5.11: The amount of CO_2 dissolved in the water phase in the reservoir at the end of the post-injection period, showing an insignificant difference across modelled cases.....134
Figure 5.12: CO_2 dissolved along the deformation bands plane for the five modelled cases.....134
Figure 6.1: Photograph showing the distribution of deformation bands at Chain Cliff outcrop, Eden Gorge, where they are clustered around a fault plane [yellow colouration]. Deformation bands are shown in black, open joints in purple and aeolian bedding surfaces in blue (courtesy of Andrew Newell).....139
Figure 6.2: Models in the study of the clusters of the bands had a spatial dimension of 100 m × 100 m × 100 with 125,000 active cells [ni=50, nj=50, nk=50]. Medium density parallel bands scenario is shown here. (a) Deformation bands' planes were generated using Fracture Network Model. (b) Fracture Network Model was imported in Scale up Fracture Network. The 3D grid form which it was generated will automatically be chosen to upscale into. As it is shown in this figure, deformation bands are dying out towards the caprock. The high permeability host rock is not shown. Low permeability bands are in dark blue. Sensitivity studies including deformation band density (high, medium and low), permeability contrasts, and orientation of the bands were designed to study the clusters of deformation bands. These scenarios are not included in this figure.....141
Figure 6.3: Five cases studied herein: a) Conjugate set of deformation bands with 0-degree intersection angle; b) Conjugate set of deformation bands with 10-degree intersection angle; c) parallel set of deformation band, parallel to the fault; d) parallel set of deformation band; perpendicular to the fault; and e) Random distribution of deformation bands (Blue: caprock, Red: fault, Green: deformation bands). 146
Figure 6.4: A) Low, medium and high density of deformation bands. The fault is not shown. B) Effects of deformation band density on flow distribution. More mobile gas appeared beneath the caprock in the models with a low to medium number of deformation bands.....150

Figure 6.5: The amount of dissolved CO_2 in the brine and mobile CO_2 in both reservoir and beneath the caprock in cases with different density of deformation bands. *151*
Figure 6.6: None of the models in the study of deformation band density reached the pressure limit of 30 bars. Note that the permeability contrast of three orders of magnitude were considered here. *151*
Figure 6.7: Dissolved CO_2 and mobile gas in the reservoir, in the fault rock and the layer below the caprock. M refers to a medium number of deformation bands. PERP refers to a parallel set of deformation bands that are perpendicular to the fault. PARA refers to a parallel set of deformation bands that are parallel to the fault. RAND refers to a random distribution of deformation bands. CON0 refers to a conjugate set of deformation bands with a horizontal intersection axis and the intersection axis in CON10 is at an angle of 10^o. PC denotes permeability contrast. For example, Case M-RAND-PC4 is the model with a medium number of randomly distributed deformation bands with six orders of magnitude host rock-deformation bands permeability contrast. For the permeability values, see Table 6.2. ..... *154*
Figure 6.8: CO_2 distribution in cases with differing permeability contrast. A) CO_2 distribution in models with conjugate sets of deformation bands with an intersection angle of 10°; and B) CO_2 distribution in cases with a parallel distribution of deformation bands. *155*
Figure 6.9: The amount of free gas beneath the caprock and fault rock in cases with various type of deformation band distributions..... *156*
Figure 6.10: Mobile gas beneath the caprock and fault plane in the presence of open fractures. *157*
Figure 6.11: Influence of open fractures in CO_2 distribution in the presence of open fractures...... *157*
Figure 6.12: The amount of free gas beneath the caprock and in the fault rock under different injection scenarios display similar trends. M refers to models with medium density of deformation bands, LR refers to low injection rate, MR to medium injection rate and HR to high injection rate. *159*
Figure 6.13: The amount of free gas beneath the caprock and in the fault rock under different well placement scenarios. M refers to models with medium density of deformation bands, F refers to the models with well placement in x=25 and y=40 and C refers to the models with well placement in x=50 and y=50. ..... *159*

List of Tables

Table 1.1: Aquifer classification based on total dissolved solids (Meyer and Croskrey 2017).....24
Table 2.1: CO_2 physical properties.....31
Table 2.2: Fold and fault dominated traps.....37
Table 2.3: Stratigraphic traps (after Biddle and Wielchowsky 1994). 38
Table 2.4: Structure and depositional systems in some industrial and pilot projects.....44
Table 2.5: Factors influencing CO_2 storage efficiency.....58
Table 3.1: Petrophysical and flow characteristics of the four rock samples used for flow simulation in Section 1 - Grayburg Formation and Section 2 - Lorca Basin (Bennion and Bachu 2006b; 2008; 2010). 71
Table 3.2: Petrophysical and flow characteristic used for flow simulation in Section 3 (Bridport Sand Formation) (Bryant, Kantorowicz and Love (1988); Bennion and Bachu (2006b; 2008; 2010). 71
Table 3.3: Injection strategy. For Bridport Sand Formation, two injection rates and two scenarios for perforation locations were considered for flow simulation. 77
Table 3.4: As the geometric volume of the storage reservoir is known, as well as its porosity [φ] and the irreducible water saturation [S_{wir}], based on the formulation 2.9 introduced by CSLF (2007) which is discussed in section 2.6.2, then the theoretical volume available for CO_2 storage V_{CO2} [sm^3] for homogeneous models is calculated and compared to total injected gas. 78
Table 4.1: The main characteristics of the Slick Rock Member (compiled by Andrew Newell and Andrew Butcher).....98
Table 4.2: Petrophysical properties of the Slick Rock Member (high permeability palaeo-reservoir) and Earthy Member (topseal) of the Entrada Sandstone Formation. 99
Table 4.3: Reservoir (Slick Rock Member) and topseal (Earthy Member) properties. 102
Table 4.4: CO_2 Injector location, perforation location and location of faults in all four models. 105
Table 4.5: Reservoir and topseal properties in Model A and Model B.....106
Table 5.1: Several significant differences between deformation bands and ordinary fractures (Fossen et al. 2007).....118
Table 5.2: Terminology, deformation mechanisms and the properties of deformation bands in various formations.....121
Table 5.3: Grid Properties and wells' location in the study of one set of conjugate bands. 125
Table 5.4: Parameters used for flow simulation. 126
Table 5.5: Sensitivity design to test the variation in hinge-line plunge. 127
Table 5.6: Sensitivity design to test permeability contrast. 128
Table 5.7: Sensitivity design to test permeability heterogeneity along deformation bands. 129
Table 6.1: Models built to study the effects of density of deformation bands on CO_2 distribution. L - low density, M - medium density, and H - high density of deformation bands. PARA - parallel distribution of deformation bands, RAND - random distribution of deformation bands, CON0 - conjugate sets with horizontal intersection axis, and CON10 - conjugate sets with an angle of 10. U refers to the undeformed model. For example, L-CON10 is a model with low-density of conjugate deformation bands with a 10-degree intersection angle.....143
Table 6.2: Permeability values used for the permeability contrast sensitivity study. M refers to medium density of deformation bands and PC refers to permeability contrast.....144
Table 6.3: Properties of deformation bands including shape and density, and density of vertical open fractures in all 36 models investigated.....147
Table 6.4: 15 scenarios were considered in order to investigate the effect of injection rate on CO_2 storage security. 148
Table 6.5: 10 scenarios were considered to study the effects of well placement on storage security. 148

Chapter 1

Introduction

1.1 Climate change and greenhouse gases

Climate change is attributed directly to the change in the composition of the atmosphere. Natural climate variability observed over the comparable time period has now been enhanced by human activity through the direct link between industrial growth and emissions (UNFCCC 1992). However, no matter how you define climate change and the perceived or real anthropogenic component toward it, the global threat remains.

Earth warms part of the incoming solar shortwave radiation and emits infrared radiation. infrared radiation is absorbed and emitted by certain atmospheric constituents. These components include water vapour (H_2O), carbon dioxide (CO_2), nitrous oxide (N_2O), ozone (O_3), and methane (CH_4) and they are primary greenhouse gases (GHGs). The downward component of the infrared radiation causes the increase in the temperature of the lower layers of the atmosphere and Earth's surface (Cubasch et al. 2013). This phenomenon is called the greenhouse effect (IPCC: Annex: I 2018). An increase in the concentration of greenhouse gases increases the scale of this effect, which contributes to global warming (Cubasch et al. 2013)

Carbon dioxide emissions make up 76% of the total annual greenhouse gas emissions (Victor et al. 2014) and have increased from 278 ppm in 1750 to 416.71 ppm on 10 January 2022 (Figure 0.1). To reduce the potential impacts of global warming, the CO_2 concentration should not exceed 500 ppm CO_2eq (Victor et al. 2014). However, the atmospheric concentrations of CO_2 have already passed 400 ppm (Figure 0.1) and are increasing at an average rate of 20 ppm per decade (Ciais et al. 2013).

Estimations have shown that anthropogenic activities have caused a warming of 0.84 °C relative to the twentieth-century (NOAA 2021) (Figure 0.2). Emission scenarios predict atmospheric CO_2 concentrations of 400-900 ppm by 2100 (Figure 0.3). Based on these scenarios, the consequential increase in global mean surface temperature is projected to

range from 0.3 °C to 4.8 °C (IPCC 2013). Loss of sea ice, sea-level rise, increase in ocean acidity, intense heat waves, extreme weather events, epidemics and droughts are some of the adverse consequences of global warming (Bernstein et al. 2008).

Figure 0.1: The Keeling Curve shows the full record of global CO_2 concentrations in the Earth's atmosphere. The latest figure on 10 January 2022 is 416.71 ppm (2.45 ppm higher from January 2021) (NOAA/ESRL 2020).

Figure 0.2: 0.84 °C increase in temperature, above the twentieth-century average, has occurred (NOAA 2020).

The largest source of man-made greenhouse gases is the energy sector and the associated combustion of fossil fuels, which are singled out as the dominant cause for the observed increase in atmospheric CO_2 concentrations (Victor et al. 2014). Fossil fuels are projected to remain the primary source of energy in many developed and developing countries for the next 30 years (BP Energy Outlook 2019). Combatting climate change and limiting a global temperature rise below 1.5 or 2 °C will require a cut in fossil fuel use and/or the captured and securely stored, usually underground, of over 1000 gigatons of CO_2 (Scott et al. 2012; Alcalde et al. 2018; Zahasky and Krevor 2020).

Figure 0.3: CO_2 concentrations based on different emission scenarios range between 400 – 900 ppm (Vuuren et al. 2011).

The large-scale deployment of carbon capture and storage (CCS), wherein CO_2 is captured from the exhaust of combustion systems, transported and injected below the surface for long term safe storage, should play an important role in meeting the climate goals as set out by the IPCC during COP21 and the Paris Agreement (IPCC 2018).

1.2 Carbon capture and storage

CCS is a key technology and a leading option that could be used to stabilise atmospheric CO_2 concentrations and to secure warming below 2 °C by removing up to 32% of CO_2 emissions up to 2060 (Ennis-King and Paterson 2005; Orr 2009; Global CCS Institute 2017). Large-scale deployment of CCS facilities is required in order to capture CO_2 from fossil fuel and biomass power plants and other large CO_2-emitting industries, such as Portland cement and lime production. This would be achieved using high-pressure pipeline networks and the subsequent storage of CO_2 by injecting it into geological formations (IPCC 2005). Given that 8Gt of CO_2 per year is required to be stored by 2050 (Scott et al. 2012), thousands of CCS facilities are necessary. If CCS technologies are not accessible, then the total cost to reach a 50% reduction in CO_2 emissions could increase by 70% (IEA 2013). Therefore, to reach net-zero GHG emissions, CCS is essential. In 2020, only 21 large-scale CCS are in operation (IEA 2019). The UK has an excellent CO_2 storage potential; however, the UK has not yet made progress in deploying large-scale CCS infrastructure. The UK's required annual CO_2 capture volumes are up to 175 $MtCO_2$ by 2050, consequently, large scale CCS should be operating in

the UK in 2026 (The Climate Change Committee 2019), with governmental funding of a least £800 million being made available (HM Treasury 2020).

Since the focus of this thesis is on CO_2 storage, the actual mechanisms of CO_2 capture and transportation are not addressed.

CO_2 can be injected and successfully stored by comprehensively evaluated deep geological formations, where a 99% retention of stored CO_2 can be achieved after 100 years; thus ensuring effective CO_2 storage (Hepple and Benson 2005; Chadwick et al. 2008). The potential geological formations that have been considered for geological storage of CO_2 are depleted oil and gas reservoirs, deep saline aquifers and un-mineable coal beds. The focus of this thesis is on depleted oil and gas reservoirs (e.g., Dance, Spencer and Xu 2009; Vidal-gilbert et al. 2010; Underschultz et al. 2011; Dance 2013) and deep saline aquifers (e.g., Chadwick, Noy and Holloway 2009; Peters et al. 2015; Celia et al. 2015; Shariatipour, Pickup and Mackay 2016; Pourmalek and Shariatipour 2019).

1.2.1 Depleted oil and gas reservoirs

Oil and gas reservoirs that once held natural accumulations of hydrocarbon could be used for CO_2 storage in the future once they are depleted (Bachu 2000). The previous entrapment of oil and gas is considered as a reliable indicator that future CO_2 injection is both secure and viable.

Oil and gas fields have many characteristics that make them promising sites for the geological storage of CO_2 (USDOE 2010), e.g., proven trap, available data and infrastructure and known reservoir properties. Furthermore, CO_2 flooding into a mature oil reservoir causes CO_2 dissolution in the oil and, by increasing the bulk volume and decreasing the oil viscosity, allows the recovery of an additional 10-15 percent of the oil in place (USDOE 2010). This process is known as Enhanced Oil Recovery or EOR. Therefore, CO_2 injection into depleted oil reservoirs is mainly associated with EOR rather than CO_2 storage. Nevertheless, the total amount that can eventually be stored in EOR operations is only a small percentage of CO_2 emissions (Bachu and Adams 2003). The Weyburn project is a successful example of a CCS-Enhanced oil recovery project. CO_2 is injected into the fractured Weyburn-Midale carbonate reservoir in Saskatchewan, Canada (Brown 2002; Preston et al. 2005; Jensen et al. 2011; Njiekak et al. 2013). It is planned that 23 $MtCO_2$ will be stored during 20-25 years of the CO_2-EOR project (IPCC 2005).

Depleted gas reservoirs are better candidates for CO_2 sequestration, as CO_2 can be injected into a depleted gas reservoir to re-pressurize it to its original pressure (Bachu 2000). The CO2CRC Otway Project is an example of a successful geological storage of CO_2 in a depleted gas field (Dance 2013).

Many hydrocarbon reservoirs that are still producing will only be available for CO_2 storage once they are fully depleted. Furthermore, the condition of the wells is of concern and will need to be evaluated, along with reservoir capacity.

An upper estimate of the storage capacity of oil and gas fields is around 900 $GtCO_2$ (IPCC 2005). A study by Zahasky and Krevor (2020) showed that to meet the 2 °C climate change scenario, a CO_2 storage capacity of 2700 Gt is needed, implying that the storage capacity of depleted oil and gas reservoirs alone is insufficient to meet that target.

1.2.2 Deep saline aquifers

Deep saline aquifers are widespread in onshore and offshore sedimentary basins (IPCC 2005). They are filled with saline groundwater (Table 1.1) and are unsuitable for human consumption or agricultural use following treatment. The composition and concentration of dissolved salts in brine differ globally (Oldenburg 2006); however, Sodium chloride (NaCl) is the main dissolved solid in saline aquifers (Oldenburg 2006).

Table 0.1: Aquifer classification based on total dissolved solids (Meyer and Croskrey 2017).

Deep saline aquifers offer the largest storage potential amongst formations, with up to 10,000 $GtCO_2$ (IPCC 2005). The storage capacity of saline aquifers is higher than depleted oil and gas reservoirs, and they occur in all sedimentary basins (Bentham and Kirby 2005). Suitable saline aquifers for the purpose of CO_2 storage are composed of high porosity and high permeability sandstones or carbonates that are capped by shale aquitards or evaporitic aquicludes (Bachu and Stewart 2002) and occur at the depth of 800 m or more. Both physical and chemical mechanisms operate simultaneously or across different time scales to trap CO_2 in saline aquifers; these are explained in Section 2.3. The Sleipner project in the North Sea is the best

example of CO_2 storage in a saline aquifer (IPCC 2005), where 1Mt CO_2 per year has been injected since 1996 via a deviated well (Chadwick et al. 2008). CO_2 is partially trapped beneath nine relatively impermeable intra-reservoir mudstone layers situated beneath the main caprock (Bickle et al. 2007).

1.3 Thesis overview

1.3.1 Motivation

At the depths required for geological storage of CO_2, the gas has a lower density than brine and is in a supercritical state. Upon injection, the CO_2 will rise, due to density differences, through high permeability rocks until it reaches a caprock where it can accumulate in structural or stratigraphic traps. These physical traps are the primary means by which CO_2 is stored in geological formations until other trapping mechanisms influence the storage process. However, leaking through conductive faults, fracture networks (Busch et al. 2010; Michael et al. 2010), rock-cement-casing assemblage (Bagheri et al. 2018; 2019) and thin caprock or gap in the caprock is an important issue.

A seal, along with a highly porous and permeable reservoir, is a critical component of a trap. A seal or caprock is formed from low permeability rock (i.e., shales and evaporites) (Biddle and Wielchowsky 1994) and has a high capillary entry pressure that inhibits the vertical flow of CO_2 (Hesse et al. 2009; Wollenweber et al. 2010).

Early industrial and trial sequestration projects have mainly relied on structural and stratigraphic trapping mechanisms. For instance, in the Weyburn-Midale geological storage project, the Midale evaporite makes a perfect trap (Njiekak et al. 2013). In the Sleipner project, CO_2 is partially trapped beneath nine, relatively impermeable intra-reservoir mudstone layers situated beneath the main caprock (Bickle et al. 2007). In Salah, Algeria, the CO_2 was injected into a relatively simple low relief domed structure (Iding and Ringrose 2010), while the Naylor Field in South Eastern Australia, used as part of the CO2CRC Otway Project, is a fault-bounded trap (Vidal-Gilbert et al. 2010). In the Quest project in Canada, CO_2 is injected in a reservoir with a number of seals (Tawiah et al. 2020).

Herein, the effects of both large-scale faults and small-scale deformation bands as structural traps and primary and secondary stratigraphic traps on CO_2 geological storage are investigated. The rationale is that, particularly, in a short time-period, the CO_2 storage process

relies on structural and stratigraphic mechanisms. Therefore, it is desirable to maximise the storage security by reducing the reliance on a regional seal by utilising primary and secondary stratigraphic traps or small-scale structural traps.

For instance, the effects of mixed facies on CO_2 storage are poorly understood but can be an important factor in many target formations. They may act as small or large stratigraphic traps and may minimise the large buoyancy force acting upon a top seal.

Research has been renewed with the realisation that bleaching caused by large fluxes of CO_2-charged fluids offers an opportunity to better understand the CO_2 storage processes. By constructing a reservoir scale flow model, this study also attempts to replicate the observed patterns of bleaching and identify potential large-scale (i.e., faults) pathways of reducing fluids.

The influence of deformation bands, at the scale of a conjugate set and at the reservoir scale, on supercritical CO_2 injection and storage has been overlooked. This study research if the reduction in effective reservoir permeability caused by deformation bands will adversely impact CO_2 injection and storage, or, by creating a large number of mini structural traps around major faults, enhance storage security at injection sites even when sandstone is juxtaposed against sandstone.

1.3.2 Aim and objectives

This thesis aims to investigate CO_2 structural and stratigraphic trapping mechanisms to ensure secure geological storage.

This will be achieved by constructing 3D static models based on different outcrops and performing flow simulations to evaluate the storage potential of heterogeneous mixed siliciclastic-carbonate systems, deformation bands, and faults.

Consequently, the specific objectives are to:

- Assess the potential of mixed siliciclastic and carbonate complex systems to act as successful stratigraphic traps by constructing 3D static models based on outcrops from the Grayburg Formation, Lorca Basin and Bridport Sand Formation,
- Identify two possible pathways for the migration of reducing fluids in the Entrada Sandstone palaeo-reservoir and determine the influence of heterogeneity at lithofacies scale by building 3D static models based on the outcrop incorporating two major faults and facies heterogeneity,

- Evaluate the potential of one conjugate set of bands to act as mini-structural traps by modelling a conjugate set resulting from the amalgamation of multiple anastomosing seams,
- Examine the impact of deformation bands on CO_2 injection and storage by undertaking a simplified flow modelling exercise incorporating information on the geometry and porosity-permeability characteristics of clusters of deformation bands from a Penrith Sandstone Formation outcrop.

1.3.3 Methodology

In order to meet the aim of this thesis, several outcrops were carefully selected to build 3D static models in Petrel software (Schlumberger 2016). The constructed models then were fed into the ECLIPSE reservoir simulator (Schlumberger 2017) to run flow simulations. Various options exist in the ECLIPSE software to investigate CO_2 storage in geological formations, such as CO2SOL (study storage in oil reservoirs), COAL (study CO_2 storage in Coal Bed methane reservoirs) and CO2STORE (study CO_2-H_2O systems with salts). In this study, the ECLIPSE 300 simulator with CO2STORE was used. The porosity and permeability used in this study were based on field observations and/or relevant literature. The depth of the reservoir models was set at depths where CO_2 is in the supercritical state. Dynamic modelling was conducted under a pressure gradient of 100 bars/Km and a temperature gradient of 25°C/km, unless otherwise stated. To maintain geomechanical stability, and avoid damage to the reservoir, it is assumed that pressure remains below 75% of the lithostatic pressure gradient (225 bars/Km) at any point within the model (Noy et al. 2012), unless otherwise stated. The relative permeability curves in all chapters are taken from Onoja and Shariatipour (2018), except for Chapter 3, which are from Bennion and Bachu (2008; 2010). A same relative permeability curve to model CO_2 displacing water and water displacing CO_2 (no hysteresis in relative permeability) has been used throughout this study. This task has been overlooked because the resulting model would be slow and expensive to run, and reservoir simulations were generally unfeasible. The computational limitation was due to the size of the models in chapters 3 and 4 and the number of cells used to model mini-structures in chapters 5 and 6. Moreover, with a continually growing CO_2 plume, a non-hysteretic formulation using properties relevant for drainage should suffice and the use of hysteretic characteristic curves was not as critical. The same argument applies if structural trapping constrains CO_2 plume movement (Doughty

2007). Moreover, the focus was on structural and stratigraphic traps and not residual trapping mechanism.

1.3.4 Thesis outline

The following provides a short overview of the thesis structure and chapter contents.

Chapter 2: background

In this chapter, the physical properties of CO_2 are reviewed and various CO_2 trapping mechanisms are presented. In addition, depositional environments and how they affect the flow distribution are discussed, alongside the importance of outcrop analogues in reservoir modelling. This chapter is ended with a detailed review of CO_2 storage simulations in subsurface geological formations.

Chapter 3: **The impact of heterogeneous mixed siliciclastic-carbonate systems on CO_2 geological storage**

In order to study stratigraphic traps, mixed siliciclastic and carbonate systems are considered. This chapter aims to systematically investigate such systems to evaluate the effect of the variability of facies on fluid flow. Three different outcrops are chosen in this study, each representing a different mixed shallow-marine system with varying heterogeneity that may form small or large stratigraphic traps.

Chapter 4: Modelling of bleached palaeo-reservoir in the Salt Wash Graben, Utah

In Chapter 4, bleached palaeo-reservoir outcrop is selected to construct a reservoir scale flow model to investigate which major faults in the study area (the Salt Wash graben and the Little Grand Wash fault) were the more likely pathway for reducing fluid (i.e., CO_2). In addition, the highly heterogeneous character of the Entrada Sandstone is modelled to test the importance of geological heterogeneity on fluid flow and the bleached zone distribution.

Chapter 5: The application of X-shaped conjugate deformation bands as structural traps

This chapter aims to explore the effects of one conjugate set of bands on fluid flow. The most important question needs to be addressed in this chapter is whether these sub-seismic reservoir heterogeneities have applications as structural traps.

Chapter 6: The Impact of deformation bands clusters on CO_2 injection and storage

This chapter aims to examine the impact of clusters of deformation bands on CO_2 injection and storage. To study the influence of clustered deformation bands, models are generalised

to investigate the effects of host rock-deformation bands permeability contrast, deformation bands density, orientation and distribution.

Chapter 7: Conclusion and recommendations

This chapter presents the main conclusion of the thesis and put forward recommendations for future work.

Chapter 2

Background

2.1 CO_2 physical properties and subsurface pressure and temperature

The behaviour of CO_2 at depth is strongly dependent on its physical properties (Ennis-King and Paterson 2002; Bachu 2003) (Table 0.1). At normal atmospheric conditions, CO_2 is a stable gas. At lower temperatures and elevated pressures CO_2 exists as a solid, and for temperatures and pressures above the critical point [31.1 $^{\circ}$C and 73.8 bars] CO_2 occurs as a supercritical fluid (Figure 0.1). In the supercritical state, the fluid has different properties than that of its gas or liquid phases (Bachu 2008). CO_2 is in a dense (500-900 kg/m^3) liquid-like state that occupies less space but behaves like a gas by occupying the available pore volume (Holloway and Savage 1993; Ennis-King and Paterson 2002; Bachu 2003; 2008). The efficiency of CO_2 stored in a supercritical state is significantly greater than storage in the gas state (Chadwick et al. 2008).

Under normal pressure and geothermal gradient, as in a typical aquifer, CO_2 exists in a supercritical state at depths of c. 800 m (Chadwick et al. 2008). However, this key depth is highly variable between and within basins. For instance, in the Alberta Basin it ranges from <0.7 to >1.2 km depending on a geothermal gradient (Bachu and Stewart 2002). In UK onshore sedimentary basins, with a geothermal gradient of 25-26 °C/km and surface temperature of 10 °C, CO_2 reaches a supercritical state at 0.80-0.85 km (Holloway and Savage 1993). The density of CO_2 increases with depth (Figure 0.2) and approaches the density of formation brine (i.e., 1,000 kg/m^3, depending on the water salinity). However, the maximum density that can be attained, in normally pressured basins, is still less than that of formation brine at that depth (≈ 800 kg/m^3). In a cold basin, this density would be achieved at 0.8-1.0 km, but in warm basins the depth would increase to 1.5-2.0 Km (Bachu 2003). At depths, in over-pressured basins, a higher CO_2 density will be achieved; however, financial and safety issues

then become a major concern (Bachu 2003). The density contrast causes CO_2 to migrate up-dip under buoyancy until it reaches a caprock. The greater density difference between CO_2 and formation brine causes stronger buoyancy forces; thus, buoyancy forces in warm basins are more significant than cold basins, leading to increased flow and reduced storage safety. The CO_2-brine viscosity ratio increases with depth. However, at the optimum depth for CO_2 storage, it ranges from 0.05 to 0.20, which results in the CO_2 attaining a higher mobility than brine; this can lead to viscous fingering (Ennis-King and Paterson 2002). Figure 0.3 shows the density and viscosity of CO_2 as a function of temperature and pressure

Table 0.1: CO_2 physical properties.

Properties			
Molecular Weight	44.01 g/mol		
Critical temperature	31.06°C		
Critical pressure	73.83 bars		
Density	468.19 Kg/m³		
Triple point temperature	-56.56°C		
Triple point pressure	5.1867 bars		
Liquid phase at 1.013 bars			
Liquid density at triple point	1178.4 kg/m³		
Gas Phase at 1.013 bars	**0°C**	**15°C**	**25°C**
Gas density	1.9763 kg/m³	1.8714 kg/m³	1.8075 kg/m³
Dynamic viscosity	1.3711E-4 Po	1.4446E-4 Po	1.4932E-4 Po
Solubility in water		8.21E-4 mol/mol	6.15E-4 mol/mol
Specific gravity	1.53	1.53	1.53
Specific volume	5.06E-1 m³/kg	5.344E-1 m³/kg	5.532E-1 m³/kg
Thermal conductivity	14.674 mW/m·K	15.844 mW/m·K	16.643 mW/m·K
Vapor pressure	34.9054 bars	50.9921 bars	64.4789 bars
Solid Phase at 1.013 bars			
Solid density	1562 kg/m³		

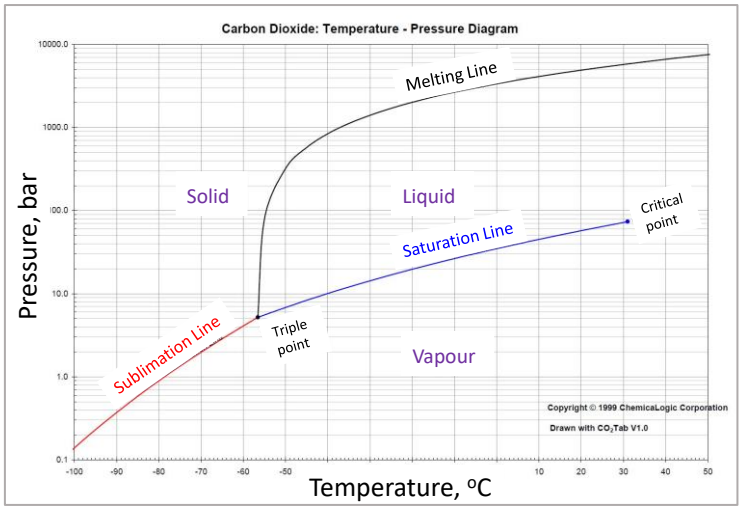

Figure 0.1: CO_2 phase diagram (ChemicaLogic Corporation 2018).

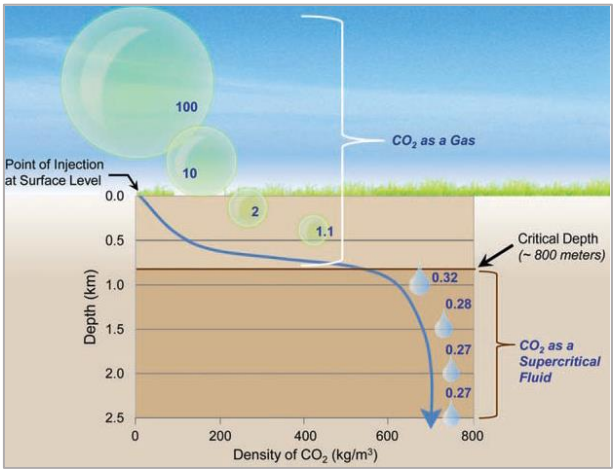

Figure 0.2: Variation of density with depth, assuming hydrostatic pressure, a geothermal gradient of 25 °C/km and surface temperature of 15 °C (IPCC 2005).

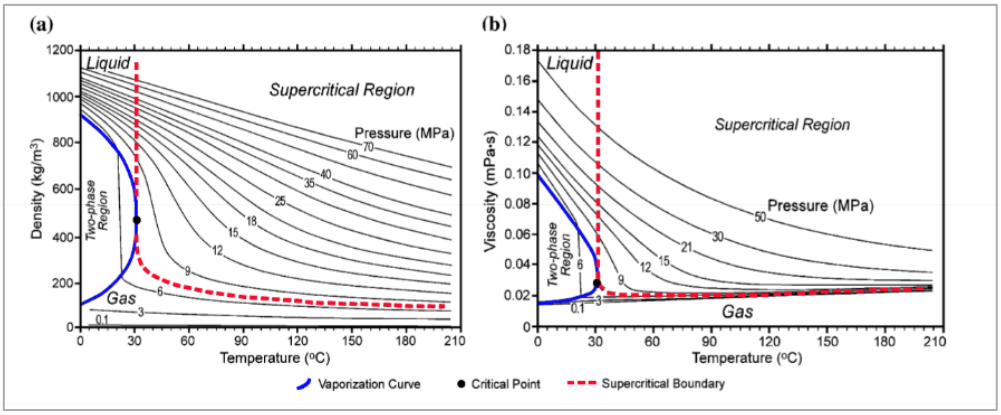

Figure 0.3: Density and viscosity of the CO_2 as a function of temperature and pressure (Nordbotten, Celia and Bachu 2005).

2.2 Driving forces

Two-phase flow in porous media has applications in several subsurface processes, including geological carbon storage (Løvoll et al. 2005). Fluid flow in CO_2 storage is controlled by hydrodynamic, buoyancy, viscosity and capillary forces. The first two driving forces oppose the latter. The relative importance of each mechanism, and the distribution of CO_2 and formation brine, are controlled by the petrophysical properties of the reservoir, density difference of liquid phases, mobility ratio, relative permeability and capillary curves and the injection strategy (Pentland et al. 2011).

Hydrodynamic forces result from pressure differences between injection and natural forces. During supercritical flow, as CO_2 is generally less viscous than the formation brine, viscous fingering may influence the flow pattern. In this case CO_2 (non-wetting fluid) may intrude into the formation brine (wetting fluid) and form preferential flow paths known as viscous fingers (Måløy, Feder and Torstien 1985; Zhou, Fayers and Orr Jr 1997; Løvoll et al. 2005; Zhang et al. 2011; Pentland et al. 2011; Islam, Chevalier and Sassi 2013).

The density difference between the supercritical CO_2 and the formation brine induces vertical flow causing the CO_2 to migrate through the liquid until it reaches a low permeability caprock. Generally, capillary forces have a lesser effect on the development of the plume than buoyancy and viscous forces (Ide, Jessen and Orr Jr 2007).

The dimensionless gravitational number, mobility ratio and capillary number can help evaluate flow patterns and distribution in the reservoir (Zhou, Fayers and Orr Jr. 1997; Nordbotten, Celia and Bachu 2005; Kopp, Class and Helmig 2009). These numbers are indirectly influenced by pressure, temperature, and salinity (Bachu 2015). The gravitational number influences the shape, extent and location of the plume in the reservoir and thereby the storage efficiency.

$$\Gamma = \frac{2\pi\Delta\rho g k \lambda_b H^2}{Q} \qquad 2.1$$

(Nordbotten, Celia and Bachu 2005)

Γ is the gravity number, $\Delta\rho$ the density difference between aquifer brine and CO_2 at *in-situ* conditions, g is the gravitational constant, K is permeability, H is thickness and λ_b is brine mobility.

$$M = \frac{\frac{k_{rnw}}{\mu_{nw}}}{\frac{k_{rw}}{\mu_w}} \qquad M = \frac{\lambda_{nw}}{\lambda_w} \qquad 2.2 \qquad \text{(Berg, Oedai and Ott 2013)}$$

M is mobility ratio, μ_{nw} is non-wetting (i.e., CO_2) viscosity, μ_w is wetting phase (i.e., brine) viscosity, λ_{nw} is non-wetting phase mobility, and λ_w is wetting phase mobility.

$$C = \frac{q\mu_{CO_2}}{T_s \cos\theta} \qquad 2.3 \qquad \text{(Espinoza, Kim and Santamarina 2011)}$$

C is the capillary number, q is the injection rate, T_s is the interfacial tension between water and CO_2 and θ is the contact angle formed by the water-CO_2 interface and the mineral surface.

2.3 CO_2 Trapping Mechanisms

To conduct any CO_2 storage project successfully, comprehensive knowledge of the physical and chemical trapping mechanisms and the ability to predict them is essential (Lu et al. 2013). Based on physical, chemical and hydrodynamic conditions in the reservoirs, different trapping mechanisms are involved in the storage processes. These mechanisms are two-fold: physical trapping and geochemical trapping (Lu et al. 2013). Physical trapping mechanisms include structural and stratigraphic traps, where the upward migration of CO_2 is inhibited by low permeability caprock; and residual or capillary trapping, where CO_2 is trapped as immobile and isolated bubbles (Juanes et al. 2006). Where no apparent structural trap exists, a CO_2 plume may be trapped because of its extremely long residence time. This trapping mechanism is known as hydrodynamic trapping (Bachu and Adams 2003). Geochemical trapping includes dissolution and mineral trapping, as CO_2 partially dissolves into the water phase (e.g., Ennis-King and Paterson 2005; Özgur 2006; Iglauer 2011). Over geological time, the dissolution products can precipitate in the reservoir as stable minerals, a permeant trapping mechanism known as mineral trapping (e.g., Andre et al. 2007; Gaus 2010; De Silva 2015). The timescales associated with each of these sequestration mechanisms differ (Alcalde et al. 2018), although they can operate simultaneously (IPCC 2005). However, during the injection period, physical trapping could be the most significant mechanism, and conversely, dissolution and mineral trapping mechanisms become more significant during the post-injection period.

This study investigates the importance of structural and primary and secondary stratigraphic traps in CO_2 geological storage, with a particular focus on small-scale deformation bands.

2.3.1 Structural and stratigraphic trapping mechanism

The successful geological storage of CO_2 is dependent on structural and stratigraphic trapping mechanisms and the presence of an impermeable seal, e.g., the Weyburn-Midale CO_2 sequestration project, Canada (Brown et al. 2017) and Sleipner Field, northern North Sea (Chadwick et al. 2008; Zhu et al. 2015; Falcon-Suarez et al. 2018). This trapping mechanism offers reliable storage in well-characterised sedimentary basins and in oil and gas fields where hydrocarbons have been trapped over geological time. Such mechanisms must guarantee the secure storage of CO_2 by minimizing the risk of leakage until other trapping mechanisms are initiated. It is important to analyse the ability of structures to retain fluids in the long-term, as storage integrity can be jeopardised by leakages through transmissive faults, fractures, leaky wells, and a thin caprock or gap in the caprock (Song and Zhang 2013).

Under thermodynamic conditions suitable for CO_2 storage, the injected CO_2 is usually in a supercritical state with a density of 30% to 40% less than that of the brine (Ennis-King and Paterson 2002). During the CO_2 injection process, the mobile CO_2 (non-wetting phase) displaces brine (wetting-phase) and is akin to the drainage process when the saturation of the non-wetting phase increases. After injection ceases the CO_2 will rise under buoyancy through high permeability pathways until it reaches a caprock and accumulates in a trap. The upward migration of the CO_2 is controlled by vertical permeability and the density difference between CO_2 and brine (Hellevang 2015).

To have a feasible trap, two basic components are required: firstly, a reservoir with high porosity and high permeability where the CO_2 can be stored, and secondly, a seal with low porosity, low permeability, and high capillary entry pressure where any further CO_2 migration is prevented. Porosity [φ] is the measure of the storage capacity, it can be primary (depositional), secondary (diagenesis) and link to fracturing. No matter the type of porosity, it is vital to have enough volume to accommodate a considerable amount of fluid. The reservoir must also allow the transmission and exchange of fluids. Permeability [K] is the measure of the ability of a fluid to flow through a reservoir. Individual reservoirs generally display lateral and/or vertical variations in their petrophysical properties (i.e., porosity and permeability), caused by depositional and/or diagenetic processes.

Low to very low permeability (µD to nD) rocks that act as a seal or caprock are often water-saturated, fine-grained clastics (i.e., clayey shale and silty shales), evaporites or organic-rich

rocks (Downey 1984), which prevent CO_2 from migrating up and out of the traps (Fleury et al. 2011). A good sealing capacity is essential for retaining the CO_2 over a long timescale.

Petroleum can be preserved in structural and or stratigraphic traps, which can be categorised into three broad types: structural, stratigraphic or a combination of both (Levorsen and Berry 1967).

Structural traps are formed due to the deformation of strata, during or after sediment deposition. The most important structural traps are fold- or faults-dominated (Figure 2.4, Table 0.2) (Biddle and Wielchowsky 1994); however, according to North (1985) purely fault-dominated traps are uncommon. Structural traps (folds and faults) which are formed due to crust movement can impede the vertical or horizontal movement of the injected CO_2 (Bachu 2008).

Fold-dominated structural traps can have a diversity of geometries. Fold is a term used to describe a curved or nonplanar arrangement of beds that are mainly formed by tectonic processes. Folds can be categorised as fault-related or fault-free (Figure 2.5, Table 0.2).

Fault-related types include fault-bend, propagation, drag and drape. Fault-free types include lift-off, chevron/kink band, diapir and differential compaction (Biddle and Wielchowsky 1994).

Fault-dominated structural traps can be categorised as normal, reverse and strike-slip (Figure 0.6) (Biddle and Wielchowsky 1994).

Figure 0.4: Structural traps. Blue is CO_2 accumulation. Red is the fault (after Biddle and Wielchowsky 1994).

Table 0.2: Fold and fault dominated traps.

				Mechanism
Structural traps	**Fold-dominated**	Fault- free	Lift-off folds	Formed due to buckling caused by stratal shortening above a decollement (Poblet and Mcclay 1996).
			Chevron/kink fold	Folds resulting from the compression along layering (Ramsay 1974).
			Diapir	Materials such as magma and salt can flow vertically or horizontally deform roof layers and form such folds (Biddle and Wielchowsky 1994).
			Differential compaction	Formed as a result of differential compaction above buried topography (Biddle and Wielchowsky 1994).
		Fault- related	Fault bend	Caused by bending of a fault-block as it moves over a non-planer fault surface (Suppe 1983).
			Fault propagation	Caused by compression in front of a fault tip during fault propagation (Suppe and Medwedeff 1990).
			Fault drag fold	Caused by frictional forces acting across a fault (Suppe 1983).
			Fault drape fold	Caused by flexure above a buried fault (Suppe 1983).
	Fault- dominated	Normal		In extensional regimes when the hanging wall moves downward relative to the footwall block, normal faults are formed (Fossen et al. 2007). They are the most common type of fault-dominated structural traps (Biddle and Wielchowsky 1994).
		Reverse		The hanging wall moves up relative to the footwall due to compressive shortening of the crust (Fossen et al. 2007).
		Strike-slip		Faults where the primary motion is horizontal and parallel to the fault plane (Reading 1980).

Figure 0.5: Fault-related folds and fault-free folds (after Biddle and Wielchowsky 1994).

Figure 0.6: Fault traps (after Biddle and Wielchowsky 1994).

Stratigraphic traps exist where stratigraphy restricts fluids in the reservoir. Stratigraphic traps can be divided into three categories: depositional or primary traps (Figure 0.7) (traps created by stratigraphic processes at the time of sediments' deposition), stratigraphic traps associated with unconformities (traps occurred beneath or above an unconformity) and secondary stratigraphic traps (traps formed as a result of post-depositional alteration) (Rittenhouse 1972) (Table 0.3). Hence, stratigraphic traps are geological structures generated by depositional and/or diagenetic processes that limit the vertical and horizontal movement of CO_2 (Bachu 2008).

Table 0.3: Stratigraphic traps (after Biddle and Wielchowsky 1994).

Figure 0.7: Primary stratigraphic traps (after Biddle and Wielchowsky 1994).

Storage in structural traps can be both advantageous and disadvantageous (Chadwick et al. 2008); for instance, the estimation of storage security and capacity in a closed trap is calculable due to the known and limited extent of CO_2. However, the reduced contact areas between the CO_2 and brine can minimise the dissolution effectiveness. Furthermore, a formation with a thick column of the CO_2 displaying a high buoyancy force acting upon a caprock and can jeopardise the storage integrity. Structural traps also have lower storage capacity when compared to open aquifers because of the potential for a rapid pressure build-up (Zhou et al. 2008; Lindeberg, Vuillaume and Ghaderi 2009). In open aquifers, there are no lateral boundaries that limit the CO_2 movement. A large contact area leads to effective dissolution; however, this can be disadvantageous as it needs to be mapped in order to identify possible leakage pathways. In addition to large-scale traps, small un-mappable traps can exist at the subsurface. They can improve the overall effectiveness of structural trapping and, by retarding plume migration, can increase the volumes that can be safely stored in the reservoirs (Nilsen, Lie and Anderson 2015). In Chapters 5 and 6, the significance of deformation bands which are small-scale structures will be investigated.

2.3.1.1 Structural trapping mechanisms at different injection sites

In this section storage projects that rely on structural and stratigraphic traps will be examined.

Sleipner Project

The Mio-Pliocene Utsira Sand is an aquifer with relatively low structural relief that has been used for CO_2 injection (Chadwick et al. 2008). The lack of a well-defined closure in such an aquifer is an issue for CO_2 geological storage (Chadwick et al. 2004). Only a small fraction of pore volume is situated within structural closures at the top of the Utsira Sand (Zweigel et al. 2000). However, the reservoir is not homogeneous sand but is comprised of high porosity and permeability sand packages separated by thin (intra-reservoir) low permeability mudstone or shaley horizons (Chadwick, Noy and Holloway 2009) (Figure 2.8). These shales are c. 1m thick and are reflected as peaks in gamma-ray, sonic and neutron density logs. A thicker shale layer, termed the 'five-metre shale', separates the uppermost sand unit from the main reservoir (Chadwick et al. 2004). These thin shale layers have drastically influenced CO_2 distribution within the reservoir, as CO_2 has migrated laterally beneath the intra-reservoir shales and subsequently ponding beneath (Chadwick, Noy and Holloway 2009). These layers may permit a more efficient dissolution of CO_2 and effectively increase the reservoir capacity. In their absence; however, the CO_2 would escape and migrate upwards to reach the next layer (Zweigel et al. 2004). In Utsira Sand, small faults would likely manifest as deformation bands with considerable permeability loss compared to the host rock (Chadwick, Noy and Holloway 2009).

Figure 0.8: Sleipner storage reservoir with inter-formational shale layers (Cavanagh and Haszeldine 2014).

CO2CRC Otway Project

The CO2CRC Otway Project is a pilot site used to examine CO_2 storage in a depleted natural gas field (Dance, Spencer and Xu 2009). The main storage mechanism is the containment of the CO_2 in structural trapping, as the Naylor Field of the Otway Project is a fault-bound trap. Gas produced from the Buttress Field is injected into the late Cretaceous Waarre C Formation (Dance 2013). The targeted formation is bound on three sides by sealed faults with an efficient seal capacity (Vidal-Gilbert et al. 2010). These faults juxtapose the reservoir against the Belfast Mudstone, an exceptionally good seal in this basin (Dance 2013). There is no evidence that methane had moved out of the reservoir via these faults (Vidal-Gilbert et al. 2010). The injected CO_2 migrated upward under buoyancy towards the top of the formation to rest below the methane gas cap, which is slightly lighter than CO_2. Small-scale sedimentary features within the reservoir affect the CO_2 distribution (Dance 2013).

In Salah CO_2 storage project

During the life span of the In Salah project, 3.8 Mt of CO_2 was stored in the subsurface (Ringrose et al. 2013). Structurally, the Krechba Field is a relatively simple anticline with four-way dip closures (Eiken et al. 2011). CO_2 was injected into the down flank of a producing gas field through three deep reach horizontal wells. The reservoir is composed of Carboniferous sandstone with a medium permeability (Iding and Ringrose 2010). Injectivity was an issue due to the low permeability matrix. The sandstones and caprock both have fractures and small faults, and the fracture permeability can enhance the overall permeability of the reservoir. To achieve optimum injectivity, the wells were designed to intersect these fractures. The operation stopped in 2011 and subsequent monitoring showed that the pressure and the injected CO_2 has migrated to the lower part of the caprock. The main explanation for this is that hydrofracturing of the lower caprock was occurred due to the high injection pressure (White et al. 2014), nonetheless, CO_2 remains secure within the storage unit (Ringrose et al. 2013; White et al. 2014).

Weyburn-Midale CCS- EOR project

The Weyburn CO_2-enhanced oil recovery project (CO2-EOR) is a very complex geological system. The oil exists in a Mississippian Midale fractured carbonate reservoir (Pendrigh 2005;

Njiekak et al. 2013). An angular unconformity juxtaposes highly porous carbonates against the impermeable Watrous Formation creating a trap. The Midale Evaporite provides the upper seal and the relatively impermeable and extensive Triassic Lower Watrous Member, lying above the Sub-Mesozoic Unconformity, provides a regional seal. The Frobisher unit forms the bottom seal to the Midale reservoir zones (Njiekak et al. 2013). The geological setting of the Weyburn-Midale project is favourable for the long-term storage of CO_2 (Preston et al. 2005) as hydrocarbons are trapped in a combined stratigraphic, diagenetic and hydrodynamic trap (Brown 2002). CO_2 leakage through the primary seal is highly unlikely and if it happens there are other zones that can act as CO_2 sinks and barriers (Preston et al. 2005).

The Snøhvit project

The target storage reservoir in the Snøhvit field is the early Jurassic Tubåen Formation (Hansen et al. 2013). The formation is composed of clean sand that can be subdivided into five units based upon interbedded shale layers that can act as barriers to flow (Grude, Landrø and Osdal 2013). The Tubåen Formation is compartmentalised by several E-W trending faults (Grude, Landrø and Osdal 2013); CO_2 has been injected into the F-segment of the block, which is located between two sealing faults (Hansen et al. 2013).

Cranfield CO_2 injection site

The main trapping mechanism of the Cranfield storage site is structural. A four-way closure of a gentle anticline provides an effective structural trap and maximum opportunity for the long-term dissolution trapping. The Upper Cretaceous D-E sand units of the Lower Tuscaloosa Formation is the target formation. The sealing properties of the NNW-SSE trending normal fault that intersects the D-E units is uncertain, but several studies showed that the fault is non-transmissive (Lu et al. 2013). The regional caprock has diverse lithologies but a suitable sealing capacity that could retain a long column of CO_2 (Lu et al. 2013).

Ketzin project

The storage formation in the Ketzin project is the upper part of the Triassic Stuttgart Formation (Kempka et al. 2013). The structural trap consists of a double anticline. The anticline, along with a multi barriers system, provides safe storage of CO_2 (Ivandic et al. 2015).

The Stuttgart Formation is overlain by the Weser Formation, which acts as the immediate caprock to the reservoir.

Quest project

CO_2 injection at Quest started in August 2015 and c. 4 million tonnes of carbon dioxide have now been stored safely via three injection wells into the Basal Cambrian Sandstone (Shell Canada 2019). This formation is a deep saline aquifer with a thickness of 45 m located at a depth of about 2 km above the Precambrian basement. The reservoir has high porosity and permeability and numerous seals, including the primary seal (Middle Cambrian Shale), secondary seal (Lower Lotsberg) and ultimate seal (Upper Lotsberg) (Tawiah et al. 2020). Table 2.4 is summarised some of the storage projects, their structures and depositional environments.

2.3.2 Hydrodynamic trapping mechanism

Deep saline aquifers, with no apparent physical trap, may exist in sedimentary basins and can have a very large storage capacity. Storage is governed by the slow transport mechanism (Bachu, Gunter and Perkins 1994) as CO_2 moves through the aquifer with or against regional groundwater flow (Bradshaw et al. 2007). The residence time of CO_2 is so high, as velocities are so low, that migration is measured in cm/yr (Bergman and Winter 1995; Bradshaw et al. 2007). The slow transport mechanism retains the CO_2 within the aquifer as the CO_2 does not reach the edges of the system. Consequently, there is no need for a structural or stratigraphic trap.

Other trapping mechanisms can also operate on the CO_2. For example, dissolution trapping can also occur, which can eliminate the buoyancy and fingering effects and thus reduces the risk of leakage (Bachu, Gunter and Perkins 1994). The trapping of CO_2 over a geological timescale is termed hydrodynamic trapping. When considering hydrodynamic trapping, it is important to know the hydrodynamics of the aquifer and CO_2 movement in relation to regional flow. For example, Larkin (2010) showed that among immature, mature and static basins, the mature basins are more suitable for such storage as the up-dip migration of CO_2 will be reduced as groundwater and buoyant flow are in opposite directions.

Table 0.4: Structure and depositional systems in some industrial and pilot projects.

Project	Structure	Depositional environment	Formation	Reference
Sleipner	Low relief dome	Shallow shelf setting	Utsira Formation	Chadwick et al. (2008)
Weyburn	Angular unconformity	Arid tidal-flat	Midale Formation	Pendrigh (2005); Njiekak et al. (2013)
In Salah	Gentle dome	Tidal deltaic	Krechba Formation	Iding and Ringrose (2010); White et al. (2014)
Frio	Steeply dipping formation due to the close proximity to a salt dome	Fluvial	Frio Formation	Hovorka et al. (2006); Xu et al. (2010)
Salt Creek	Asymmetrical anticline	Delta	Tensleep Formation	Bickle et al. (2017); Doherty et al. (2017)
Snohvit	Fault trap	Deltaic to fluvial	Tubåen Formation	Grude, Landrø and Osdal (2013); Hansen et al. (2013)
Gorgon	Small scale structural/stratigraphic traps and no need for large scale traps	Deep water slope	Dupuy Formation	Flett et al. (2009)
Ketzin	Anticline	Fluvial	Stuttgart Formation	Kempka et al. (2014); Ivandic et al. (2015)
Otway	Fault trap	Fluvial	Warre C Formation	Vidal-Gilbert et al. (2010); Underschultz et al. (2011); Dance (2013)
Quest	Open aquifer	shallow marine to tidal	Basal Cambrian	Tawiah et al. (2020)
Bunter	Number of simple 4-way dip-closed structures	Arid to semi-arid fluvial	Bunter Sandstone	Williams et al. (2013)
Cranfield	Gentle four-way anticline	Fluvial	D-E units of the Lower Tuscaloosa Formation	Hovorka et al. (2011); Lu et al. (2013)
Captain	No specific structural traps	Shelf	Captain Sandstone Formation	Jin et al. (2012); Williams et al. (2016)
Bell Creek	Monocline and stratigraphic trap	Near-shore marine	Muddy Formation	Gorecki et al. (2012); Hamling et al. (2013)

2.3.3 Residual trapping mechanism

The capillary or residual trapping mechanism has been explored by various authors (Kumar et al. 2004; Juanes et al. 2006; Krevor et al. 2011; Pentland et al. 2011; Krevor et al. 2015). it is attractive over the short- to medium-term (Bachu 2008) and can contribute to storage security. Capillary or residual trapping mechanisms are active at the pore-level (Kumar et al. 2004) and characterised by the irreversibility of multiphase flow, especially relative permeability hysteresis within the porous medium (Juanes et al. 2006). Simulation studies have shown that a considerable amount of CO_2 can be immobilised by the capillary trapping mechanism (Krevor et al. 2011).

Generally, supercritical CO_2 is the non-wetting phase in sedimentary rocks that are suitable for geological storage and formation brine is the wetting phase (Iglauer, Pentland and Busch 2014). During its injection into saline aquifers, the CO_2 invades the pore space and saturation increases at the front of the plume. This process is called drainage, as the brine is drained from the pore space. CO_2 migrates vertically away from the injection well as a continuous and connected mass until it reaches the caprock. However, there is not a complete displacement as high capillary entry pressure prevents the formation brine from being drained from the smallest pore in the medium. After injection ceases, water saturation increases at the trailing edge and formation brine encroaches into the pore space filled with CO_2. This process is referred to as imbibition. As brine prefers to imbibe into smaller pores, disconnected and isolated bubbles of CO_2 are left, which are effectively immobile. This remaining CO_2 is described as trapped saturation and this is where the relative permeability of the CO_2 drops to zero and it cannot flow out of the pore system (Figure 2.9A) (Juanes et al. 2006). This trapping mechanism can occur naturally or can be induced by the injection of water slugs with alternating CO_2 injection, which maximises water imbibition (Juanes et al. 2006; Qi, Laforce and Blunt 2009). However, where the maximum CO_2 saturation and zero water relative permeability are obtained during the drainage process, trapped saturation cannot be reached (Juanes et al. 2006; Burnside and Naylor 2014). Residual trapping enhances the dissolution trapping since small droplets of CO_2 dissolve faster than large droplets of CO_2 (Iglauer 2011). This mechanism, therefore, improves storage security, capacity and limits the ultimate distribution of injected CO_2 (Krevor et al. 2015).

2.3.4 Dissolution trapping

Another mechanism involves the trapping of CO_2 as a dissolved solute in the aqueous phase. CO_2 solubility in the aqueous phase is a function of pressure, temperature and salinity (Spycher, Pruess and Ennis-King 2003). CO_2 solubility increases with pressure and reduces with increasing temperature and salinity. The salt type (i.e., NaCl, KCl, Na_2SO_4, etc.) also affects CO_2 solubility (Iglauer 2011). In subsurface geology considered for CO_2 storage, with elevated pressures and temperatures, the pressure-effect compensates the temperature-effect and CO_2 dissolution increases with depth. The amount and rate of dissolved CO_2 in the aqueous phase depend on the relative permeability curve, and values of residual water- and residual gas saturation. The higher the residual water saturation the greater the dissolution of CO_2 during the injection period. Less residual gas saturation allows for a higher CO_2 dissolution rate as the contact area between CO_2 and brine increases (Ennis-King and Paterson 2005). This is because the interfacial area has an essential role in the mass transfer kinetics and subsequent CO_2 dissolution (Iglauer 2011). Large quantities of CO_2 can be stored in geological media by this mechanism, with an increase in the storage capacity by a factor of two (Firoozabadi and Cheng 2010). The downside, however, is the slowness of the process, which can occur over millennia (IPCC 2005).

CO_2 and brine form a reactive system, as CO_2 dissolves in water to form aqueous carbon dioxide CO_2(aq). This results in the production of bicarbonate and a decrease in reservoir pH to ≈3. The second reaction is the slowest (Iglauer 2011):

$$CO_2(sc) + 3H_2O \rightleftharpoons CO_2(aq) + 3H_2O \quad (2.4)$$

$$CO_2(aq) + H_2O \rightleftharpoons H_2CO_3 \quad (2.5)$$

$$H_2CO_3 \rightleftharpoons HCO_3^- + H^+ \quad (2.6)$$

$$HCO_3^- \rightleftharpoons CO_3^{2-} + H^+ \quad (2.7)$$

CO_2 dissolved in brine is transported by three mechanisms: molecular diffusion, mechanical dispersion and convection. These mechanisms can operate concurrently or independently (Özgur 2006) and further contribute to the process of dissolution (Ennis-King and Paterson 2002; 2005; Iglauer 2011).

Molecular diffusion is a time-dependent process caused by random molecular motions linked to the concentration gradient. When two miscible fluids with different concentrations, e.g., brine saturated with CO_2 and undersaturated brine, flow through a porous medium,

dispersion occurs. This is because: i) fluids move faster through the centre of the pores. ii) fluid travels faster through larger pores. iii) some of the fluid will encounter longer travel pathways due to the tortuosity of a medium.

When CO_2 dissolves in the reservoir formation brine the density of the water increases unlike most other gases (Ennis-King and Paterson 2005). According to Lindeberg and Bergmo (2003), saturated brine is 10 kg/m^3 denser than unsaturated brine and this leads to convective mixing (Figure 2.9B). Low permeability caprock with high capillary entry pressure hinders the upward migration of a low-density plume (Juanes et al. 2006; Qi, Laforce and Blunt 2009). High buoyancy CO_2 tends to bypass much of the available reservoir pore volume, which reduces storage capacity. Eventually, the injected CO_2 is distributed below the caprock as a thin or thick mobile layer, depending on the seal geometry (Ennis-King and Paterson 2005). CO_2 can dissolve in the underlying single aqueous phase. Only the top of the water column is in contact with the CO_2 (gas-brine interface). At this stage the dissolution is controlled by molecular diffusion. Diffusion causes the dissolved CO_2 to be transported further away from this surface. The dissolution of CO_2 increases the density of the aqueous phase creating gravitational instability, which destabilises the system. When a sufficient thickness of CO_2-saturated brine has been formed, convection starts to occur (Ennis-King and Paterson 2005; Riaz et al. 2006; Özgur 2006; Iglauer 2011; Ranganathan et al. 2012). The dominant mechanism in CO_2 dissolution is convective mixing, which is much faster than diffusion (Ennis-King and Paterson 2005).

Figure 0.9: (A) Residual trapping and (B) Dissolution trapping (after Zulczewski et al. 2012; Dong and Blunt 2009).

2.3.5 Mineral trapping

Over time, CO_2 reacts with the formation brine to form carbonic acid. The formation of this weak acid causes the pH to drop and the acid reacts with and breaks down minerals that function as cation donors (De Silva, Ranjith and Perera 2015). The precipitation of new stable mineral assemblages can thus contribute to mineral trapping. For instance, the dissolution of albite results in the precipitation of dawsonite and chalcedony, and the dissolution of chlorite results in precipitation of siderite, dolomite, kaolinite and chalcedony (Gaus 2010). Dawsonite may be the dominant secondary carbonate that forms and traps CO_2 (Gao et al. 2013). This mechanism strongly depends on the availability of reactive minerals in the aquifer. Some feldspar and clay minerals have a dissolution rate many orders of magnitude slower than carbonate minerals (Andre et al. 2007), thus such trapping mechanism takes place over thousands or millions of years. During the initial injection period the amount of CO_2 that can be immobilised by this trapping mechanism is almost negligible (Bachu et al. 2007). Nonetheless, this storage mode is permanent and has a large capacity, which makes it an attractive long-term storage option.

2.4 Depositional environment

Sediments can accumulate in a variety of basinal environments due to a combination of physical, chemical and biological processes (Boggs 2014). There is a close relationship between the depositional process and rock properties, as depositional environments determine sediment distribution, grain size and sorting (Bjørlykke 2014). Consequently, depositional environments control the heterogeneity, internal features and quality of reservoirs (Okwen, Yang and Frailey 2014; Ringrose and Bentley 2015). The classification of reservoirs and aquifers in relation to their depositional environments include:

- Fluvial reservoirs
- Aeolian reservoirs
- Tidal-deltaic reservoirs
- Shallow-marine reservoirs
- Deep-marine reservoirs
- Carbonate reservoir (Figure 2.10)

2.4.1 Fluvial reservoirs

These are complex systems generated by the erosional, transportational and depositional activities of rivers (Tucker 2009; Boggs 2014). Various types of fluvial deposits exist which demonstrated a unique set of properties. Comprehensive knowledge of these differences is crucial in the evaluation of a subsurface reservoir geology (Slatt 2013). Fluvial deposits are important hydrocarbon reservoirs and aquifers and possible injection sites. These reservoirs are known for their inherent heterogeneous stratigraphic architecture. Many of these reservoirs are characterised by multiple and laterally discontinuous sand bodies producing complex spatial patterns (Lu et al. 2012). Sand-body geometry, orientation and petrophysical properties influence fluid flow and result in variable connectivity and tortuous flow pathway (Deveugle et al. 2011). Fluids flow in high permeability paths in fluvial reservoirs (Dressel et al. 2010).

The Cranfield CO_2 injection site (Section 2.3.1.1) is a coarse-grained complex fluvial sandstone demonstrating various degrees of lithological and petrophysical heterogeneity (Lu et al. 2013). CO_2 flow paths in this type of reservoir are very complex, which leads to increased interaction between the brine and CO_2 and thus higher dissolution trapping.

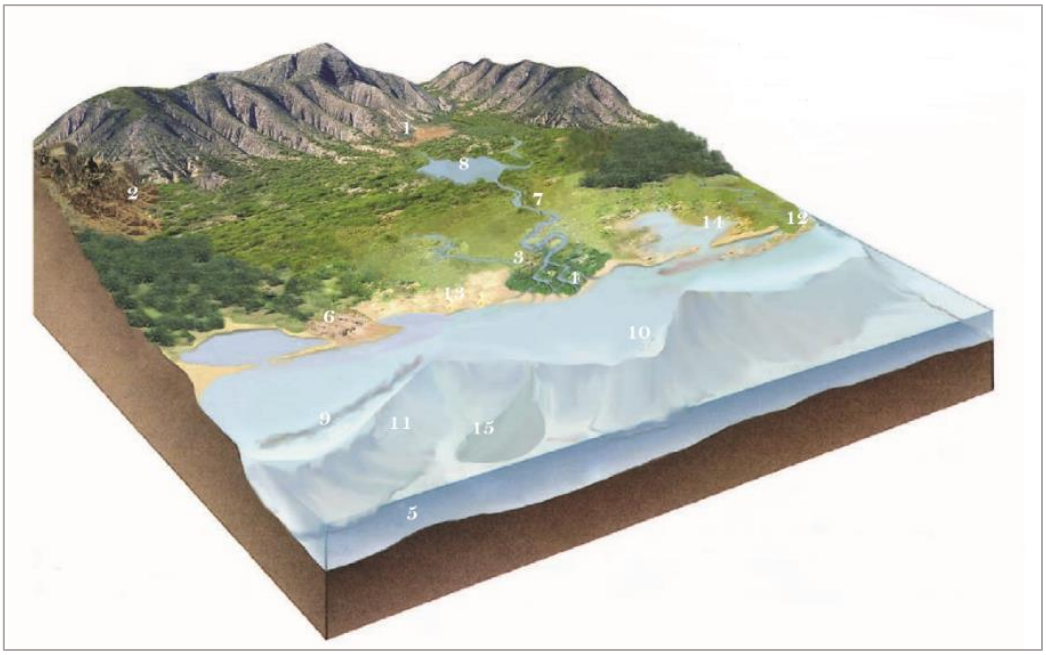

Figure 0.10: Depositional environments (USDOE 2010). 1) Alluvial, 2) Basalt, 3) Swamp, 4) Deltaic, 5) Deep marine, 6) Aeolian, 7) Fluvial, 8) Lacustrine, 9) Reef, 10) Shelf, 11) Slope, 12) Beach and barrier Island, 13) Beach, 14) Tidal flat, 15) Turbidite.

2.4.2 Aeolian reservoirs

These sediments are generated by the activities of wind under arid conditions (Boggs 2014). These deposits are well-sorted with a good porosity-permeability relationship. They produce thick, extensive and high-quality reservoirs with high net-to-gross ratios (Ringrose and Bentley 2015). Recent studies showed that aeolian reservoirs can display permeability that is extremely anisotropic (North and Prosser 1993). Aeolian deposits can be heterogeneous, especially at the small-scale. This arises from the permeability contrast between laminae. Within aeolian systems, the primary direction of injected CO_2 is parallel to the palaeo-wind direction at the time of deposition (Dressel et al. 2010). In this study, outcrops in Chapter 4, 5 and 6 specifically were deposited in aeolian environments.

2.4.3 Deltaic reservoirs

Deltaic sediments occur in marginal-marine environments where rivers empty sedimentary load into oceans or smaller standing bodies of water such as lakes. Based on the strength of fluvial, wave and tide input, they can be classified as the river-, wave-, or tide-dominated deltas (Tucker 2009). Sediment properties vary between and within these types and making deltaic reservoirs complex systems. They have distinctive fluid flow patterns due to their internal architecture, with reservoir performance dominated by the orientation and continuity of sand and shale layers that act as reservoirs and barriers (Slatt 2013). In reservoir modelling, fluvial and wave-dominated deltas are included alongside shallow marine deposits.

2.4.4 Shallow-marine reservoirs

Shallow-marine sandstones form one of the most prolific reservoirs with high recovery factor Howell et al. (2008). They are described as depositional systems which show the influence of both marine and continental processes (Stow, Reading and Collinson 1996).

Such systems have been studied greatly, for example, Manzocchi, Ringrose and Underhill (2008) and Howell et al. (2008) studied these systems and concluded that both large-scale architecture and small-scale lamination influence oil production. Shallow-marine reservoirs are being used (or are considered) as industrial storage projects or test sites for CO_2 sequestration [see Table 2 4]. They generally have a high storage efficiency (Okwen, Yang and

Frailey 2014) as they exhibit good sorting and high porosity (Bjørlykke 2014). Mixed facies outcrops investigated in Chapter 3 were deposited in shallow-marine environments. Numerous siliciclastic-carbonate shallow-marine sequences can be found globally. Carbonate and siliciclastic sediments can mix due to spatial variations in depositional environments caused by sea-level change or variations in sediment supply (Boggs 2014). Therefore, siliciclastic facies may interfinger carbonate facies (Boggs 2014). These types of deposits have received less attention with regards to CO_2 storage purposes. In Chapter 3, the significance of mixed facies deposited in shallow-marine environment on CO_2 storage and stratigraphic trap performance will therefore be investigated.

2.4.5 Deep-marine reservoirs

Deep-marine siliciclastic deposits are the result of mass-flow. Their extent is constrained by surrounding topography, termed confinement. This concept is especially important as there is a direct link between confinement and permeability, e.g., unconfined demonstrates a layered architecture with a low Kv/Kh ratio; however, in a confined system the kv/Kh ratios are higher. One of the unique aspects of such systems is the existence of stratigraphic traps, especially in unconfined architecture (Ringrose and Bentley 2015).

2.4.6 Carbonate reservoirs

Extensive carbonate aquifers in the Middle East have huge CO_2 storage capacity (El-maghraby and Blunt 2013). Carbonates are generally deposited in shallow, warm and clear marine environments (Tucker and Wright 2009); however, deeper-water carbonates, which originate from shelf deposits and transported by various processes, have also been identified (Boggs 2014). Biological, chemical and detrital processes can form carbonate areas (Ahr 2011). Carbonates, at the time of deposition, can show various levels of primary porosity up to c. 40-70%, but porosity can decrease to 5-15% in older rocks as it is lost with burial. The diagenesis processes that act on depositional porosity can both enhance and reduce primary porosity and create new pore types. Dissolution, cementation, compaction and pressure solution, recrystallisation and replacement are all diagenetic processes that can alter primary depositional porosity. Some original flow pathways are altered by processes such as cementation or compaction and become barriers to fluid flow (Ahr 2011). Carbonate

reservoirs can be divided into depositional, digenetic and fracture reservoirs (Ahr 2011). In reservoir modelling, carbonate reservoirs are difficult to reproduce (Ringrose and Bentley 2015) as they demonstrate different types of porosity, while pore size and shape distribution can be uniform or extremely heterogeneous. Porosity-permeability relationships are highly varied (Ahr 2011). Other than the complexity of their diagenetic history, the mechanical properties of carbonates also differ from siliciclastic sediments, and their brittle nature makes them more prone to fractures under differential stress. Reservoirs with fractures have a significant effect on fluid flow as they increase reservoir permeability. Naturally fractured reservoirs [NFRs] are abundant in sedimentary basins and according to Burchette (2012) more than half of the world's remaining conventional oil and gas fields are held in extensively fractured carbonate reservoirs. Fractures and faults exist at various scales, from centimetres to 100 km. Fluid flow in NFRs can be modelled using a dual-porosity approach, which is also known as sugar cube approach, and also using Discrete Fracture Network modelling (DFN). In dual-porosity modelling one porosity is associated with the matrix blocks and another with fractures and vugs (Kazemi et al. 1976) (Figure 2.11). In DFN modelling, structural features are explicitly populated in the reservoir models. Although the carbonate depositional environments are categorised as if only carbonate sediments are present, mixed carbonate and siliciclastic sediments exist in many stratigraphic successions (Chiarella, Longhitano and Tropeano 2017).

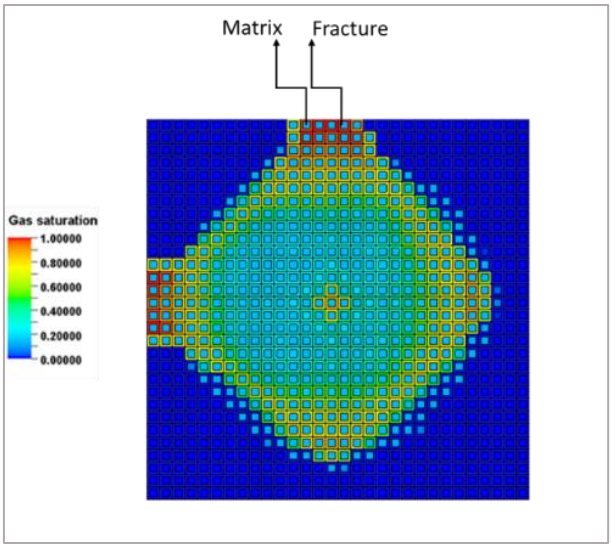

Figure 0.11: Dual porosity modelling. Two simulation cells are associated with each block, one for high porosity-low permeability matrix and one for low porosity-high permeability fractures.

2.5 Heterogeneity

Many studies have explored how geological heterogeneities caused by stratigraphic factors affect flow, storage capacity and effectiveness (Ghanbari, Pickup and Mackay 2006; Flett, Gurton and Weir 2007; Ambrose et al. 2008; Lengler, Lucia and Kühn 2010; Hovorka et al. 2011; Deng et al. 2012; Goater, Bijeljic and Blunt 2013; Sundal et al. 2013; Asharf 2014), as CO_2 can be confined in numerous small or large stratigraphic traps.

As explained above, the depositional environment controls the internal stratigraphic architecture and therefore the distribution of properties (i.e., porosity, permeability, wettability, etc.), which in turn controls the CO_2 migration pattern, storage capacity, effectiveness and seal capacity (Ambrose et al. 2008). In homogeneous reservoirs, CO_2, as a buoyant liquid, migrates upwards as there are no permeability barriers to hinder flow. Therefore, CO_2 bypasses the reservoir and, consequently, the contact area between the CO_2 and brine is reduced, resulting in less dissolution storage capacity. In the case of heterogeneous reservoirs, the upward movement of the CO_2 is restricted while the lateral movement of CO_2 is promoted. Therefore, CO_2-brine interaction increases which assists CO_2 dissolution trapping (Ambrose et al. 2008). Green et al. (2009) investigated the effects of vertical heterogeneity on the movement of mobile and dissolved CO_2. They noted that convection started much later in homogeneous models. Ennis-King and Paterson (2005) showed that convection improves the overall dissolution trapping mechanism. The column of CO_2 that acts on the caprock is reduced in heterogeneous reservoirs. This is because CO_2 is distributed more evenly and the higher percentage of the reservoir volume is swept, leading to higher seal capacity (Ambrose et al. 2008). However, the percentage of heterogeneity needs to be considered. This is because reservoir quality is decreased by heterogeneity, and the storage efficiency may reduce due to the localised build-up of pressure.

Rasmusson et al. (2016) and Flett, Gurton and Weir (2007) indicated that decreasing the sand/shale ratio, corresponding to a gradual decrease in reservoir quality, progressively hindered the buoyant migration of the plume. This increase in the tortuosity of the CO_2 migration pathways resulted in a reduction in the rate of residual gas trapping through hysteresis effects. However, since less CO_2 accumulates under the caprock, the risk of leakage is minimised. The numerical modelling of the Ketzin test site indicated that small-scale

heterogeneity increases the sharpness of the CO_2 front, and therefore, the volume of the reservoir which is affected by injected CO_2 is enhanced (Lengler, Lucia and Kühn 2010).

2.6 Storage capacity

Several classification systems are used to describe CO_2 storage resource (CSLF 2007; IEA-GHG 2008; CO2CRC 2008; Gorecki et al. 2009; USDOE 2010; SPE 2017) (Figure 2.12). To calculate the storage capacity, the type and position in the table (IEA-GHG 2008, CO2CRC 2008, Gorecki et al. 2009, USDOE 2010, SPE 2017) or pyramid (CSLF 2007) must be specified (Global CCS Institute 2008).

All classifications, except for USDOE (2010), begin by assuming that the total pore volume within a geological system, after considering the fundamental characteristics, is accessible for storage and can be utilised to its full capacity. In the CSLF classification, this is known as 'Theoretical Capacity'. This upper limit is unrealistic as restrictions always limit the full utilization of pore volume. In the 'Theoretical Capacity' estimation, no technical limitations are considered. When the geological and technical constraints are applied to the estimation, terms such as 'Effective Storage Capacity' [CSLF] and 'CO_2 Resource Estimates' [USDOE] are employed.

After considering regulatory, infrastructure and general economic limits the term 'Practical Capacity' is used. This is equivalent to the 'CO_2 Capacity Estimate' [CSLF, USDOE] and 'Operational Storage Capacity' [CO2CRC]. The 'Proved subset' in IEA-GHG (2008), CO2CRC (2008), Gorecki et al. (2009) and SPE (2017), and 'Matched Storage Capacity' in CSLF (2007) is calculated with reasonable certainty using geoscientific and engineering analysis and a detailed matching of large stationary CO_2 sources with suitable geological storage sites. The 'Probable' and 'Possible' subsets are defined using future techno-economic scenarios.

The estimation of CO_2 storage capacity based on methodologies such as CSLF and USDOE is termed volumetric. Methodologies based on analytical and numerical simulation of CO_2 are called dynamic, as time is a variable. Such CO_2 storage capacity calculations may be undertaken at various scales: national, basin, regional, local and site-specific (Bachu et al. 2007). Volumetric and dynamic estimates can be used for regional- and local-scale, respectively (Bachu 2015). Various methodologies (e.g., CSLF, USDOE and US Geological

Survey) are used to estimate CO_2 storage capacity of depleted oil and gas reservoirs and deep saline aquifers (Bachu et al 2007; USDOE 2010).

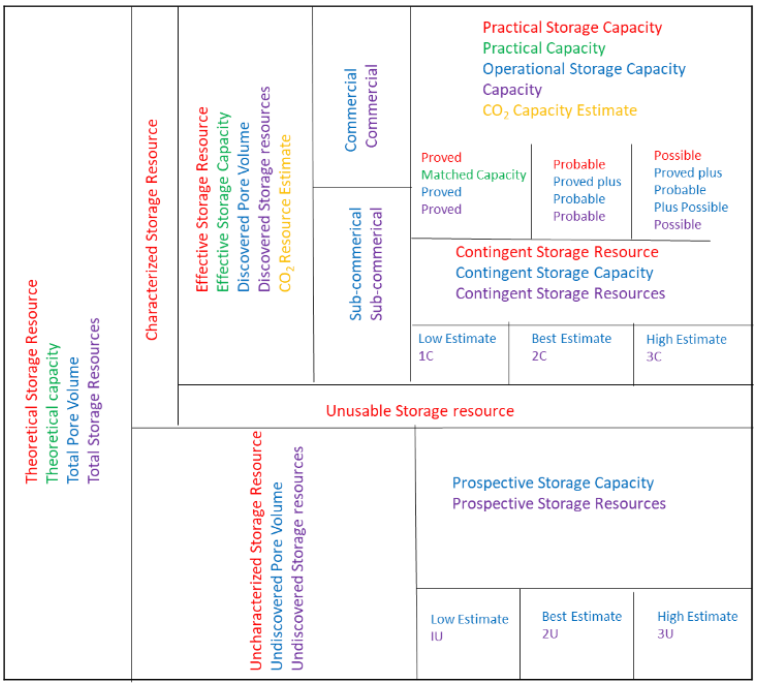

Figure 0.12: Different CO_2 storage capacity classifications are proposed. They are shown in one table for comparison. Red is Goercki et al. (2009), blue is CO2CRC (2008), Purple is SPE (2017), Green is CSLF (2007) and yellow is USDOE (2010).

2.6.1 Oil and gas reservoirs

The estimation of CO_2 storage capacity in oil and gas reservoirs is relatively simple when compared to aquifers and coal beds, as the former are better researched and are discrete bodies. When estimating the capacity of oil and gas reservoirs it is assumed that the volume previously filled by oil and gas is now available for CO_2 storage. This assumption is not applicable in reservoirs that were subjected to water flooding or are in contact with an aquifer. Based on reservoir pressure conditions, the volume of CO_2 that can be injected into depleted reservoirs may be lower or higher than the volume previously occupied by the oil and gas. Moreover, as reservoirs may not have been filled with fluids to their spill points, the injected CO_2 can be utilised this extra pore volume.

A review of the CSLF capacity estimation methodology is offered:

- For gas reservoirs:

$$M_{CO2t} = \rho_{CO2r} \times R_f \times (1 - F_{IG}) \times OGIP \times \left[\frac{P_s \times Z_r \times T_r}{P_r \times Z_s \times T_s}\right] \qquad 2.8$$

where M_{CO2t} is the mass of injected CO_2, ρ_{CO2r} is CO_2 density, R_f is recovery factor, F_{IG} is the fraction of injected gas, OGIP is initial gas in place, P, T, and Z are pressure, temperature and gas compressibility factors, respectively.

- For oil reservoirs:

$$M_{CO2t} = \rho_{CO2r} \times [R_f \times OOIP/B_f - V_{iw} + V_{pw}] \quad 2.9$$

Where OOIP is the initial oil in place, B_f is the formation volume factor, V_{iw} and V_{pw} are the volume of injected and produced water.

- Based on reservoir geometry:

$$M_{CO2t} = \rho_{CO2r} \times [R_f \times A \times h \times \varphi \times (1 - S_w) - V_{iw} + V_{pw}] \quad 2.10$$

Where A, h, φ, and S_w are area, thickness, porosity and water saturation, respectively.

There are various mechanisms involved in the CO_2 storage process that can reduce the volume that is occupied by the CO_2. The effective reservoir capacity for CO_2 storage can be obtained by multiplying the total capacity by the capacity coefficient, which is less than 1.

- CSLF effective storage capacity methodology in oil and gas reservoir:

$$M_{CO2e} = C_m \times C_b \times C_h \times C_w \times C_a \times M_{CO2t} \equiv C_e \times M_{CO2t} \quad 2.11$$

where M_{CO2e} is effective storage capacity, the subscripts m, b, h, w, a are mobility, buoyancy, heterogeneity, water saturation and aquifer strength, respectively. C_e is the capacity coefficient.

- USDOE capacity estimation methodology:

$$M_{CO2t} = E \times \rho_{CO2r} \times A \times h \times \varphi\ (1 - S_w) \quad 2.12$$

Where E is CO_2 storage efficiency factor.

2.6.2 Deep saline aquifers

The capacity estimation in saline aquifers is challenging (Bachu et al. 2007) as various trapping mechanisms and timescales are involved in the storage of CO_2. CSLF methodology can be applied for structural and stratigraphic traps and the USDOE can be applied for the whole aquifer.

- CSLF capacity estimation methodology in deep saline aquifers:

Theoretical storage capacity:

$$V_{CO2t} = V_{trap} \times \varphi \times (1 - S_{wirr}) \equiv A \times h \times \varphi \times (1 - S_{wirr}) \qquad 2.13$$

where V_{trap} is trap volume and S_{wir} is irreducible water saturation.

Effective storage capacity:

$$V_{CO2e} = C_c \times V_{CO2t} \qquad 2.14$$

where C_c is a capacity coefficient.

- USDOE capacity estimation methodology in deep saline aquifers:

$$M_{CO2} = A \times h \times \varphi \times \rho_{CO2} \times E \qquad 2.15$$

where E is the effective storage factor.

CO_2 storage efficiency is described as:

$$E = \frac{V_{CO_2}}{V_{\varphi}} \qquad 2.16$$

where E is storage efficiency, V_{CO_2} the volume of CO_2 injected into an aquifer rock volume and V_{φ} is the pore space in that volume (Goodman et al. 2013). CO_2 storage efficiency depends on several factors. These factors can be divided into four categories (Bachu 2015):

1. Aquifer characteristics,
2. Aquitard characteristics,
3. Injection strategy characteristics, and
4. Regulatory constraints.

These factors play an important role in the evolution of CO_2 in an aquifer. Table 0.5 summarised these factors and their impacts on CO_2 storage efficiency and hence capacity. These factors may have positive or negative effects on CO_2 storage efficiency as they, directly or indirectly, affect the gravity number and the mobility ratio [see Equations 2.1 and 2.2].

Several attempts have been made to calculate the storage efficiency by considering a combination of the aforementioned factors. The methodologies and results vary greatly. However, Goodman et al. (2013) have compared different methodologies and concluded that for open systems the storage efficiency ranges between 1.5% and 3.6% (CSLF 2007; USDOE 2010) and for a closed system between 0.3% and 1.2% (Zhou et al. 2008). Szulczewski et al. (2012) consider migration-limited and pressure-limited capacity of between 0.4% and 7.2%.

Table 0.5: Factors influencing CO_2 storage efficiency.

Factor	Comments	Reference
Aquifer thickness	Higher storage efficiency is achieved by thin aquifers [see gravity number equation 2-1: section 2.2].	Espie and Woods (2014)
Kv/Kh	In higher Kv/Kh ratios, CO_2 tends to rise rapidly towards the top. This results in a concave vertical shape of the plume, thus reducing the storage efficiency. More CO_2 dissolves in the brine at lower kv/kh values.	Hongjun et al. (2010); Shariatipour et al. (2014)
Heterogeneity	Heterogeneity generally increases CO_2 storage efficiency in high permeability aquifers. In contrast, in low-permeability aquifers, where CO_2 storage is limited by pressure build-up, storage efficiency is reduced.	Flett, Gurton and Weir (2007); Goater and Bijeljic Blunt (2013)
Lithology	Reef limestones have the lowest storage efficiency. Several types of clastic depositional settings demonstrate the highest storage efficiency.	Gorecki et al. (2009)
Depositional environment	Shelf carbonates demonstrate the lowest storage efficiency, while fluvio-deltaic clastics demonstrate the highest storage efficiency.	Okwen, Yang and Frailey (2014)
Aquifer dip	The velocity of the migration is proportionally amplified by increases in aquifer slope, which reduces storage efficiency.	Espie and Woods (2014)
Pressure	The density and viscosity of both fluids (i.e., CO_2 and brine) are increased by increasing pressure, although indirectly, pressure affects the gravity number and mobility ratio and increases storage efficiency.	Bachu (2015); Nordbotten, Celia and Bachu (2005)
Temperature	The density and viscosity of both fluids (i.e., CO_2 and brine) increase with decreasing temperature. Higher *in situ* temperature leads to higher CO_2 buoyancy and a higher mobility ratio, decreasing storage efficiency.	Bachu (2015)
Salinity	Water density and viscosity are increased by increasing salinity. Higher salinity also decreases the solubility of the CO_2 in the water phase which decreases the dissolution capacity.	Bachu (2015)
$k_{rCO2-max}$	Storage efficiency is decreased by increasing maximum relative permeability to CO_2. [See 2-2 equation: Section 2.2].	Okwen, Yang and Frailey (2014)
Irreducible water saturation	Storage efficiency is increased by decreasing irreducible water saturation.	Nordbotten and Celia (2006); (Okwen, Stewart and Cunningham (2010)
The number and distribution of CO_2 injection wells	Storage efficiency is augmented by increasing the number of injection wells; however, well interference may lead to unacceptable pressure build-up.	Wang, Zhang and Wu (2013)
Sealing caprock	Generally, seals will not allow CO_2 flow; however, some seals, such as shales, may allow pressure dissipation and brine leakage into the seal. This is dependent on seal lithology and in turn seal permeability. For example, evaporites with very low permeability create a closed aquifer as they do not allow leakage and pressure dissipation, thus, decreasing the CO_2 storage capacity.	Zhou et al. (2008)

2.7 Storage security

To consider CCS as an effective mitigation tool for emissions capture and climate change mitigation, CO_2 must be confined for 10 ka years and leakage to the atmosphere must be below 0.001-0.01% per annum (Hepple and Benson 2005). Two possible sources of CO_2 leakage are from storage units and storage facilities (Leung et al. 2014). Figure 2.13 illustrates various leakage mechanisms.

To contain CO_2 in porous reservoirs a seal or caprock must overlie the storage unit (IEAGHG 2011). Seals are low permeability rocks with a high capillary entry pressure. The key lithologies for seals are shales and evaporites. The permeability of shales (aquitards) ranges from 1 µD to 0.1 mD. Evaporites (aquicludes) have a permeability of c. 10^{-6} mD (Bachu 2015). To describe a seal capacity, which is the ability of a seal to confine the injected CO_2 for geological time, three aspects need to be investigated: seal -capacity, -geometry and -integrity (IEAGHG 2011). Seal capacity is defined as the CO_2 column height that can be retained in the geological media. CO_2 has a lower density than brine and rises through the reservoir under buoyancy. The upward migration of CO_2 continues until the CO_2 movement is restricted by sealing caprock.

At the caprock-reservoir interface, when the trap is filled to its seal capacity, there is a balance between capillary and buoyancy pressure. When buoyancy pressure exceeds the capillary entry pressure, the CO_2 can enter the seal pores. Capillary pressure is controlled by three factors: the size of the pore throats [r], CO_2-water interfacial tension [σ] and CO_2 wettability to the rock in the presence of the formation brine - expressed by the contact angle [θ] as shown by Laplace equation below:

$$P_{c=} \frac{2\sigma COS\theta}{r} \qquad 2.17$$

The seal capacity and the CO_2 column height are increased by reducing the size of pore throats and the contact angle between the CO_2 and water, and by increasing the interfacial tension between CO_2 and water. If depleted gas reservoirs are considered for CO_2 storage, the sealing capacity of the caprock needs to be re-evaluated, as the interfacial tension of the CO_2-water system is less than the CH_4-water. Therefore, the capacity of seals in gas reservoirs or oil reservoirs with a gas cap may not be sufficient to seal the injected CO_2 (Li et al. 2005).

Figure 0.13: Leakage mechanisms: A) CO_2 escapes through a thin caprock or gap in the caprock; B) CO_2 Leaks due to higher CO_2 pressure than capillary entry pressure; C) CO_2 escapes through faults and fracture networks; D) CO_2 escapes via poorly completed injection wells; E) CO_2 escapes via abandoned wells; F) CO_2 is transported out of the storage unit by natural flow; G) CO_2 migrates beyond the regional caprock (IEAGHG 2011).

In addition to capillary leakage, the diffusive loss may also reduce seal capacity (Song and Zhang 2013). CO_2 can migrate through the pore space of a caprock saturated with water by molecular diffusion; the diffusive loss is a continuous and dominant process. However, significant leakage by this mechanism can only be expected over a geological timescale (Busch et al. 2010).

Seal geometry refers to seal thickness and seal areal extent. The seal capacity is not a function of seal thickness. In practice, however, the likelihood that thin seals are subjected to fracturing is high (IEAGHG 2011).

Many basins have reservoirs and seals packages. For example, in the Sleipner field, sandstone layers are divided by intraformational shale seals, which are barriers to flow. They form local traps and assist to CO_2 dissolution and, therefore, the reliance on a regional seal is reduced. The study of Gibson-poole et al. (2009) showed that an average CO_2 column height of around 500 m can be retained by such intraformational shale layers.

Root (2007) investigated the relationship between depositional environments and a seal's area and thickness and demonstrated that a shelf depositional environment and fluvial overbank facies provide the most extensive and most limited seals, respectively.

Seal integrity describes the seal's tendency to develop new conducting faults or to reactivate dormant faults and is a function of lithology. Using an integrity factor (1-0), lithologies such as halite or organic shale are least likely to form structural permeability as they are ductile lithologies and their integrity factor approaches 1. An increase in the carbonate content of the shale will cause the integrity factor to move towards 0 (IEAGHG 2011).

2.7.1 Faults, fractures and deformation bands

The faulting and fracturing of reservoirs are of concern as they provide potential leakage paths for the injected CO_2. In addition, the simulation of such reservoirs is extremely challenging. Discovering a site with a homogenous caprock without any faults or fractures is unlikely (Rutqvist and Tsang 2002). Therefore, the study of fault and fracture is necessary, covering aspects such as spatial distribution, orientation, dimension, interconnectedness, aperture and conductivity (Iding and Ringrose 2010). These structures mainly have a tectonic origin; although, anthropogenic activities such as CO_2 injection can create such structures. They are formed when stress exceeds the strength of the rock. Generally, only faults that are seismically resolvable have been included in models, because of model resolution and central processing unit (CPU) cost.

Faults and fractures modify the permeability of the rock and may enhance or reduce CO_2 flow (Faulkner et al. 2010; Manzocchi et al. 2010). Faults can create a seal by juxtaposing a reservoir against a seal or by forming a low permeability fault zone, as explained in Section 2.3.1. As they act as traps for hydrocarbons, they can potentially trap injected CO_2. However, by forming flow pathways through the caprock they can also jeopardise storage security.

As flow across faults is an important concept in petroleum and CO_2 storage, transmissibility needs to be calculated. Transmissibility is a function of fault permeability, fault thickness and fault displacement. The transmissibility multiplier (a numerical device) varies from 0 (completely seal) to 1 (completely open) (Manzocchi and Walsh 1999). Up-fault flow is also very important as vertical permeability can be three orders of magnitude higher than across-fault permeability (Faulkner et al. 1998).

Deformation bands (also known as cataclastic faults (Fisher and Knipe 2001), faults (Manzocchi et al. 1998) and (micro)fractures (Gabrielsen and Koestler 1987), etc.)) are narrow tabular zone of localised strain that cannot be identified by seismic imaging (Fowles and Burley 1994). Generally, the formation of deformation bands causes a reduction in porosity and permeability in high quality reservoirs, in contrast to fractures. In Chapters 5 and 6, deformation bands of the Penrith Sandstone are used for CO_2 flow simulation to assess the extent to which these features can act as effective mini-traps and contribute to secure CO_2 geological storage.

2.8 Outcrop

One of the main issues regarding reservoir modelling is constructing the heterogeneous distribution of reservoir properties (Howell, Martinus and Good 2014), as it is challenging to map small layers and structures such as fractures (Buckley et al. 2010).

Input data used for flow simulation is mainly obtained from wells and seismic surveys, data with differing resolutions. The wells offer high vertical resolution and restricted lateral resolution. In contrast, the seismic profiles offer data from vast areas but lack vertical resolution (Howell, Martinus and Good 2014). Consequently, sub-seismic features within the reservoir that may influence fluid flow are not resolved by seismic surveys (Manzocchi et al. 2008). To have an accurate and detailed representation of the heterogeneity in the subsurface, outcrop analogues such as cliff sections are used (Buckley et al. 2010; Howell, Martinus and Good 2014). The data obtained from outcrops are either soft- (qualitative) or hard data (quantitative). Soft data provide modellers with a better conceptual understanding of the depositional system and facies distribution. Hard data includes the geometry, thickness and length of layers (Howell, Martinus and Good 2014). These data are finally used to undertake flow simulation experiments for hydrocarbon fields and potential CO_2 storage sites (Buckley et al. 2010).

One of the issues regarding outcrops is their quality and the exposure of structures (Rotevatn et al. 2009), and another is finding an adequate analogue. Although it is necessary to select an outcrop based on data that is required to be incorporated into models, sometimes it is necessary to use composite data from several outcrops to construct a model that accurately represents a system (Howell, Martinus, and Good 2014).

Light Detection and Ranging (LiDAR) is a popular surveying technique because of its accuracy and high resolution (5 to 10 mm resolution). It produces a dense point cloud in a relatively short time (Slob and Hack 2004). Each point is represented by a coordinate in 3D space. Wilson et al. (2011) used LiDAR data to link outcrop fracture observations to create 3D DFN (discrete fracture network) model.

Throughout this research, outcrops are used to construct precise static models. For example, in Chapter 3 various outcrops demonstrate mixed facies (Grauburg Formation, Lorca Basin, and Bridport Sand Formation) are used to study CO_2 stratigraphic entrapment. In Chapter 4, the Jurassic Entrada Sandstone outcrop is employed to test the importance of geological

heterogeneity on fluid flow. The importance of faults, as flow conduits in the region, is also investigated. In Chapters 5 and 6, deformation bands in the Penrith Sandstone outcrop are used for CO_2 flow simulation.

2.9 CO_2 storage simulations in subsurface geological formation

Mathematical models and numerical simulators are required to tackle safety, feasibility and economic issues in CO_2 storage. Various techniques are used by industry and researchers to model CO_2 flow in saline aquifers, including analytical models (e.g., Nordbotten, Celia and Bachu 2005; Zhou et al. 2008; Mathias et al. 2011), streamline simulations (Qi 2008), vertical equilibrium (Gasda, Nordbotten and Celia 2009) and conventional 3D simulations (e.g., Kempka et al. 2013; Shariatipour, Pickup and Mackay 2016). 3D simulations have fewer shortcomings when compared to other techniques used to model more complex reservoirs with high pressure and temperature ranges. The existing simulators for CO_2 storage in geological media are mainly from codes that were originally developed for the oil and gas industry (Jiang 2011). The simulation of CO_2 geological storage is more challenging than modelling of oil and gas reservoirs, as it requires a broader range of spatio-temporal scales. Simulators are chosen based on their specific applications and capabilities. The Eclipse reservoir simulator has been employed in this study. Schlumberger's ECLIPSE has two software packages: ECLIPSE Black Oil (E100) and ECLIPSE Compositional (E300). ECLIPSE compositional with CO2STORE option has been especially developed for CO_2 storage and can accurately compute the density, viscosity and compressibility of CO_2 as a function of temperature and pressure. For the CO2STORE option, three phases are considered: a CO_2 rich phase, a H_2O rich phase and a solid phase. The CO_2 gas density and viscosity are calculated based on the studies of Spycher and Pruess (2005); Fenghour, Wakeham and Vesovic (1998) and Vesovic et al. (1990). The mutual solubilities of CO_2 and H_2O are based on the study of Spycher and Pruess (2005) and (2009), and calculated for CO_2-H_2O systems under typical CO_2 storage conditions: 12-250 °C and up to 600 bars. The salts are assumed to stay in the liquid phase unless the SOLID option is used.

2.10 Summary

Given the importance of structural and stratigraphic traps for the safe geological storage of carbon dioxide, this thesis tries to use various outcrops to build three-dimensional static models and then conduct flow simulations to address the gaps in our knowledge.

Initially, different types of mixed siliciclastic-carbonate outcrops deposited in shallow-marine environments are selected. These outcrops demonstrate various types of mixing that may affect flow. The goal is to study their storage potential and their effect on storage security by forming stratigraphic traps.

In another study, flow simulation, for the first time, was conducted using a Utah outcrop to establish the main pathways for reducing fluids. These palaeo-reservoirs were deposited in a range of aeolian environments. The pathway for reducing fluids is uncertain and the main pathways for reducing fluids are not known. For example, it is not known which fault in the area acted as a seal to the reducing fluid and which one was a conduit.

Deformation bands as small-scale structural features have not been considered in CO_2 flow simulation. They have not been evaluated as mini structural traps. Moreover, it is uncertain, as clusters, if they have the potential to minimise the reliance on a major proximal fault. Therefore, these features are considered to evaluate their potential for safe geological storage of CO_2.

Chapter 3

The impact of heterogeneous mixed siliciclastic-carbonate systems on CO_2 geological storage

3.1 Introduction

Along with structural traps (folds and/or faults), stratigraphic traps, where variations in local stratigraphy are the main element in the trapping of fluids, can create an effective trapping mechanism (Hovorka et al. 2004; Shariatipour, Pickup and Mackay 2016).

An excellent example of profiting from the stratigraphic trap for the geological storage of CO_2 is the Sleipner project in Norway, where CO_2 is injected into the Utsira Formation - shallow marine deposit. Variations in the depositional environments have provided reservoir and seal combinations (stratigraphic trap) that can help store CO_2 effectively (Bickle et al. 2007).

However, among all the shallow-marine depositional settings, mixed siliciclastic and carbonate systems (and associated heterogeneities) have not been studied for CO_2 geological storage. Consequently, the impact of mixed facies on CO_2 storage is poorly understood but may be an important factor in many target formations. This research, therefore, aims to systematically investigate the different styles of stratigraphic heterogeneity in mixed siliciclastic and carbonate systems to evaluate their effect on fluid flow. This will help determine their potential as stratigraphic traps for CO_2 geological storage.

The key questions addressed in the chapter include:

1) How do facies' interplay and associated sediment heterogeneity, in mixed systems, influence fluid flow?
2) Could alternating carbonate and sandstone facies, with contrasting permeability, form the reservoir and non-reservoir intervals?

A detailed understanding of facies can be achieved by using an outcrop analogue to construct realistic 3D reservoir models (Brandsæter et al. 2005; Barnaby and Ward 2007; Newell and Shariatipour 2016; Newell et al. 2019). Three outcrops are chosen in this study, each representing a mixed shallow-marine system with varying heterogeneity that may act as a

small or large stratigraphic trap. These depositions display various types of heterogeneities that may be suitable for CO_2 confinement. The three 3D models are based on the: 1. Grayburg Formation (US), which displays spatial permeability linked to variations in the mixture of siliciclastic and carbonate sediments; 2. Lorca Basin outcrop (Spain), which demonstrates interfingering of clastic and carbonate facies; and 3. Bridport Sand Formation outcrop (UK), an example of a layered reservoir with thin carbonate-cemented horizons.

3.2 Mixed siliciclastic-carbonate systems

Numerous clastic-carbonate shallow-marine sequences can be found around the world in both recent and geological settings (Mount 1985; Tucker 2003). These systems are comprised of both terrigenous siliciclastic material and transported or *in-situ* carbonates (Mount 1985; Zecchin and Catuneanu 2017). This mixed depositional system can display a transition from entirely siliciclastic to entirely carbonate (Zecchin and Catuneanu 2017).

A high flux of siliciclastic sediments into a marine setting generally has a negative effect on carbonate production and the two facies are thus often segregated (Catuneanu et al. 2011). However, there are a number of processes which may bring them into contact, including transportation and mixing of siliciclastic and carbonate sediments due to rare but extreme events (e.g., storms); biogenic production of carbonate on siliciclastic substrates; and sediment mixing along faulted or other high-relief marine margins where continental and marine environments interact (Mount 1985). Interactions between siliciclastic and carbonate deposits may continue into the burial diagenesis phase, where carbonates may induce widespread cementation and porosity reduction in siliciclastic rocks (Bryant, Kantorowicz and Love 1988).

Geological formations composed of both siliciclastic and carbonate deposits can exhibit spatiotemporal facies variability, where facies occupy discrete but coeval belts or vary through geological time. High-frequency fluctuations in relative sea-level, climate change or sediment supply can lead to alternations in the predominance of siliciclastic or carbonate sedimentation (Zecchin and Catuneanu 2017). For example, carbonate facies will often dominate during transgressive systems tracts (TST), when large areas of the continental margin are brought into a zone of high carbonate productivity, while continental clastics dominate following high-stand and falling-stage systems tracts (FSST) (Catuneanu et al. 2011).

Mixed carbonate and siliciclastic formations can show great variability in lithofacies from carbonate grainstone to quartz sandstone (Bryant, Kantorowicz and Love 1988; Barnaby and Ward 2007).

The variation in lateral and vertical heterogeneities, resulting from mixed deposits, may form baffles and barriers that influence flow behaviour (Chiarella et al. 2017) and may help form stratigraphic traps as alternating carbonate and sandstones, with contrasting permeability, could form the reservoir and non-reservoir intervals (McNeill et al. 2004).

Heterogeneity in such systems can occur at the bed, lithofacies and stratigraphic scales (Tucker 2003; Chiarella et al. 2017). Studying the effects of facies change on fluid distribution using 3D models can provide additional insight into potential CO_2 geological storage. In this study, only stratigraphic scale structures were considered. Due to computational limitations finer scales were ignored, although such systems can show scale-independent similarities (Ringrose and Bentley 2015; Chiarella et al. 2017).

3.3 Introduction to the case studies

Three case studies were selected, each displaying different styles of siliciclastic-carbonate mixing. One example comes represents cyclic interbedding, another from the interaction of carbonate and siliciclastic environments along a 'steep' continental-marine margin, and finally mixing due to storm processes.

3.3.1 Grayburg Formation – Siliciclastic-Carbonate Cyclical Interbedding

The Permian Basin is a major hydrocarbon producing area in the southern US. The Grayburg Formation (Late Permian) of the Permian Basin is a shallow-marine mixed siliciclastic–carbonate sequence displaying significant heterogeneity due to the cyclical interbedding of major lithofacies (McNeill et al. 2004). This formation is subject to enhanced oil recovery (EOR) using waterflooding and gas injection, while the non-reservoir equivalent succession is considered for wastewater disposal (He et al. 2019). The mixed carbonate and siliciclastic rocks were categorised into seven end-member lithofacies: six carbonate lithofacies (from packstone-wackstone to ooid grainstone) and one siliciclastic lithofacies (quartz sandstone) (Barnaby and Ward 2007) (Figure 0.1). Finer siliciclastics, such as claystone and siltstone, did not occur.

3.3.2 Lorca Basin – Steep Marine Margin Setting

The Tortonian Stage (Late Miocene) Parilla Formation of the Lorca Basin, Spain, exhibits siliciclastic-dominated, mixed siliciclastic-carbonate and carbonate-dominated cycles. The mixed cycles have developed mid-ramp, bordering an alluvial fan system (Thrana and Talbot 2006) (Figure 0.2). Alluvial deposits interfinger with marginal marine and carbonate ramp facies and offer a good record of sea-level change. The Lorca Basin succession has been chosen as it exemplifies facies with interfingering siliciclastic and carbonate deposits.

3.3.3 Bridport Sand Formation – Mixing by Storm Processes

The early Jurassic Bridport Sand Formation outcrops at Bridport on the Dorset coast of southern England, UK, and is a reservoir rock of the Wytch Farm onshore field (Morris, Hampson and Johnson 2006). The outcrop offers an appropriate analogue for several Jurassic oil and gas fields in the North Sea where thin carbonate-cemented horizons compartmentalise shallow-marine sandstones (Kantorowicz, Bryant and Dawans 1987; Bryant, Kantorowicz and Love 1988). The formation is strongly bioturbated and forms part of a mixed clastic-carbonate shallow-marine system (Morris, Hampson and Johnson 2006). Permeability heterogeneity arises from the preferential cementation of bioclastic-rich and clay-poor sediments (Bryant, Kantorowicz and Love 1988). The continuous carbonates within friable sands may act as an extensive barrier, while the discontinuous cemented horizons can act as local baffles to fluid flow (Morris, Hampson and Johnson 2006) (Figure 0.3).

The Bridport Sands are overlain by the Inferior Oolite Group; and these, in turn, are overlain by the mudstones of Lower Fuller's Earth Member. Towards the top, the frequency of cemented horizons increases and their thickness decreases (Bryant, Kantorowicz and Love 1988). Extensive cement horizons exist in the subsurface (Bryant, Kantorowicz and Love 1988).

3.1 Methodology

A range of numerical simulations was conducted in order to investigate the effects of heterogeneity change in bivariate facies on CO_2 flow, distribution, storage capacity and security. For this purpose, static geological models were generated in Schlumberger's Petrel software (Schlumberger 2016). The static models were based largely on published

information of stratigraphic architecture (Bryant et al. 1988; Thrana and Talbot 2006; Barnaby and Ward 2007) and supplemented, in the case of the Bridport Sands, with new observations from outcrop laser scans. Dynamic modelling studies were conducted using ECLIPSE 300 (Schlumberger 2017) with the CO2STORE module.

Figure 0.1: Stratigraphic cross-section from promontory G showing major facies in Grayburg Formation (Parker 2013).

Figure 0.2: Outcrop photo and stratigraphic of the Miocene-age Lorca Basin (Thrana and Talbot 2006).

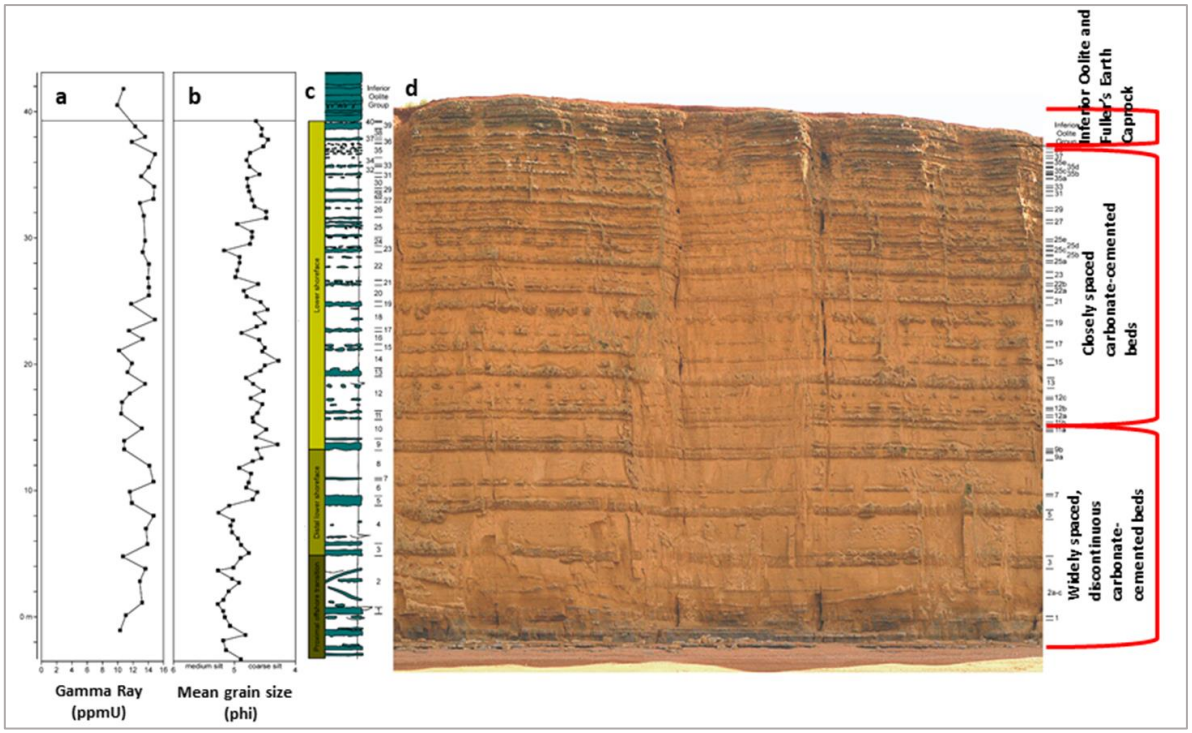

Figure 0.3: Bridport Sand Formation: (a) Outcrop gamma-ray profile; (b) mean grain size data; (c) lithology and interpreted facies (cemented bands is in teal); (d) and outcrop photo of Bridport Sand Formation showing Inferior Oolite, closely spaced carbonate-cemented beds and widely spaced, discontinuous carbonate-cemented beds (modified after Hampson et al. 2014).

3.1.1 Flow Modelling

The depth of the reservoir models was set at 1000 metres with the injected CO_2 in the supercritical state. Dynamic modelling was conducted under an initial pressure of 100 bars and an isothermal condition of 42 °C (using a temperature gradient of 25 °C/km). It was initially assumed that the reservoir was entirely saturated with brine. The constraints for injection were that CO_2 must remain within the storage boundary and the injection pressure pulse was not permitted beyond the domain. In addition, although values differ between published authors and basins (Breckels and van Eekelen 1982; Law and Bachu 1996; Moss et al. 2003; Noy et al. 2012; Goater, Bijeljic and Blunt 2013), the injection pressure limit was set at 90% of the fracturing pressure for Section 1 and Section 2 (Law and Bachu 1996; Bachu 2015) and 75% of the lithostatic pressure for Section 3 (Noy et al. 2012), in order to maintain geomechanical stability and avoid damaging the reservoir.

The relative permeability and capillary pressure curves used in this study were based on the results of Bennion and Bachu (2006a, 2006b; 2008; 2010), representing comparable facies and conditions (Figure 0.4, 3.5 and 3.6, Table 0.1 and 3.2). They offered relative water-CO_2 permeability data for sandstone, carbonate, shale and anhydrite rocks, which allow detailed

numerical simulations of a CO_2 injection and sequestration process (Bennion and Bachu 2005) and are used throughout this chapter (Figure 0.4). They showed the end-point values and shape of the capillary pressure curve attributed to pore size distribution and rock heterogeneity. The porosity and permeability values for Sections 1 and 2 are based on their studies. The properties for the third section (Table 3.2) are based on the study of Bryant, Kantorowicz and Love (1988). No hysteresis in relative permeability was considered. This study was designed to examine the impact of stratigraphic variability within mixed siliciclastic and carbonate formations and thus no conductive faults, fractures, or leaky wellbores were included in the model.

Table 0.1: Petrophysical and flow characteristics of the four rock samples used for flow simulation in Section 1 - Grayburg Formation and Section 2 - Lorca Basin (Bennion and Bachu 2006b; 2008; 2010).

Table 0.2: Petrophysical and flow characteristic used for flow simulation in Section 3 (Bridport Sand Formation) (Bryant, Kantorowicz and Love (1988); Bennion and Bachu (2006b; 2008; 2010).

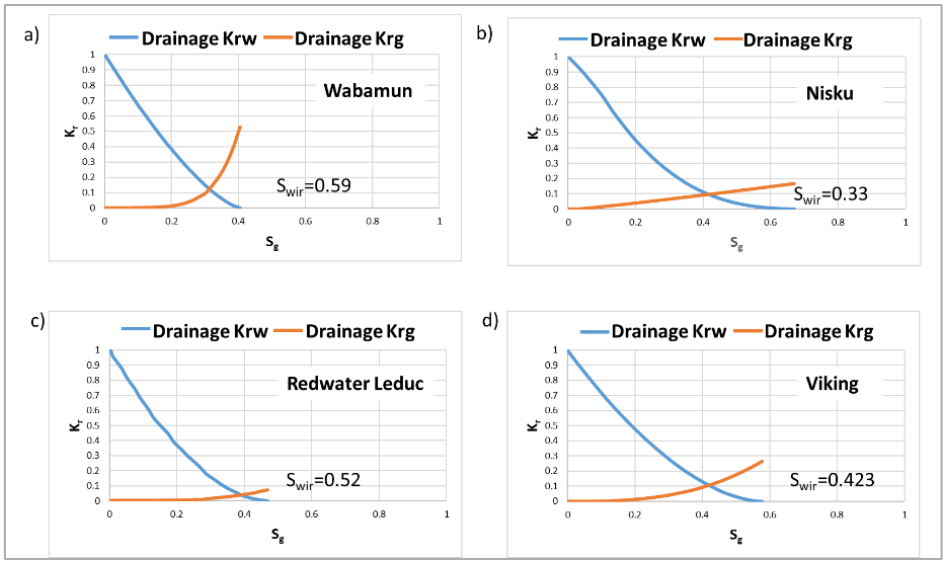

Figure 0.4: Relative permeability curves used throughout this study: a) Wabamun carbonate; b) Nisku carbonate; c) Redwater Leduc carbonate; and d) Viking Sandstone. K_r is relative permeability (K_{rw} relative permeability for water and K_{rg} relative permeability for gas) and S_g is gas saturation.

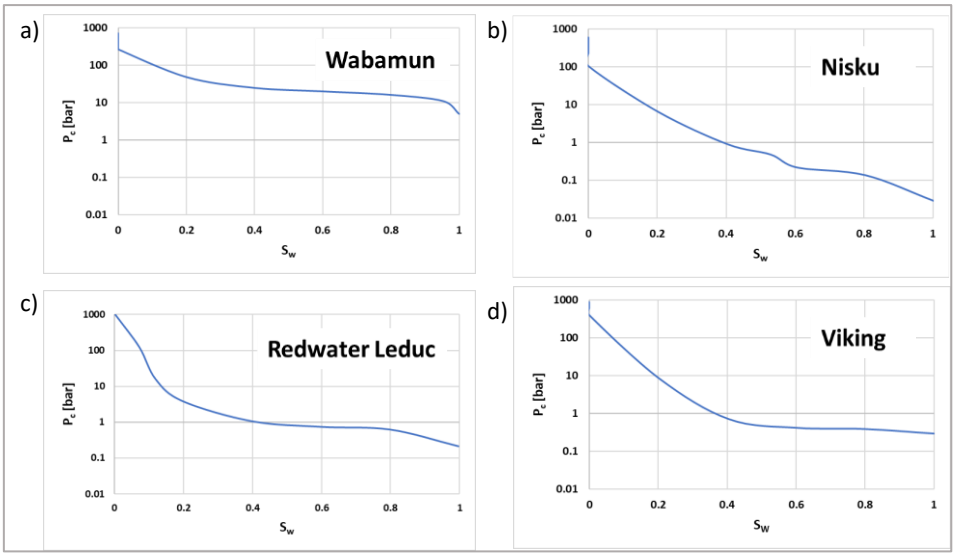

Figure 0.5: Capillary pressure curves used throughout this study: a) Wabamun carbonate.; b) Nisku carbonate; c) Redwater Leduc carbonate; and d) Viking Sandstone.

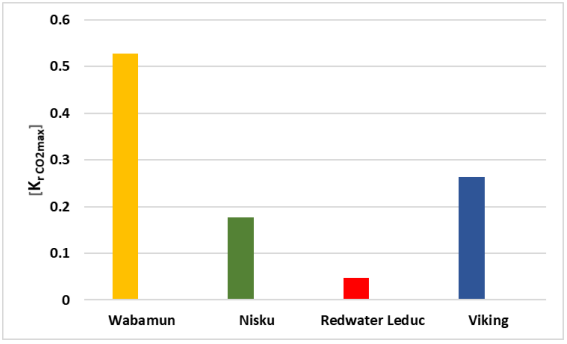

Figure 0.6: Comparing all endpoint relative permeability [$K_{rco2max}$]to CO_2 at irreducible water saturation [S_{wir}].

3.1.2 Reservoir models

The 3D geological models were constructed as closed aquifers assuming that intact, un-faulted regionally extensive low permeability shale layers exist below and above the models. As the lateral boundaries were also closed to flow, the pressure build-up constrains capacity (Mathias et al. 2011). Each model was uniformly gridded in the three main dimensions.

3.1.2.1 Section 1 – Grayburg Formation

All models had a spatial dimension of 1000 m × 1000 m × 100 m, which was discretised into a total of 200,000 active cells [ni=100 × nj=100 × nk=20]. Six major carbonate lithofacies, from low porosity and permeability packstone-wackstone to high porosity and permeability ooid grainstone, and one coarse grain siliciclastic lithofacies, are recognised in the Grayburg Formation (Barnaby and Ward 2007). The modelling is a simplified version of the Grayburg Formation and investigated carbonate and siliciclastic lithology percentages based on the study of Barnaby and Ward (2007), where the quartz sand fraction can range from <10 percent to >90 percent.

Sequential indicator simulation (SIS) which is a geostatistical technique has been used here to generate the facies' distribution. This method is mainly applied where the shape of the bodies is not certain. To test the impact of varying ratios of sandstone to carbonate on flow distribution and storage security, nine models were considered (Figure 0.7b) from 10 percent sandstone to 90 percent sandstone (i.e., 10:90…90:10). These values were assigned manually. The variogram type used here was exponential with the nugget of 0.01. Range which is the maximum distance where sample values are dependent on each other was assigned 1000 in major horizontal direction, 1000 in minor direction normal to the major and 0 in vertical direction. The azimuth which is the orientation of the major direction and dip were assigned 0. Two additional models, pure carbonate and pure sandstone, were also constructed. Unlike the deterministic method which presents only one model of the reservoir, the stochastic method can provide unlimited possibilities or "realisations". Choosing the best realisation for flow modelling is the key to predicting flow movement within a reservoir. However, for the purpose of this study, this scenario seems to be sufficient. Figure 0.7a shows the static models from the pure sandstone model, models with varying percentages of sandstone and carbonate and the pure carbonate model, respectively. For each realisation, three models with three different carbonate petrophysical properties (Bennion and Bachu 2010), but the

same sandstone petrophysical properties, (Bennion and Bachu 2008) were input for the flow simulation (Table 0.1). Eventually, 31 models were constructed. As carbonate rocks are generally more complex in nature than siliciclastic rocks (e.g., Lucia 2007; Ahr 2011), the values for the sandstone facies were kept unchanged for all models. The Viking sandstone studied by Bennion and Bachu 2005; 2006b; 2008) was used herein, which is a clean sandstone that exhibits a unimodal pore size distribution. Three carbonates with varying properties were used, namely:

1. Wabamun Carbonate - a low permeability succession with a unimodal pore size distribution with few macropores (Bennion and Bachu 2010). Its high threshold capillary pressure is due to the preponderance of micropores and thus, it is assumed that these facies can act as a barrier to flow and add to storage capacity and security, forming a stratigraphic trap.
2. Nisku carbonate - a homogenous matrix, resulting in a uniform and less concentrated flow, with the assumption that it can boost effective sweep.
3. Redwater Leduc Reef carbonate - categorised as a high permeability carbonate in Bennion and Bachu (2010) and was assumed to be suitable for CO_2 storage as it has higher pore volume (Table 0.1).

The contrast in permeability between the carbonate and sandstone in Model 1 is approximately four orders of magnitude with the transmissibility of 0.00077 cP.rm^3/day/bars for the carbonate facies, in Model 2 it is less than one order of magnitude with the transmissibility of 1.9612 cP.rm^3/day/bars for the carbonate facies while in Model 3 it is 0.18 order of magnitude with the transmissibility of 15.221 cP.rm^3/day/bars for the carbonate facies. The standardised transmissibility of sandstone is 9.9340 cP.rm^3/day/bars.

One vertical CO_2 injection well was added in the centre of the model and completed at layers 18 to 20. To study the plume migration, a volume flow rate of 9000 m^3/day CO_2 was injected over 10 years, followed by 150 years post-injection period where only density differences create flow. The CO_2 injection rate was chosen to be around the total planned storage of a Sleipner. The well was controlled by a surface rate with a maximum pressure limit of 200 bars (Table 3.3).

3.1.2.2 Section 2 – Lorca Basin

The model had dimensions of 1000 m × 1000 m × 40 m, discretised into 195,000 active cells [ni=50 × nj=50 × nk=78]. The static geological model was constructed to capture the

interfingering of carbonate facies with alluvial clastic facies (Figure 3.8) that was seen in the outcrop (Thrana and Talbot 2006). Such a system does not contain closed compartments. A truncated Gaussian Simulation was used to generate the transitional, interfingering contact between the two facies belts. The petrophysical properties of this mixed system are not available, therefore, the input values were taken from (Table 0.1). For comparison purposes, one homogenous sandstone model (LB-PS) was also used for flow simulation. The injection strategy is summarised in Table 3.3.

Figure 0.7: (a) Static reservoir models (1000 m × 1000 m × 100 m) from pure sandstone (GF-PS), varying ratio of sandstone to carbonate, and pure carbonate (GF-PC). C refers to carbonate and S refers to sandstone. (b) The percentage of each facies in each model is denoted by a number. For example, the case GF-10S-90C is a model with 10 percent sandstone and 90 percent carbonate (Pourmalek et al. 2022).

Figure 0.8: Static model (1000 m × 1000 m × 40m) of the mixed clastic-carbonate system of the Lorca Basin (Pourmalek et al. 2022).

3.1.2.3 Section 3 – Bridport Sand Formation

The laser scanning of the Bridport outcrop at Dorset was used to construct static model (Figure 3.9). The model has dimensions of 2100 m × 2100 m × 60 m discretised into 588,000 active cells [ni=70 × nj=70 × nk=120]. Models were smaller than the 5 km coastal outcrop due

to computational limitations. The permeability and porosity of sands and cemented horizons are summarised in Table 3.2. Although four types of cementations were recognised at the Bridport outcrop (Bryant, Kantorowicz and Love 1988), only laterally extensive sheets, which are continuous in three dimensions, were considered for flow simulation. A detailed study of fractures was ignored due to the limited grid resolution. In addition, these fractures were cemented and probably not conduits for flow. In contrast to the previous example, where facies interfingered at the mid-ramp, the cemented layers had compartmentalised the formation at the outcrop. Similar and extensive layers may also be present subsurface (Bryant, Kantorowicz and Love 1988).

Figure 0.9: Static models (2100m × 2100m × 60m) of Bridport Sand Formation were constructed based on the laser-scanned image. Towards the top of this sequence, the frequency of cemented horizons increases and their thickness decreases. The 3D extent of cemented layers was 90%, 70%, 50% and 10% of the model. Here only the model BPS-2 with 70% cemented layers is shown (Pourmalek et al. 2022).

The 3D extent of layers in models BPS-1, BPS-2, BPS-3, and BPS-4 was 90%, 70%, 50% and 10%. As only 61% of the cemented layers at the outcrop extended over 90% of the coastal outcrop, a model with cemented horizons of varying extent was also considered, one which more closely matched that observed at the Bridport outcrop (BPS-5). In each model number of cemented horizons were modelled based on the location and their disposition as observed in the laser scanned image (Figure 3.18d). CO_2 injection rates were set at 20,000 and 30,000 sm^3/day, with the well located in the centre of the model. Models with low injection rate (20,000 sm^3/day) were labelled "LI" and models with high injection rate (30,000 sm^3/day) were labelled "HI". CO_2 was injected for 10 years through perforations below the most bottom cemented layer, followed by 100 years recovery period. As the sands are isolated by extensive cemented horizons, well perforation was also used across the entire model thickness. It is important to know whether the storage capacity improves when different injection designs are used, while still guaranteeing storage security (Table 3.3). For

comparison purposes, one homogenous sandstone was also used for flow simulation (PBS-PS-HI and PBS-PS-LI).

Table 0.3: Injection strategy. For Bridport Sand Formation, two injection rates and two scenarios for perforation locations were considered for flow simulation.

Case	Injector location	Perforation location	Injection rate [m^3/day]	Injection period [years]	Recovery period [years]
Grayburg Formation	(i=50, j=50)	(K=18-20)	9000	10	150
Lorca Basin	(i=25, j=25)	(K=34-38)	5000	10	100
Bridport Sand Formation	(i=35, j=35)	(K=95-115)	20000	10	100
		(K1=95-115; K2=93-96; K3=88-91; K4=83-86; K5=78-81; K6=73-76; K7=68-71; K8=64-66; K9=60-62; K10=56-58; K11=52-54; K12=48-50; K13=44-46; K14=40-42; K15=37-38; K16=34-35; K17=31-32; K18=28-29; K19=25-26; K20=21-23)			
		(K=95-115)	30000		
		(K1=95-115; K2=93-96; K3=88-91; K4=83-86; K5=78-81; K6=73-76; K7=68-71; K8=64-66; K9=60-62; K10=56-58; K11=52-54; K12=48-50; K13=44-46; K14=40-42; K15=37-38; K16=34-35; K17=31-32; K18=28-29; K19=25-26; K20=21-23)			

3.2 Results

3.2.1 Section 1 – Grayburg Formation

The results of models with low permeability carbonate (Wabamun Formation, Model 1) demonstrate the highest value of dissolved CO_2 in the water phase in models with less carbonates (Figure 0.10). One extensive low permeability layer occurred at layer 15 from

Model GF-C20-S80. As a result, the upward migration of CO_2 was completely restricted resulting in a plume that was not uniformly developed towards the caprock (

Figure *0.12*). As a consequence, the highest gas concentrations beneath the caprock were observed in the pure sandstone (GF-PS) or the model with 10 percent carbonate (GF-C10-S90-L). This is because CO_2 migration was not hindered by the low permeability carbonate layer. As the percentage of carbonate facies increases and permeability decreases the ability of a reservoir to transmit fluid is considerably reduced. Consequently, poor levels of injectivity were observed in high percentage carbonate and pure carbonate models (GF-C80-S20-L, GF-C90-S10-L and GF-PC-L). In these three models, very low injectivity was achieved compared to other models (e.g., 96%, 5%, and 3% of the cumulative injected gas in models GF-C80-S20-L and GF-C90-S10-L and GF-PC-L, respectively). Bottom hole pressure instantaneously reached the constraint limit in models GF-C90-S10-L and GF-PC-L. In GF-C80-S20-L the CO_2 could be injected into the reservoir until the 9th year of the injection period. Figure 0.13 compares the total CO_2 injected, the amount of dissolved CO_2 in the water phase, and the pressure in the model at the end of the simulation period in the pure carbonate model (GF-PC-L) and pure sandstone models (GF-PS). This graph shows how the bottom hole pressure limit was quickly reached in models with a low sandstone-carbonate ratio resulted in project failure due to injectivity issues.

Theoretical volume available for CO_2 storage, V_{CO2} [sm^3], for homogeneous models is calculated and shown in Table 3.4. As it is evident, in GF-PS, GF-PC-M and GF-PC-H, total gas injected never reached half of the theoretical volume available. Total gas injected into GF-PC-L is significantly less than other models due to low porosity and permeability which resulted in injectivity issue.

Table 0.4: As the geometric volume of the storage reservoir is known, as well as its porosity [φ] and the irreducible water saturation [S_{wir}], based on the formulation 2.9 introduced by CSLF (2007) which is discussed in section 2.6.2, then the theoretical volume available for CO_2 storage V_{CO2} [sm^3] for homogeneous models is calculated and compared to total injected gas.

	V_{CO2} [sm^3]	**Total injection [sm^3]**	**[%]**
GF-PC-L	3.24 E+06	9.19 E+05	28.3
GF-PC-M	6.50 E+06	3.24 E+06	49.9
GF-PC-H	8.06 E+06	3.24 E+06	40.2
GF-PS	1.14 E+06	3.24 E+06	28.4

The optimum heterogeneity rate in models GF-C20-S70-L and GF-C30-S80-L makes them the most suitable configurations for CO_2 injection, as injection security, capacity and injectivity were achieved.

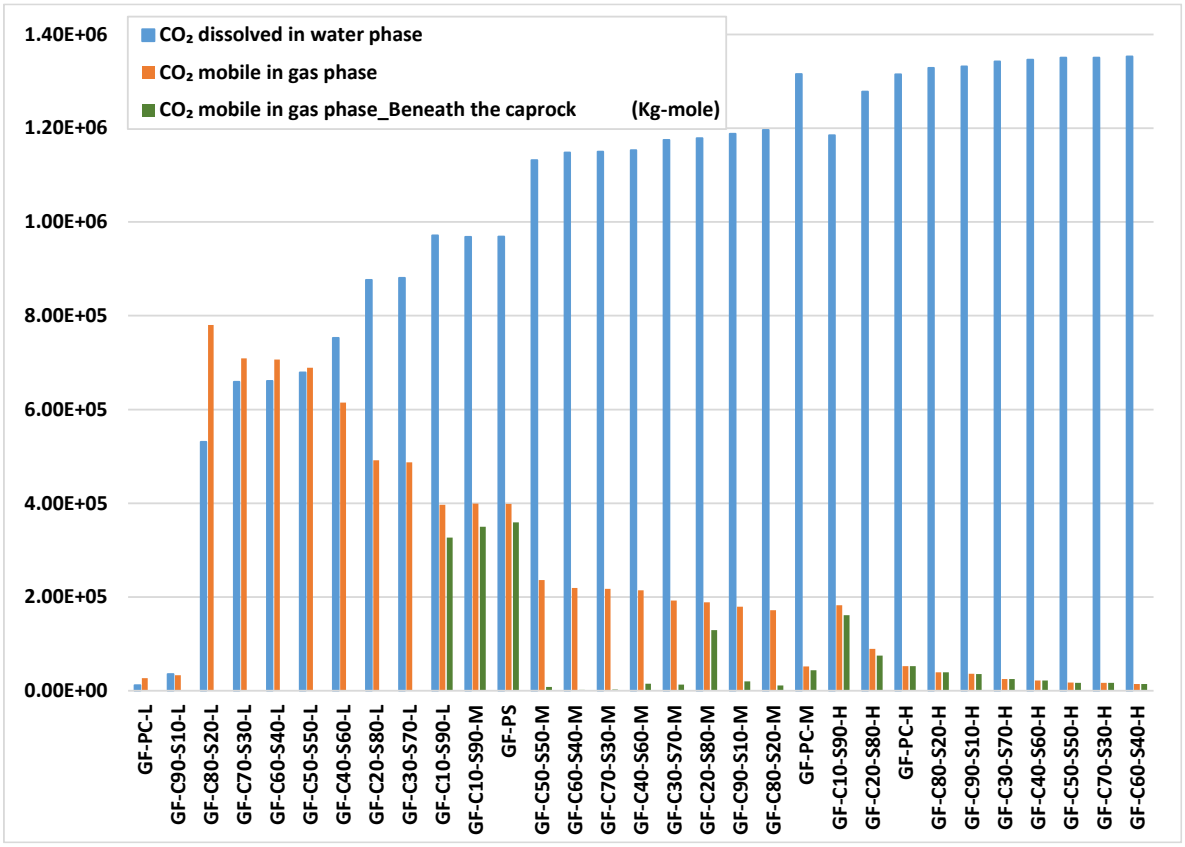

Figure 0.10: Dissolved and mobile CO_2 in the reservoir and Mobile CO_2 beneath the caprock in all models investigated in Section 1. L, M and H refer to low, medium and high permeability carbonate facies and GF refers to Grayburg Formation. For properties see Table 0.1.

The results of models with medium permeability carbonate (Nisku Formation, Section 1 – Model 2) demonstrate that the injected CO_2 developed vertically under the effect of buoyancy (reflecting the lower density of CO_2 relative to brine) until it reached the caprock where it moved out laterally beneath it (Figure 0.14). The flow distribution towards the caprock was relatively symmetrical. As expected, CO_2 showed a uniform flow in the pure sandstone and pure carbonate models. The lateral movement of the CO_2 beneath the caprock caused the lower permeability carbonates to influence the distribution of injected CO_2. The rate of dissolution trapping was highest in the homogenous, pure carbonate (GF-PC-M) model (Figure 0.10). The CO_2 plume approached a cylindrical shape around the injection well. However, the radius of the CO_2 plume around the well is smaller in the case of pure sandstone (GF-PS). Smaller effective permeability in GF-PC-M causes weaker buoyancy forces resulting in the wider footprint of the CO_2 around the injector and high resident time. Higher pressure

in the storage formation was also achieved. Figure 0.10 also shows that the volume of free gas beneath the caprock in the pure sandstone model was significantly higher than for the pure carbonate model, as CO_2 bypassed much of the model and accumulated beneath the caprock. As a result of added heterogeneity, only small patches of free gas can be seen beneath the caprock in the heterogeneous models (e.g., GF-C50-S50-M) (Figure 0.10).

The results of models with high permeability carbonate (Redwater Leduc Formation, Model 3) show that the amount of dissolved CO_2 in the pure sandstone (GF-PS) was less than in pure carbonate (GF-PC-H) (Figure 0.10). Lower CO_2 effective permeability in GF-PC-H resulted in higher resident time and higher CO_2-brine interaction. Therefore, there is higher dissolution in this model. Higher CO_2 effective permeability in GF-PS facilitated upward migration resulted in higher gas accumulation beneath the caprock and lower CO_2 dissolved in the water phase. Therefore, the highest amount of CO_2 accumulated beneath the caprock was still observed in the pure sandstone model (GF-PS). The plume was less distorted compared to low permeability carbonate facies models (Figure 0.15).

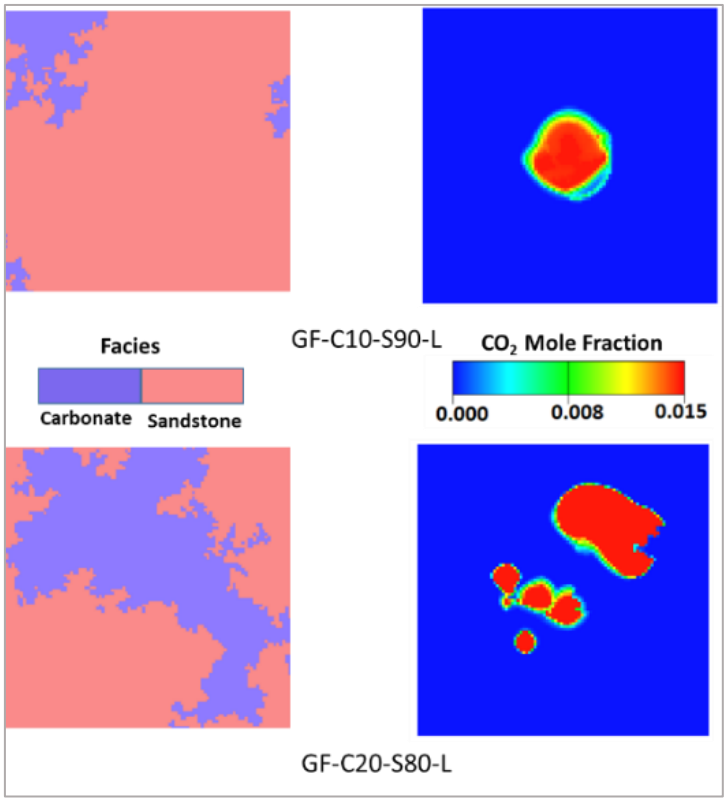

Figure 0.11: A low permeability layer developed across the entire model, from GF-C20-S80. This layer hindered the upward migration of CO_2 and allowed the lateral migration.

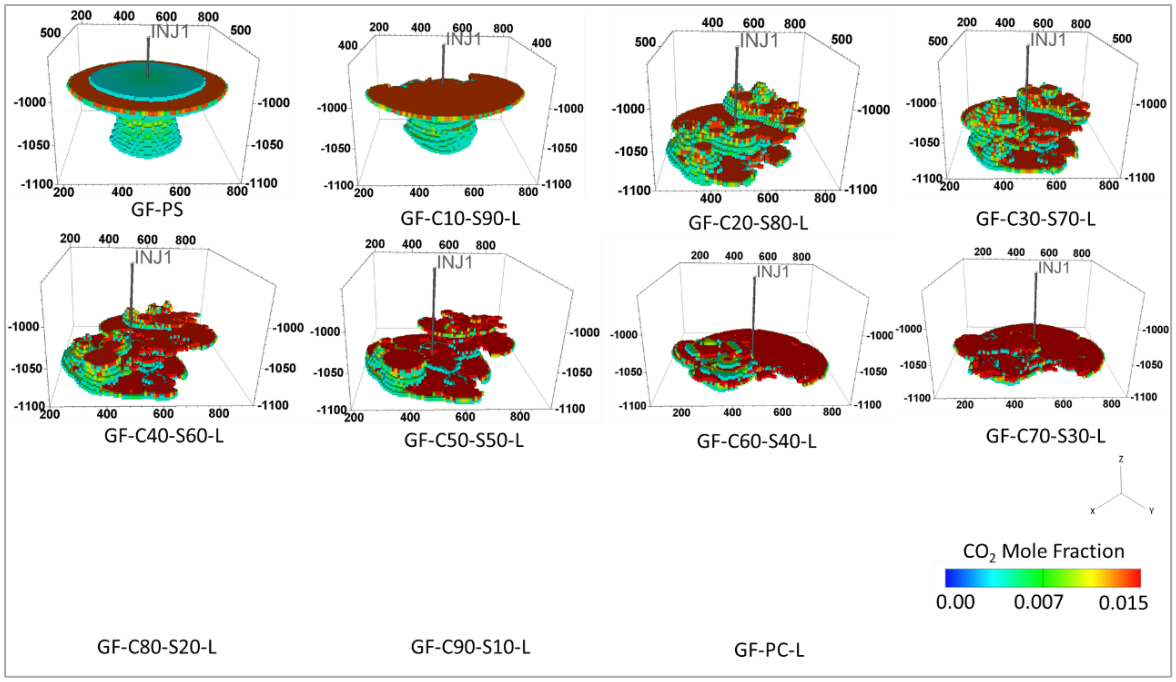

Figure 0.12: Flow distribution in models with different sandstone-carbonate ratios. The properties of low permeability carbonate (L) were used for the carbonate facies in Model 1 (Table 0.1). CO_2 migration towards the caprock is completely restricted in models with decreasing sandstone-carbonate ratios. Flow models with injectivity problems are not shown. GF refers to Grayburg Formation, C to carbonate, and S to sandstone.

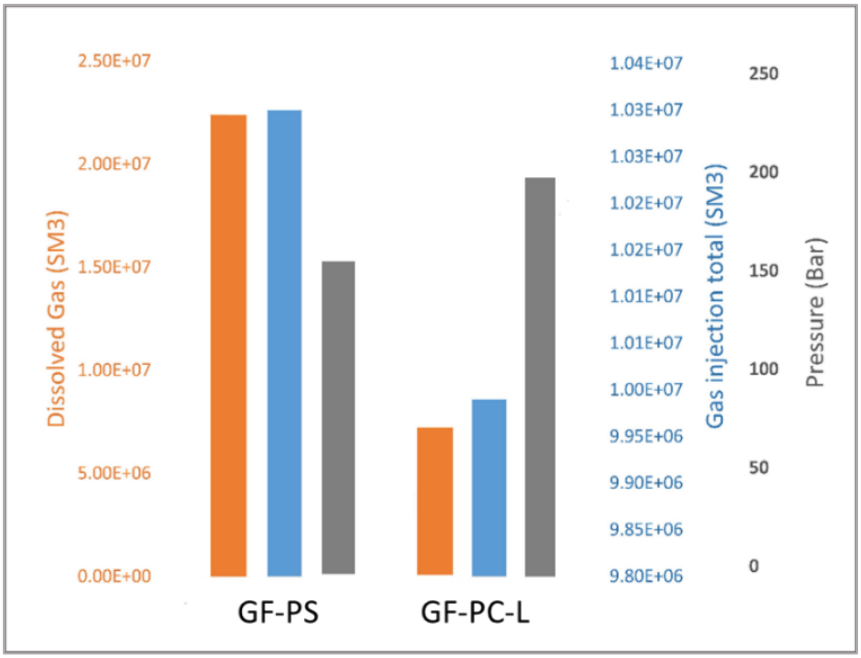

Figure 0.13: Average field pressure, cumulative CO_2 injection and amount of dissolved CO_2 in the water phase in the pure sandstone model (GF-PS) and pure low carbonate model (GF-PC-L). GF refers to Grayburg Formation, C to carbonate, and S to sandstone.

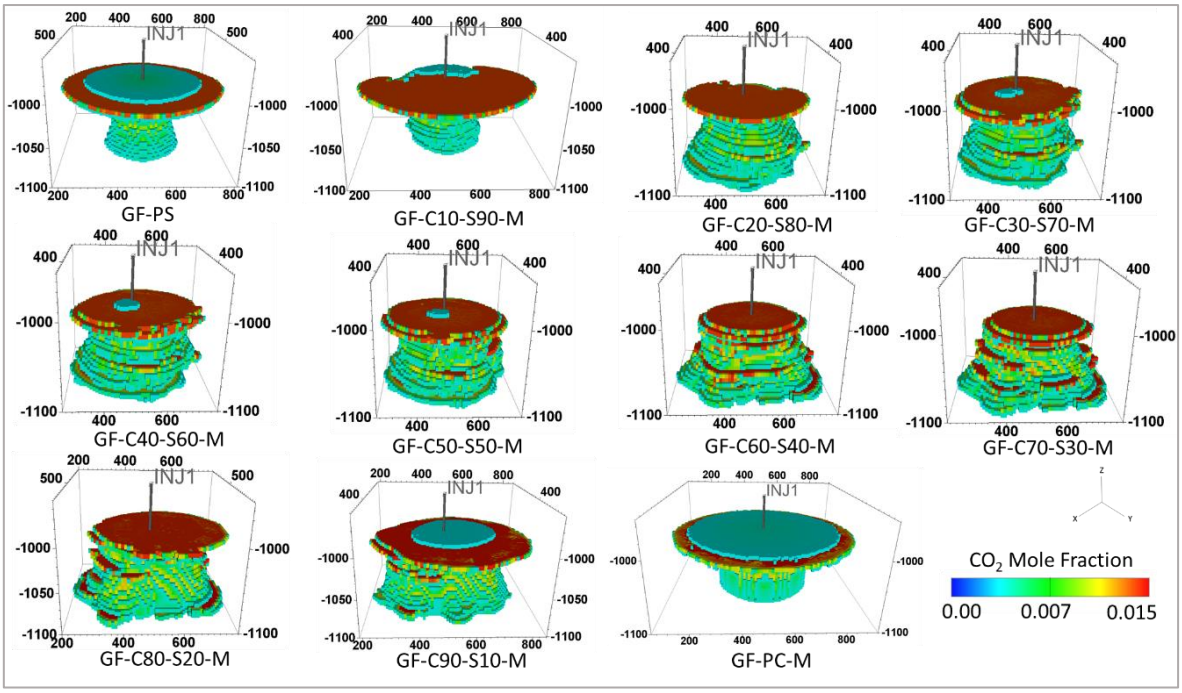

Figure 0.14: Flow distribution in models with different sandstone-carbonate ratios. The properties of medium permeability Nisku carbonate were used for carbonate facies in Model 2 (Table 3.1). GF refers to Grayburg Formation, C to carbonate, and S to sandstone.

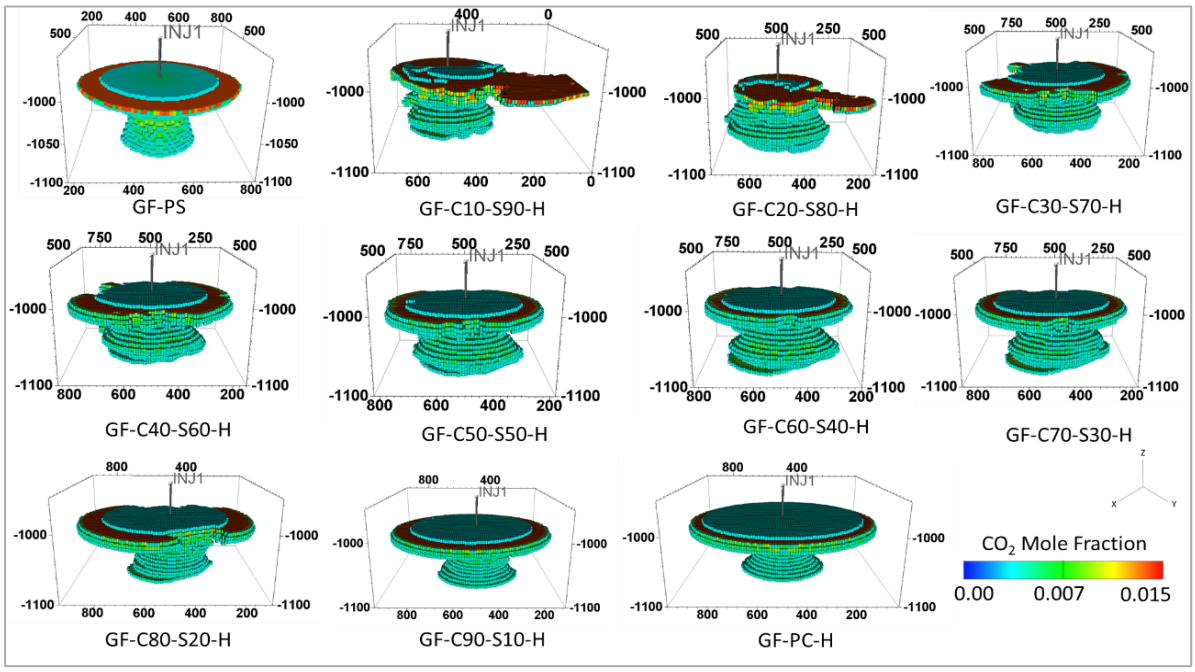

Figure 0.15: Flow distribution in models with different sandstone-carbonate ratios. The properties of high permeability carbonate were used for the carbonate facies in Model 3 (Table 3.1).

3.2.2 Section 2 – Lorca Basin

The CO_2 distribution within the mixed interfingered system with varying petrophysical properties is shown in Figure 0.16. In these models, the plume developed asymmetrically towards the top and was completely distorted, which reflects the interaction between

buoyancy forces and facies-controlled heterogeneity. The degree of plume distortion is dependent on the permeability contrast. As the heterogeneity in permeability arose across the interfingering facies, the discontinuities interrupted the vertical movement of CO_2, which was retained in the lower part of Model LB-CL-S. Alternatively, most of the CO_2 reached the caprock in Model LB- CH-S.

Larger volumes of mobile CO_2 existed beneath the caprock in the homogeneous model (LB-PS) than the model with high permeability carbonate facies (LB-CH-S) (Figure 0.17). This is due to the intrinsic heterogeneity (and associated properties) involved in this model caused by interfingered facies, where CO_2 upward migration is disturbed. This facilitated more interaction between the brine and CO_2, which increased the amount of dissolved CO_2 in the water phase and decreased the amount of mobile gas beneath the caprock.

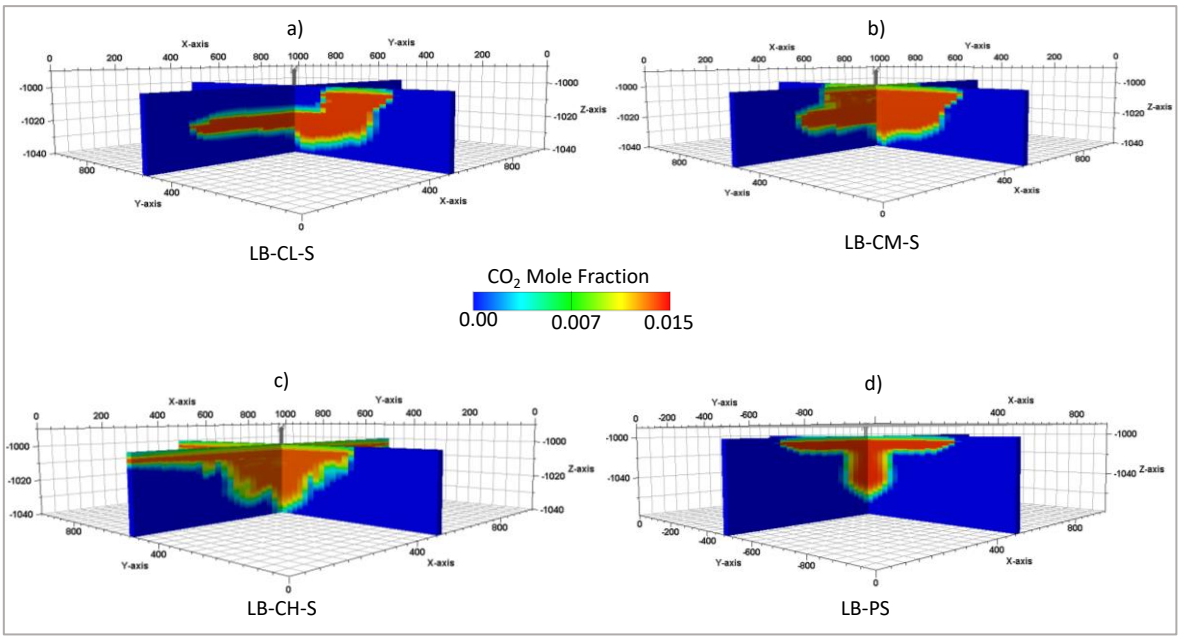

Figure 0.16: CO_2 mole fraction in the model with a) Low permeability carbonate (LB-CL-S); b) Medium permeability carbonate (LB-CM-S); c) High permeability carbonate (LB-CH-S); and d) Homogeneous model (LB-PS). The properties of the sandstone facies properties remained constant throughout the simulation. LB refers to Lorca Basin. For properties see Table 3.1.

3.2.3 Section 3 – Bridport Sand Formation

The CO_2 distribution within the Bridport Sand Formation is shown in Figure 3-18. The results demonstrate that the amount of mobile CO_2 in homogeneous models was considerable in the high permeability layer beneath the caprock compared to models with cemented horizons (Figure 0.19). For both injection scenarios and all models with cemented horizons, except the 10% (BPS-4), no mobile CO_2 occurred in the overlying Inferior Oolite. In all models CO_2 only

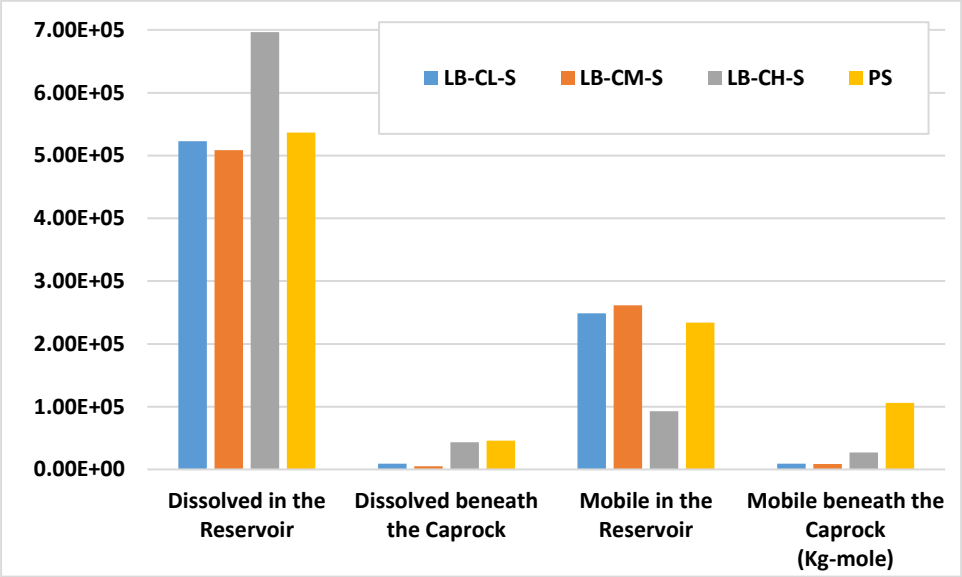

Figure 0.17: Dissolved and mobile CO_2 in the reservoir and beneath the caprock. For the properties see Table 3.1. LB refers to Lorca Basin.

partially filled the sands. In BPS-4 the injected CO_2 was seen to escape laterally towards the high permeability strata and the Fuller's Earth caprock. As stated earlier, the high-density cemented fracture system was not modelled, as they are confined in well-cemented horizons (Bryant, Kantorowicz and Love 1988). It was deduced that the amount of CO_2 trapped as a dissolved phase is insignificantly less in models where all the sand layers were perforated. Figure 0.20 demonstrates the pressure and dissolved CO_2 in each sand layer when the CO_2 was injected across the whole succession. The amount of dissolved CO_2 was increased as the area covered by CO_2 was increased. In the middle layers (40-42), where most coverage was observed, a higher amount of dissolved CO_2 was seen in the water phase. However, as the sand layers thickened towards the bottom of the reservoir (e.g., 68-71), the CO_2 formed a narrow plume around the well, resulting in less dissolution.

The effectiveness of such mixed systems depends on a mobile gas that reaches any leakage points (i.e., transmissible faults, corroded wells or gaps in the caprock). Figure 0.21 compares the free gas beneath the caprock for all cases considered here. Pure sandstone models (GR-PS, LB-PS, and PBS-PS-HI and LI) are the least secure scenarios. Bridport Sand Formation cases are the safest, except for the scenario with the least extensive cemented sheets. The Grayburg Formation cases are the least secure.

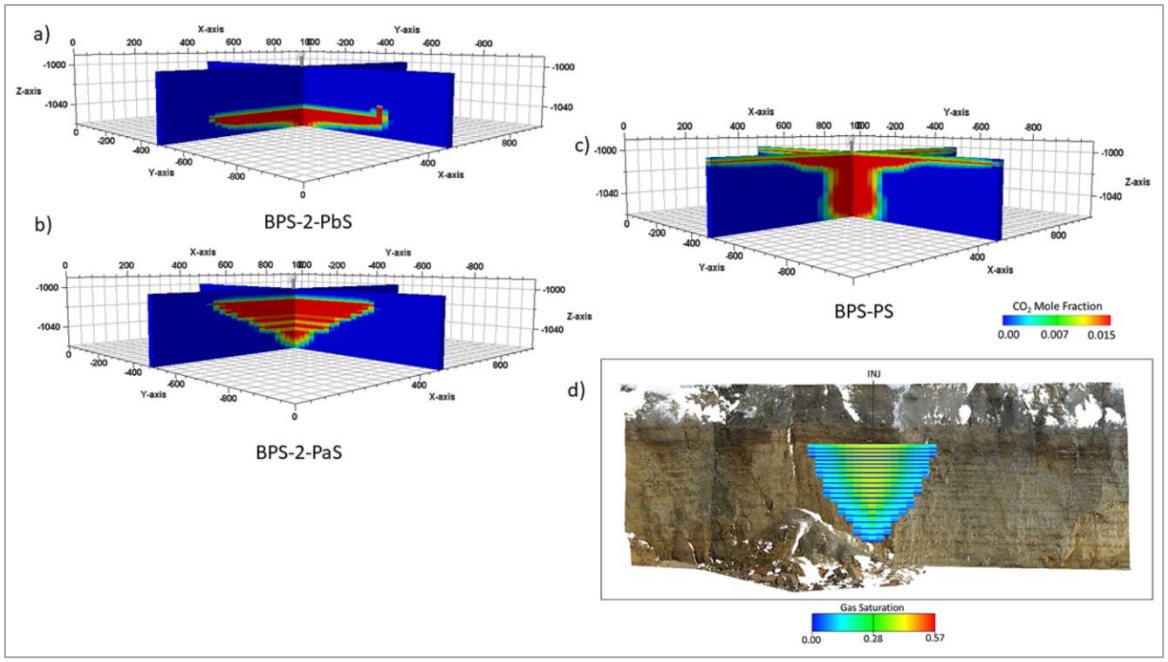

Figure 0.18: CO_2 mole fraction in the model BPS-2 with 70% cemented layers. CO_2 was injected through perforations: (a) into the bottommost sand layer (PbS); and (b) through all sand layers (PaS). (c) Homogeneous model (BPS-PS). (d) Results of the Eclipse dynamic-flow simulation shown on the vertical plane of the laser-scanned digital outcrop of the Bridport Sand Formation that was used to build the static models. The sandstone facies properties remained constant throughout the simulation. BPS, Bridport Sand Formation. For properties, see Table 3.2.

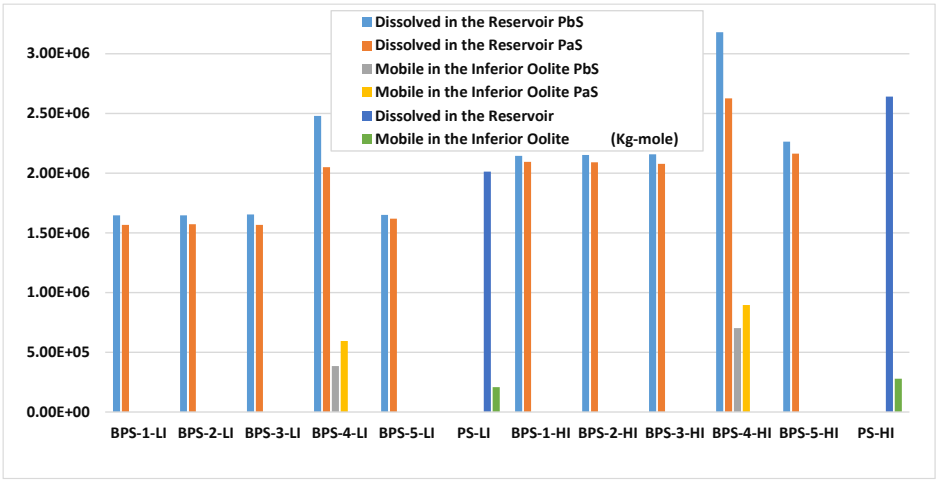

Figure 0.19: Dissolve CO_2 in the reservoir and mobile CO_2 in the high permeability layer (Inferior Oolite) in models with 20,000 Sm^3 (LI) and 30,000 Sm^3 injection rates (HI). In these models, CO_2 was injected through perforations into the bottom-most sand layer (PbS) or through all sand layers (PaS). BPS refers to Bridport Sand Formation. BPS refers to Bridport sand Formation. PS-HI and PS-LI are homogeneous sandstone models with high and low injection rates, respectively.

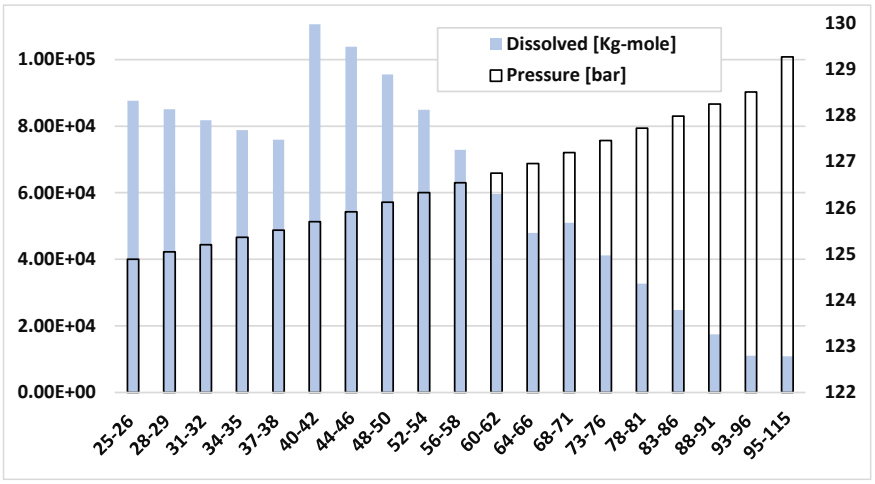

Figure 0.20: CO_2 and the pressure in the sands. The x-axis shows the layers where the well is open to CO_2 injection.

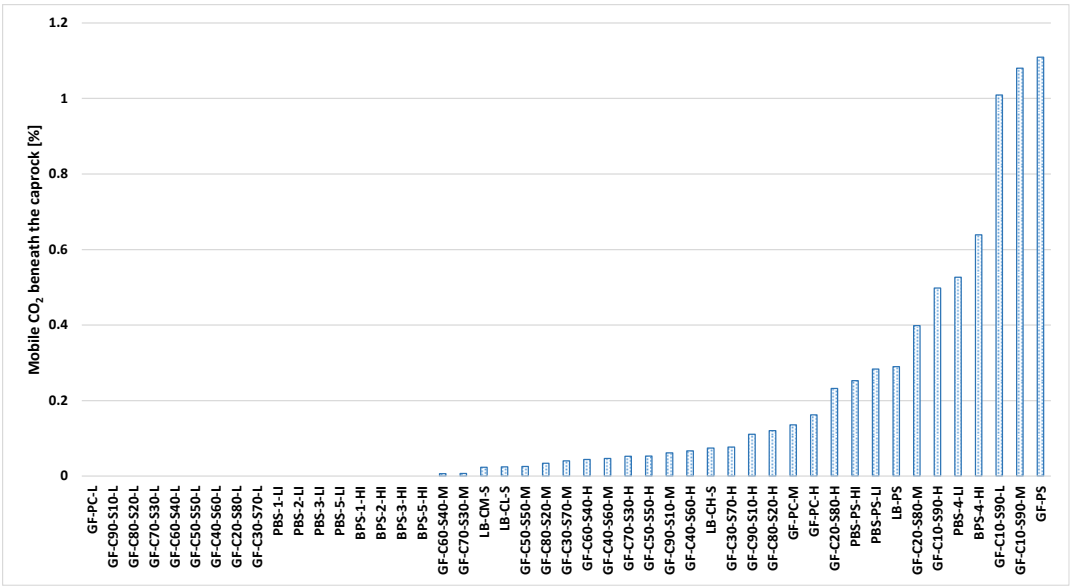

Figure 0.21: Percentage of the free gas beneath the caprock in all cases. GF: Grayburg Formation, LB: Lorca Basin, and PBS Bridport Sand Formation.

3.3 Discussion

The effectiveness of CO_2 storage may be enhanced by sediment heterogeneity arising from the distribution of low permeability facies, as they facilitated the lateral migration of CO_2 which can result in longer flow paths and thus increase volume available (Hovorka et al. 2004; Flett, Gurton and Weir 2007; Lengler, Lucia and Kühn 2010; Goater et al. 2013). In this study, the increase in low permeability facies did not lead to an increase in storage capacity because of a low permeability layer developed from model GF-C20-S80 (Figure 0.11). The reduction in available volume, storage capacity and reservoir communication are linked to the low porosity and permeability of the Wabamun carbonate facies (Section 1, Model 1). The presence of this layer was not reflected in the results of the flow simulations in Model 2 and

Model 3 of the Grayburg Formation as high permeability contrast would cause considerable flow heterogeneity. The high permeability contrast (i.e., four orders of magnitude) in Model 1 affects flow so that injected CO_2 could not migrate vertically and instead accumulated at the bottom of the reservoir (

Figure *0.12*). This explains the irregular shaped plume in Model 1 compared to Models 2 and 3 which behave more homogeneously. In particular, low viscosity gas reservoirs are sensitive to higher contrasts in permeability and justify a simple modelling exercise (Ringrose and Bentley 2015).

Static models herein are but one of many options in order to study flow; however, the results demonstrate the significance of localised geology on flow characteristics in complex 3D systems.

Heterogeneity needs to be considered as injectivity generally decreases with increasing heterogeneity (e.g., Lengler et al. 2010) and the storage efficiency decreases with localised pressure build-up (Goater et al. 2013). Although a decrease in high permeability lithology could result in injection problems and limit CO_2 storage capacity, even low-permeability aquifers can be utilised for CO_2 geological storage if high permeability 'sweet zones' exist close to the injector. These zones can improve injectivity and reduce reservoir pressure (Hester and Harrison 2010); alternatively, a misplaced injection well may result in project failure as seen in Model 1, in scenarios with low sandstone-carbonate ratios.

In contrast, both facies in Model 2 were relatively homogenous, with a unimodal pore size distribution, uniform matrix (Bennion and Bachu 2006a; 2006c) and insignificant permeability differences (less that order of magnitude). The injected CO_2 showed a relatively uniform sweep around the injection well and towards the caprock. The results in Model 2, particularly in the heterogeneous models, is driven by the small permeability differences between the two facies. The heterogeneity provided by the association of two facies can add to reservoir security. However, the reduced permeability in some parts of the reservoir, where carbonate facies delay the upward migration of the CO_2, was not sufficient to completely inhibit the flow towards the caprock. Carbonate facies had considerably higher permeability values (46 mD) than typical seals (e.g., Shale=1.00E-08 mD).

The dissolved CO_2 in heterogeneous models was also marginally higher than in the pure carbonate scenario of Model 3, since the permeability of the carbonate facies is only 0.18 order of magnitudes higher than the permeability of sandstone facies. The lower the

permeability contrast, the less irregular the plume. Although Sifuentes et al. (2009) showed that heterogeneous models had a higher CO_2 dissolved in the water phase and a lower mobile CO_2 in the reservoir, these facets depended on effective permeability, permeability contrast of facies, and heterogeneity rate in these models.

In the case of Lorca Basin scenario, the CO_2 plume was distributed by facies discontinuities, which led to improved CO_2 dissolution trapping, as the interfacial area has an essential role in the transfer and subsequent dissolution of CO_2 (Iglauer 2011). The degree of plume distortion is also dependent on the permeability contrast. The degree of interruption by these discontinuities is higher in Model with low permeability carbonate, and the plume is retained in the lower part of the reservoir.

The sandstone/shale cycles offer effective confinement in hydrocarbon and CO_2 storage systems (e.g., Sleipner project (Chadwick et al. 2008)). In the case of the Bridport Sand Formation, the lateral continuity of these thin cemented layers will most likely have a significant impact on plume development towards the caprock and hence the volume of CO_2 sequestration in the layered systems. Banded carbonates can inhibit vertical CO_2 migration, act as a stratigraphic trap and reduce the reliance on a top seal, and thus seal failure is extremely unlikely. Consequently, the storage effectiveness of the system is dependent on the fidelity of these cemented horizons.

The flow modelling of these systems demonstrates that facies mixing and associated sediment heterogeneity have different influences on CO_2 storage capacity and security.

In the case of the Grayburg Formation, storage security and capacity were not controlled by heterogeneity alone but influenced by the permeability of each facies; their permeability contrast, the degree of heterogeneity and the relative permeability characteristic of the system. In the case of the Lorca Basin, heterogeneity through interfingering of the carbonate and clastic facies improved the storage security regardless of their facies permeability. For the Bridport Sand Formation, the existence and continuity of extended sheets of cemented carbonate contributed to storage security but not storage capacity.

The long-term storage security of CO_2 in such systems depends on the amount of free gas that reaches existing leakage points. Overall, these mixed systems contribute to the safe storage of CO_2 as insecure scenarios are associated with pure sandstone and carbonate or models with high sandstone-carbonate ratio. Among the three outcrops studied herein, the safest scenario is the Bridport Sand Formation, although this is dependent on the continuity of

cemented layers. The least secure scenario is the Grayburg Formation as the cemented bands in Bridport Sand Formation inhibited the vertical migration of CO_2. However, in the case of Grayburg Formation, heterogeneity in the models either cause the compartmentalization of the reservoir, thus reducing CO_2 dissolution, or allowed CO_2 to escape via gaps towards the caprock.

3.4 Conclusion

In this study, three formations with differing styles of heterogeneity were explored, including variable siliciclastic-carbonate ratio, interfingering of carbonate and sand facies and a succession with narrow cemented bands. All three styles of heterogeneity are deposited within a mixed siliciclastic-carbonate system. These lithofacies, and their associated physical properties, were systematically modelled to determine how they influenced injected CO_2 flow, and, as such, determine their potential as stratigraphic trap for the safe geological storage of CO_2.

This study has demonstrated that facies interplay and sediment heterogeneity have a varying influence on fluid flow, storage capacity and security. In the example of the Grayburg Formation storage security and capacity were not controlled by heterogeneity alone but influenced by facies permeability, permeability contrast and the relative permeability characteristic of the system. Based on the petrophysical properties of each facies, stratigraphic heterogeneity can limit connectivity and significantly increase injection pressure. In the Lorca Basin, heterogeneity achieved through the interfingering of the carbonate and clastic facies, improved the storage security regardless of their permeability. For the Bridport Sand Formation example, the existence of extended sheets of cemented carbonate contributed to storage security but not storage capacity. This study demonstrates the significance of these systems for safe CO_2 geological storage, as stratigraphic heterogeneity is likely be a significant feature of future storage sites. These mixed systems can minimise the large buoyancy force that act upon the top seal thus reducing the reliance of the storage security on the caprock. They can also increase the contact area between injected CO_2 and brine, thereby promoting CO_2 dissolution.

Chapter 4

Modelling of bleached palaeo-reservoir in the Salt Wash Graben, Utah

4.1 Introduction

There are significant uncertainties in modelling the fate of injected CO_2 over a long time period (Pourmalek and Shariatipour 2019). Natural CO_2 fields, as analogues for CO_2 storage projects, may provide new insight regarding CO_2 in the subsurface (i.e., its dissolution in brine, [re-]action with rock minerals, escape via faults and corroding of the top-seals) (Bickle and Kampman 2013). In places CO_2 is actively escaping from natural reservoirs (e.g., Little Grand Wash and Salt Wash graben in central Utah, USA), primarily along faults, but elsewhere CO_2 has been securely stored in geological formations for extensive time-periods (e.g., Bravo Dome, New Mexico and McElmo CO_2 fields, Colorado) and has been produced for commercial purposes (Allis et al. 2001).

The study of potential subsurface reservoirs and aquifers for CO_2 storage is both challenging and expensive. Knowledge of the geological controls on fluid movement is obtained from seismic surveys and well data, such as core and downhole geophysical logs. Such subsurface data sets leave an information gap between relatively coarse scale seismic and fine scale well data. In the oil and gas industry, the study of rock outcrops has long been used to fill this gap, offering analogues on the shape and dimensions of geological heterogeneities at the metre to decametre scale (e.g., Rotevatn et al. 2009; Buckley et al. 2010; Wilson et al. 2011).

Although new technologies, such as terrestrial laser scanning, have significantly increased the range of information that can be obtained from outcrops (Howell, Martinus and Good 2014), there are difficulties in making a direct link between geological heterogeneity of an outcrop and subsurface fluid movement. Therefore, the study of outcrops with preserved palaeo-reservoir systems is important; and more specifically, those palaeo-reservoirs where the

migrating fluids have left a permanent fingerprint by chemically changing the rock matrix (Newell et al. 2019). A common example of this fingerprint is the grey bleaching resulting from the reduction of red-bed terrestrial sandstones by fluids. This phenomenon is particularly widespread across the Colorado Plateau of the Southwestern United States. The bleaching of red Mesozoic sandstones by fluids provides a remarkable visual record of their pathway through highly permeable sandstones and fractures (Chan et al. 2000; Beitler, Chan and Parry 2003; Haszeldine et al. 2005; Wigley et al. 2012). The importance of bleached palaeo-reservoirs for understanding fluid flow in the subsurface has long been recognised (Chan et al. 2000; Beitler, Chan and Parry 2003). However, research has been renewed with the realization that bleaching caused by large fluxes of CO_2-charged fluids offers an opportunity to better understand the processes associated with the geological storage of CO_2 as part of a wider climate change mitigation strategy (Bickle, Kampman and Wigley 2013; Bickle and Kampman 2013; Burnside et al. 2013; Wigley et al. 2013).

A high proportion of the recent work on outcrop analogues has focussed on the bleached Jurassic palaeo-reservoirs of eastern Utah. Research has explored the role of fractures on fluid flow (Dockrill and Shipton 2010), the geochemistry of rock-fluid interaction (Bickle and Kampman 2013; Kampman et al. 2016) and the long-term integrity of CO_2-reservoir topseals (Kampman, et al. 2016). However, while many authors have studied the bleached palaeo-reservoirs around Green River (Dockrill and Shipton 2010; Bickle, Kampman and Wigley 2013; Kampman. et al. 2016), there has been no attempt to construct a reservoir scale flow model that tries to replicate the observed patterns of bleaching (an outcrop proxy for the distribution of CO_2-charged reducing-fluids) and the regional pathways of buoyant CO_2-charged fluids into the former reservoir. Three main questions are to be addressed:

1) Can flow simulators, which are critical to understand the feasibility and long-term security of geological carbon storage, successfully replicate the distribution of bleaching observed in the reservoir analogue?
2) Can flow simulation replicate potential pathways for reducing fluids?
3) Do palaeo-reservoirs provide an insight into how geological heterogeneity and complexity should be incorporated into static geological models (increasing the time and cost of computer simulation) for the realistic modelling of CO_2 sequestration?

4.2 Geological setting

4.2.1 Location

The Middle Jurassic Entrada Sandstone (exposed near Green River, Utah, northern Paradox Basin of the Colorado Plateau) has been the subject of recent CO_2 storage-related research (Kampman et al. 2014; 2016). The intracratonic Paradox Basin is an ovate structure situated in Southeastern Utah and Southwestern Colorado. The Entrada Sandstone is potentially a good analogue for many Permian and Triassic red-bed aeolian-dominated reservoirs that are considered important targets for geological CO_2 storage on the NW European continental shelf (Newell and Shariatipour 2016). The study site is located 13 km south of the town of Green River in East Central Utah (38.865 N 110.098 W) on a WNW-ESE trending fault system, recently termed the Salt Wash Graben (Pearce et al. 2011; Wigley et al. 2013; Ogata et al. 2014) (Figure 0.1).

4.2.2 Entrada Sandstone Formation

The focus of this chapter is a palaeo-reservoir that occurs as a narrow, elongate outcrop of Middle Jurassic Entrada Sandstone, on the crest of the Green River anticline. At Salt Wash graben the Entrada Sandstone is 43 to 170 m thick and subdivided into the Slick Rock and the Earthy members (Doelling 2001) (Figure 0.2). The Slick Rock Member is comprised of alternating cross-bedded aeolian sandstone and wavy-laminated silty sandstone.

The Slick Rock Member represents the permeable palaeo-reservoir rock for CO_2 charged fluids. The Earthy Member sharply overlies the Slick Rock Member and is a muddy fine-grained sandstone. The Earthy Member is 20-30 m thick and forms a topseal to the aeolian sandstone reservoir.

4.2.3 Structure

Faults and related fractures can have a considerable role in determining the relative movement of subsurface fluids. Faults can form barriers to flow by juxtaposing a high-permeability reservoir against a low-permeability seal, or by generating low-porosity and low-permeability fault rocks. However, fault leakage is a trap limitation, caused by the juxtaposition of a reservoir unit against a high-permeability unit, or the formation of a fracture network along the fault plane.

Figure 0.1: (A) Study area (black rectangle) is adjacent to the Salt Wash graben. NNW plunging Green River anticline is truncated by two major faults of the Salt Wash graben and Little Grand Wash fault (Allis et al. 2001; Doelling 2001). Faults are shown in red, anticlinal axes in black and selected geological formations are coloured and labelled from the Utah Geological Survey Map 180 (Newell et al. 2019). (B) Aerial photograph of the study area. Red line is the bleached area and the blue line is the Slick Rock Member (palaeo-reservoir). Red stars indicate the location of the two logged sections in Figure 0.4.

Figure 0.2: The Entrada Sandstone comprises the Slick Rock Member, which is the high permeability sandstone to silty sandstone palaeo-reservoir and the Earthy Member, which is a low permeability muddy sandstone topseal (courtesy of Andrew Newell and Andrew Butcher).

The shallow NNW plunging open Green River anticline was formed as a result of evaporate migration and dissolution in the Paradox Basin (Dockrill and Shipton 2010). The fold axis of the Green River anticline is truncated by the Little Grand Wash fault and the Salt Wash graben, where CO_2-charged groundwater emanates from a series of geysers and springs (Shipton et al. 2004; Dockrill and Shipton 2010). As seen in Figure 0.1, the Entrada Sandstone outcrops on the northern footwall of the Salt Wash graben.

The Little Grand Wash fault is an EW trending structure that is 30 Km long, with an average dip of 70° to the south). This fault juxtaposes Late Jurassic and Cretaceous sediments at the surface. The geometry and depth of this fault are undefined, but drilling records show that this fault may offset rocks of Upper Carboniferous age (Dockrill and Shipton 2010).

The WNW trending Salt Wash Graben is a 20 km long and part of a 31 km structure that consists of the Salt Wash and Ten Mile grabens. This structure juxtaposes Mid-Jurassic and Cretaceous deposits at the surface. The Cretaceous Cedar Mountain Formation is exposed in the central part of the Salt Wash Graben, implying a downthrow of c. 200 m (Newell et al. 2019) (Figure 4.1). Several faults, which run parallel to the Green River Anticline, link the Salt Wash graben and Little Grand Wash fault (Figure 0.1). The study of Dockrill and Shipton (2010) demonstrated how structural control influenced the vertical migration of fluids through a thick sequence of sandstone and shale. Faults have promoted parallel fluid flow rather than cross-fault flow, as permeability increased parallel to the faults and in the absence of sealing

capacity of the caprocks. This is shown by extensive bleaching and the numerous travertine deposits located at the northern footwall of Salt Wash graben and Little Grand Wash fault.

4.2.4 Burial history

Nuccio and Condon (1996) reconstructed the burial (geohistory curves) and thermal histories for six areas within the Paradox Basin. Near Green River in Utah, the Middle Jurassic Entrada Formation was probably buried to a depth of 2560 m and from the middle-late Eocene was brought rapidly back to the surface.

4.2.5 Field and laboratory methods

Field data was collected by Andrew Newell and Andrew Butcher over six-days. The details of field and laboratory methods can be found in Newell et al. (2019). Field data were gathered on geological boundaries, dip and strike of bedding, lithofacies, grain-size and sorting, sandstone permeability (using a TinyPerm II Portable Air Permeameter), locations of major faults and fractures, and the extent of bleaching in the palaeo-reservoir. Sedimentary logs were recorded from the Entrada Sandstone at the western and eastern ends of the bleached zone [as shown in Figure 0.4]. Laboratory analyses included the measurement of gas permeability and pore throat size distributions by means of a MICP tests. Thin sections were cut and examined under a scanning electron microscope (SEM) to obtain additional data on grain morphology, composition, pore cements and clays. Field observations and Laboratory analyses were used for lithofacies classification (Table 4.1). As explained in the methodology (Section 4.3), associated properties of each lithofacies were input to static models and were used to simulate flow within the bleached palaeo-reservoir.

4.2.6 Lithofacies of the Entrada Sandstone Formation

4.2.6.1 Slick Rock Member – Palaeo-reservior lithofacies

The Slick Rock Member of the Entrada Sandstone Formation comprises sandstone-dominated lithofacies (Figure 0.5). The grain-size and sorting ranges from clean to argillaceous-rich sandstones, accompanied by a change in sedimentary structures. The key characteristics of the Slick Rock Member are summarised in Table 0.1. Aeolian dune sandstones are usually composed of clean, cross-bedded sandstone (Figure 0.5A). The presence of cross-bedded

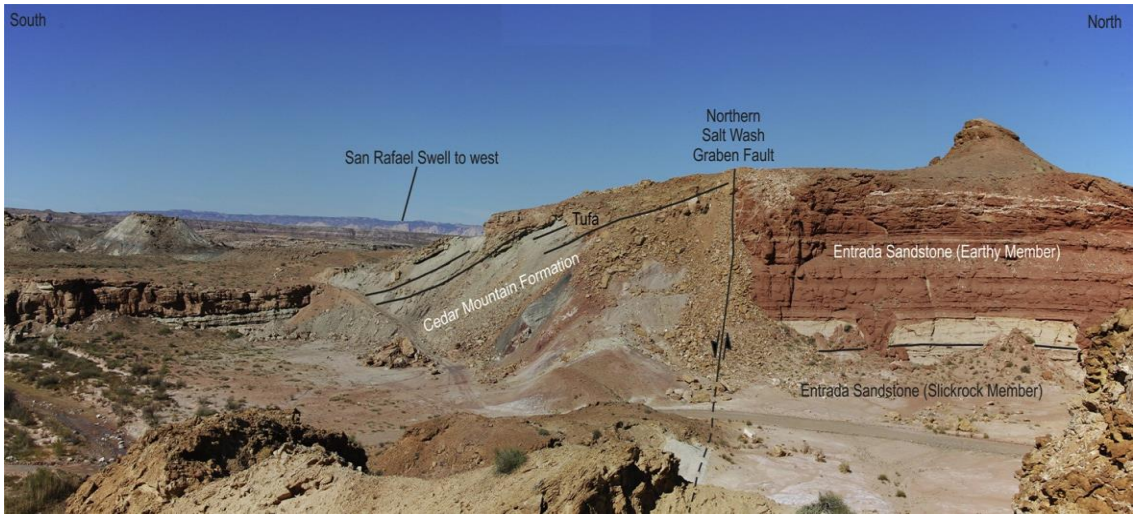

Figure 0.3: The abrupt truncation of the Slick Member and Earthy Member of the Entrada Sandstone Formation against the Cedar Mountain Formation (lower Cretaceous). The bleaching also extends into the Earthy Member (topseal) (courtesy of Andrew Newell and Andrew Butcher).

structures implies that these structures would have developed at the slip-face, on dry substrates above the groundwater table where wind could generate bedforms from loose sand.

Wind-ripple laminated sandstones (Figure 0.5B) are comparable to aeolian dune sandstone in terms of sediment composition, although they differ by displaying horizontal or low-angle lamination. These structures would have deposited on dry mobile substrates around the flanks of dunes. They may have formed on low relief aeolian sand sheets where dunes were absent.

These two lithofacies occur interbedded with silty sandstone or clayey silty sandstone showing irregular wavy or highly convolute lamination. They are shown in Figure 0.5C and D, respectively. These sandstones are fine-grained and share many of the petrographic and reservoir properties of the overlying Earthy Member. It is possible that these lithofacies were formed on damp or wet substrates within low lying interdune areas that intersected the water table (Crabaugh and Kocurek 1993).

The sandstones of this member were mostly, but not entirely, deposited in a range of aeolian environments that periodically interacted with a shallow groundwater table (Crabaugh and Kocurek 1993). Typically, wet and dry aeolian lithofacies within the Slick Rock Member alternate on a scale of roughly one metre. Frequently they show ‘drying-upward cycles’. In this arrangement muddy wet interdune deposits pass upwards, through wavy laminated sandstones and wind-ripple laminated sandstones, into cross-bedded aeolian dune sandstones.

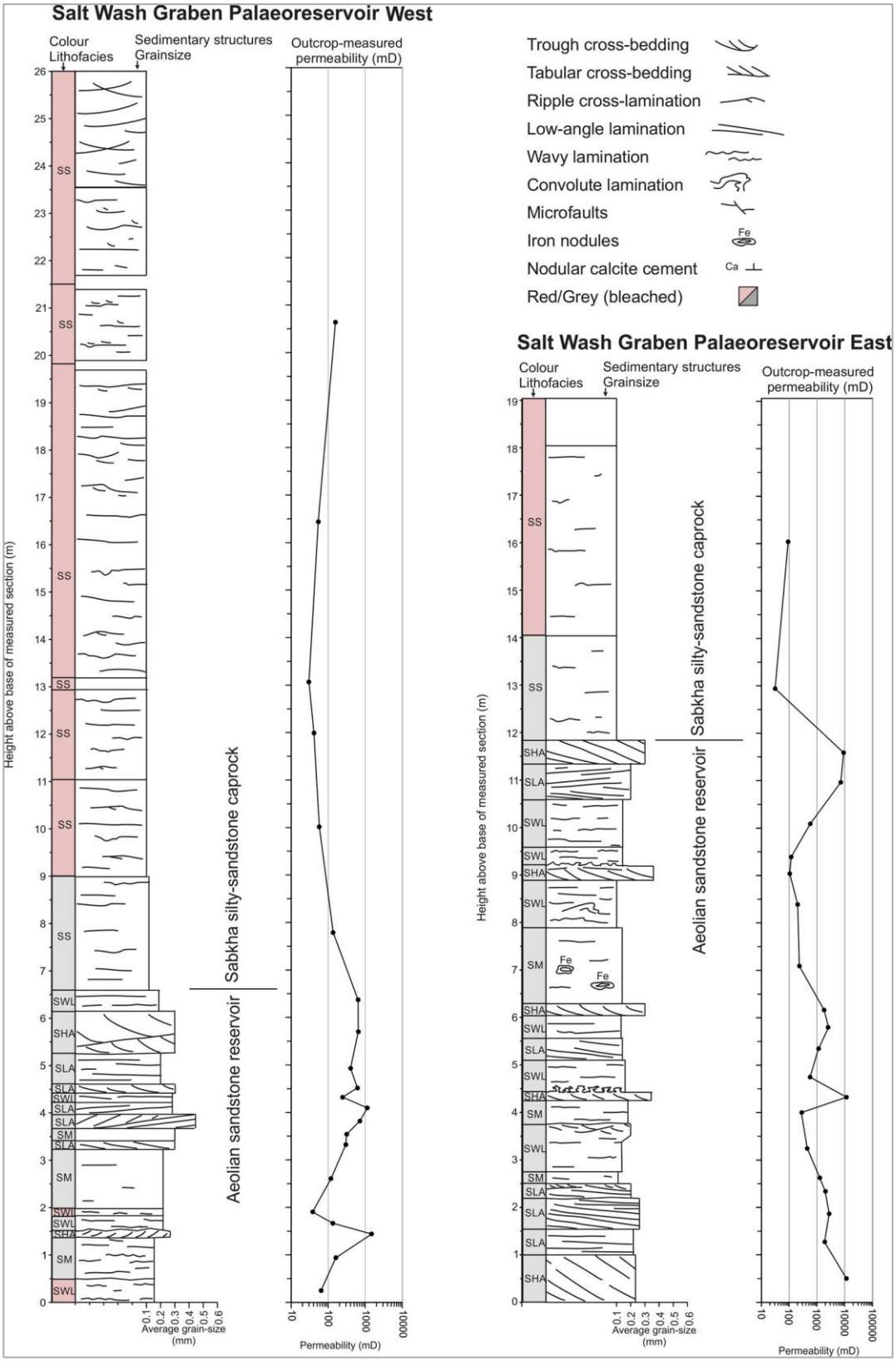

Figure 0.4: Sedimentology log of the upper Slick Rock Member and lower Earthy Member of the Entrada Sandstone Formation. The location of these sections is shown as red stars in Figure 0.1 (measured by Andrew Newell and Andrew Butcher).

Table 0.1: The main characteristics of the Slick Rock Member (compiled by Andrew Newell and Andrew Butcher).

Code	Description	Interpretation	Typical permeability
SHA	Sandstone, high-angle cross-bedded. Tough or tabular cross-bedded with foresets reaching a maximum angle of around 28 degrees. Wedge-shaped or parallel laminated foresets. Composed of fine-medium grained sand, moderately to well-sorted, quartz-rich.	Mobile aeolian dunes with curved or straight crests. Lamination results from grain-flow and grain fall on dune avalanche faces.	1000–10000mD
SLA	Sandstone, low-angle lamination. Typically displays well-developed pin-stripe lamination with alternation of cm-thick, fine-medium sand laminate and mm-thick fine-very fine sand. Quartz-rich, bimodal grain-size distribution.	Migration of wind-ripples on low relief sand sheets or dune aprons	1000–10000mD
SM	Sandstone, massive. Structureless sandstone, or one showing only occasional faint lamination. Very fine to medium grained, sorting generally poor.	Sand accretion in damp interdune areas	100–1000mD
SWL	Sandstone, wavy laminated. Irregular wavy discontinuous lamination, occasionally convolute lamination. Poorly sorted with common silty and very fine-grained sand laminae.	Sand accretion in damp to wet, water saturated, interdune areas	100–1000mD
SMC	Massive or faintly bedded sandstone with ferruginous concretions and wavy lamination, undulating erosion surfaces and channel fills.	Channel fills	100–1000mD
SS	Silty sandstone, discontinuous wavy lamination, massive, occasionally convolute. Very poorly sorted admixture of sand, silt and clay	Deposition on sandflats and sabkha, salt crusts probably important in trapping sediment	0.1–10 mD

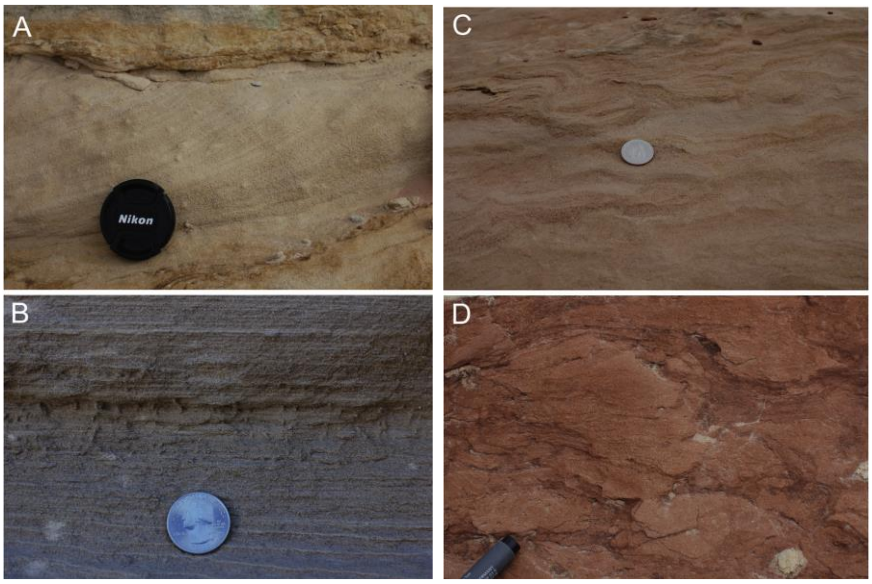

Figure 0.5: Four main sandstone lithofacies within the Slick Rock Member: (A) High angle cross-bedded dune sandstones; (B) Low-angle wind-ripple laminated sandstone; (C) Wavy and convolute laminated sandstone damp interdune deposits; and (D) Massive and muddy wet interdune sandstones. Permeability generally decreases from A to D (courtesy of Andrew Newell and Andrew Butcher).

4.2.6.2 Earthy Member – Topseal lithofacies

This is a thick unit of well-cemented, silty sandstone deposited in sabkha or a muddy sandflat in an arid marginal marine environment. The Earthy Member sharply overlies the Slick Rock Member (Figure 0.2). The Earthy Member is generally reddish brown; however, extensive grey bleaching extends for several metres into the Earthy Member at some location. Highly variable fabrics are recognizable in the Earthy Member; for instance, irregular pods of fine-grained sediment are isolated by the highly convolute lamination of silt and clay. Table 4.2 summarises the petrophysical properties of these two members of the Entrada Sandstone Formation.

Table 0.2: Petrophysical properties of the Slick Rock Member (high permeability palaeo-reservoir) and Earthy Member (topseal) of the Entrada Sandstone Formation.

	Horizontal Permeability [mD]	Vertical Permeability [mD]	Porosity [φ]	Pore throats size [µm]
Slick Rock Member	1600	830	0.25	26.5
Earthy Member	0.38	0.25	0.08	0.4

4.2.7 Reducing agents

Bleaching of the red-beds in the Colorado Plateau is connected to the migration of reducing fluids. Wigley et al. (2012) identified CO_2-rich brines containing quantities of dissolved CH_4 as the main cause of bleaching in the Middle Jurassic Entrada sandstones, near the town of Green River. Other authors have proposed different reducing agents, including hydrocarbons, organic acids, methane, H_2S, promoting alternate or multiple fluids regimes (Beitler, Chan and Parry. 2003; Haszeldine et al. 2005).

Haematite grains give the red appearance to the red sandstone. CO_2-rich brines have bleached the red sandstones by dissolution of the haematite (Fe_2O_3). Haematite and goethite coatings are formed under humid, well-drained conditions (Wigley et al. 2012). Under normal pore fluid conditions, Ferric (Fe^{3+}) is immobile and insoluble; however, acidic or reducing fluids will initiate a series of reactions which reduce ferric to soluble ferrous (Fe^{2+}). Ferrous can be removed and transported, thus discolouring the red-beds.

4.2.8 Regional fluid pathways

Wilkinson, Gilfillan and Haszeldine (2008) demonstrated that approximately 0-20% of the CO_2 originates from the mantle and the rest from the crust. These reducing fluids would have moved upwards through faults and then laterally into transmissive sandstone formations (Chan et al. 2000; Wigley et al. 2013). The fluids could have migrated upwards through the faults of the Salt Wash graben and the Little Grand Wash fault before moving southwards along the crest of the north-plunging Green River Anticline (Figure 0.6).

The upward migration of the reducing fluids was inhibited by the low permeability Earthy Member, which acted as a topseal; although, there was a long-term diffusion into the Earthy Member (Kampman et al. 2016). The palaeo-reservoir was then breached by NNW-trending fractures related to extension movement across the crest of the Green River Anticline. The vertical escape of the reducing fluids has caused the bleaching of these fractures (Figure 0.7).

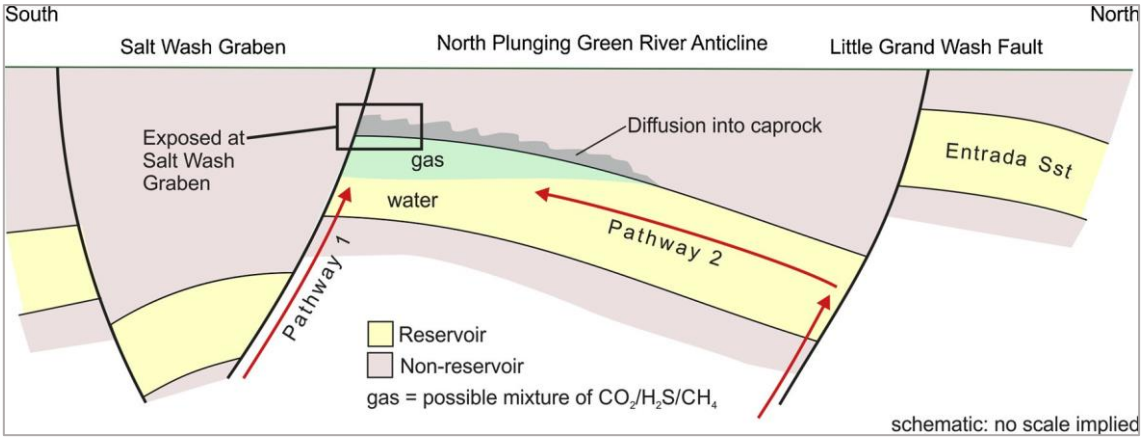

Figure 0.6: Two possible pathways for the migration of reducing fluids from depth into the Entrada Sandstone palaeo-reservoir at Salt Wash graben. Pathway 1 is via northern fault of Salt Wash graben. Pathway 2 is via Little Grand Wash fault.

4.2.9 Distribution of the bleaching

Bleaching occurs in a broadly semi-circular area 1150 m across (parallel to the Salt Wash Graben fault) and 408 m wide (perpendicular to the Salt Wash Graben fault) on the crest of the Green River Anticline (Figure 0.1B). The upper contacts between bleached and unbleached Entrada Sandstone are well exposed along the western and eastern margins of the palaeo-reservoir. Although the thickness of the bleaching is at least 13 m, the bleaching; however, could extend to an unknown depth into the unexposed Slick Rock Member. The full lateral extent is unknown as bleached sediment is covered by younger strata to the north.

The bleached-unbleached contact always appears above the contact between the Slick Rock Member and the Earthy Member. From the top of the Slick Rock Member, the grey-red reduction front ranges from 2 m to a maximum of 4 m. Within the Slick Rock reservoir lithofacies, the bleaching is distributed uniformly and crosses lithofacies boundaries (Figure 0.7A). The sedimentological differences between these lithofacies do not seem to have had an impact on the migration of the reducing fluids. Only the well-cemented and relatively muddy wet interdune deposits remain (partially) unbleached. It suggests that these lithofacies acted as low permeability (0.1-1 mD) baffles (Figure 0.7B) and consequently fluid diffusion would have been slow (Kampman et al. 2016). Other lithofacies within the Slick Rock Member, those with high permeabilities (1000-10000 mD), would have provided relatively rapid flow paths.

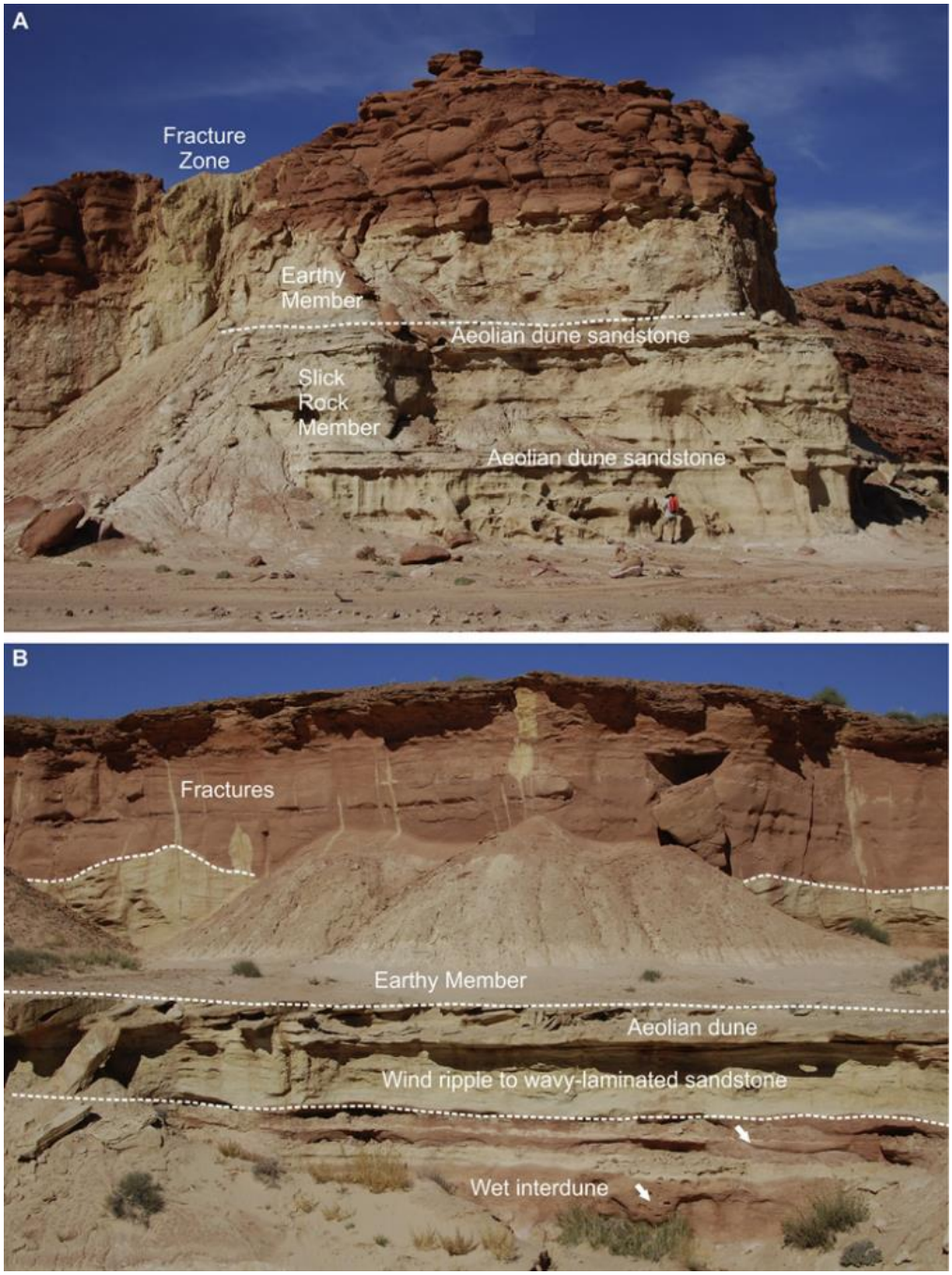

Figure 0.7: (A) East and (B) West of the palaeo-reservoir showing uniform bleaching of the Slick Rock Member. The bleached zone extends c. 4 m into the Earthy Member. Features associated with numerous fractures were formed where reducing fluids escape vertically through the fracture cluster (courtesy of Andrew Newell and Andrew Butcher).

4.3 Methodology

4.3.1 Justification for numerical modelling

Thus far, there has been no attempt to construct a reservoir scale flow model in order to replicate the observed patterns of bleaching produced by CO_2-charged reducing-fluids. The modelling programme undertaken here has two main objectives, firstly: to investigate the

regional pathways for the ingress of buoyant CO_2-charged fluids into the reservoir and; secondly, to examine the influence of heterogeneity on fluid flow at lithofacies' scale. Moreover, the Earthy Member seal provides an opportunity to investigate the properties and influence of a tight seal.

4.3.2 Reservoir model

The grid for the dynamic flow model had dimensions of 1500 m × 2000 m × 90 m and was discretised into 225,000 active cells [ni=75, nj=100, nk=30]. The grid spacing was uniform in the x, y and z directions throughout the model. A geological model was constructed in Petrel (Schlumberger 2016) and captures the essential observed geometry of the palaeo-reservoir as an NNW plunging anticline with up-dip closure against a fault (Figure 0.8). The palaeo-reservoir (Slick Rock Member of the Entrada Sandstone Formation) was subdivided into dipping facies each with a thickness of around 5 m. The facies model replicates, simplistically, the stacked beds of wet interdune, damp interdune and aeolian dune deposits within the Slick Rock Member, with each facies assigned a permeability of 10, 100, and 1000 mD and a porosity of 5, 15, and 25%, respectively. A permeability anisotropy of 0.1 was assumed for the reservoir. The permeability and porosity of the Earthy Member of Entrada Sandstone Formation, which acted as a topseal, was set at 0.1 mD and 0.01%, respectively. The reservoir and topseal properties used in the model are summarised in Table 0.3.

Table 0.3: Reservoir (Slick Rock Member) and topseal (Earthy Member) properties.

	Reservoir (Slick Rock Member)			**Topseal (Earthy Member)**
Property	lithofacies 1	lithofacies 2	lithofacies 3	Lithofacies 4
Porosity [%]	25	15	5	0.01
Rock permeability [mD]	1000	100	10	0.1

4.3.3 Flow modelling

The bleaching fluid was a low temperature (c. 27 °C) CO_2-saturated brine with a salinity of 2.5-7.0 wt% (Bodnar 2003; Wigley et al. 2012). As such, it is assumed that the bleaching occurred at a depth shallower than the probable maximum burial depth (2.5 km); hence, the depth was set at 1 km, with CO_2 in a supercritical state.

In order to predict the fate of injected CO_2 in the reservoir, numerical models need information on the relative permeability and capillary pressure of the CO_2-brine system

(Bennion and Bachu 2008). The experimental data on these two parameters are scarce, therefore, empirical formulations have been used to construct the capillary pressure (P_c), saturation (S) and relative permeability (k_r) relationship (Pc-S-k_r relationship). To generate the P_c-S-k_r relationships, numerical modelling studies have generally assumed the generic value for the pore size index typical of a sedimentary reservoir chosen for CO_2 storage (e.g., Rutqvist, Birkholzer and Tsang 2008; Birkholzer, Zhou and Tsang 2009; Oostrom et al. 2016). This value is considered constant for the entire storage formation regardless of the geological heterogeneity of the model. This assumption ignores any variation in the average pore size of rock lithologies within the layered reservoir, and since flow is dependent on the P_c-S-k_r relationship, the accuracy of the simulation results is jeopardised (Onoja and Shariatipour 2018). Herein, relative permeability and capillary pressure curves for different lithologies are taken from Onoja et al. (2019) and Onoja and Shariatipour (2018). Their study revealed that sediment gradation influenced CO_2 migration. Drainage relative permeability curves and capillary pressure curves used in this chapter are shown in Figure 0.9. Flow distribution was modelled under an isothermal condition of 27 °C and an initial pressure of 100 bars at 1000 m depth with the hydrostatic gradient of 0.1 bars/m. Initially, it was assumed that the reservoir contained 100% brine, with the mole fraction of 0.98 and 0.02 for water and NaCl, respectively. The simulations were performed using the ECLIPSE 300 compositional simulator with the CO2STORE option (Schlumberger 2017).

To maintain geomechanical stability and avoid damage to the reservoir, the injection pressure needs to remain below 80% of the lithostatic pressure at any point within the model (Breckels and van Eekelen 1982; USEPA 1994). The fracture pressure gradient varies from 0.108 to 0.205 bars/m in different regions in the United States; 0.18 bars/m fracture pressure was used in this study. The wells were controlled by the surface rate, with a maximum pressure limit of 180 bars. During simulation studies, the pressure did not reach this constraint. CO_2 was injected for 20 years followed by 1000 years post-injection period used to study the CO_2 plume migration.

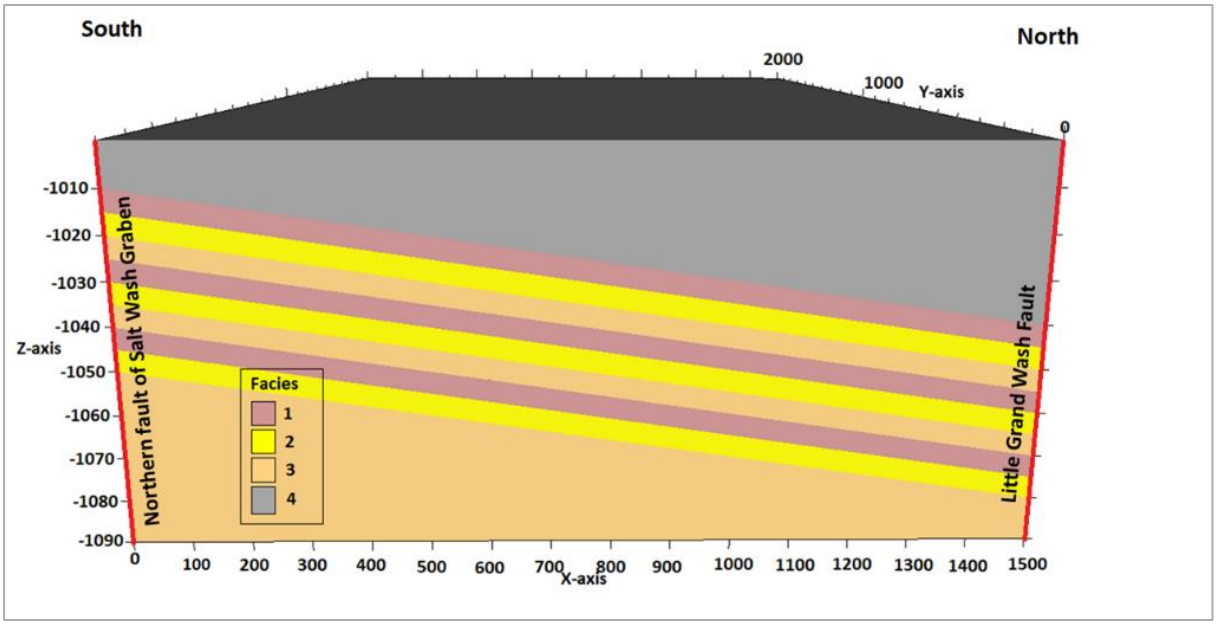

Figure 0.8: Reservoir model showing the distribution of lithofacies (Table 4.3) used for flow simulations. Little Grand Wash (LGW) fault is placed at the right-end of the model and the northern fault of the Salt Wash graben (SWG) is placed to the left-hand side of the model. Facies 1 permeability is 1000 mD, Facies 2 is 100 mD, Facies 3 is 10 mD and Facies 4 is 0.01 mD.

Figure 0.9: (a) Drainage relative permeability curve and; (b) Drainage capillary pressure curve for facies 1 (sandstone), facies 2 (silty sandstone), facies 3 (muddy sandstone) and facies 4 (sandy siltstone) (Onoja and Shariatipour 2018; Onoja et al. 2019).

4.3.3.1 Modelling to test regional pathways

The pathway for the ingress of buoyant reducing fluid into the Entrada Sandstone palaeo-reservoir is still uncertain, with possible routeways via the northern bounding fault of the Salt Wash graben and the Little Grand Wash fault further to the north (Figure 0.6). Numerical simulations were conducted to investigate which of these two major faults was the more likely pathway. To do so, three models were considered. In Model 1, a CO_2 injector well was completed on the left-side of the 3D model (southern-end) to simulate a fluid pathway from the northern fault of the Salt Wash graben. In Model 2, CO_2 was injected from the right-hand side of the 3D model (northern-end) and a source of CO_2 from the Little Grand Wash fault.

The injection rate was 4000 sm^3/day in these two models. In another study (Model 3), it was assumed that both faults were pathways, so injector wells were placed on both sides of the model. The injection rate was set at 8000 sm^3/day in Model 3 (4000 sm^3/day for each well). In all three models CO_2 was injected from the uppermost high-permeability layer (Table 0.4). The primary justification for such an injection point comes from field evidence that shows localised bleaching in the uppermost high-permeability sandstone, just below the caprock, on the flanks of the palaeo-reservoir (Figure 0.2). These uppermost high-permeability layers are, therefore, likely to have formed pathways for buoyant reducing fluids moving into the reservoir (Shariatipour, Pickup and Mackay 2016). The transmissibility of the faults was assumed to be 0 in j direction, thus acting as a lateral barrier to flow.

Table 0.4: CO_2 Injector location, perforation location and location of faults in all four models.

	Injector location	Location of Perforation	Location of the Faults
Model 1	(i=1, j=50)	(k=11-12)	i:1-1, j:1-100, k:1-30
Model 2	(i=75, j=50)	(k=11-12)	i:75-75, j:1-100, k:1-30
Model 3	(i=1, j=50) and (i=75, j=50)	(k=11-12)	i:1-1, j:1-100, k:1-30 i:75-75, j:1-100, k:1-30

4.3.3.2 Modelling to test the effect of seal properties

The Earthy Member sharply overlies the Slick Rock Member, and the reduction front (grey-red contact) is located 2-4 m above the Slick Rock Member. Figure 0.7 is suggesting that the Earthy Member acted as an imperfect seal into which the CO_2 ingress was through slow diffusion. To test the effects of seal properties two models were considered, one using properties of the Earthy Member obtained from the field study with a porosity and permeability of 0.01% and 0.1 mD, respectively (Model 1). In Model 2, a tight seal with a porosity value of 0.01% and permeability of 10^{-6} mD was used.

4.3.3.3 Modelling to test the impact of reservoir heterogeneity

To test the impact of reservoir heterogeneity on flow two models were compared. Model A was configured as previously described and shown in static mode of Figure 0.8 with facies varying in permeability across four orders of magnitude up to a maximum value of 1000 mD. To account for the possibility of higher permeability values for aeolian sandstones, Model B was modified to include facies with a permeability range across six orders of magnitude up to a maximum of 10,000 mD (Table 0.5).

Table 0.5: Reservoir and topseal properties in Model A and Model B.

Model A	Reservoir (Slick Rock Member)			Topseal (Earthy Member)
Property	lithofacies 1	lithofacies 2	lithofacies 3	lithofacies 4
Porosity [%]	25	15	5	0.01
Permeability [mD]	1000	100	10	0.1

Model B	Reservoir (Slick Rock Member)					Topseal (Earthy Member)
Property	lithofacies 1	lithofacies 2	lithofacies 3	lithofacies 4	lithofacies 5	lithofacies 6
Porosity [%]	35	25	20	15	10	0.01
Permeability [mD]	10,000	1000	100	10	1	0.1

4.4 Results

The first model tested whether the palaeo-reservoir was filled via the northern bounding fault of the Salt Wash Graben, with CO_2 injected from the left-hand side of the model (Figure 0.10). During the injection period, the simulation results demonstrate that, due to injection pressure, CO_2 migrated laterally through the uppermost high-permeability layer near the injection well and migrated into the base of the topseal (Figure 0.10a). However, in the subsequent shut-in period (Figure 0.10b), CO_2 moved upwards under buoyancy, migrated through the low-permeability Earthy Member topseal, and ultimately may have reached the surface. At the end of the simulation, it is observed that CO_2 mainly migrated vertically through the imperfect seal rather than downdip through high permeability lithofacies. Figure 0.11 provides the (a) front and (b) top view of the CO_2 mole fraction at the end of the simulation and shows that CO_2 migration was limited to the area near the injection well. Overall, this model does not appear to be a good analogue for the bleaching seen in the palaeo-reservoir, which extends over a considerably larger area 1150 m parallel to the Salt Wash graben and 408 m perpendicular to the Salt Wash Graben fault (Figure 0.1B).

In the second model, CO_2 was injected through the uppermost high permeability layer of the Slick Rock reservoir from the northern boundary of the model, simulating a pathway via the Little Grand Wash fault. The injection location was downdip from the palaeo-reservoir in the northern region of the north-plunging Green River Anticline. Figure 0.12 shows the CO_2 mole fraction during the injection period and post-injection period. During the injection period, CO_2 migrated up-dip away from the well through the high-permeability carrier bed due to

buoyancy forces and diffused into the bottom part of the topseal. After 20 years, the injection was stopped and the simulation was continued for 1000 years. During this period CO_2 continued to migrate up dip through both the Slick Rock Member and base of the Earthy Member. Depending on injection rates, CO_2 might reach the other side of the model that is impervious to flow. Figure 0.13 illustrates the front view and top view of the CO_2 mole fraction when CO_2 was injected from a down-dip location on the Little Grand Wash fault. In this case, the flow was distributed across a broader area than what had been observed from injection via the northern bounding fault of the Salt Wash graben. The model appears to provide a closer match to bleaching observed in the palaeo-reservoir. In particular, through:

(1) The broad area of bleaching observed within the main reservoir zone on the anticlinal crest [see Figure 4.1B]

(2) The greater penetration of bleaching into the topseal in the main fold-crest reservoir [see Figure 0.7]

(3) The general localisation of flow within high-permeability carrier beds in parts of the reservoir distal from the fold crest [see Figure 0.2].

A primary fluid source from the Little Grand Wash fault also matches the observations of Dockrill and Shipton (2010), where fault travertine deposits are particularly thick and well-developed, while those along the Salt Wash Graben are less so.

It is possible that both faults were routes for fluids into the palaeo-reservoir and this scenario was explored in a third model. Figure 0.14 illustrates the CO_2 mole fraction at the end of this simulation. Modelling indicates that some component of up-dip migration of CO_2-charged fluids from the Little Grand Wash fault was required to produce the observed patterns of bleaching.

Figure 4.15 shows how caprock properties contribute to storage security. A higher CO_2 mole fraction was observed in Model 1 with an imperfect Earthy Member. If the immediate seal to the reservoir is not completely secure it is essential to evaluate the integrity of the regional caprock. To maintain the security of the storage project, and ensure sufficient containment of the injected CO_2, it is necessary to consider the optimum injection pressure to avoid CO_2 migration through the caprock by exceeding the capillary entry pressure (Pruess 2006).

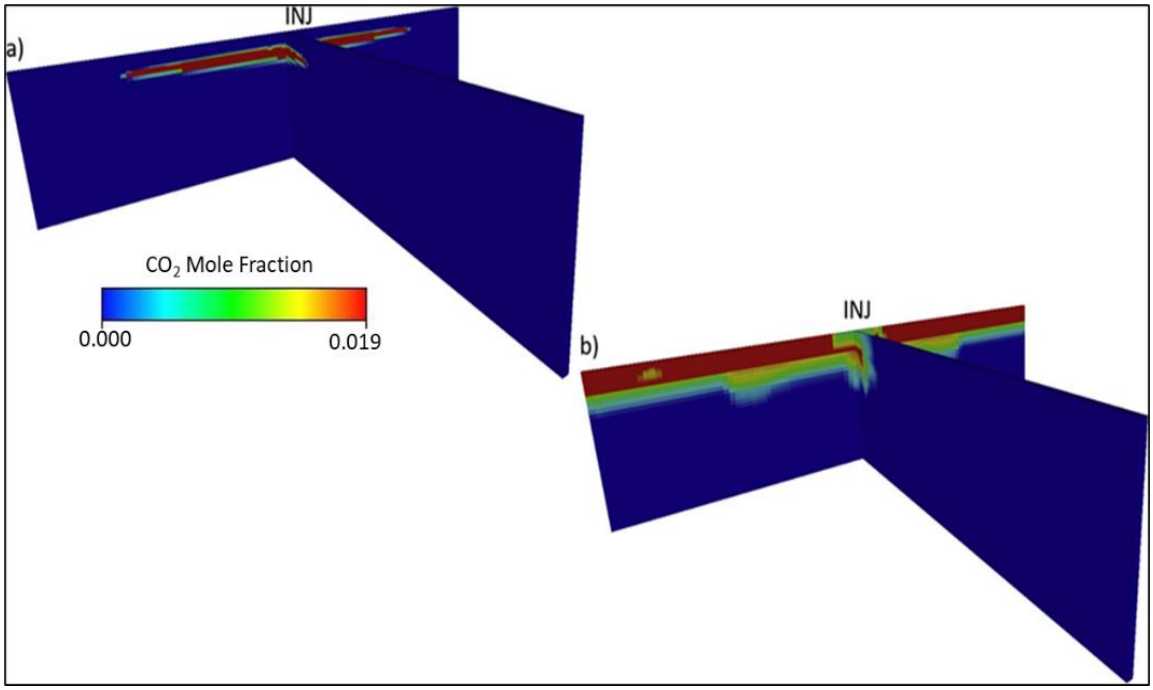

Figure 0.10: a) CO_2 mole fraction at the end of the 20 years injection period and (b) At the end of the 1000 years post-injection period. CO_2 pathway is northern fault of the Salt Wash graben. INJ = Injection points.

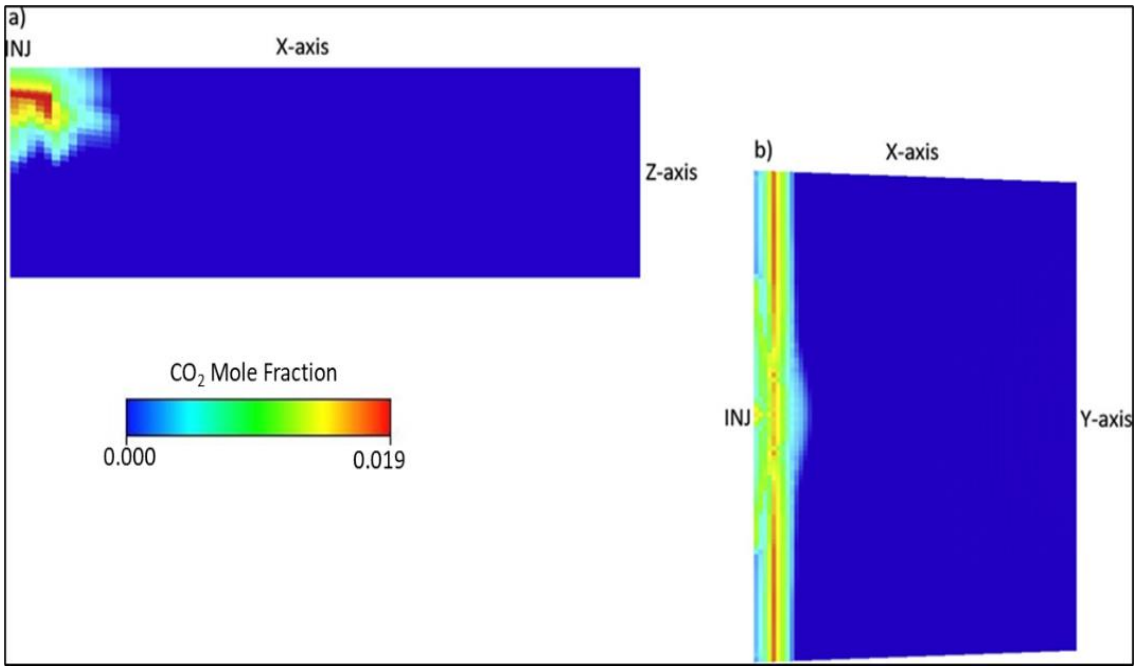

Figure 0.11: a) Front view and (b) Top view of the CO_2 mole fraction at the end of the simulation. CO_2 pathway is northern fault of the Salt Wash graben. INJ = Injection points.

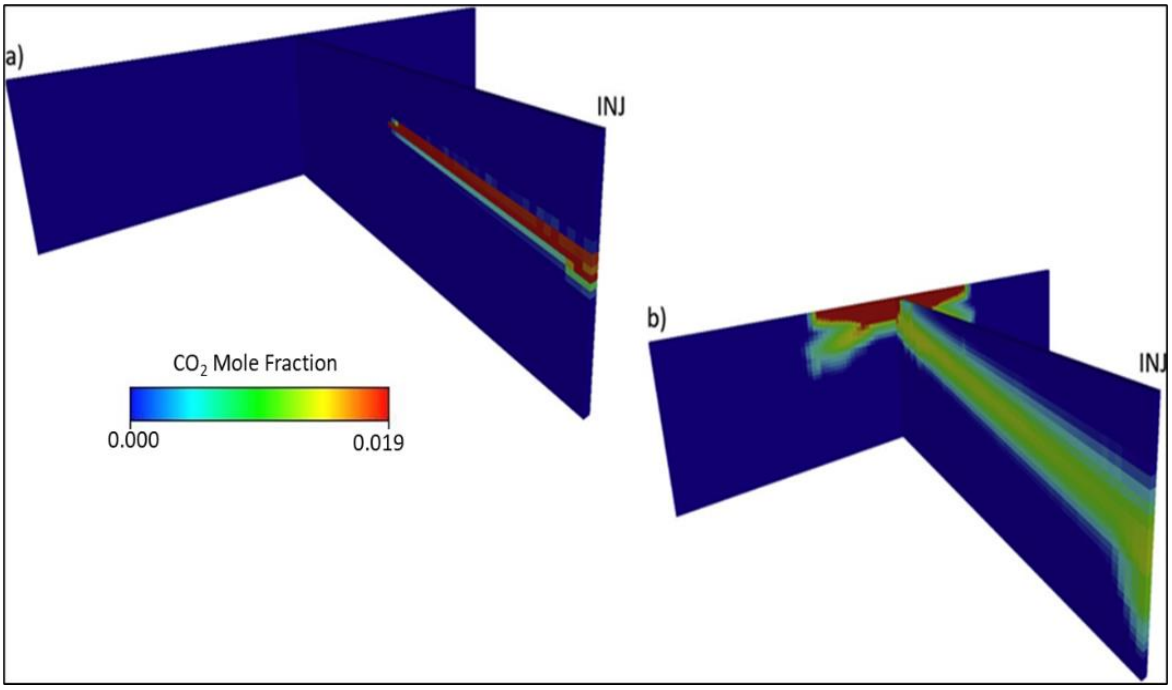

Figure 0.12: a) CO_2 mole fraction at the end of the 20 years injection period and (b) At the end of the 1000 year post injection period. CO_2 pathway is the Little Grand Wash fault. INJ = Injection points.

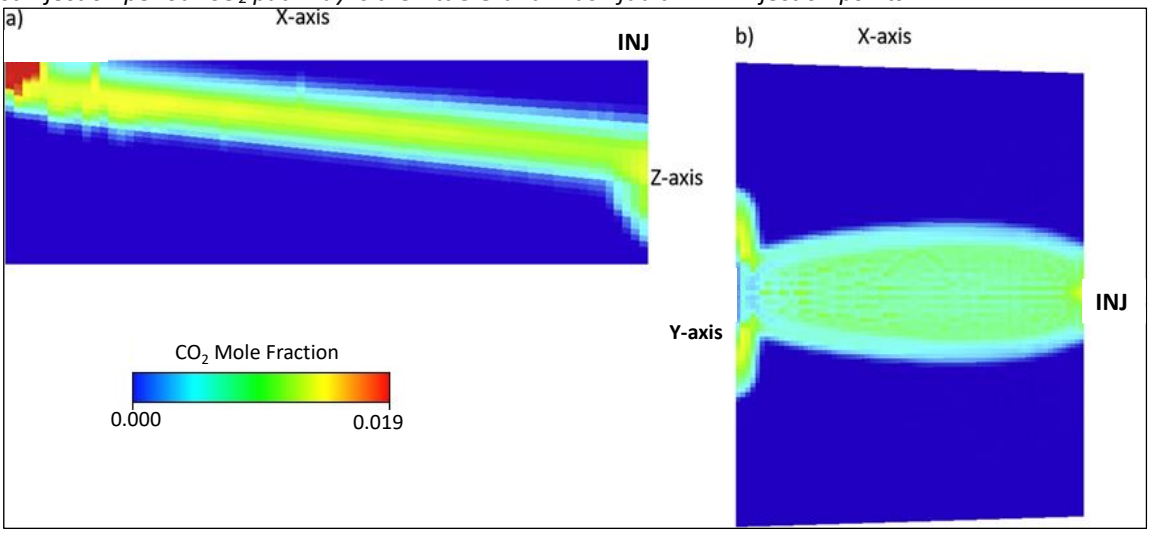

Figure 0.13: a) Front view and (b) Top view of CO_2 mole fraction when CO_2. Injected from the right-hand side of the model. CO_2 pathway is the Little Grand Wash fault. INJ = Injection points.

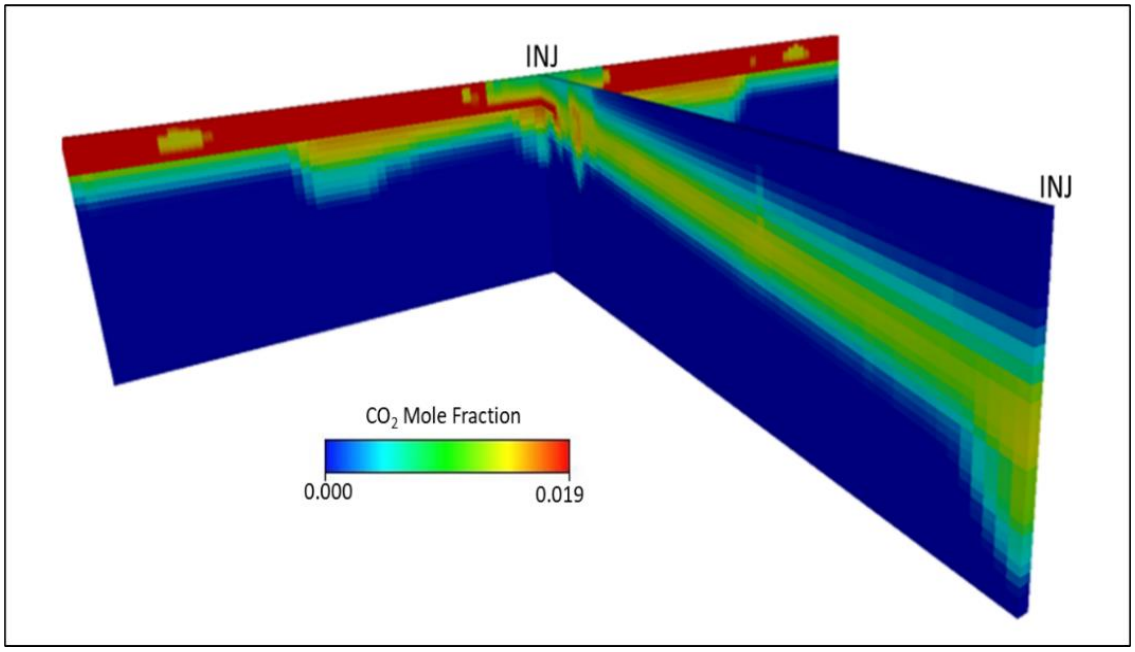

Figure 0.14: CO_2 mole fraction in Model 3. CO_2 pathways is both the Little Grand Wash fault and Salt Wash graben.

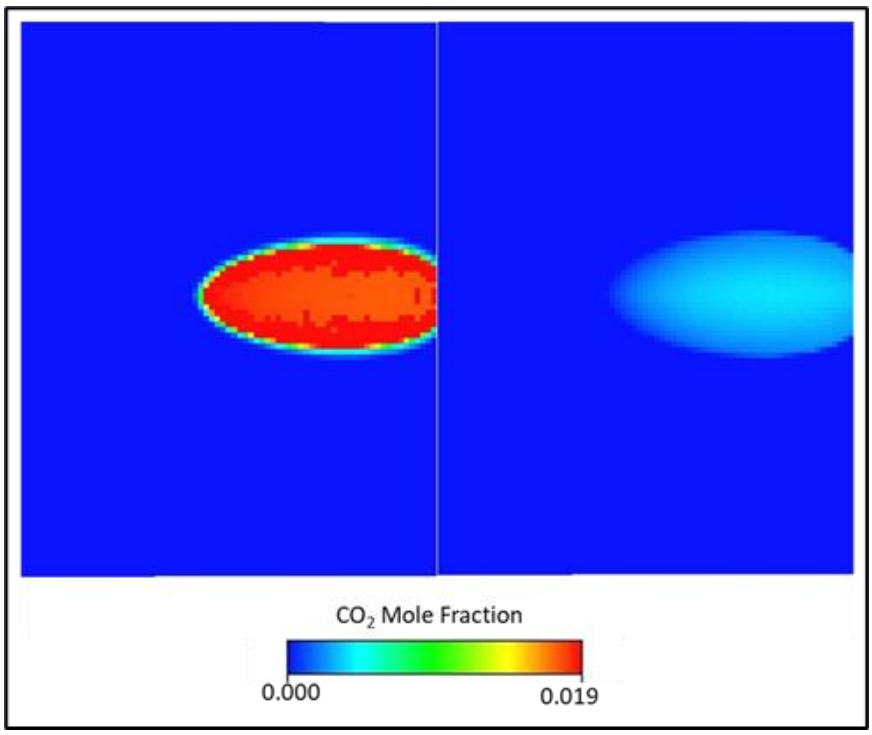

Figure 0.15: CO_2 mole fraction at the base of the imperfect seal (left) and tight seal (right).

Figures 4.16 and 4.17 show the total amount of dissolved CO_2 and pressure in the base of the topseal in Model 1 and Model 2, respectively.

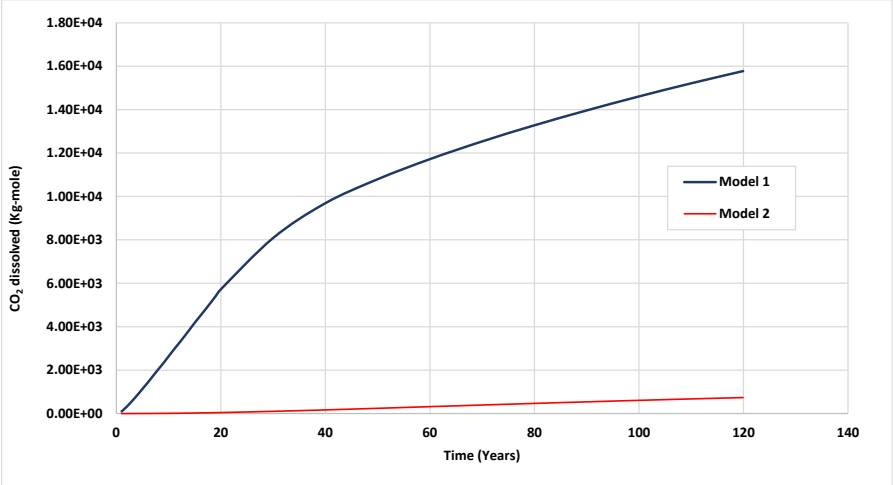

Figure 0.16: Amount of CO_2 dissolved in the base of the topseal in Model 1 and Model 2.

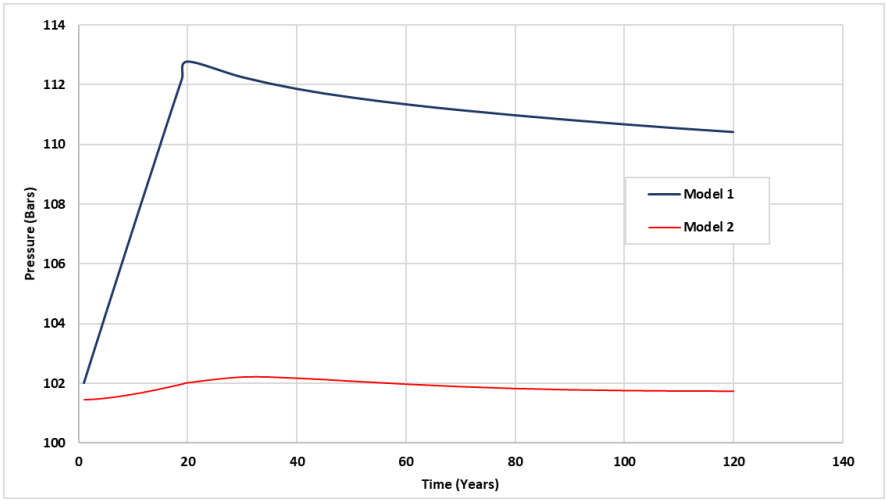

Figure 0.17: Amount of pressure increase in the base of the topseal in Model 1 and Model 2.

Both models, in the test on the impact of reservoir heterogeneity, displayed a uniform and widespread distribution of injected CO_2 consistent with the observed distribution of bleaching (Figure 4.18). Figure 4.19 plots the amount of dissolved CO_2 against time in the two models and shows that CO_2 dissolution is significantly higher in Model B than Model A during the injection period. In Model B, layers with high permeability (10,000 mD) allowed for a faster migration of CO_2; and consequently, the CO_2 plume covered a broader area more quickly, increasing the contact with formation brine causing more CO_2 dissolution (around 42%). However, at the end of simulation study, CO_2 swept uniformly across all lithofacies boundaries with different permeability values resulting in an equal volume of CO_2 dissolution in the brine of both models.

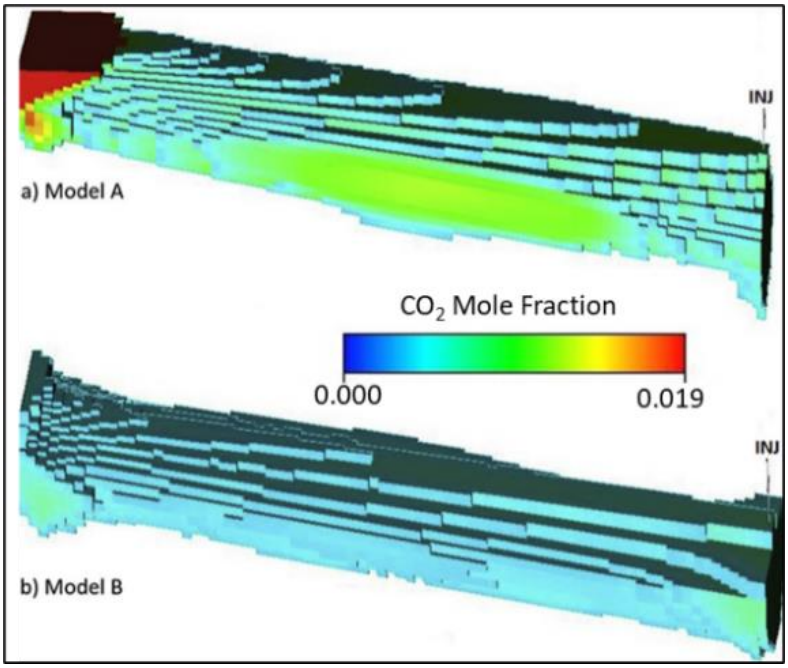

Figure 0.18: (a) Distribution of CO_2 in the model with a permeability range of four orders of magnitude (see Table 4.5 Model A). (b) Distribution of CO_2 in the model with a permeability range of six orders of magnitude (see Table 4.5 Model B). Both scenarios result in a relatively uniform distribution of CO_2 across the boundaries of layered lithofacies.

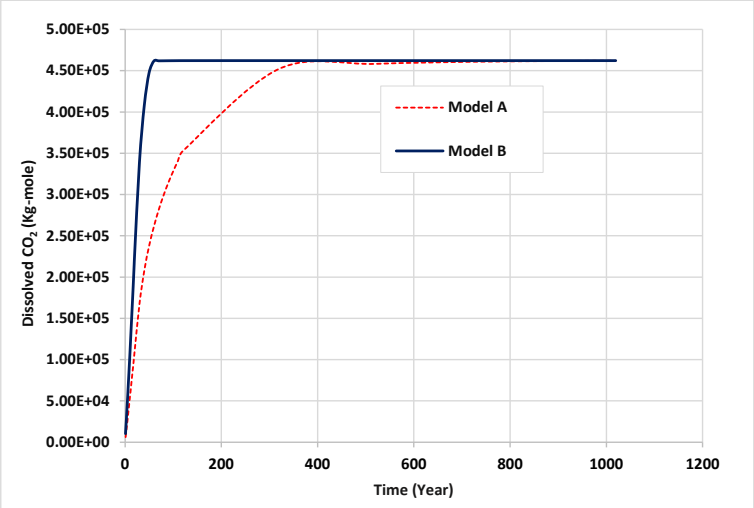

Figure 0.19: Total amount of CO_2 dissolution in the brine in Model A and Model B.

4.5 Discussion

The Entrada Sandstone Formation exhibits a high degree of heterogeneity; this is a typical characteristic of 'wet aeolian' facies. The main assumption of this study was that the Entrada Sandstone Formation should have had a significant influence on the distribution of CO_2 charged reducing fluids and thus the distribution of bleached sediment. However, the analyses of outcrops show that within the Slick Rock Member, the palaeo-reservoir, lithofacies boundaries and heterogeneity had relatively little impact on the distribution of

bleaching; even though large permeability ranges of at least three orders of magnitude have been recognised at the outcrop. Flow simulations on models of the Slick Rock Member palaeo-reservoir confirms the outcrop observations. In the modelling study, relatively little confinement of injected CO_2 within layers of highly contrasting permeability was observed. The study demonstrates a relatively uniform distribution of injected CO_2 even where the target formation displays considerable heterogeneity and permeability contrasts.

However, it is also necessary to consider the nature of the invasive fluids in order to justify the outcrop and modelling observations. At the Salt Wash graben the fluids were likely to have been low viscosity brines enriched with CO_2 and CH_4 (Wigley et al. 2013) rather than high viscosity oils. The results of this study would thus appear to validate Flora's Rule (Ringrose and Bentley 2015), a general rule of thumb that has its foundation in the viscosity term in the Darcy flow equation:

$$u = \frac{-k}{\mu} \nabla(p) \qquad 4.1$$

Where u is velocity, k is permeability, μ is viscosity and $\nabla(p)$ is pressure gradient.

Flora's rule states that while viscous fluids such as oil might be sensitive to one or two orders of permeability variation for a given porosity class, gas reservoirs might be sensitive to three-orders of magnitude. Therefore, some heterogeneities may behave quite similar in gas reservoirs. The important practical significance of the Flora's Rule is in understanding how much detail is needed when reservoir modelling. It can be argued that some reservoirs may not require complex and detailed reservoir models, especially those involving low viscosity fluids. A high degree of permeability heterogeneity is required to explain the rationale of a complex modelling exercise (Bentley and Ringrose 2018).

This appears to have been the case for the palaeo-reservoir in the Salt Wash graben where bleaching is uniform across lithofacies boundaries. The widespread bleaching within this palaeo-reservoir suggests that detailed lithological information may not be required to achieve a realistic simulation.

It was also assumed that as bleaching was widespread adjacent to the northern fault of the Salt Wash graben, this fault was the main flow pathway for CO_2 charged reducing fluids; however, the flow simulations suggest otherwise. Given the present structural configuration of the Entrada Sandstone Formation at Salt Wash graben, some component of up-dip fluid migration from the Little Grand Wash fault towards the Salt Wash graben was required.

Modelling studies reproduce the observed patterns of bleaching. One result of this study confirms, as with previous studies, that the two major faults did not act as seals and were leakage paths for fluids.

Both the analysis of outcrop and flow simulation suggests that a knowledge of lithofacies variation and structural configuration is essential to gain a full understanding of the pathways of transient flow. The significance of reservoir lithofacies variation on the long-term distribution of fluids only diminished when a permanent and perfect seal is guaranteed; otherwise, the lithofacies can reduce the reliance on a topseal.

4.6 Conclusions

The Entrada Sandstone Formation is an exhumed palaeo-reservoir and example of a wet aeolian deposition system. The complex metre-scale layered heterogeneity is the production of the migration and accretion of aeolian dune and wet interdune deposits. The Entrada Sandstone Formation is potentially a useful analogue for comparable continental red-bed formations that are being consideration for CO_2 geological storage on the NW European continental shelf. On the Colorado Plateau, the Entrada Sandstone Formation has been significantly bleached as a result of iron-oxide reduction due to the high fluxes of CO_2-charged reducing fluids. Therefore, this sandstone offers an excellent opportunity to understand how reducing fluids migrate and accumulate within heterogeneous aeolian deposits.

A series of flow models have been constructed and run to study fluid migration paths, and to investigate the level of heterogeneity and geological details required to accurately simulate flow, and thus lead to a reduction in the time and cost of computer simulations.

It is highly probable that the main CO_2 pathways, which caused the bleaching of the Entrada Sandstone Formation and changed the red sandstone to grey, were via the Little Grand Wash fault or the Little Grand Wash fault and northern fault of the Salt Wash graben. However, it is very unlikely that the Salt Wash graben was the sole pathway for the Green River as the anticline is plunging with up-dip closure against the Salt Wash graben. Some components of up-dip migration of CO_2-charged fluids from the Little Grand Wash fault was required to produce the observed patterns of bleaching.

A modelling study of a bleached palaeo-reservoir within the Entrada Sandstone Formation has helped test and validate Flora's Rule. The Flora Rule, which has its foundation in the viscosity term in Darcy flow equation, indicates that a gas reservoir is only sensitive to

permeability contrasts of three orders of magnitude. Despite the geological heterogeneity and strong permeability contrasts in the Entrada Sandstone Formation observed at the outcrop, the bleaching is uniformly distributed across lithofacies boundaries. This has been supported herein by flow modelling. It can be concluded that the geological heterogeneity of a reservoir needs to be sufficiently high, and that a range of 1-10^3 mD should not greatly impede the relatively uniform distribution of CO_2 charged fluids throughout a reservoir. This research reveals that the full spectrum of lithofacies is not required when modelling with fluids of lesser viscosity (i.e., CO_2), as they are less sensitive to heterogeneity than high viscosity fluids.

Of significance are the properties of the seal when entrapping injected CO_2. The seal in the study area is the Earthy Member, which has a higher permeability and porosity than typical seals and this has allowed CO_2 diffusion into the seal of up to 4 m. This outcome has been repeated in the simulation studies. The results indicate that the optimum injection rate and perforation location can enhance CO_2 storage security when the topseal has atypical caprock properties.

Chapter 5

Application of X-shaped conjugate deformation bands as structural traps

5.1 Introduction

Permian and Triassic sandstone formations of continental aeolian origin are considered to be important target sites for the geological storage of CO_2 in the sedimentary basins of NW Europe, e.g., the Permian Collyhurst Sandstone of the East Irish Sea Basin (Gamboa et al. 2019) and the Permian Leman Sandstone of the Southern North Sea Basin (Holloway et al. 2006). Aeolian sandstone formations offer a good storage potential as they are often thick, have a high porosity-permeability and are relatively homogeneous. However, their reservoir potential can be impacted on by the formation of deformation bands (Shipton et al. 2002), as these structures are linked to the reduction of effective permeability.

Deformation bands have highly variable geometries and dimensions [review by Fossen et al. 2017] but, in general terms, often occur as X-shaped conjugate sets composed of intersecting planes with opposing dip direction. This chapter aims to analyse the effects of a single conjugate set of deformation bands on CO_2 flow. This research is important as it provides an idea of the flow at the scale of one conjugate set of bands, which helps to understand the flow at a reservoir scale. The outcrop analogue observed in the Permian Penrith Sandstone Formation of NW England has implications for the flow simulations applied here.

The key questions addressed in the chapter are:

1) How does the geometrical architecture of a single conjugate set of bands influence the CO_2 flow?
2) How much permeability contrast is needed for a set to trap CO_2 effectively?
3) Does the permeability contrast along deformation bands affect the flow?
4) Importantly, do these sub-seismic reservoir heterogeneities have applications as structural traps?

5.2 Origin and characteristics of deformation bands

Structures resulting from different modes of failure are classified by Aydin, Borja and Eichhubl (2006) into deformation bands and sharp discontinuities. In contrast to failure in stiff and low-porosity rocks, which cause the formation of extensional and shear fractures (Fossen et al. 2007), rock failure in a porous granular material (φ>15%), such as sandstones and conglomerates (Aydin and Johnson 1983; Fisher and Knipe 2001; Aydin, Borja and Eichhubl 2006; Nicol et al. 2013; Fossen et al. 2017) or carbonate grainstone (Tondi et al. 2006; Fossen et al. 2017; Rotevatn et al. 2017), can produce millimetre to centimetre-thick, tabular-planar, low displacement deformation features of localised strain, termed deformation bands (Aydin 1978). The differences between deformation bands and fractures are summarised in Table 0.1.

The term deformation band was introduced by Aydin (1978), but they are also known as cataclastic faults (Fisher and Knipe 2001), shear bands (Menéndez, Zhu and Wong 1996), microfaults (Jamison and Stearns 1982) and granulation seams (Pittman 1981) (Table 0.2). Although deformation bands can extend for tens or hundreds of metres (Aydin 1978; Aydin and Johnson 1983; Fossen et al. 2007), they cannot, however, be identified through seismic imaging (Fowles and Burley 1994) and they remain unrecognised in many sandstone aquifers and reservoirs (Sternlof, Pollard and Durlofsky 2006). These structural heterogeneities can develop in non-tectonic and tectonic settings (extensional or contractional) (Jamison and Stearns 1982; Fisher and Knipe 2001; Ballas, Fossen and Solivia 2015; Zuluaga et al. 2016; Fossen et al. 2017). In a contractional regime deformation bands are widely and evenly distributed, whereas in an extensional regime they are concentrated around major faults (Solum et al. 2010; Soliva et al. 2013; Schueller et al. 2013; Zuluaga et al. 2016). From an individual deformation band to a slip plane, the offset can be from a few millimetres to tens of metres (Jamison and Stearns 1982; Aydin and Johnson 1983; Antonellini and Aydin 1994).

Deformation bands can be classified kinematically (Aydin, Borja and Eichhubl 2006) into three end-members: dilation, compaction and shear deformation bands; however, a combination of the three is common.

Table 0.1: Several significant differences between deformation bands and ordinary fractures (Fossen et al. 2007).

Deformation bands	Occur in highly porous granular media	Tabular discontinuities	Maximum of a few centimetres displacement	Maintain or increase cohesion	Reduction in porosity and permeability
Ordinary fractures	Occur in non-porous and low porosity media	Sharp discontinuities	Metre scale displacement	Cohesion is lost or reduced	Increase in permeability

They can also be classified in terms of the main deformation mechanism operating during their formation. The processes of deformation in a porous granular material are facilitated by the presence of pore space that allows for several deformation mechanisms. These deformation mechanisms are controlled, in turn, by internal (rock properties) and external factors (burial depth and stress state) (e.g., Fossen et al. 2007; Ballas, Fossen and Solvia 2015). Host rock properties include mineralogy, grain size, shape, sorting, cementation and porosity. The main mechanisms involved in the formation of deformation bands are grain reorganisation (Twiss and Moores 1992; Du Bernard et al. 2002, Rawling and Goodwin 2003); cataclasis (Aydin 1978; Aydin and Johnson 1983; Underhill and Woodcock 1987; Du Bernard et al. 2002; Rawling and Goodwin 2003; Saillet and Wibberley 2010; Rotevatn and Fossen 2011; Fossen et al. 2015); phyllosilicate smearing (Antonellini and Aydin 1994; Fisher and Knipe 2001); and dissolution and cementation (Leveille et al. 1997; Tondi et al. 2006; Fossen et al. 2007). In porous siliciclastic rocks, grain reorganisation and cataclasis are primary mechanisms, with dissolution and cementation often secondary (Aydin 1978; Antonellini and Aydin 1994; Leveille et al. 1997; Fisher and Knipe 2001; Fossen et al. 2007; Rotevatn and Fossen 2012). These mechanisms result in various types of deformation bands, include disaggregation, phyllosilicate and cataclastic bands each with different petrophysical properties (e.g., porosity, permeability and capillary entry pressure) that can impact fluid flow.

5.3 Petrophysical properties of deformation bands and their effect on fluid flow

Deformation bands can act as both flow conduits and flow barriers; however, most observations have shown that deformation bands reduce porosity and permeability to some extent (Aydin 1978; Underhill and Woodcock 1987; Antonellini and Aydin 1994; Shipton et al. 2002; Rotevatn et al. 2008; Ballas, Fossen and Solvia 2015). Permeability reduction depends on the type of deformation band. While disaggregation bands generally have little or no

impact on the porosity and permeability, phyllosilicate bands, a sub-category of disaggregation band, can reduce permeability by five orders of magnitude (Fisher and Knipe 2001). Cataclastic bands, in extreme cases, can result in a permeability reduction of up to six orders of magnitude (e.g., Underhill and Woodcock 1987; Antonellini and Aydin 1994; Fisher and Knipe 2001; Shipton et al. 2002), and commonly two to four orders of magnitude relative to the host rock (e.g., Torabi, Fossen and Alaei 2008). Deformation bands have a porosity of about one order of magnitude less than the surrounding host rock (Aydin and Johnson 1983; Antonellini and Aydin 1994; Torabi and Fossen 2009; Griffiths et al. 2016). In deformation bands where cataclasis is well-developed, capillary entry pressure measurements confirm the effective local sealing capacity of these structures with respect to the non-wetting phase (Antonellini and Aydin 1994; Torabi, Fossen and Alaei 2008; Torabi and Fossen 2009; Torabi, Fossen and Braathen 2013). Table 0.2 summarised the terms used in the literature for deformation bands, deformation mechanisms and the properties of deformation bands in various formations.

Porosity, permeability (from zero to two or three orders of magnitude (Fossen et al. 2007; Torabi, Fossen and Alaei 2008)) and thickness also vary along the bands (Rotevatn et al. 2013). Using flow simulations, Rotevatn et al. (2017) investigated the permeability and flow effects of individual deformation bands in porous carbonate rocks, concluding that deformation bands may have a greater influence than previously thought. In some lower permeability host rock, they found that deformation bands seriously impede flow when the permeability of the bands is one or two orders of magnitude less than the low to medium permeability host rock. This contradicts previous studies that have been shown that deformation bands must have a large permeability contrast (three to four orders of magnitude) relative to the host rock to affect flow (e.g., Zuluaga et al. 2016). Furthermore, it is previously indicated by Ringrose and Bentley (2015) and Newell et al. (2019) that gas reservoirs might only be sensitive to three orders of magnitude permeability contrast. Given the contradicting results and since it is not yet clear how much permeability contrast is necessary for the deformation bands to act as flow barriers, particularly in gas reservoirs, this study expands our knowledge on the effects of these structures in such reservoirs.

5.4 Deformation bands: an outcrop analogue

5.4.1 Penrith Sandstone of NW England

The Lower Permian Penrith Sandstone Formation of north-west England is a classic example of a high porosity aeolian sandstone that contains numerous deformation bands (Fowles and Burley 1994). The Penrith Sandstone consists of up to 460 m of aeolian cross-bedded sandstone (Lower Permian Rotliegend equivalent) contained within the fault-bounded Vale of Eden Basin (Figure 0.1). It unconformably overlies Carboniferous deposits and is conformably overlain by the Upper Permian Eden Shale and Triassic St Bees Sandstone (Figure 0.2) (Arthurton and Wadge 1981). The Penrith formation is red-brown and composed mostly of well-rounded and well-sorted fine to coarse-grained sandstone.

5.4.2 Deformation bands in Penrith Sandstone

Deformation bands in the Penrith Sandstone are typically seen as low porosity white bands standing out against a background of porous and undeformed red sandstone on weathered outcrop surfaces (Figure 0.3). As recognised elsewhere (Aydin and Johnson 1983), the bands show a continuum of development from millimetre-wide seams which offset stratigraphic markers by a few millimetres (Figure 0.3a), through to anastomosing clusters several centimetres thick (Figure 0.3b) and occasional zones of up to one metre thick, with slip surfaces developed along the margin (Figure 0.3c). The length of the deformation bands is highly variable. Seers and Hodgetts (2016) showed that individual deformation band segments are typically around 0.7 m in length, but these can combine to form zones of deformation bands that are often 1-10 m in length in a vertical direction and may extend for 15 m or more in the bedding parallel (horizontal) plane. The deformation bands typically dip at high angles of 60-85 degrees and form two sets with opposing dip azimuths (Figure 0.4). Deformation bands and band clusters demonstrate a wide range of dihedral angles (most commonly between 35-95^{o}) in the extensional regime (Fossen et al. 2017).

Table 0.2: Terminology, deformation mechanisms and the properties of deformation bands in various formations.

Case	Name	Mechanism	Property	References
Simpson Group, Oklahoma, USA	Granulation seam	Cataclasis	Reduced porosity and permeability	Pittman (1981)
Nubian Sandstone, Suez rift	Cataclastic slip band	Cataclasis	Reduced porosity and permeability	Du Bernard et al. (2002)
Sandstone of Savage Creek marine terrace, northern California, USA	Dilation bands	Granular flow with dilational component	Transient increase in porosity and permeability	Du Bernard, Eichhubl and Aydin (2002)
The Brent Group and equivalent, North Sea	Fault	Compaction, dissolution and cementation	In clean sandstone, they show the same value. In clay rich sandstones show permeability reduction	Fisher and Knipe (2001)
The Rotliegendes	Fault	Cataclasites and cementation	Reduced porosity and permeability	Fisher and Knipe (2001)
Navajo and Entrada Sandstones, Utah, USA	Deformation bands or small faults	Cementation, movement of grains, cataclasis	Reduced porosity and permeability	Aydin (1978)
Sandstone of the Troll Field, northern North Sea	Micro fracture		Permeability is reduced. No significant effects on reservoir communication	Gabrielsen and Koestler (1987)
Navajo Sandstone, USA	Deformation-band shear zones	Mechanical grain fracturing	Reduced porosity and permeability	Davis et al. (2000)
Penrith Sandstone, NW England	Cataclastic slip band	Cataclasis and mechanical dilation	Reduction in properties due to cataclasis and enhancement of properties due to dilation	Fowles and Burley (1994)
Wingate Sandstone, Colorado, USA	Microfaults	Intergranular cataclastic flow	Porosity and permeability reduction	Jamison and Stearns (1982)

Figure 0.1: (a) Map showing the location of the Eden field site in north-west England. (b) Geological map of the Vale of Eden Basin and distribution of the Penrith Sandstone, Eden Shale and St Bees Sandstone (Lafare, Peach and Hughes et al. 2016).

Figure 0.2: Outcrops of the Penrith Sandstone are within the Eden Gorge overlain by Eden Shale and St Bees Sandstone formations. NE-SW trending faults, which form in association with the deformation bands, are also presented (Pourmalek et al. 2021).

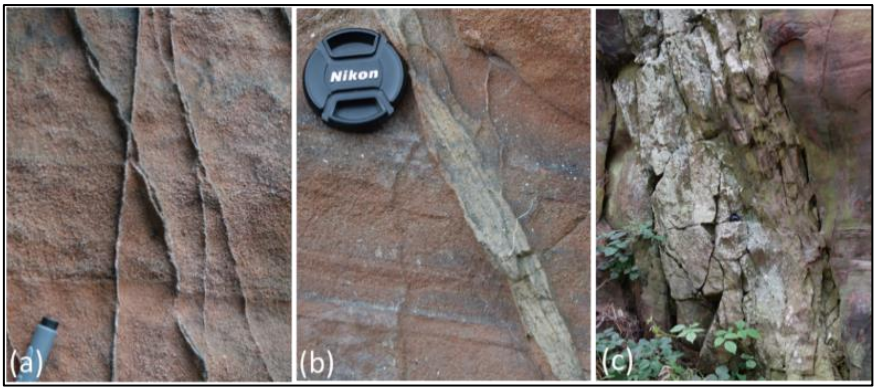

Figure 0.3: Variations in deformation band development from (a) Millimetre-wide bands showing conjugate cross-cutting arrangement; (b) Multiple anastomosing bands forming a zone several centimetres across; and (c) Thick zone composed of multiple bands with slip surface on the hanging wall (right hand) side (courtesy of Andrew Newell).

Figure 0.4: Typical arrangement of deformation bands in conjugate sets with a dihedral angle of c. 45 degrees [shown in the figure]. This value is used for the acute angle of intersection between two cross-cutting deformation bands throughout the flow modelling (courtesy of Andrew Newell).

5.5 Methodology

A range of numerical simulations was conducted in order to investigate x-shaped deformation bands and their influence on CO_2 flow. For this purpose, static models are based on the observations gathered from a Penrith Sandstone outcrop (i.e., porosity, permeability, shape and maximum thickness) that have implications for the flow simulations (Pourmalek et al. 2021). The static models were generated in Petrel software (Schlumberger 2016). Dynamic modelling studies were conducted using ECLIPSE 300 (Schlumberger 2017) with the CO2STORE module. For this study, a step-by-step incremental change of parameters (dihedral angle, hinge line plunge and permeability contrast) are followed in order to isolate and evaluate the effects of a conjugate set on flow movement. The results of this study will help

establish how important and effective sub-seismic scale structural heterogeneities (i.e., conjugate deformation bands) are when considering high-porosity sandstones as potential subsurface storage for CO_2.

5.5.1 Reservoir model

A simplified sandbox model with a spatial dimension of 20 m × 20 m × 20 m was developed and discretised into a total of one million active cells [ni=100, nj=100, nk=100] (Table 0.3). It is assumed that the host rock is homogeneous, and by doing so, the effects of deformation bands on fluid flow are isolated. In this chapter, to accurately calculate the influence of deformation bands on fluid flow, a discrete fracture network was used to account for a set of conjugate bands. A discrete fracture network [DFN] refers to a computational model that explicitly represents the geometrical properties of fractures, joints or deformation bands (Lei, Latham and Tsang 2017). Deformation bands were given a thickness of 20 cm, which was the minimum cell size at which the reservoir modelling software was still able to operate and the modelling was computationally feasible. In sandstone formations, deformation bands of this thickness can result from the amalgamation of multiple anastomosing seams (Figure 0.3b). Two surfaces were included in the 3D static model that dip in opposite directions and were cross-cutting. The dimensions of the planes representing the deformation bands were set at 10 m in a horizontal direction, 12.5 m in a vertical direction and had a thickness of 20 cm. As acknowledged in other studies (e.g., Fowles and Burley 1994), true dimensions are generally difficult to determine with any accuracy from most two-dimensional outcrops and are probably highly variable depending on the often high connectivity of individual deformation bands. These nominal dimensions, however, seemed reasonable based on the outcrop evidence and the published data (Fossen et al. 2007). The acute angle of intersection between two deformation bands was set at 45^{o} (Figure 0.4 and Figure 0.6), representing a typical mid-range value for conjugate sets of compactional deformation bands in an extensional basin setting (Fossen et al. 2017). However, an acute angle of 90^{o} was also investigated in Section 5.6.1. The corresponding cells of these two surfaces were given the values of the deformation bands porosity and permeability, based on the sensitivity study under consideration (Table 0.5, Table 0.6 and Table 0.7).

Table 0.3: Grid Properties and wells' location in the study of one set of conjugate bands.

Property	Value
Model dimension	20 m × 20 m × 20 m
Number of Cells	ni=100, nj=100, nk=100
Average cell size	20 cm x 20 cm x 20 cm
Injectors' location	INJ1= (i=50, j=50) INJ2= (i=51, j=50) INJ3= (i=50, j=51) INJ4= (i=51, j=51)

5.5.2 Flow simulation

No flow boundaries were considered for sides of the models. Each model was uniformly gridded in the three main dimensions. As shown in Figure 0.5, the permeability of the deformation bands is up to six orders of magnitude less than the permeability of the host rock. The porosity and permeability for the host rock and deformation bands were based on field samples of Penrith Sandstone (Pourmalek et al. 2021). The results agree with observations from other studies (e.g., Torabi, Fossen and Alaei 2008; Torabi and Fossen 2009; Torabi, Fossen and Braathen 2013; Ballas, Fossen and Slovia 2015; Fossen et al. 2017), which show that deformation bands can reduce sandstone permeability by several orders of magnitude. However, in this chapter, these values were based on preliminary field and laboratory studies and permeability contrast between a conjugate set and the sandstone matrix across three orders of magnitude was tested (Table 0.6).

The burial depth of northern England geology is much debated (Turner et al. 1995), with the Vale of Eden supposedly being buried to ≤ 3 km during the early Tertiary (Lewis et al. 1992). Thus, the depth of the reservoir model was set at 2000 metres with the injected CO_2 in the supercritical state. Dynamic modelling was conducted under an initial pressure of 214 bars (pressure gradient of 107 bars/Km at a salinity of 100,000 ppm) and an isothermal condition of 65 °C (using a temperature gradient of 25°C/km). It was initially assumed that the reservoir was fully saturated with brine (100% water saturation). To maintain geomechanical stability and avoid damage to the reservoir, it was assumed that pressure remains below 75% of the lithostatic pressure gradient (225 bars/Km) at any point within the model (Noy et al. 2012). The wells were controlled by the surface rate with a maximum pressure limit of 340 bars. During simulations, the pressure did not reach the pressure constraint. The same fluid properties were used for all models. The relative permeability curves (Figure 0.9, Table 0.4) were taken from Onoja and Shariatipour (2018), while no hysteresis in relative permeability was considered in this study. Dynamic modelling details are summarised in Table 0.4. Four

vertical CO_2 injection wells were added for the sake of symmetrical CO_2 migration and completed at layers 65 to 70 (Table 0.3). To study the plume migration, 30 Sm^3 CO_2 per day was injected over 10 days followed by a one-year post-injection period where only density difference creates flow. The models examined how changing four parameters of the deformation bands might influence CO_2 distribution: a) the plunge angle of the hinge line between two cross-cutting deformation bands; b) the acute angle of two cross-cutting deformation bands; c) the permeability contrast between a conjugate set and host rock; and d) the variation in permeability along the deformation bands.

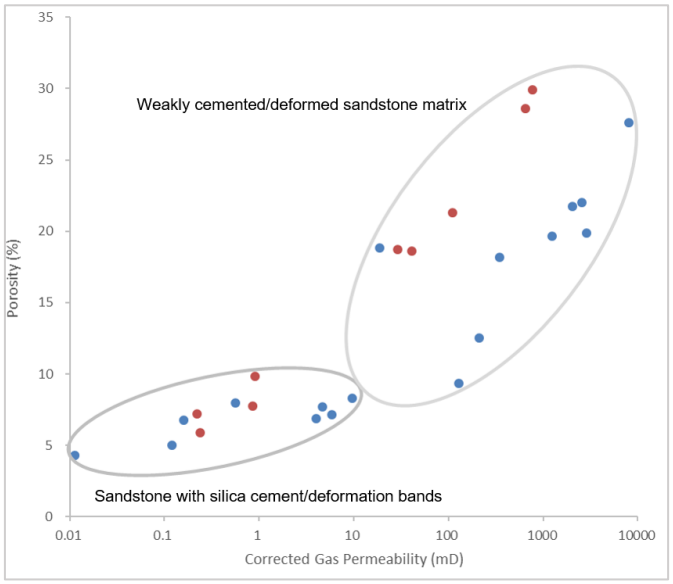

Figure 0.5: Porosity and permeability measurements from samples of the Penrith Sandstone Formation outcrop. Blue dots are core plugs measurements based on liquid re-saturation (porosity) and nitrogen gas permeability tests. Red dots are porosity estimated by the image analysis and a predicted Carman-Kozeny permeability calculated from the total porosity and specific surface area. Both types of measurements demonstrate that host rock has a porosity of 10-30%, while the sandstone with deformation bands has a porosity <10%. Permeability decreases by several orders of magnitude in rocks with bands (courtesy of Andrew Newell and Antoni Mildowski).
Table 0.4: Parameters used for flow simulation.

Parameter	Value
Temperature at datum [°C] (Thermal gradient 25°C/km)	65
Pressure at datum [bars] (pressure gradient of 107 bars/Km)	214
Salinity (Nacl) [ppm]	100,000
Irreducible brine saturation (S_{wr})	0.3
Maximum brine saturation	1.0
End-point relative permeability to brine	1.0
End-point relative permeability to CO_2	1.0

5.5.3 Sensitivity design

5.5.3.1 Sensitivity design to test variation in hinge-line plunge

Deformation bands within the aeolian Penrith Sandstone, and in many other comparable high-porosity sandstones, generally occur as conjugate sets composed of two intersecting planes with opposing dip azimuths (Fossen et al. 2017) (Figure 0.3 and Figure 0.4). While most attention has focussed on the magnitude and tectonic significance of the dihedral angle between the two inclined planes (Fossen et al. 2017), it is likely that the plunge angle of the hinge line could also vary with respect to the horizon, either because of syntectonic processes or subsequent tilting of the entire geological formation. In most geological outcrops this parameter is extremely difficult to measure directly, but it might have an impact on the capture and storage of CO_2 by, for example, modifying the spill point. To test the impact of varying the hinge-line plunge on flow and storage capacity three scenarios were investigated: a) the hinge line was horizontal (CASE A); b) the hinge line dips at an angle of 5^o (CASE B); and c) the hinge line dips at an angle of 10^o (CASE C) (Figure 0.6). For comparative purposes, a model with entirely homogeneous geology and no deformation bands was also run (CASE D) (Table 0.5). For all models the permeability of the deformation bands and the host rock were set at 0.22 mD and 646 mD, respectively (Figure 5.5, Table 0.5). The domain had a pore volume of 2.288×10^3 m^3. A conjugate set of deformation bands enclose a pore volume of 50 m^3 and were assumed to act as a local structural trap. A dihedral angle of 90^o, reported by Fossen et al. (2017), was also used for flow simulation.

Table 0.5: Sensitivity design to test the variation in hinge-line plunge.

	Deformation band			Host rock	
	Intersection angle	**Porosity [%]**	**Permeability [mD]**	**Porosity [%]**	**Permeability [mD]**
CASE A	0^o	7.23	0.22	28.6	646
CSAE B	5^o	7.23	0.22	28.6	646
CASE C	10^o	7.23	0.22	28.6	646
CASE D				28.6	646

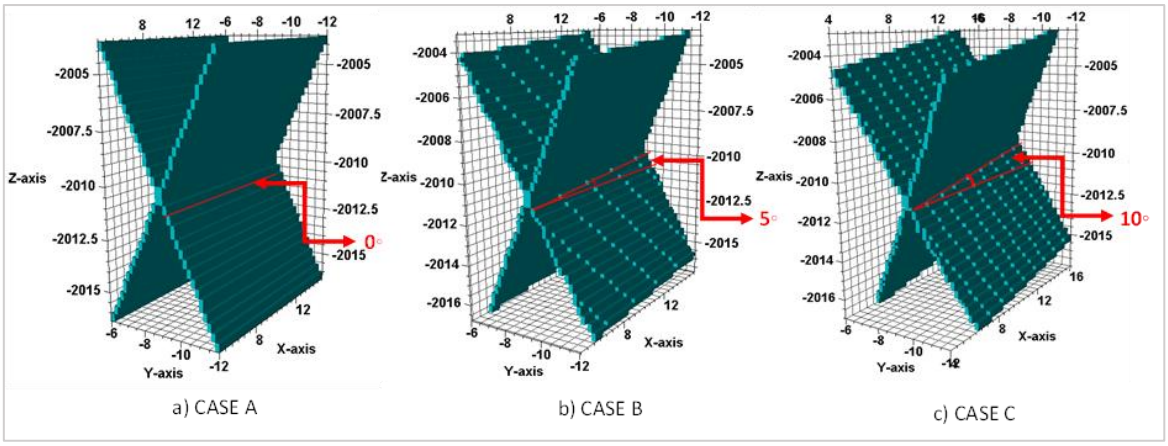

Figure 0.6: A scenario of a single conjugate set of bands. A sandbox model with a spatial dimension of 20 m × 20 m × 20 m with a total of one million active cells [ni=100, nj=100, nk=100] was constructed. Two inclined planes (conjugate deformation bands) in opposite directions which were mutually cross-cutting were included in the model (shown in dark green). Three structures with varying hinge-line plunge were considered in the sensitivity study of Section 4.1: a) Intersection angle with the horizon is zero; b) Intersection axis is at an angle of 5°; and c) Intersection axis is at an angle of 10°. The angles are shown in red.

5.5.3.2 Sensitivity design to test the permeability contrast between host rock and a conjugate set

To test the influence of permeability contrast between deformation bands and host rock (in the context of CO_2 storage), models were run while varying the permeability of the deformation bands and the host rock. CASE A from the previous section, where the axis of intersection between the conjugate deformation bands was horizontal, was used as a base case. Four models were created: CASE A-1, CASE A-2, CASE A-3, and CASE A-4 with different host rock-deformation band permeability contrast. The values used for the Penrith Sandstone are within the range of published works; however, only up to three orders of permeability contrasts were considered here (Table 0.6). It has been assumed the high capillary threshold across deformation bands with high sealing properties (Torabi et al. 2013).

Table 0.6: Sensitivity design to test permeability contrast.

	Deformation band		Host rock	
	Porosity [%]	Permeability [mD]	Porosity [%]	Permeability [mD]
CASE A-1	7.23	0.22	28.6	646
CSAE A-2	9.82	0.91	29.9	770
CASE A-3	5.86	0.24	18.6	41
CASE A-4	7.74	0.85	18.7	29

5.5.3.3 Sensitivity design to test permeability heterogeneity along deformation bands

Torabi and Fossen (2009) examined samples from the North Sea Brent Group; Entrada Sandstone, San Rafael Desert, Utah; and the Nubian Sandstone, Sinai, Egypt. They suggested that lateral variations in porosity and permeability are common and can change from zero to two-three orders of magnitude. Property variations along bands may reduce their sealing capacity. In this section, the effects of permeability heterogeneity along the deformation bands on plume shape and storage security were investigated. CASE A from Section 5.5.3.1 was taken considering two scenarios. In scenario one, permeability was homogenous along the bands and three cases with different permeability values were considered: CASE A-HO-0.01, CASE A-HO-0.1, and CASE A-HO-1. In scenario two, permeability had heterogeneous distribution along the bands and two cases with two orders of magnitude permeability contrast along the bands were considered: CASE A-HE-0.1 with higher average permeability contrast than CASE A-HE-0.01. The permeability of the host rock is homogeneous throughout [1000 mD] in order to isolate the effect of permeability variation along the bands. Reservoir conditions (pressure, temperature and salinity) are presented in Table 0.4 and the relative permeability curves are shown in Figure 4.9. Table 0.7 presents the permeability values used in this section.

Table 0.7: Sensitivity design to test permeability heterogeneity along deformation bands.

	Permeability along the bands [mD]	**Host rock Permeability [mD]**
CASE A-HO-0.01	0.01	1000
CASE A-HO-0.1	0.1	1000
CASE A-HO-1	1	1000
CASE A-HE-0.01	0.01-0.1-1	1000
CASE A-HE-0.1	0.1-1-10	1000

5.6 Results and discussion

5.6.1 The effects of bands intersection angle on CO_2 storage security and flow distribution

The storage capacity of each set of conjugate deformation bands is a function of the host rock porosity and the closure size. The upwards movement of CO_2 is driven by the buoyancy contrast between the lighter CO_2 and denser formation brine. When a deformation band was introduced into the model it filled with CO_2 up to its spill point and then the gas escaped in

the X direction (Figure 0.7a, b and c), ascended towards the upper layers. In CASE A, the CO_2 plume showed a symmetrical distribution along the intersection axis. In the models where the conjugate deformation bands had a tilted intersection, the CO_2 plume tended to migrate under buoyancy up-dip along the intersection axis resulting in an asymmetrical plume along the axis. In the homogenous model (CASE D), with no deformation band, the CO_2 plume migrated vertically and was distributed symmetrically around the injection wells (Figure 0.7d). A higher acute intersection angle between two deformation bands would increase the pore volume available for CO_2 and thereby improve storage security. Figure 0.8 demonstrates the difference in flow distribution, at the end of the injection period, between two models with an acute angle of 45 degrees (Figure 0.8a) and 90 degrees (Figure 0.8b). CO_2 escaped the enclosed volume earlier and formed a larger plume outside the conjugate bands in the model with an acute angle of 45°, unlike the model with an acute angle of 90°. The porosity loss, because of localised deformation band formation, does not seriously compromise the ability of the sandstone reservoir to store fluid or affect its storage capacity (Antonellini and Aydin 1994). However, as observed, it can improve storage security even where the intersection axis between two low permeability planes is inclined.

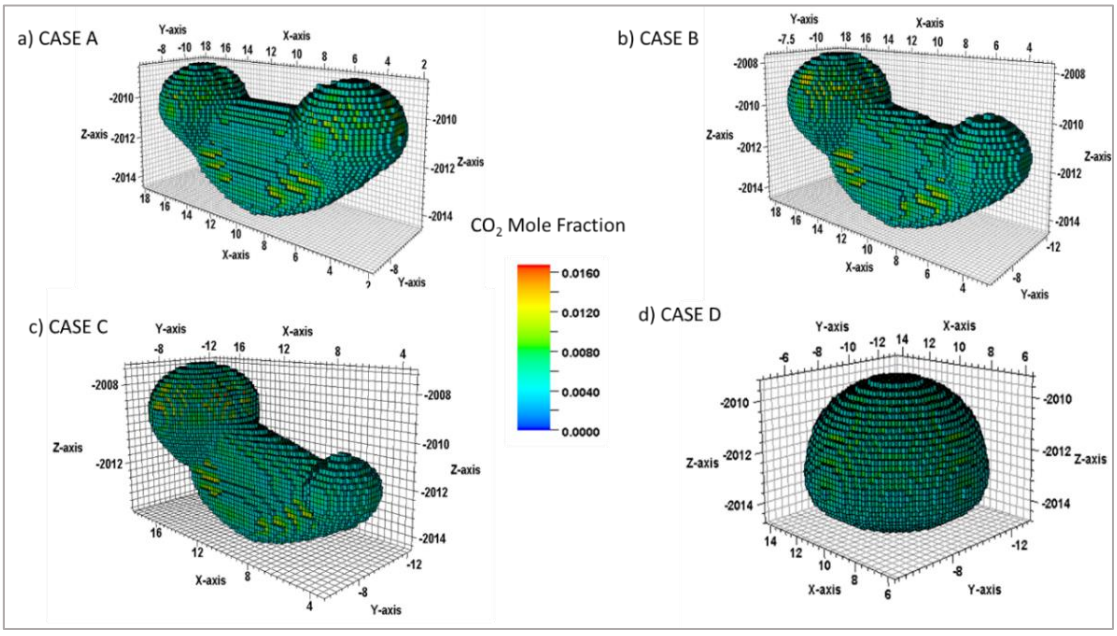

Figure 0.7: The effects of variation in hinge-line plunge on CO_2 distribution. The deformation band filled with CO_2 up to its spill point then the gas escaped in the X direction and ascended towards the upper layers. In CASE A the CO_2 plume shows a symmetrical distribution along the intersection axis. In CASE B and CASE C, the CO_2 plumes are asymmetrical along the axis. The homogenous model (CASE D) showed a symmetrical CO_2 plume around the injectors.

Figure 0.8: a) Plan view of the CO_2 mole fraction in the model with an acute angle of 45 degrees; and b) Model with an acute angle of 90 degrees. At the end of the post-injection period the CO_2 plume developed outside the enclosed volume in the model where bands had an acute angle of 45 degrees, while CO_2 has not yet left the enclosed volume in the model with an acute angle of 90 degrees. The dihedral angles used here are within the range reported by Fossen et al. (2017).

5.6.2 The effects of contrasting host rock-deformation band permeability on CO_2 distribution

Deformation bands can substantially modify fluid flow (Antonellini and Aydin 1994); however, the extent to which these structures influence the injected CO_2 distribution will depend on the permeability contrast between the host rock and the deformation bands (Fossen and Bale 2007; Rotevatn et al. 2009; Zuluaga et al. 2016; Rotevatn et al. 2017). Significant differences in permeability between the undeformed host rock and faults are essential for the latter to act as a seal and significantly impede fluid flow (Fisher and Knipe 2001). Permeability differences are insufficient for most faults studied by Fisher and Knipe (2001) and consequently they could only impede the non-wetting phase at low saturation. Modelling results based on typical permeability ranges for the host rock and deformation bands within the Penrith Sandstone (Figure 5-5, Table 0.6) are shown in Figure 0.9.

The contrast in permeability in the deformation band-host rock was sufficiently high to create a reliable mini-structural trap in CASE A-1 and CASE A-2 (regardless of the closure size) (Figure 0.9a and b). Deformation bands with smaller permeability contrast, although can affect flow, they are unable to block flow completely (CASE A-3 and CASE A-4) (Figure 0.9c and d). To impede flow effectively the permeability of the deformation bands needs to be at least three orders of magnitude less than the host rock. These results disagree with the study of Rotevatn

et al. (2017) who concluded that a permeability contrast of more than one-two orders of magnitude is necessary for deformation bands to impede flow. This inconsistency arises from the fact that gas reservoirs (here supercritical CO_2 injection) are only sensitive to three orders of magnitude permeability differences (Ringrose and Bentley 2015; Newell et al. 2019), which differs from the fluid modelled by Rotevatn et al. (2017) - a two-phase flow simulations, with water displacing oil. Hence, the fluids under investigation are a key factor when studying heterogeneities. In the context of the structural entrapment of CO_2 higher contrast scenarios (more specifically, three orders of magnitude) provide more effective traps.

Aside from CO_2 that is structurally trapped in the host rock beneath the intersecting plane, the properties of the host rock also influenced CO_2 storage capacity and security by influencing the amount of CO_2 that can be dissolved in the water phase. For example, a high host rock permeability in CASE A-1 and CASE A-2 contributed to trapping through increased brine and CO_2 interaction (Figure 0.10).

The CO_2 distribution across the deformation bands, in four cases, is displayed in Figure 0.9. The amount of dissolved CO_2 in the brine was seen to be greater where deformation bands have a higher permeability and porosity. Although the modelling approach is simplified it does show the significance of (i) host rock permeability; (ii) host rock-deformation band permeability contrast; and (iii) deformation band closure size on effective permeability and fluid flow.

5.6.3 The effect of permeability heterogeneity along the deformation bands

The previous section has shown that the deformation bands and host rock permeability contrast affect fluid flow, and this is based on the magnitude of the contrast. In this section, the permeability variation along the deformation bands was investigated. Figure 0.11 compares cases with and without a permeability variation and demonstrates that it had an insignificant influence on the total amount of CO_2 that became dissolved in the water phase in the reservoir. This means that CO_2 did not leak from the higher permeability areas along the deformation bands. The total level of dissolution in the reservoir depends on the permeability of the reservoir and deformation bands. Since permeability variation along the bands was two orders of magnitude, and was relatively low, it did not have a significant effect on the plume shape or the quantity of dissolved CO_2 in the reservoir.

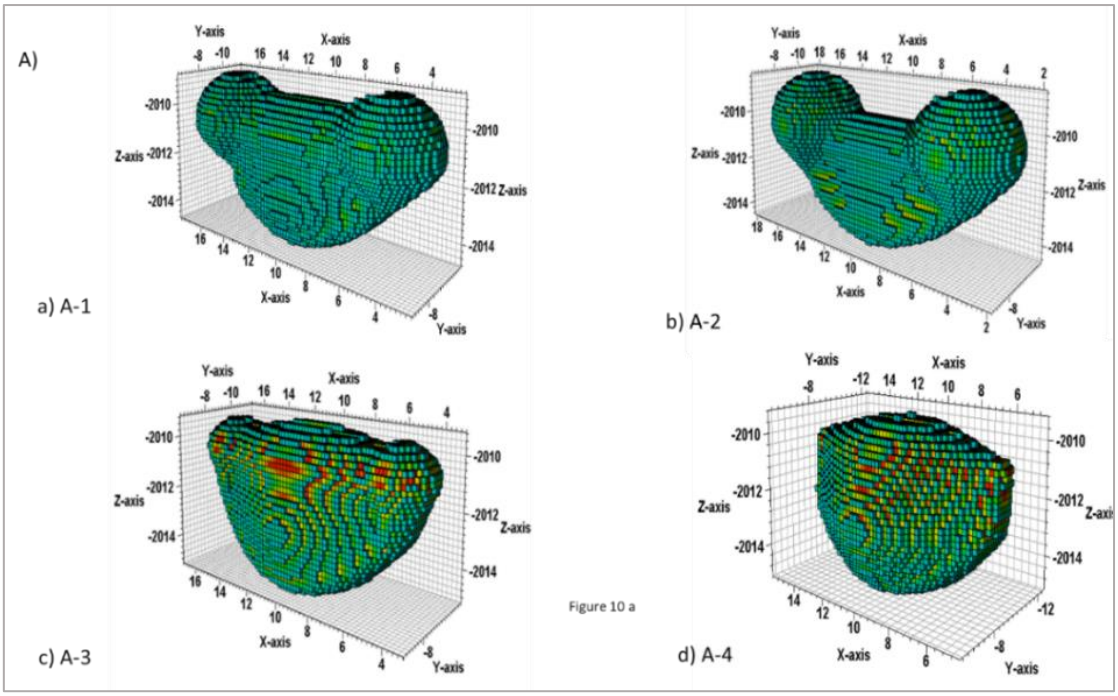

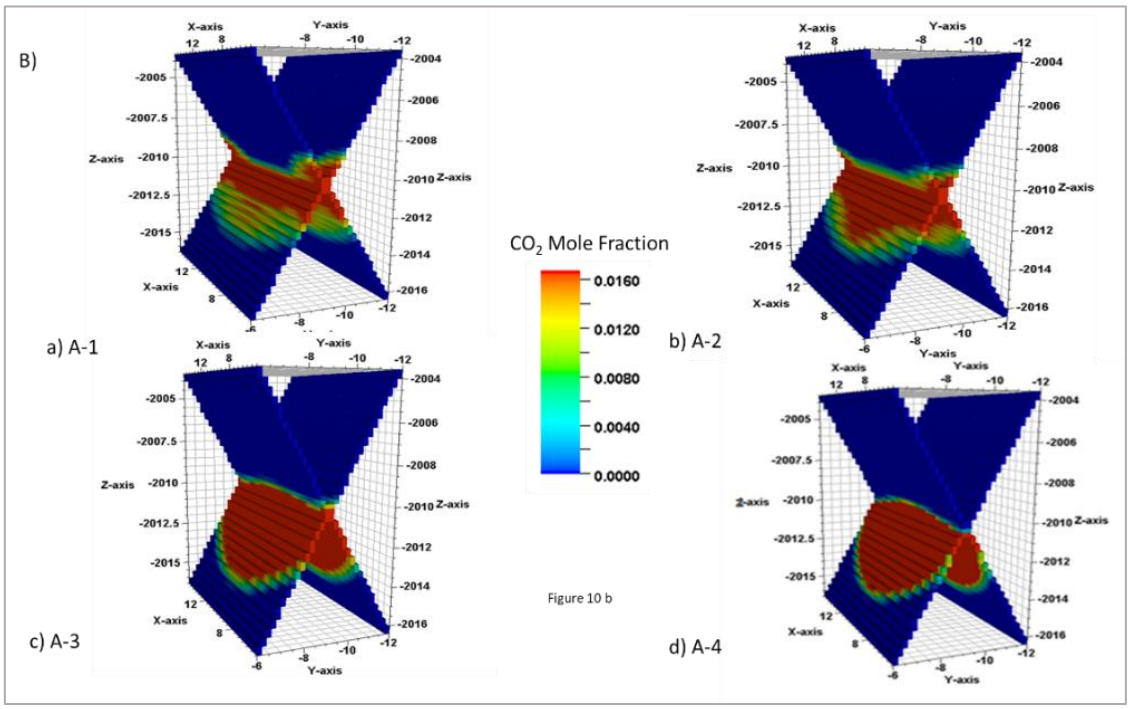

Figure 0.9: A) The effect of deformation band-host rock permeability contrast on CO_2 distribution. B) CO_2 distribution across the deformation bands plane.

Figure 5.11 shows the amount of dissolved CO_2 along the deformation bands in all five modelled cases at the end of the injection period. Obviously, the amount of dissolved CO_2 depends on the average permeability along the band, the higher the average band permeability the more dissolved CO_2 in the water phase.

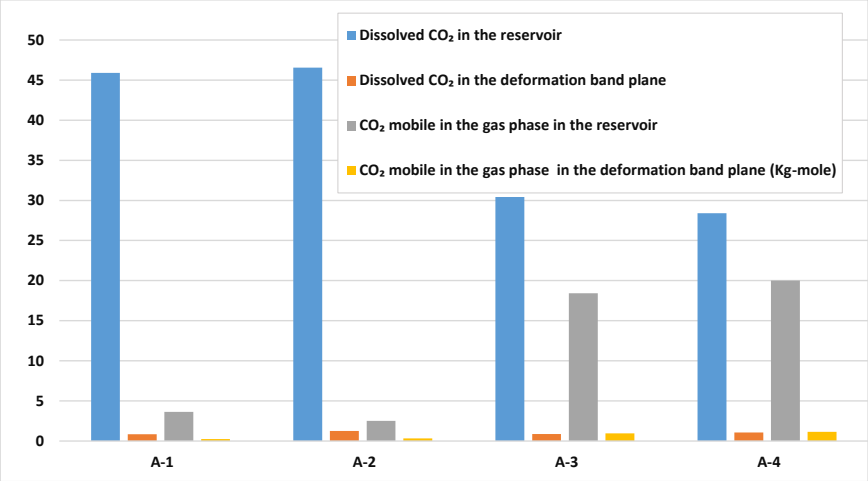

Figure 0.10: Dissolved CO_2 and mobile CO_2 in the reservoir and the deformation band plane at the end of the simulation period. See Figure 5.9 for associated models and Table 5.6 for the porosity and permeability values.

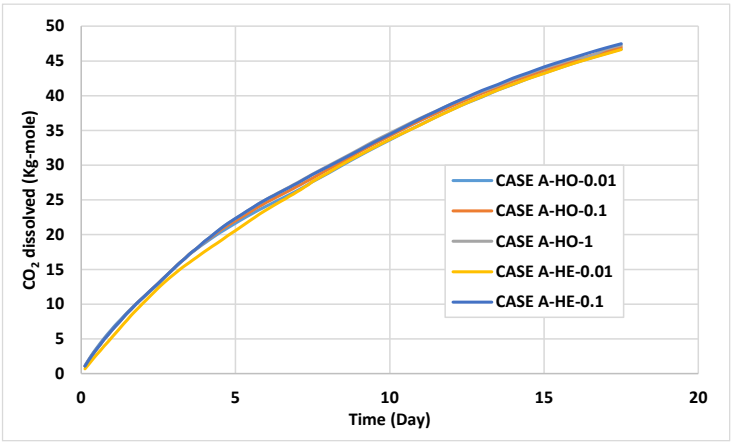

Figure 0.11: The amount of CO_2 dissolved in the water phase in the reservoir at the end of the post-injection period, showing an insignificant difference across modelled cases.

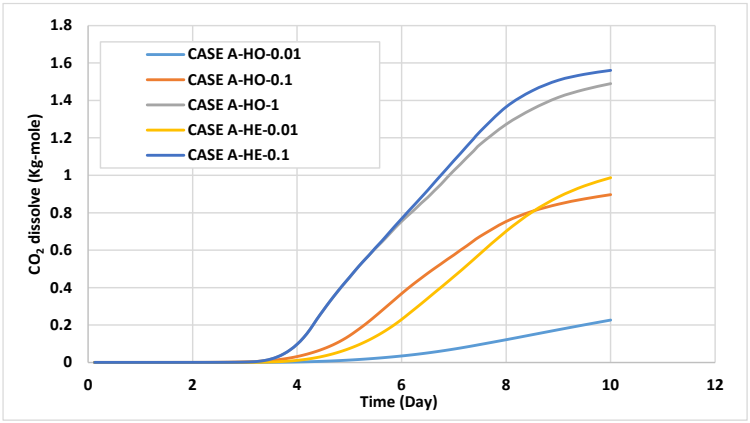

Figure 0.12: CO_2 dissolved along the deformation bands plane for the five modelled cases.

5.7 Conclusion

The extent to which deformation bands can act as efficient mini-traps for the geological storage of CO_2 has been assessed in this chapter. Deformation bands within the aeolian Penrith Sandstone occur as conjugate sets. In the first attempt, only a single set of conjugate deformation bands was considered for flow simulation. The results demonstrate that although a set of X-shaped deformation bands does not compromise the storage capacity, it can improve storage security as a result of their geometry by structurally trap the injected CO_2. Among the cases studied herein, deformation bands with the horizontal hinge line offer the safest scenario. It also has been shown that the higher the acute angle between two intersecting deformation bands, the greater the amount of CO_2 that can be trapped structurally. Deformation bands can extensively influence CO_2 distribution, which depends on their permeability when compared to that of the host rock, as the level of permeability contrast creates considerable flow heterogeneities. In some cases the deformation band-host rock permeability contrast was insufficient (at one order of magnitude) to act as a reliable mini structural trap. However, even in these cases, deformation bands can affect flow. In cases with three orders of magnitude permeability contrast, deformation bands can block the CO_2 migration and act as an efficient mini trap. A variation in permeability along the deformation bands has little effect on storage security and safe CO_2 storage; however, this is dependent on the average permeability of the bands.

Chapter 6

The Impact of deformation bands clusters on CO_2 injection and storage

6.1 Introduction

Several authors have established how deformation bands can have significant effects on subsurface flow in hydrocarbon reservoirs (Manzocchi et al. 1998; Rotevatn et al. 2008; Rotevatn and Fossen 2011; Fachri et al. 2013; Antonellini et al. 2014; Zuluaga et al. 2016; Qu and Tveranger 2016; Rotevatn et al. 2017). However, despite the potential importance of high-porosity aeolian sandstones for CO_2 storage, the impact of deformation bands on supercritical CO_2 injection and storage has been overlooked and has not been tested using flow simulation.

When sandstone is faulted against shale, the small pore apertures of the shale, despite the petrophysical properties of the fault, may form an up-dip seal. However, when sandstone is juxtaposed against sandstone by faulting, the concern is the sealing capacity of the fault, as fluids can escape up-dip via any leaky points. Due to the abundance of low permeability deformation bands around major faults it seems likely that faults may operate as seals even when a sandstone is juxtaposed against a sandstone.

It is uncertain whether the reduction in effective reservoir permeability caused by deformation bands will adversely impact CO_2 injection and storage, or, by creating a large number of mini structural traps, they may enhance storage security at injection sites and reduce the reliance on maintaining the integrity of a single stratigraphic seal. Consequently, this chapter aims to examine the impact of this commonly developed structural configuration on CO_2 injection and storage. To achieve this aim, a flow modelling was constructed that incorporates information on the geometry and porosity-permeability characteristics of deformation bands from the Permian Penrith Sandstone Formation of NW England clustered around a fault plane (Figure 0.1). The key questions addressed in this chapter include:

1) How does the density of the deformation bands influence fluid communication and storage security?
2) How does deformation bands orientation, with regards to a major fault, affect storage security?
3) How might the permeability of the deformation bands, relative to the host rock, affect the effectiveness of CO_2 storage?
4) How do open joints, in the presence of deformation bands, affect storage security?

6.2 Effects of deformation bands on fluid flow

The effect of deformation bands on fluid flow dynamics and production performance has been addressed by various researchers using flow simulations (Matthäi et al. 1998; Olsson 2000; Sternlof, Pollard and Durlofsky 2006; Rotevatn and Fossen 2011; Rotevatn et al. 2013; Qu and Tveranger 2016; Zuluaga et al. 2016; Qu, Tveranger and Fachri 2017; Rotevatn et al. 2017). These studies have shown that deformation bands in siliciclastic, and carbonate reservoirs or aquifers are responsible for some distinctive flow-related phenomena including increased flow tortuosity, improved sweep efficiency, delayed water breakthrough and pressure compartmentalisation. Their results demonstrate the importance of including damage zones (i.e., deformation bands) when investigating high-porosity and faulted reservoirs.

For instance, Sternlof, Pollard and Durlofsky (2006) performed a set of flow simulations on compaction bands based on a data from the Aztec Sandstone, Nevada, USA. They reported profound effects on subsurface flow, anisotropic reservoir flow properties and variable production efficiency. They also observed the tendency for fluids to channel along the main deformation band trends.

A fluid flow simulation study was performed by Rotevatn et al. (2009) on a pervasive system of cataclastic deformation bands associated with a soft-linked relay ramp. Their results show how deformation bands impact flow tortuosity, sweep efficiency, water breakthrough and pressure communication. However, the results were critically dependant on the permeability and density of deformation bands.

Rotevatn and Fossen (2011) used a sandstone reservoir analogue during fluid flow simulations, with their results showing the effect of a low-permeable process zone on

pressure compartmentalisation, flow tortuosity and sweep efficiency. It was observed that sweep efficiency enhancement caused elements of an otherwise bypassed reservoir to still produce.

Fachri, Rotevatn and Tveranger (2013) continued the study of Rotevatn et al. (2009) by generating a reservoir model of the relay ramp using a truncated Gaussian simulation, which they then compared to the previous deterministic approach (Rotevatn et al. 2009). Using this method, they were able to capture details of fluid flow in reservoirs with small-scale heterogeneities (i.e., deformation bands).

By simulating flow through a contractional folded unit with deformation bands, Zuluaga et al. (2016) demonstrated that deformation bands with a permeability constant of three orders of magnitude higher relative to the host rock will influence fluid flow by delaying water breakthrough and enhancing sweep efficiency. However, a low permeability contrast (of one to two orders of magnitude) was seen to have little effect on flow.

Qu and Tveranger (2016) carried out flow simulations using models constructed with and without damage zones; their simulation showed the importance of including damage zones when investigating faulted reservoirs as lower permeability deformation bands result in different reservoir responses.

Rotevatn et al. (2017), using simulations, showed that deformation bands seriously impede flow when the permeability of the deformation bands is one-two orders of magnitude less than the host rock.

Previous studies have focused on the effect of deformation bands on petroleum production and management. The effects of conjugate deformation bands on fluid flow, however, have not been explored, nor the effects of these structures on the geological storage of CO_2. In addition, contradicting results in many published studies make further investigation of such structural heterogeneity necessary, as at present it is unclear whether deformation bands have any practical implications in CO_2 storage.

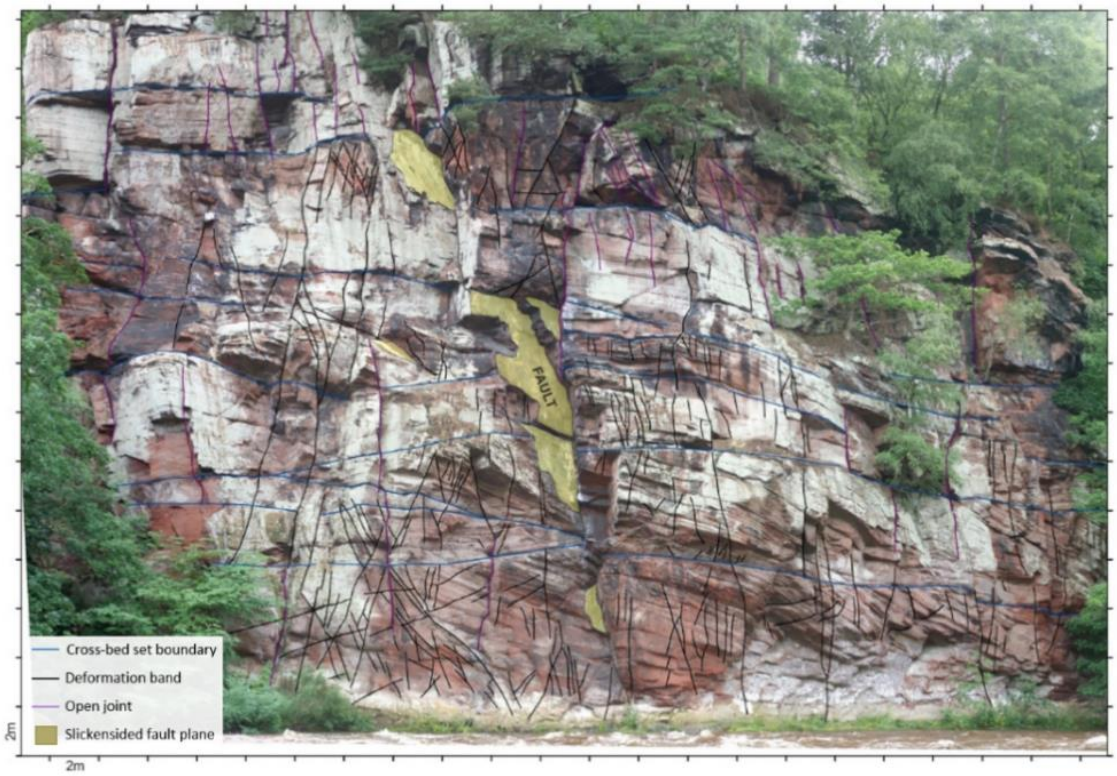

Figure 0.1: Photograph showing the distribution of deformation bands at Chain Cliff outcrop, Eden Gorge, where they are clustered around a fault plane [yellow colouration]. Deformation bands are shown in black, open joints in purple and aeolian bedding surfaces in blue (courtesy of Andrew Newell).

6.3 Methodology

Given that in real-world situations, deformation bands do not generally occur as isolated sets but in dense clusters, several numerical simulations were configured in order to investigate the influence of deformation bands on CO_2 geological storage. To study the clusters of deformation bands, models were generalised to investigate the effects of deformation band density, orientation, distribution and petrophysical properties. For these models a wider range of permeability contrast, compared to previous chapter, was considered (up to six orders of magnitude) (Figure 0.5). This represents the range found in the Penrith Sandstone and in other studies (e.g., Fisher and Knipe 2001; Torabi and Fossen 2009; Fossen et al. 2017). The static models were generated in Schlumberger's Petrel software. Dynamic modelling studies were conducted using ECLIPSE 300 (Schlumberger 2017) with the CO2STORE module. For this study, the models were intentionally kept simple, with a step-by-step variation of parameters in order to isolate and evaluate the key factors governing flow movement in such reservoirs.

6.4 Reservoir Model

To generate a fracture/deformation bands model in Petrel standard processes such as facies modelling and petrophysical modelling are conducted prior to fracture modelling. The framework for the geological models is comprised of the horizontal top surface and the horizontal base surface. 3D static models with a spatial dimension of 100 m × 100 m × 100 m with 125,000 active cells [ni=50, nj=50, nk=50] were generated (Figure 0.2). Each model was uniformly gridded in the three main dimensions. It was assumed that the deformation bands were present across the model and that they disappeared upward as they enter the low porosity caprock. It was also assumed that the host rock is homogeneous throughout, by doing so, the effects of deformation bands on fluid flow is isolated.

To accurately calculate the contribution of deformation bands to fluid flow, a discrete fracture network (DFN) was used to explicitly populate the deformation bands in the reservoir models. This is especially valuable where features (i.e. deformation bands) are anticipated to control the behaviour of the system (Alghalandis 2017). The deformation bands can be implemented in reservoir models using on either a stochastic or deterministic method. In DFN models features are generally implemented as stochastic models, where numerous realisations offer a quantitative measure for uncertainty and variability (Dershowitz et al. 1998). To incorporate clusters of deformation bands into the models, a discrete fracture network was created using the stochastic method but guided and constrained by available outcrop data. To model these structural heterogeneities, certain initial observations must be inputted into the static models, using Fractur Network Modelling in Petrel, including the distribution and the extent of the deformation bands, the geometry of the deformation bands, their orientation and permeability. The first step is to assign the density of the deformation bands. The shape and length of the deformation bands also need to be specified in Petrel. It was assumed that the deformation bands were close to square in all models. The orientation of the bands (dip, dip azimuth, etc...) also needs to be assigned in the fracture modelling. Assigning the permeability of the bands is the last step in creating a discrete fracture network. After assigning properties, the associated deformation band surfaces can be imported to the Scale-up Fracture Network Properties in Petrel. The Scale-up Fracture Network process converts the discrete fracture network into the properties that are essential for the simulator. The results, porosity and permeability, are exported and used for flow simulation in Eclipse 300.

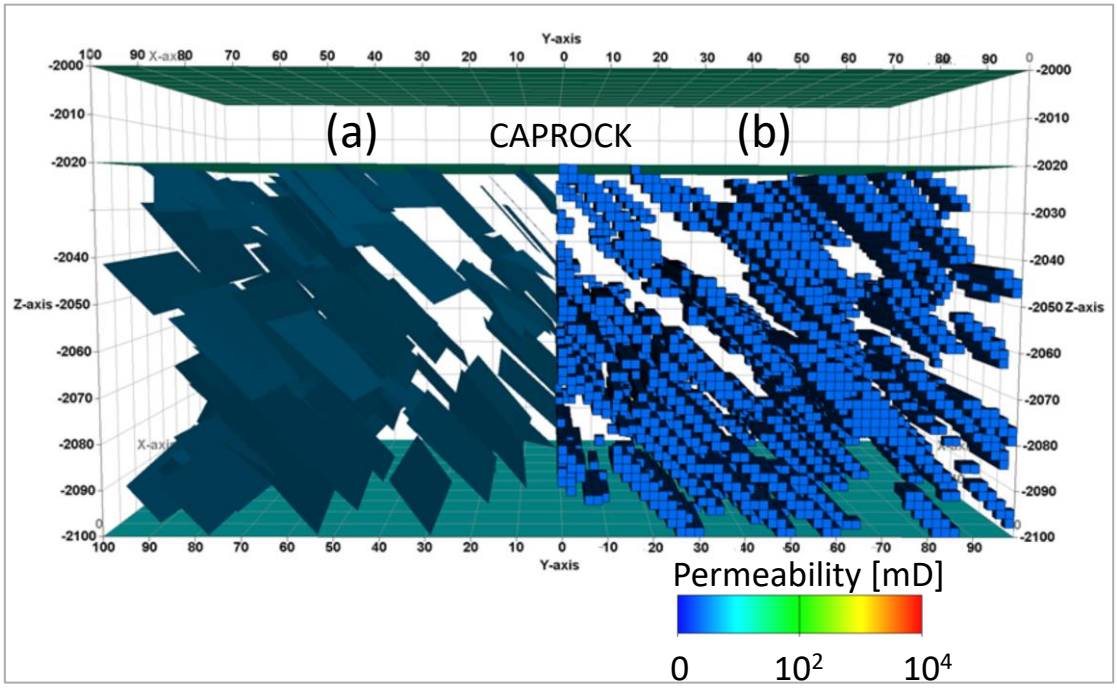

Figure 0.2: Models in the study of the clusters of the bands had a spatial dimension of 100 m × 100 m × 100 with 125,000 active cells [ni=50, nj=50, nk=50]. Medium density parallel bands scenario is shown here. (a) Deformation bands' planes were generated using Fracture Network Model. (b) Fracture Network Model was imported in Scale up Fracture Network. The 3D grid form which it was generated will automatically be chosen to upscale into. As it is shown in this figure, deformation bands are dying out towards the caprock. The high permeability host rock is not shown. Low permeability bands are in dark blue. Sensitivity studies including deformation band density (high, medium and low), permeability contrasts, and orientation of the bands were designed to study the clusters of deformation bands. These scenarios are not included in this figure.

6.5 Flow simulation

One injector well was placed in the centre of the model, chosen to maximise the volumetric sweep efficiency and well away from the boundaries. For the flow simulation workflow and dynamic modelling details see Section 5.5.2.

6.6 The effects of clustered deformation bands on CO_2 storage

In most geological settings deformation bands do not occur as single isolated features, but as dense clusters of conjugate sets that mutually cross-cut each other (Figure 6.1). The deformation bands are formed prior to the development of a slip surface on a normal fault. As this develops the deformation bands will ultimately form a damage zone on either side of the main fault plane. Figure 0.1 provides an illustration of this scenario for the Penrith Sandstone with a high density of deformation bands located either side of a slip surface that has developed on the outer face of a thick zone of deformation bands (Figure 0.3c). Similarly,

the measurement of deformation bands in the Wingate sandstone, Colorado National Monument (Jamison and Stearns 1982) and Moab Member, Entrada Sandstone (Antonellini and Aydin 1994) shows a clear correlation between the high density of deformation bands and their proximity to the fault. Schueller et al. (2013) identified a logarithmic decrease in the number of deformation bands away from the fault core.

The simulation studies examine the influence of clusters of deformation bands on CO_2 distribution in the reservoirs, with a focus on:

1. The effects of varying the density of deformation bands (Section 6.6.1.1);
2. The effects of varying the permeability contrast between the host rock and dense clusters of deformation bands (Section 6.6.1.2);
3. The impact of introducing a high transmissibility fault at the proximity of a dense cluster of deformation bands, simulating the common scenario found in extensional basin settings where the deformation bands occur in a damage zone around a fault (Section 6.6.1.3);
4. The impacts of open joints observed in the outcrop (Figure 6.1) (Section 6.6.1.4);
5. The effects of injection rate and well location (Section 6.6.1.5).

6.6.1 Sensitivity design

6.6.1.1 Deformation band density

For the first sensitivity study three models, with different density of deformation bands were considered. To assign the density of these features in the models, Petrel provides parameter P30 (number of fractures per volume), parameters P31 (fracture length per volume), parameter P32 (fracture area per volume), and P33 (fracture volume per volume). Parameter P30 was used to build three cases that are identified by the label “H” (high density of deformation band, six per metre), “M” (medium density of deformation band, three per metre) and “L” (low density of deformation band, one per metre). Deformation bands in cases with “H” might be considered representative of a geological scenario proximal to a normal fault, while those labelled “L” might be more distal to a fault. For each case deformation bands with different distribution patterns were modelled using the Fisher model method in Petrel: parallel, random and conjugate sets. PARA refers to the parallel distribution of deformation bands and RAND refers to the random distribution of deformation bands. In CON0 the

conjugate sets of deformation bands had a horizontal intersection axis and the intersection axis in CON10 was at an angle of 10. A control case, which was undeformed, was labelled "U"; hence, 13 cases were investigated (Table 0.1). The objective of this section is to investigate the influence of deformation band density on CO_2 storage security and capacity.

Table 0.1: Models built to study the effects of density of deformation bands on CO_2 distribution. L - low density, M - medium density, and H - high density of deformation bands. PARA - parallel distribution of deformation bands, RAND - random distribution of deformation bands, CON0 - conjugate sets with horizontal intersection axis, and CON10 - conjugate sets with an angle of 10. U refers to the undeformed model. For example, L-CON10 is a model with low-density of conjugate deformation bands with a 10-degree intersection angle.

	Number of Deformation band patches in the model	**Distribution**	**Permeability [mD]**	
			Deformation band	Host rock
L-PARA	Low	Parallel	0.91	770
L-RAND		Random	0.91	770
L-CON0		Conjugate 0	0.91	770
L-CON10		Conjugate 10	0.91	770
M-PARA	Medium	Parallel	0.91	770
M-RAND		Random	0.91	770
M-CON0		Conjugate 0	0.91	770
M-CON10		Conjugate 10	0.91	770
H-PARA	High	Parallel	0.91	770
H-RAND		Random	0.91	770
H-CON0		Conjugate 0	0.91	770
H-CON10		Conjugate 10	0.91	770
U	None			770

6.6.1.2 Host rock and deformation band permeability contrast

Plume irregularities are exacerbated by increased contrast in permeability, which has significant ramifications for CO_2 storage security. In order to investigate the effects of permeability contrast on CO_2 storage, eight different scenarios were considered. The permeability of the host rock was increased from 10 mD in PC1 to 10,000 mD in PC4, while the permeability of the deformation bands remained constant (at 0.01 mD). In addition, four other models with permeability contrasts of one to three orders of magnitude were considered. The values from Penrith Sandstone (Table 0.2 and Figure 0.5) and the literature (e.g., Torabi, Fossen and Alaei 2008) were covered. Medium density of deformation bands was used for all flow models; consequently, all cases were assigned the label "M". Also, eight undeformed cases were used for comparative purposes (UNDEFORMED-1 to UNDEFORMED-8). The permeability of deformation bands and host rock are presented in Table 0.2. A fault

can act as both a barrier and conduit to the flow. Here one dipping high transmissibility fault was introduced to all models by a conventional fault transmissibility multiplier (Manzocchi et al.1999). It is assumed that this fault has a permeability of 2000 mD and transmissibility of 34.108 cP.rm^3/day/bars.

Table 0.2: Permeability values used for the permeability contrast sensitivity study. M refers to medium density of deformation bands and PC refers to permeability contrast.

	Distribution	**Permeability [mD]**	
		Host Rock	**Deformation band**
M-CON0-PC1	Conjugate (angle of 0^o)	10	0.01
M-CON0-PC2		100	0.01
M-CON0-PC3		1000	0.01
M-CON0-PC4		10000	0.01
M-CON0-PC5		646	0.22
M-CON0-PC6		770	0.91
M-CON0-PC7		41	0.24
M-CON0-PC8		29	0.85
M-CON10-PC1	Conjugate (angle of 10^o)	10	0.01
M-CON10-PC2		100	0.01
M-CON10-PC3		1000	0.01
M-CON10-PC4		10000	0.01
M-CON10-PC5		646	0.22
M-CON10-PC6		770	0.91
M-CON10-PC7		41	0.24
M-CON10- PC8		29	0.85
M-PARA-PC1	Parallel	10	0.01
M-PARA-PC2		100	0.01
M-PARA-PC3		1000	0.01
M-PARA-PC4		10000	0.01
M-PARA-PC5		646	0.22
M-PARA-PC6		770	0.91
M-PARA-PC7		41	0.24
M-PARA-PC8		29	0.85
M-PERP-PC1	Perpendicular	10	0.01
M-PERP-PC2		100	0.01
M-PERP-PC3		1000	0.01
M-PERP-PC4		10000	0.01
M-PERP-PC5		646	0.22
M-PERP-PC6		770	0.91
M-PERP-PC7		41	0.24
M-PERP-PC8		29	0.85
M-RAND-PC1	Random	10	0.01
M-RAND-PC2		100	0.01
M-RAND-PC3		1000	0.01
M-RAND- PC4		10000	0.01
M-RAND-PC5		646	0.22
M-RAND-PC6		770	0.91
M-RAND-PC7		41	0.24
M-RAND-PC8		29	0.85

6.6.1.3 Deformation bands geometry and location against high transmissibility fault

In extensional settings deformation bands generally occur in association with normal faults. This section describes how this geological scenario might influence storage security. To cover a range of structural possibilities, five models were considered in which the orientation of the deformation bands was varied relative to the transmissive fault plane. The Fisher model method is used to assign various orientation by inputting mean dip (0-90), mean dip azimuth (0-360) and concentration for fractures ranges from 0 (wide scatter) to 100 (focused distribution). In Case M-PARA, deformation bands are parallel to one another and the high transmissibility fault. In M-PEPR, the deformation bands were parallel to each other but perpendicular to the fault. In M-RAND, the deformation bands had a random distribution. In M-CON0, a conjugate set of deformation bands had a horizontal intersection axis and the intersection axis in M-CON10 is at an angle of 10^{o} (Figure 0.3). A medium density of deformation bands setting (three per metre) was used in all cases. The permeability of deformation bands and the host rock were set at 0.91 mD and 770 mD, respectively M-CON0 broadly replicates the type of geological scenario was observed in the Penrith Sandstone (Figure 0.1).

6.6.1.4 Deformation bands and fractures

In many reservoirs the presence of open fractures may increase its effective permeability, thus neutralizing the effect of low permeability deformation bands (Rotevatn et al. 2017). For instance, Tindall (2006) demonstrated that crosscutting joints may form pathways for fluid flow across deformation bands. The switch in the failure mode is a result of lithification and quartz cementation and a change in loading conditions (Aydin, Borja and Eichhubl 2006). Thus, these features almost always postdate deformation bands in sandstones. However, as quartz cementation occurs locally, deformation bands and joints may form simultaneously in different parts of a sandstone (Fossen et al. 2007).

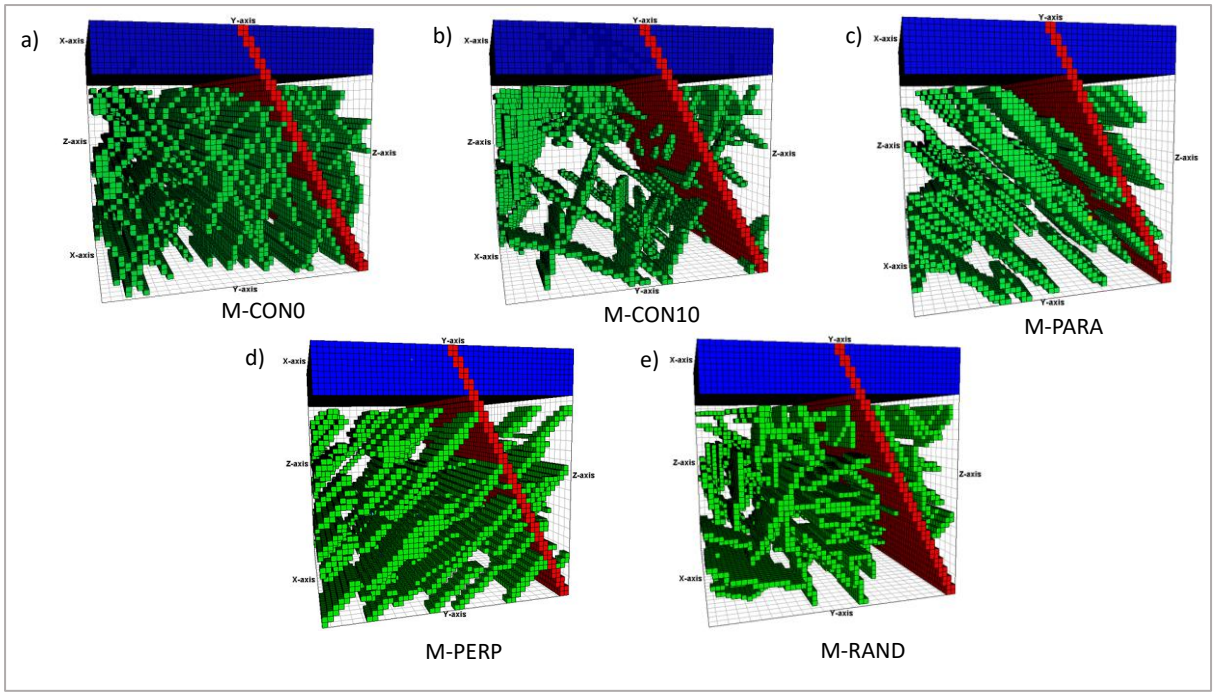

Figure 0.3: Five cases studied herein: a) Conjugate set of deformation bands with 0-degree intersection angle; b) Conjugate set of deformation bands with 10-degree intersection angle; c) parallel set of deformation band, parallel to the fault; d) parallel set of deformation band; perpendicular to the fault; and e) Random distribution of deformation bands (Blue: caprock, Red: fault, Green: deformation bands).

In previous sections, the effect of open fractures (joints) has not been considered, because introducing joints can cloud the effect of deformation bands, which are the main focus of the chapter. In the Penrith Sandstone outcrop (Figure 0.1) open joints are present, and to produce more realistic models joints were added to this study. Four different distributions of deformation bands (parallel deformation bands and parallel to a fault, parallel deformation bands and perpendicular to a fault, random deformation bands and conjugate deformation bands) with three densities (high, medium, and low) were constructed. The density of deformation bands is the same as in Section 6.6.1.1. Consequently, 12 deformation band models were constructed. For each model, three different joints densities (high, medium and low) were also considered: high joint density, six per metre; medium joint density, three per metre; and low joint density, one per metre. In all, 36 models were considered (Table 0.3). As shown by Aydin, Borja and Eichhubl (2006), joints in sandstones are generally perpendicular to the layers, therefore, all joints were modelled as vertical structures. For example, the case CON0-H-L had high a density of conjugate deformation bands with a horizontal intersection axis and low density joints. The permeability of the deformation bands, fractures and host rock were set to 0.01 mD, 2000 mD, and 1,000 mD, respectively.

Table 0.3: Properties of deformation bands including shape and density, and density of vertical open fractures in all 36 models investigated.

	Density of deformation bands	**Density of joints**	**Distribution**
CON0-H-L	High	Low	Conjugate (0° angle)
CON0-H-M		Medium	
CON0-H-H		High	
CON0-M-L	Medium	Low	
CON0-M-M		Medium	
CON0-M-H		High	
CON0-L-L	Low	Low	
CON0-L-M		Medium	
CON0-L-H		High	
PARA-H-L	High	Low	Parallel to a fault
PARA-H-M		Medium	
PARA-H-H		High	
PARA-M-L	Medium	Low	
PARA-M-M		Medium	
PARA-M-H		High	
PARA-L-L	Low	Low	
PARA-L-M		Medium	
PARA -L-H		High	
PERP-H-L	High	Low	Perpendicular to a fault
PERP-H-M		Medium	
PERP- H-H		High	
PERP-M-L	Medium	Low	
PERP-M-M		Medium	
PERP-M-H		High	
PERP-L-L	Low	Low	
PERP-L-M		Medium	
PERP-L-H		High	
RAND-H-L	High	Low	Random
RAND-H-M		Medium	
RAND- H-H		High	
RAND-M-L	Medium	Low	
RAND-M-M		Medium	
RAND-M-H		High	
RAND-L-L	Low	Low	
RAND-L-M		Medium	
RAND-L-H		High	

6.6.1.5 Injection rate and well location

The cases introduced in Section 6.6.1.3 were used and three injection rates were applied for each case. Permeability of the bands was set to 0.91 mD and host rock to 770 mD.The cases with "LR" had a low injection rate (100 sm^3/day), "MR" medium injection rate (250 sm^3/day) and "HR" a high injection rate (525 sm^3/day). The highest injection rate is the maximum that can be used before the system reaches the pressure constraint of 340 bars and causes damage to the reservoir. Various injection rates are modelled to identify trends in mobile gas

accumulation in the fault rock and beneath the caprock with different shape of deformation bands (Table 0.4).

The placement of the injector well and its relationship to CO_2 storage security was also explored by considering two well locations using static models in Section 6.6.1.3. In cases with "C" the injector was centred in the model (well location: x=50 and y=50), and in cases with "F" the well was placed far from the fault (well location: x=25 and y=40). The injection rate was of 250 sm^3/day (Table 0.5).

Table 0.4: 15 scenarios were considered in order to investigate the effect of injection rate on CO_2 storage security.

	Distribution	Deformation band density	Injection rate
M-LR-PARA	Parallel	Medium	100 sm^3/day
M-MR-PARA			250 sm^3/day
M-HR-PARA			525 sm^3/day
M-LR-PERP	Perpendicular	Medium	100 sm^3/day
M-MR-PERP			250 sm^3/day
M-HR-PERP			525 sm^3/day
M-LR-RAND	Random	Medium	100 sm^3/day
M-MR-RAND			250 sm^3/day
M-HR-RAND			525 sm^3/day
M-LR-CON0	Conjugate 0 (angle of 0^o)	Medium	100 sm^3/day
M-MR-CON0			250 sm^3/day
M-HR-CON0			525 sm^3/day
M-LR-CON10	Conjugate 10 (angle of 10^o)	Medium	100 sm^3/day
M-MR-CON10			250 sm^3/day
M-HR-CON10			525 sm^3/day

Table 0.5: 10 scenarios were considered to study the effects of well placement on storage security.

	Distribution	Deformation band density	Injection rate	Well Location
M-C-PARA	Parallel	Medium	250 sm^3/day	x=50 and y=50
M-F-PARA				x=25 and y=40
M-C-PERP	Perpendicular	Medium	250 sm^3/day	x=50 and y=50
M-F-PERP				x=25 and y=40
M-C-RAND	Random	Medium	250 sm^3/day	x=50 and y=50
M-F-RAND				x=25 and y=40
M-C- CON0	Conjugate 0 (angle of 0^o)	Medium	250 sm^3/day	x=50 and y=50
M-F- CON0				x=25 and y=40
M-C- CON10	Conjugate 10 (angle of 10^o)	Medium	250 sm^3/day	x=50 and y=50
M-F- CON10				x=25 and y=40

6.7 Result and discussion

6.7.1 Investigating the effects of deformation band density on CO_2 storage

In the undeformed case (U) the resultant plume was uniform and symmetrical. Figure 0.4A and B illustrates the density of deformation bands and CO_2 distribution in the case of low density (L-CON10), medium density (M-CON10) and high density (H-CON10) of conjugate sets of deformation bands. The impact of deformation band density on plume geometry was apparent. As the number of deformation bands increased in the model, the vertical and lateral movements became restricted and the plume became progressively distorted. Less CO_2 reached the caprock where there is a higher density of deformation bands. These results imply that, in general, deformation bands inhibited the vertical movement of CO_2. More mobile gas was observed beneath the caprock in the homogeneous model without deformation bands and with runs using a low to medium number of deformation bands (Figure 0.4 and Figure 0.5).

The volume of dissolved CO_2 in brine and mobile CO_2 in both the reservoir and beneath the caprock are shown in Figure 0.5. Although insignificant, the greatest amount of CO_2 dissolved in the water phase and the lowest degree of mobile CO_2 was observed in the homogeneous model without deformation bands (U) and in models with low deformation bands. The amount of free gas beneath the caprock was lower in the models with a higher number of deformation bands.

Fossen and Bale 2007, Rotevatn et al. 2009 and Fachri, Rotevatn and Tveranger 2013 have previously indicated that a significant concentration of low permeability bands is needed for deformation bands to have considerable negative effects on productivity. This is because the abundance of these structural heterogeneities, which can extend to tens or hundreds of metres (Aydin 1978) with various orientations (Rotevatn et al. 2009), may cause extensive compartmentalisation and represents a major barrier to fluid flow. In the CO_2 storage context, for deformation bands to contribute to secure storage, a number of deformation bands that do not overly damage reservoir communication nor reduce bulk porosity, that improves the sweep efficiency, block the upward movement of CO_2, and do not cause injectivity issue is necessary. As pressure buildup is sensitive to reservoir permeability, an exceptionally high number of low permeability bands will cause injectivity issues. In this study, the number of deformation bands observed at the Penrith Sandstone outcrop (reported also by Aydin (1978)

for deformation bands in aeolian sandstone), and modelled with three orders of magnitude permeability contrast, did not cause injectivity issues but can contribute to the secure storage of CO_2. In the case of extensional settings these structures can improve security, as high density deformation bands occur in the proximity of the fault. In this study, a higher density of deformation bands decreased the amounts of free gas beneath the caprock and in the fault plane and delayed the CO_2 arrival time to the top of the reservoir.

However, reservoir communication was slightly impaired, resulting in an insignificantly lower volume of CO_2 being dissolved in the water phase. As CO_2 could not reach all parts of the reservoir there was less CO_2 and brine interaction. This produced results in contrast to the study of Zuluaga et al. (2016), as they had previously shown that the ability of fluids to saturate the reservoir, namely sweep efficiency, is improved by deformation band occurrence.

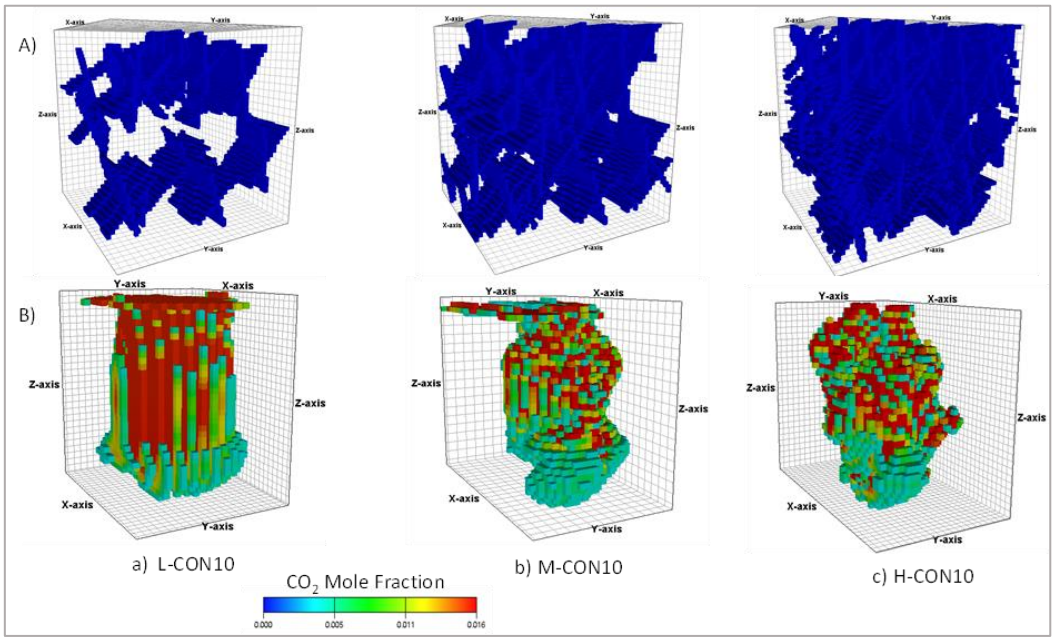

Figure 0.4: A) Low, medium and high density of deformation bands. The fault is not shown. B) Effects of deformation band density on flow distribution. More mobile gas appeared beneath the caprock in the models with a low to medium number of deformation bands.

This outcome is based on the fact that these low permeability features may redirect fluids to parts of the reservoir that would otherwise be bypassed. Therfore, how the reservoir is compartmentalised by these structural features, and the difference in spatial distribution, may have had negetive effect on the overall sweep in this study, which can cause decreased dissolution of CO_2 in the water phase. Therefore, we can not conclude deformation bands genearlly improve sweep.

One unexpected result was that the main portion of injected CO_2 was blocked from the caprock, not because of the conjugate shape of the deformation bands, but their density (Figure 0.5). Consequently, when considering the role of such structural heterogeneities in reservoirs, it is important to evaluate each reservoir separately in terms of the number of the bands, their location against larger structures, their geometry, properties and continuity.

Reservoir pressure is shown in Figure 0.6. None of the runs in this section reached the failure limit of the 340 bars, even in the scenarios with the highest number of low permeability deformation bands.

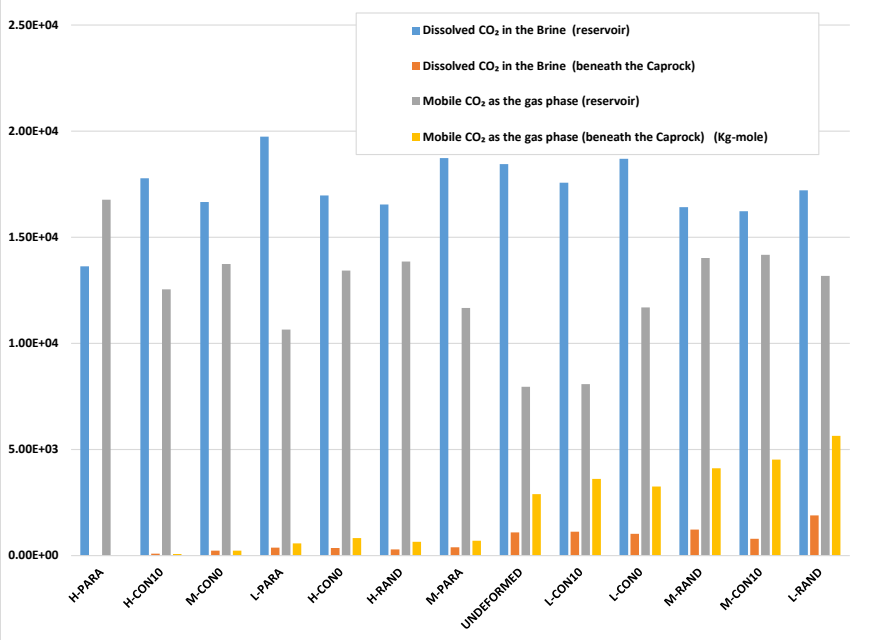

Figure 0.5: The amount of dissolved CO_2 in the brine and mobile CO_2 in both reservoir and beneath the caprock in cases with different density of deformation bands.

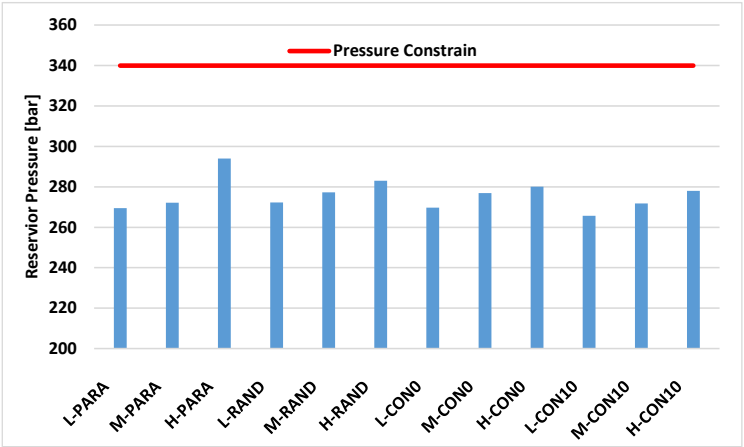

Figure 0.6: None of the models in the study of deformation band density reached the pressure limit of 30 bars. Note that the permeability contrast of three orders of magnitude were considered here.

6.7.2 The effects of host rock and deformation band permeability contrast on CO_2 storage

The dissolved and mobile gas in the storage formation, the fault rock and the layer below the caprock in models, where a permeability contrast variation between the host rock and the clusters of deformation bands exist, are illustrated in Figure 0.7. The high permeability of the host rock resulted in a higher dissolved CO_2 content as a result of increased brine and CO_2 interaction (e.g., M-PERP-PC4). Consequently, the highest mobile CO_2 in the models was observed in the reservoirs with a low permeability host rock (e.g., M-CON0-PC1). The shape of the modelled deformation bands had no significant effect on the amount of dissolved CO_2 in either the brine or the mobile gas in the storage formation.

During the injection and post-injection periods the highest free gas beneath the caprock was observed where the host rock exhibited a high permeability, with either a random distribution of deformation bands or conjugate sets of deformation bands (e.g., M-RAND-PC3 and M-CON10-PC5). No free phase CO_2 reached the caprock where the host rock had a low permeability (e.g., M-PARA-PC1).

An insignificant amount or no free gas was detected in the fault rock where deformation bands were parallel to the transmissible fault (e.g., M-PARA-PC4). Cases with a perpendicular distribution of deformation bands against the fault were among those with the highest amount of free gas in the fault rock (along with CON10). Even in M-PEPR-PC1, PC2 and PC7 (low permeability host rock), free CO_2 reached the fault plane. The earliest breakthrough of CO_2 to the caprock and the leaky fault occurred in PERP cases where the host rock had a high permeability. This is because the CO_2 plume was directed towards the caprock and fault by i) buoyancy forces; ii) the presence of a perpendicular set of deformation bands; while iii) the high permeability of the host rock increased CO_2 flow velocity.

The CO_2 distribution in cases with conjugate and paralleled deformation bands are illustrated in Figure 0.8. One large, sub-symmetrical plume formed around the injector and migrated upwards due to buoyancy forces (in all PC1 and PC8 cases). The plume shapes lacked radial symmetry and were irregular in cases with a higher permeability contrast (in all PC3, PC4, PC5 and PC6 cases). The impact of the deformation bands on the flow was significant in these cases. The overall shape of the plume changed as deformation bands varied, regardless of density and permeability contrast (compare Figure 0.8A and 6.8B).

The long term CO_2 storage security of such systems depends on the amount of free gas that reaches the transmissible faults or caprock, as there is an increased risk of leakage. This is not only controlled by the permeability contrast, but also by the permeability of the host rock itself. Many researchers have not included the effect of host rock permeability in their sensitivity analyses (Rotevatn et al. 2009; Fachri, Rotevatn and Tveranger 2013; Zuluaga et al. 2016). The study by Rotevatn et al. (2017) on carbonate rocks considered various permeabilities for the host rock. However, as the porosity and permeability values for both the host rock and the deformation band samples were lower for the carbonate rock, their study cannot be extrapolated to a siliciclastic reservoir with very high permeabilities. In the study of clusters of deformation bands, the deformation bands permeability remained below 0.91 mD throughout, with the host rock permeability ranging from 10 to 10,000 mD (Table 6.2). The storage security was jeopardised in models where the host rock had medium to high permeability and a permeability contrast above three orders of magnitude (see models PC2-PC3-PC4-PC5, and PC6 in Figure 0.7), as free gas reached the caprock and/or leaky fault. Although models with low host rock permeability have shown insignificant mobile gas beneath the caprock or the fault plane, they exhibited a higher free gas in the system. They also may cause injectivity problems in higher densities.

Fachri, Rotevatn and Tveranger 2013 and Rotevatn et al. (2017) argued that decreasing deformation band permeability (higher permeability contrast) results in a complex waterfront shape and slow fluid propagation. In this study, although a more tortuous flow pattern was observed in the high permeability contrast models, faster flow propagation was observed due to higher host rock permeability.

Permeability contrast is, therefore, not the only criterion that needs to be considered while injecting CO_2 into a very high permeability reservoir with deformation bands, for low-density CO_2 in such a reservoir passes such heterogeneities and can reach a caprock that may contain leakage points. In contrast to what we previously thought, conjugate sets of deformation bands did not significantly contribute to CO_2 storage security or block CO_2 in models with the high permeability host rock.

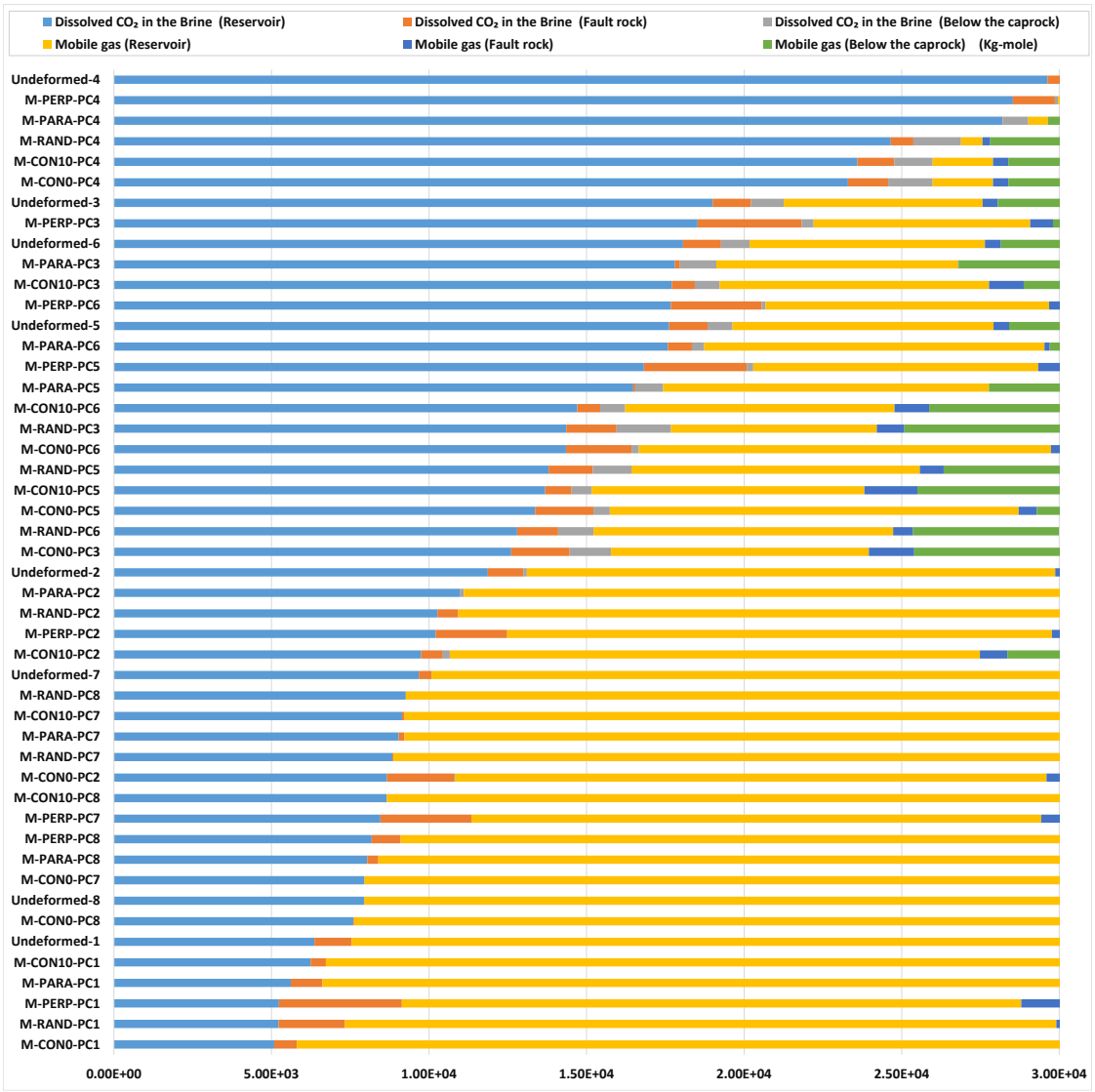

Figure 0.7: Dissolved CO_2 and mobile gas in the reservoir, in the fault rock and the layer below the caprock. M refers to a medium number of deformation bands. PERP refers to a parallel set of deformation bands that are perpendicular to the fault. PARA refers to a parallel set of deformation bands that are parallel to the fault. RAND refers to a random distribution of deformation bands. CON0 refers to a conjugate set of deformation bands with a horizontal intersection axis and the intersection axis in CON10 is at an angle of 10^o. PC denotes permeability contrast. For example, Case M-RAND-PC4 is the model with a medium number of randomly distributed deformation bands with six orders of magnitude host rock-deformation bands permeability contrast. For the permeability values, see Table 0.2.

6.7.3 The effects of deformation bands geometry and their location against high transmissibility fault

The results for the amount of free gas beneath the caprock and in the fault, for the five cases investigating the geometry and distribution of the bands, are shown in Figure 0.9. The highest amount of mobile gas both in the fault zone and beneath the caprock was observed in M-CON10 and M-RAND. M-CON0 was the most secure model as both the free CO_2 beneath the caprock and the fault rock were relatively low. None of the model runs showed complete

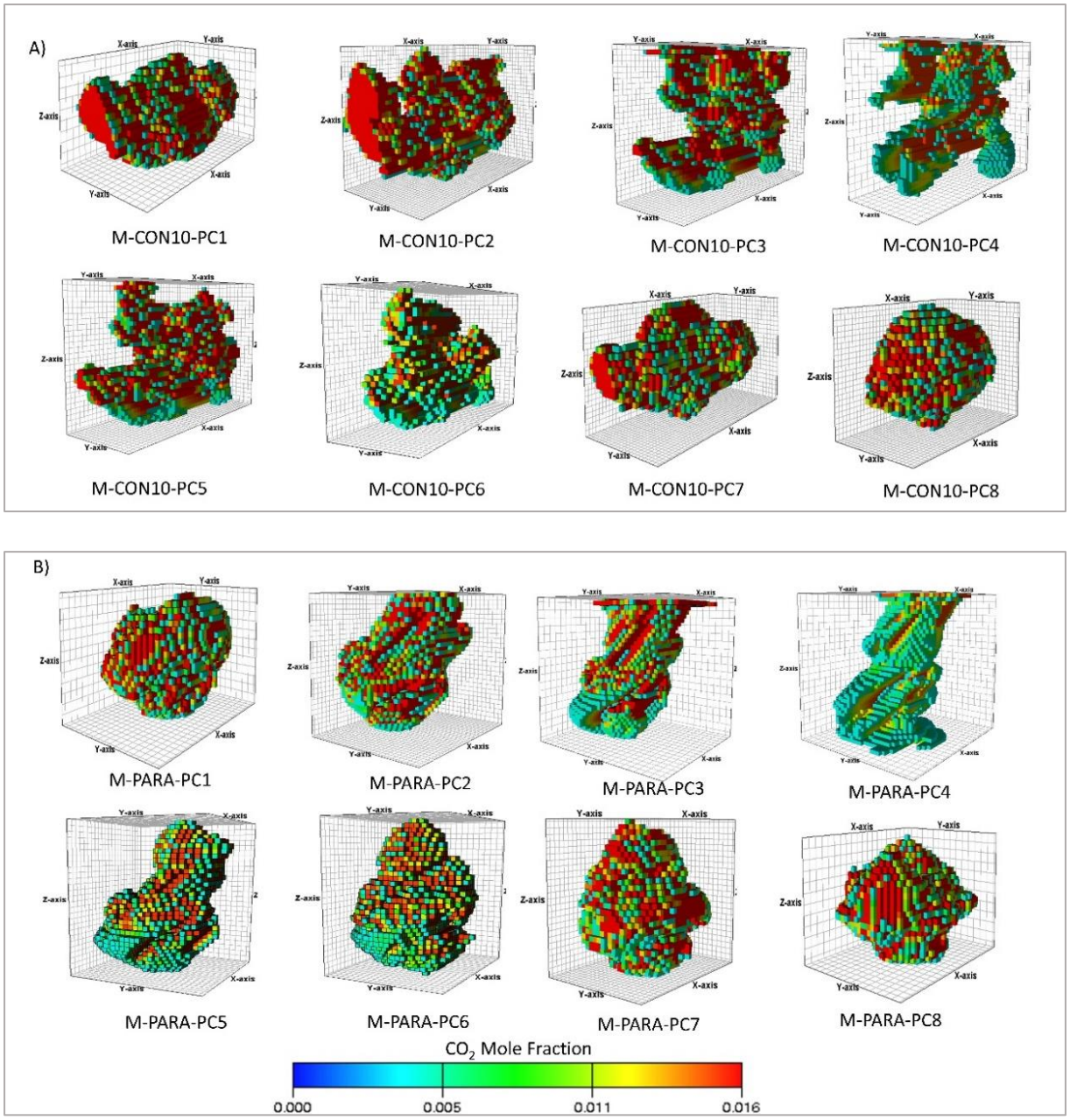

Figure 0.8: CO_2 distribution in cases with differing permeability contrast. A) CO_2 distribution in models with conjugate sets of deformation bands with an intersection angle of 10°; and B) CO_2 distribution in cases with a parallel distribution of deformation bands.

obstruction of CO_2 movement towards the leaky fault and the caprock. Even in the M-PARA model, when most of CO_2 redirected away from the fault, CO_2, as free gas, was still detected in the fault plane. This is because a medium density of deformation bands was used in the modelling study in this section. Investigating the effect of deformation bands geometry showed that the solid geometry of deformation bands can inhibit or accentuate CO_2 migration towards the caprock or transmissible fault. This is to be expected, as the deformation bands in M-CON10 retained injected CO_2 for only a short time period. The CO_2 then migrated along the intersection angle to eventually reach the caprock or transmissible fault. In cases where

the deformation bands were randomly distributed, the free movement of CO_2 occurred in some parts of the reservoir where sufficient gaps allowed for a possible escape towards the caprock and fault.

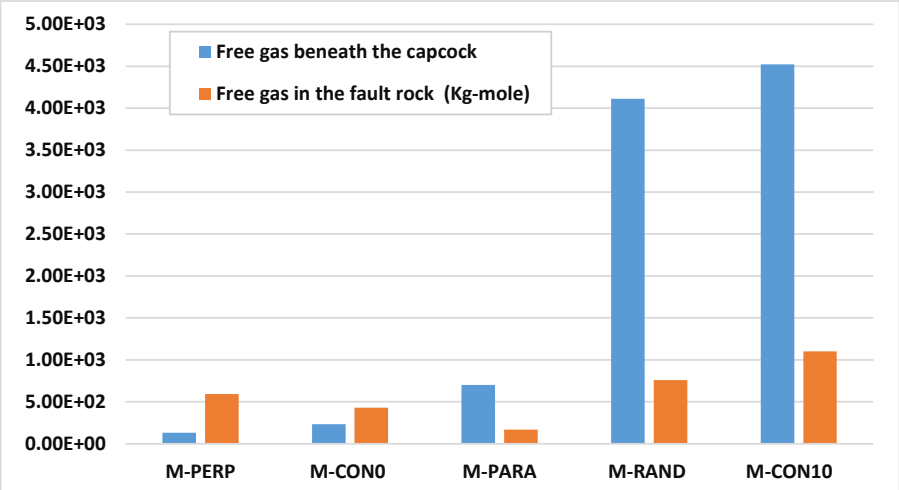

Figure 0.9: The amount of free gas beneath the caprock and fault rock in cases with various type of deformation band distributions.

6.7.4 Combined effects of deformation bands and fractures on CO_2 storage security

Comparing models with and without open fractures shows a considerable reduction in storage security, even in the models with a low number of fractures (Figure 0.10). The amount of mobile gas beneath the caprock was significantly higher than in the fault as open joints in the outcrop were aligned towards the caprock and not the fault plane (Figure 6.1). The shape and orientation of deformation bands did not have a significant effect on storage security. However, the models with conjugate deformation bands were among the least secure, and the models with parallel deformation bands perpendicular to the faults were among the most secure configurations (e.g., cases PERP-M-L and PERP-M-H). In the presence of open fractures CO_2 covered an extensive area beneath the caprock forming various potential leakage sources. Figure 0.11 demonstrates how open fractures contribute to CO_2 distribution. Fractures significantly compromised storage security, nevertheless, a high number of deformation bands in the presence of the open fractures did not necessarily guarantee storage security.

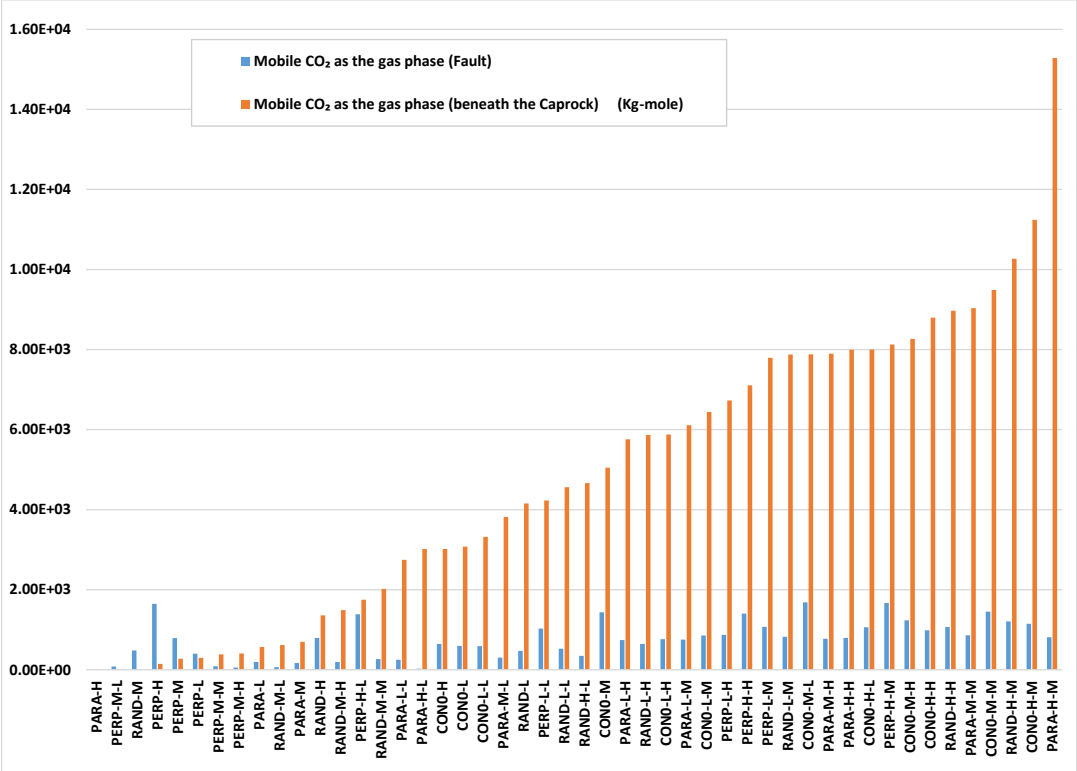

Figure 0.10: Mobile gas beneath the caprock and fault plane in the presence of open fractures.

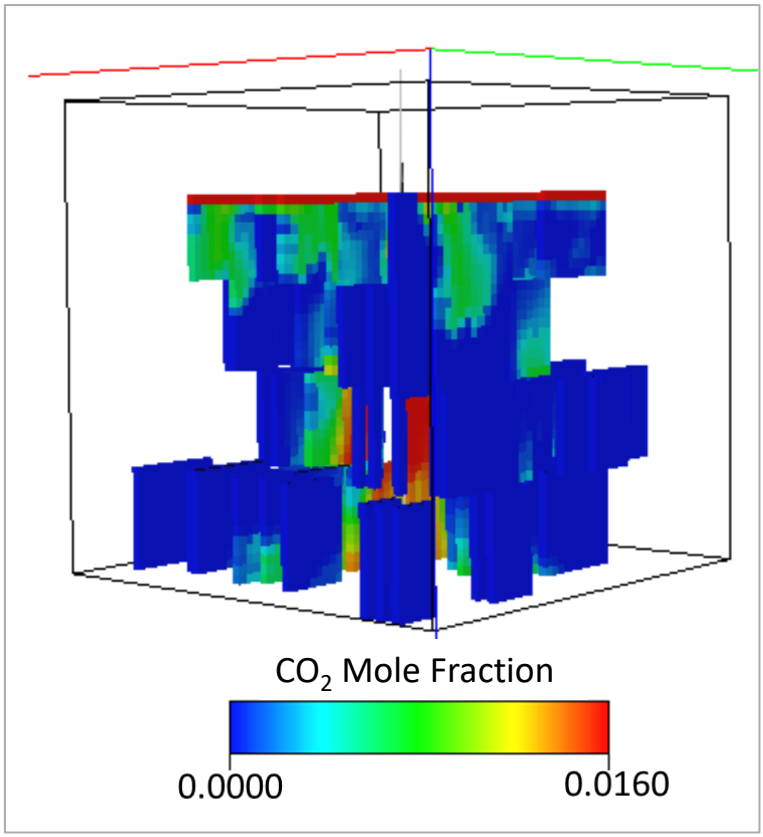

Figure 0.11: Influence of open fractures in CO_2 distribution in the presence of open fractures.

The following section addresses the improvements in storage capacity and security resulting from various injection scenarios and well placements.

6.7.5 The effects of injection rate and well location on CO_2 storage security in a deformed reservoir

As observed in the previous study, M-RAND and M-CON10 appeared to be the least secure in regard to CO_2 retention. Outcomes were repeated at high, medium and low injection rates. These two cases, again, had the highest free gas accumulation at the top of the reservoir across all three injection rate scenarios and are the least secure configurations for CO_2 storage (Figure 0.12). The most secure cases were models with sets of conjugate deformation bands with a horizontal intersection angle. Models with perpendicular distribution against the fault did not follow the trends discussed above. While low and medium injection rates were amongst the most secure cases, a high injection rate indicated a high volume of free gas beneath the caprock, as more CO_2 was directed towards the fault. CO_2 had moved upwards via the fault and ultimately accumulated with the CO_2 that had already reached the caprock.

The optimum injection rate is of key importance for the types of reservoirs studied herein. With high injection rates the CO_2 may leak through proximal high transmissibility faults, thus limiting the storage effectiveness and diminishing injection security. In addition, deformation band density and permeability contrast also need to be taken into consideration, as cases with a high number of deformation bands, in low permeability host rock, can lead to injectivity issues and potential project failure.

The amount of mobile gas in the caprock, in cases where the well was far from the fault was less than when the well was placed in the centre of the model, as free phase CO_2 was unable to reach the fault. Clearly, well placement has a considerable effect on CO_2 storage security and can help guarantee safer storage by avoiding any faults in the vicinity of the injection wells (Figure 0.13).

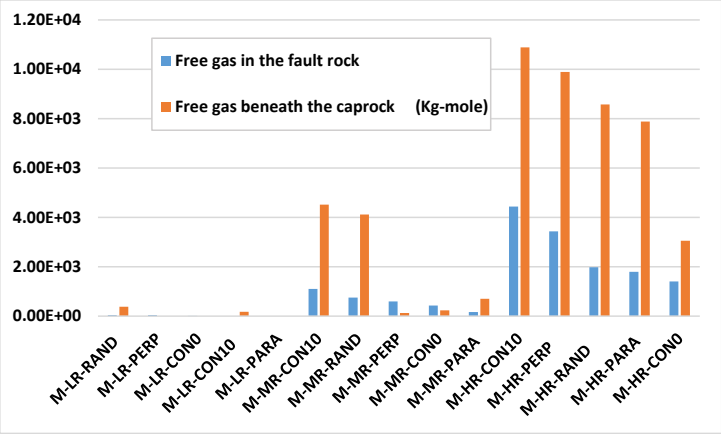

Figure 0.12: The amount of free gas beneath the caprock and in the fault rock under different injection scenarios display similar trends. M refers to models with medium density of deformation bands, LR refers to low injection rate, MR to medium injection rate and HR to high injection rate.

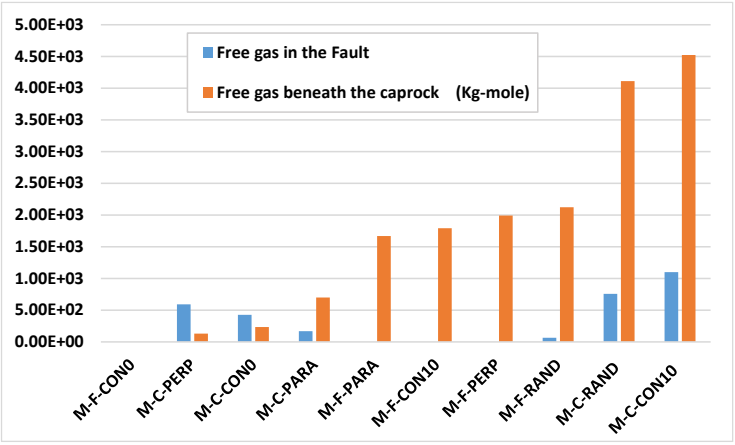

Figure 0.13: The amount of free gas beneath the caprock and in the fault rock under different well placement scenarios. M refers to models with medium density of deformation bands, F refers to the models with well placement in x=25 and y=40 and C refers to the models with well placement in x=50 and y=50.

6.8 Conclusion

Deformation bands mainly occur as dense clusters of conjugate sets that mutually cross-cut each other. The sensitivity study performed here was designed to study the effects of deformation band density and geometry; host rock and deformation band permeability contrast; and host rock permeability on CO_2 storage capacity and security. While the resultant plume was uniform and symmetrical in an undeformed case, the plume became progressively distorted as the number of deformation bands increased in the model. Deformation bands will delay the upward migration of CO_2 and reduce reliance on the top seal. The modelling studies suggest that the presence of deformation bands alone may not be a positive contributor to CO_2 storage. Deformation bands need to be abundant, but not overly damage

reservoir communication, nor reduce its bulk porosity. They also need to improve sweep efficiency, block the upward movement of CO_2 and more importantly, not cause injectivity issues. The number of deformation bands that were observed at the Penrith Sandstone outcrop, and modelled with three orders of magnitude permeability contrast, did not cause injectivity issues and did contribute to the secure storage of CO_2.

The plume shape lacked radial symmetry and irregularities were exaggerated by increasing permeability disparities. The amount of the free gas reaching the caprock or the leaky fault is not only controlled by permeability variation, but also by the permeability of the host rock, both of which have considerable ramifications for CO_2 storage security.

As deformation bands generally occur in association with normal faults, in one scenario a high transmissibility fault was introduced into a dense cluster of deformation bands. The geometry and the location of the deformation bands against a leaky fault have significant effects on the security of CO_2 storage. Some types of deformation bands demonstrated a more positive contribution to storage security (e.g., deformation bands in conjugate configuration with horizontal intersection angle), while others jeopardised storage security by increasing the amount of free gas that can reach the caprock or leaky fault (e.g., deformation bands perpendicular to the fault).

The presence of open fractures may increase the effective reservoir permeability, thus neutralizing the effect of low permeability deformation bands (Rotevatn et al. 2017). This may have a positive effect on the recovery of oil. However, in the case of the CO_2 storage, especially when they were aligned, as in the case of Penrith Sandstone, they considerably reduced storage security towards the caprock, even in models with few fractures.

To improve storage capacity and security, it is necessary to consider the optimum injection rate and well placement. High injection rates may limit storage effectiveness and diminish injection security as CO_2 may leak through proximity high transmissibility faults. Avoiding a fault in the vicinity of the injection wells can better guarantee safe storage.

Chapter 7

Conclusion and recommendation

7.1 Conclusion

The successful geological storage of CO_2 is dependent on structural and stratigraphic trapping mechanisms and the presence of an impermeable seal. Herein, the effects of both large-scale faults and small-scale deformation bands as structural traps and primary and secondary stratigraphic traps on CO_2 geological storage were investigated. The aim was to investigate whether stratigraphic heterogeneity and mini structural traps can reduce the reliance on a single stratigraphic seal and therefore improve storage security.

Stratigraphic heterogeneity influences fluid flow, storage capacity and effectiveness - as CO_2 can be confined in numerous small or large stratigraphic traps. In Chapter 3, three formations with different styles of heterogeneity were explored. These different styles of heterogeneity are provided by shallow-marine mixed siliciclastic-carbonate systems. The lithofacies, with their associated physical properties, were systematically modelled, using outcrop, to determine how they influenced CO_2 flow, and their potential as stratigraphic trap for the safe geological storage of CO_2. These three examples allowed the examination of variable siliciclastic and carbonate ratios [Grayburg Formation], interfingering carbonate and sand facies [Lorca Basin] and a succession with narrow cemented bands [Bridport Sand].

This study has revealed that facies interplay and associated sediment heterogeneity have a varying control on fluid flow, storage capacity and security.

- In the Grayburg Formation storage security and capacity were not controlled by heterogeneity alone, but influenced mainly by the permeability of each facies, their permeability contrast and the relative permeability characteristic of the system. Based on the petrophysical properties of each facies, stratigraphic heterogeneity can limit connectivity and significantly increase injection pressure.

- In the Lorca Basin heterogeneity through interfingering of the carbonate and clastic facies improved the storage security regardless of permeability.
- For the Bridport Sands the existence of extended sheets of cemented carbonate contributed to storage security but not storage capacity.

This study demonstrates the significance of these systems for safe CO_2 geological storage, as stratigraphic heterogeneity is likely to be a significant feature of many future storage sites. They can minimise the large buoyancy force that acts on the top seal and reduce the reliance of storage security on the caprock. They also increase the contact area between injected CO_2 and brine, thereby promoting CO_2 dissolution.

In Chapter 4, the Entrada Sandstone was investigated. This exhumed palaeo-reservoir is an analogue for continental red-bed formations considered as geological storage for CO_2 on the NW European continental shelf. The Entrada Sandstone has been significantly bleached as a result of iron-oxide reduction due to high fluxes of CO_2 charged reducing fluids and offers an excellent opportunity to understand how reducing fluids migrate and accumulate within heterogeneous aeolian deposits.

A series of flow modelling exercises were undertaken to study the possible fluid migration paths and to investigate the amount of heterogeneity and geological details that are needed in flow simulations in order to reduce the time and cost of computer simulations.

- Through flow modelling, it is highly probable that the main CO_2 pathways, which caused the bleaching of the Entrada Formation, are either the Little Grand Wash fault or both the Little Grand Wash fault and northern fault of the Salt Wash graben. It is highly unlikely that the Salt Wash graben was solely involved in this process as the Green River anticline is plunging with up-dip closure against the Salt Wash graben. In other words, some component of up-dip migration of CO_2-charged fluids from the Little Grand Wash fault was required to produce the observed patterns of bleaching.
- The modelling of a bleached palaeo-reservoir within the Entrada Sandstone helped validate Flora's Rule. Despite geological heterogeneity and strong permeability contrasts at the Entrada Sandstone outcrop, the bleaching was distributed uniformly across the boundaries of interlayered lithofacies and has been verified by flow modelling. In conclusion, reservoir heterogeneity needs to be sufficiently high and the range 1-10^3 mD should not greatly impede the relatively uniform distribution of CO_2 charged fluids throughout a reservoir. The modelling exercise revealed that the full

spectrum of lithofacies was not required in this case study as fluids with a lower viscosity (i.e., CO_2) are less sensitive to heterogeneity than higher viscosity fluids.

- Of significance is the seal properties when entrapping injected CO_2. The seal in the study area, the Earthy Member, has a higher permeability and porosity than typical seals, allowing for CO_2 diffusion into the seal of up to 4 m. This was repeated in simulation studies. The results indicate that the optimum injection rate and perforation location can enhance CO_2 storage security when the topseal has atypical caprock properties.

The extent to which deformation bands can act as efficient mini-traps for the geological storage of CO_2 was assessed in Chapter 5. Deformation bands within the aeolian Penrith Sandstone occur as conjugate sets. In this chapter, only a single set of conjugate deformation bands was considered for flow simulation.

- The results demonstrate that although one set of conjugate deformation bands does not compromise the storage capacity, it can improve storage security because of their geometry and the subsequent structural trapping of injected CO_2.
- Among the cases studied, deformation bands with the horizontal hinge line present the safest scenario.
- It also has been demonstrated that the higher the acute angle of the two intersecting deformation bands the more CO_2 that can be trapped structurally.
- Deformation bands can significantly influence CO_2 distribution, which depends on their permeability when compared to the host rock, as permeability contrast can create considerable flow heterogeneities. In some cases, the deformation band-host rock permeability contrast was insufficient (at one order of magnitude) to act as a reliable mini structural trap. However, even in these cases, deformation bands can affect flow. In cases with three orders of magnitude permeability contrast, deformation bands can completely block CO_2 migration and act as an efficient mini trap.
- Although variation in permeability, along the deformation bands, has little effect on storage security and safe CO_2 storage, this is dependent on the average permeability of the bands.

Chapter 6 evaluated the extent to which clusters of deformation bands can contribute to secure geological storage of CO_2. Data from the Penrith Sandstone was used to build static geological models and to simulate supercritical CO_2 injection into high-quality reservoirs with low porosity and permeability deformation bands. Deformation bands mainly occur as dense clusters of conjugate sets that are cross-cutting. The sensitivity study performed here was designed to study the effects of deformation band density, geometry, and host rock and deformation band permeability contrasts on CO_2 storage capacity and security.

- In undeformed cases the plume was uniform and symmetrical but became progressively distorted as the number of modelled deformation bands increased. The simulations indicate that the presence of the deformation bands alone may not be a positive contributor to CO_2 storage. Deformation bands need to be abundant, but not overly damage reservoir communication, nor reduce its bulk porosity. They also need to improve sweep efficiency, block the upward movement of CO_2 and more importantly, not cause injectivity issues. The number of deformation bands that were observed at the Penrith Sandstone outcrop, and modelled with three orders of magnitude permeability contrast, did not cause injectivity issues and did contribute to the secure storage of CO_2.
- The plume shape lacked radial symmetry and irregularities were exaggerated by increasing permeability disparities. The amount of the free gas reaching the caprock or the leaky fault is not only controlled by permeability variation, but also by the permeability of the host rock, both of which have considerable ramifications for CO_2 storage security.
- As deformation bands generally occur in association with normal faults, a high transmissibility fault was introduced into a dense cluster of deformation bands. The geometry and location of these deformation bands, against a leaky fault, significantly affect storage security. Some types of deformation bands demonstrated a more positive contribution to storage security, e.g., deformation bands in conjugate configuration. Other types of bands were jeopardised storage security by increasing the amount of free gas that can reach the caprock or the leaky fault, e.g., deformation bands perpendicular to the fault.
- The presence of open fractures may increase reservoir effective permeability, thus neutralizing the effect of low permeability deformation bands. This may have a

positive effect on the recovery of oil. However, in the case of CO_2 storage, especially when they are aligned, as in the case of Penrith Sandstone, towards the caprock, the open fractures considerably reduced storage security, even in models with few fractures.

- To improve storage capacity and security, it is necessary to consider the optimum injection rate and well placement. High injection rates may limit storage effectiveness and diminish injection security as CO_2 may leak through proximity high transmissibility faults. Avoiding a fault in the vicinity of the injection wells can better guarantee safe storage.

7.2 Future work

Considering all discussions and analyses through this research, several topics for further work have emerged which could improve our understanding of CO_2 trapping in structural and stratigraphic traps.

In Chapter 3, other mixed systems such as lower carbonate – upper clastic sequences and lower mudrock – upper carbonate sequences can be investigated. In addition, many more realisations can be used in the case of Grayburg Formation, and as carbonates are reactive, reactive transport modelling can be undertaken.

In Chapter 4, other fluid (i.e., oil') and mixed fluid (water and CO_2 + H_2S) migration, as suggested by authors (i.e., Haszeldine et al. 2005) for the bleaching of the sandstones, can be simulated.

In Chapter 5, a variation of thickness along the band needs to be investigated to test its significance on CO_2 storage security.

In Chapter 6, the heterogeneous distribution of permeability along the bands, and heterogeneous permeability of deformation bands within a reservoir, can be studied.

References

Ahr, W.M. (2011) *Geology of Carbonate: The Identification, Description, and Characterization of Hydrocarbon Reservoirs in Carbonate Rocks.* John Wiley & Sons.

Alcalde, J., Flude, S., Wilkinson, M., Johnson, G., Edlmann, K., Bond, C.E., Scott, V., Gil, S.M. V, Ogaya, X., and Haszeldine, R.S. (2018) 'Estimating Geological CO2 Storage Security to Deliver on Climate Mitigation'. *Nature Communications* [online] 1 (9), 1–13. available from <https://doi.org/10.1038/s41467-018-04423-1>

Alghalandis, Y.F. (2017) 'ADFNE: Open Source Software for Discrete Fracture Network Engineering, Two and Three Dimensional Applications'. *Computers and Geosciences* [online] 102 (September 2016), 1–11. available from <http://dx.doi.org/10.1016/j.cageo.2017.02.002>

Allis, R., Chidsey, T., Gwynn, W., Morgan, C., White, S., Adams, M., and Moore, J. (2001) 'Natural CO2 Reservoirs on the Colorado Plateau – Candidates for CO2 Sequestration'. *Proceedings of the First National Conference on Carbon Sequestration* 14–17

Ambrose, W.A., Lakshminarasimhan, S., Holtz, M.H., Núñez-López, V., Hovorka, S.D., and Duncan, I. (2008) 'Geologic Factors Controlling CO2 Storage Capacity and Permanence: Case Studies Based on Experience with Heterogeneity in Oil and Gas Reservoirs Applied to CO2 Storage'. *Environmental Geology* [online] 54 (8), 1619–1633. available from <https://doi.org/10.1007/s00254-007-0940-2>

Andre, L., Audigane, P., Azaroual, M., and Menjoz, A. (2007) 'Numerical Modeling of Fluid – Rock Chemical Interactions at the Supercritical CO2 – Liquid Interface during CO2 Injection into a Carbonate Reservoir, the Dogger Aquifer (Paris Basin, France)'. *Energy Conversion and Management* [online] 48 (6), 1782–1797. available from <https://doi.org/10.1016/j.enconman.2007.01.006>

Antonellini, M. and Aydin, A. (1994) 'Effect of Faulting on Fluid Flow in Porous Sandstones: Petrophysical Properties'. *AAPG bulletin* [online] 78 (3), 355–377. available from <https://doi.org/10.1306/BDFF90AA-1718-11D7-8645000102C1865D>

Antonellini, M., Cilona, A., Tondi, E., and Zambrano, M. (2014) 'Fluid Flow Numerical Experiments of Faulted Porous Carbonates, Northwest Sicily (Italy)'. *Marine and Petroleum Geology* [online] 55, 186–201. available from <http://dx.doi.org/10.1016/j.marpetgeo.2013.12.003>

Arthurton, R.S. and Wadge, A.J. (1981) *Geology of the Country around Penrith: Memoir for 1:50,000 Geological Sheet 24*.

Aydin, A. and Johnson, A.M. (1983) 'Analysis of Faulting in Porous Sandstones'. *Journal of Structural Geology,* [online] 5 (1), 19–31. available from <https://doi.org/10.1016/0191-8141(83)90004-4>

Aydin, A. (1978) 'Small Faults Formed as Deformation Bands in Sandstone'. in *Rock Friction and Earthquake Prediction*. Birkhäuser, Basel, 913–930

Aydin, A., Borja, R.I., and Eichhubl, P. (2006) 'Geological and Mathematical Framework for Failure Modes in Granular Rock'. *Journal of structural geology* [online] 28 (1), 83–98.

available from <https://doi.org/10.1016/j.jsg.2005.07.008>

Bachu, S., Bonijoly, D., Bradshaw, J., Burruss, R., Holloway, S., Christensen, N.P. and Mathiassen, O.M. (2007) 'CO2 Storage Capacity Estimation: Methodology and Gaps'. *International Journal of Greenhouse Gas Control* [online] 1 (4), 430–443. available from <https://doi.org/10.1016/S1750-5836(07)00086-2>

Bachu, S., Gunter, W.D. and Perkins, E.H. (1994) 'Aquifer Disposal of CO2: Hydrodynamic and Mineral Trapping'. *Energy Conversion & Management* [online] 35 (4), 269–279. available from <https://doi.org/10.1016/0196-8904(94)90060-4>

Bachu, S. (2000) 'Sequestration of CO2 in Geological Media: Criteria and Approach for Site Selection in Response to Climate Change'. *Energy Conversion & Management* [online] 41 (9), 953–970. available from <https://doi.org/10.1016/S0196-8904(99)00149-1>

Bachu, S. (2003) 'Screening and Ranking Sedimentary Basins for Sequestration of CO2 in Geological Media in Response to Climate Change'. *Environmental Geology* 44 (3), 277–289

Bachu, S. (2008) 'CO2 Storage in Geological Media: Role, Means, Status and Barriers to Deployment'. *Progress in energy and combustion science* [online] 34 (2), 254–273. available from <https://doi.org/10.1016/j.pecs.2007.10.001>

Bachu, S. (2015) 'Review of CO2 Storage Efficiency in Deep Saline Aquifers'. *International Journal of Greenhouse Gas Control* [online] 40 (September 2015), 188–202. available from <http://dx.doi.org/10.1016/j.ijggc.2015.01.007>

Bachu, S. and Adams, J.J. (2003) 'Sequestration of CO2 in Geological Media in Response to Climate Change: Capacity of Deep Saline Aquifers to Sequester CO2 in Solution'. *Energy Conversion and management* [online] 44 (20), 3151–3175. available from <https://doi.org/10.1016/S0196-8904(03)00101-8>

Bachu, S. and Stewart, S. (2002) 'Geological Sequestration of Anthropogenic Carbon Dioxide in the Western Canada Sedimentary Basin: Suitability Analysis'. *Journal of Canadian Petroleum Technology* [online] 41 (02). available from <https://doi.org/10.2118/02-02-01>

Bagheri, M., Shariatipour, S.M., and Ganjian, E. (2018) 'A Review of Oil Well Cement Alteration in CO2-Rich Environments'. *Construction and Building Materials* [online] 186, 946–968. available from <https://doi.org/10.1016/j.conbuildmat.2018.07.250>

Bagheri, M., Shariatipour, S.M., and Ganjian, E. (2019) 'Prediction of the Lifespan of Cement at a Specific Depth Based on the Coupling of Geomechanical and Geochemical Processes for CO2 Storage'. *International Journal of Greenhouse Gas Control* [online] 86 (September 2018), 43–65. available from <https://doi.org/10.1016/j.ijggc.2019.04.016>

Ballas, G., Fossen, H., and Soliva, R. (2015) 'Factors Controlling Permeability of Cataclastic Deformation Bands and Faults in Porous Sandstone Reservoirs'. *Journal of Structural Geology* [online] 76, 1–21. available from <http://dx.doi.org/10.1016/j.jsg.2015.03.013>

Barnaby R.J and Ward W. B (2007) 'Outcrop Analog for Mixed Siliciclastic – Carbonate Ramp Reservoirs — Stratigraphic Hierarchy, Facies Architecture, and Geologic Heterogeneity:

Grayburg Formation'. *Journal of Sedimentary Research* [online] 77 (1), 34–58. available from <https://doi.org/10.2110/jsr.2007.007%0A>

Beitler, B., Chan, M.A., and Parry, W.T. (2003) 'Bleaching of Jurassic Navajo Sandstone on Colorado Plateau Laramide Highs: Evidence of Exhumed Hydrocarbon Supergiants?' *Geology* [online] 31 (12), 1041–1044. available from <https://doi.org/10.1130/G19794.1%0A>

Bennion, B. and Bachu, S. (2005) 'Relative Permeability Characteristics for Supercritical CO2 Displacing Water in a Variety of Potential Sequestration Zones in the Western Canada Sedimentary Basin'. *SPE Annual Technical Conference and Exhibition. Society of Petroleum Engineers. 9-12 October* [online] (9–12 October). available from <https://doi.org/10.2118/95547-MS>

Bennion, D.B. and Bachu, S. (2006a) 'Dependence on Temperature, Pressure, and Salinity of the IFT and Relative Permeability Displacement Characteristics of CO2 Injected in Deep Saline Aquifers'. *SPE Annual Technical Conference and Exhibition. Society of Petroleum Engineers.* [online] (24–27 September). available from <https://doi.org/10.2118/102138-MS>

Bennion, D.B. and Bachu, S. (2006b) 'Supercritical CO2 and H2S — Brine Drainage and Imbibition Relative Permeability Relationships for Intergranular Sandstone and Carbonate Formations'. *SPE Europec/EAGE Annual Conference and Exhibition.* [online] (12–15 June). available from <https://doi.org/10.2118/99326-MS>

Bennion, D.B. and Bachu, S. (2006c) 'The Impact of Interfacial Tension and Pore - Size Distribution / Capillary Pressure Character on CO2 Relative Permeability at Reservoir Conditions in CO2-Brine Systems'. *SPE/DOE Symposium on Improved Oil Recovery. Society of Petroleum Engineers.* [online] (22–26 April). available from <https://doi.org/10.2118/99325-MS>

Bennion, D.B. and Bachu, S. (2008) 'Drainage and Imbibition Relative Permeability Relationships for Supercritical CO2 / Brine and H2S / Brine Systems in Intergranular Sandstone, Carbonate, Shale, and Anhydrite Rocks'. in *SPE Reservoir Evaluation & Engineering*. held 2008. 487–496

Bennion, D.B. and S Bachu (2010) 'Drainage and Imbibition CO2 / Brine Relative Permeability Curves at Reservoir Conditions for Carbonate Formations'. *SPE Annual Technical Conference and Exhibition. Society of Petroleum Engineers.* [online] (12–15 June), 1–18. available from <https://doi.org/10.2118/134028-MS>

Bentham, M. and Kirby, G. (2005) 'CO2 Storage in Saline Aquifers'. *Oil & gas science and technology* [online] 60 (3), 559–567. available from <https://doi.org/10.2516/ogst:2005038>

Bentley, M. and Ringrose, P. (2018) 'Future Directions in Reservoir Modelling: New Tools and "Fit-for-Purpose" Workflows'. *Geological Society, London, Petroleum Geology Conference series* [online] 8 (1), 537–546. available from <http://pgc.lyellcollection.org/lookup/doi/10.1144/PGC8.40>

Berg, S., Oedai, S., and Ott, H. (2013) 'Displacement and Mass Transfer between Saturated and Unsaturated CO2 – Brine Systems in Sandstone'. *International Journal of*

Greenhouse Gas Control [online] 12, 478–492. available from <http://dx.doi.org/10.1016/j.ijggc.2011.04.005>

Bergman, P.D. and Winter, E.M. (1995) 'Disposal of Carbon Dioxide in Aquifers in the US'. *Energy Conversion and Management* [online] 36 (6–9), 523–526. available from <https://doi.org/10.1016/0196-8904(95)00058-L>

Du Bernard, X., Labaume, P., Darcel, C., Davy, P. and Bour, O. (2002) 'Cataclastic Slip Band Distribution in Normal Fault Damage Zones, Nubian Sandstones, Suez Rift'. *Journal of Geophysical Research: Solid Earth* 107 (B7), ETG-6

Du Bernard, X., Eichhubl, P., and Aydin, A. (2002) 'Dilation Bands: A New Form of Localized Failure in Granular Media'. *Geophysical Research Letters* 29 (24), 1–4

Bernstein, L., Bosch, P., Canziani, O., Chen, Z., Christ, R., Davidson, O., Hare, W., Karoly, D., Kattsov, V., Kundzewicz, Z., Liu, J., Lohmann, U., Manning, M., Matsuno, T., Menne, B., Metz, B., Mirza, M., Nicholls, N., Nurse, L., Pachauri, R., Palutikof, J., Qin, D., Ravindranath, N., Reisinger, A., Ren, J., Riahi, K., Rosenzweig, C., Schneider, S., Sokona, Y., Solomon, S., Stott, P., Stouffer, R., Sugiyama, T., Swart, R., Tirpak, D., Vogel, C., and Yohe, G. (2008) *Climate Change 2007: Synthesis Report Summary for Policymakers*. 12–17

Bickle, M., Kampman, N. and Wigley, M. (2013) 'Natural Analogues'. in *Reviews in Mineralogy and Geochemistry* [online] vol. 77. 15–71. available from <https://doi.org/10.2138/rmg.2013.77.2>

Bickle, M., Chadwick, A., Huppert, H.E., Hallworth, M., and Lyle, S. (2007) 'Modelling Carbon Dioxide Accumulation at Sleipner: Implications for Underground Carbon Storage'. *Earth and Planetary Science Letters* [online] 255 (1–2), 164–176. available from <https://doi.org/10.1016/j.epsl.2006.12.013>

Bickle, M. and Kampman, N. (2013) 'Lessons in Carbon Storage from Geological Analogues'. *Geology* [online] 41 (4), 525–526. available from <https://doi.org/10.1130/focus0420132.1>

Bickle, M., Kampman, N., Chapman, H., Ballentine, C., Dubacq, B., Galy, A., Sirikitputtisak, T., Warr, O., Wigley, M., and Zhou, Z. (2017) 'Rapid Reactions between CO2 , Brine and Silicate Minerals during Geological Carbon Storage: Modelling Based on a Field CO2 Injection Experiment'. *Chemical Geology* [online] 468 (December 2016), 17–31. available from <http://dx.doi.org/10.1016/j.chemgeo.2017.07.031>

Biddle, K.T. and Wielchowsky, C.C. (1994) 'Hydrocarbon Traps'. in *The Petroleum System-from Source to Trap*. vol. 60. AAPG Memoir, 219–235

Birkholzer, J.T., Zhou, Q., and Tsang, C. (2009) 'Large-Scale Impact of CO2 Storage in Deep Saline Aquifers: A Sensitivity Study on Pressure Response in Stratified Systems'. *International Journal of Greenhouse Gas Controlas control,* [online] 3 (2), 181–194. available from <https://doi.org/10.1016/j.ijggc.2008.08.002>

Boggs Jr, S. (2014) *Principles of Sedimentology and Stratigraphy*. Pearson Education

BP Energy Outlook (2019) *2019 Edition*. London, United kingdom

Bradshaw, J., Bachu, S., Bonijoly, D., Burruss, R., Holloway, S., Peter, N., and Magne, O. (2007) 'CO2 Storage Capacity Estimation: Issues and Development of Standards'. *International Journal of Greenhouse Gas Control* [online] 1 (1), 62–68. available from <https://doi.org/10.1016/S1750-5836(07)00027-8>

Brandsæter, I., Mcilroy, D., Lia, O., Ringrose, P., and Næss, A. (2005) 'Reservoir Modelling and Simulation of Lajas Formation Outcrops (Argentina) to Constrain Tidal Reservoirs of the Halten Terrace (Norway)'. *Petroleum Geoscience* [online] 11 (1), 37–46. available from <https://doi.org/10.1144/1354-079303-611>

Breckels, I.M. and van Eekelen, H.A.M. (1982) 'Relationship between Horizontal Stress and Depth in Sedimentary Basins'. *Journal of Petroleum Technology* [online] 34 (09), 2191–2199. available from <http://www.onepetro.org/doi/10.2118/10336-PA>

Brown, K., Whittaker, S., Wilson, M., Srisang, W., Smithson, H., and Tontiwachwuthikul, P. (2017) 'The History and Development of the IEA GHG Weyburn-Midale CO2 Monitoring and Storage Project in Saskatchewan, Canada (the World Largest CO2 for EOR and CCS Program)'. *Petroleum* [online] 3 (1), 3–9. available from <http://dx.doi.org/10.1016/j.petlm.2016.12.002>

Brown, L.T. (2002) *Integration of Rock Physics and Reservoir Simulation for the Interpretation of Time-Lapse Seismic Data at Weyburn Field, Saskatchewa*. Doctoral dissertation, Colorado School of Mines. Arthur Lakes Library

Bryant, D., Kantorowicz, J.D., and Love, C.F. (1988) 'The Origin and Recognition of Laterally Continuous Carbonate-Cemented Horizons in the Upper Lias Sands of Southern England'. *Marine and Petroleum Geology* [online] 5 (2), 108–133. available from <https://doi.org/10.1016/0264-8172(88)90018-9>

Buckley, S.J., Enge, H.D., Carlsson, C. and Howell, J.A. (2010) 'Terrestrial Laser Scanning for Use in Virtual Outcrop Geology'. *The Photogrammetric Record* [online] 25 (131), 225–239. available from <https://doi.org/10.1111/j.1477-9730.2010.00585.x>

Burchette, T.P. (2012) 'Carbonate Rocks and Petroleum Reservoirs: A Geological Perspective from the Industry'. *Geological Society, London, Special Publications* [online] 370 (1), 17–37. available from <https://doi.org/10.1144/SP370.14>

Burnside, N.M. and Naylor, M. (2014) 'Review and Implications of Relative Permeability of CO2/Brine Systems and Residual Trapping of CO2'. *International Journal of Greenhouse Gas Control* [online] 23, 1–11. available from <http://dx.doi.org/10.1016/j.ijggc.2014.01.013>

Burnside, N.M., Shipton, Z.K., Dockrill, B., and Ellam, R.M. (2013) 'Man-Made versus Natural CO2 Leakage: A 400 k.y. History of an Analogue for Engineered Geological Storage of CO2'. *Geology* [online] 41 (4), 471–474. available from <https://doi.org/10.1130/G33738.1>

Busch, A., Amann-Hildenbrand, A., Bertier, P., Waschbuesch, M., and Krooss, B.M. (2010) 'The Significance of Caprock Sealing Integrity for CO2 Storage'. *SPE International Conference on CO2 Capture, Storage, and Utilization. Society of Petroleum Engineers.* [online] (10–12 November). available from <https://doi.org/10.2118/139588-MS>

Catuneanu, O., Galloway, W.E., Kendall, C.G.S.C., Miall, A.D., Posamentier, H.W., Strasser, A., and Tucker, M.E. (2011) 'Sequence Stratigraphy: Methodology and Nomenclature'. *Newsletters on Stratigraphy* [online] 44 (3), 173–245. available from <http://dx.doi.org/10.1127/0078-0421/2011/0011>

Cavanagh, A.J. and Haszeldine, R.S. (2014) 'The Sleipner Storage Site: Capillary Flow Modeling of a Layered CO2 Plume Requires Fractured Shale Barriers within the Utsira Formation'. *International Journal of Greenhouse Gas Control* [online] 21 (2014), 101–112. available from <http://dx.doi.org/10.1016/j.ijggc.2013.11.017>

Celia, M.A., Bachu, S., Nordbotten, J.M. and Bandilla, K.W. (2015) 'Status of CO2 Storage in Deep Saline Aquifers with Emphasis on Modeling Approaches and Practical Simulations'. *Water Resources Research* 51 (9), 6846–6892

Chadwick, A., Arts, R., Bernstone, C., May, F., Thibeau, S., and Zweigel, P. (2008) *Best Practice for the Storage of CO2 in Saline Aquifers - Observations and Guidelines from the SACS and CO2STORE Projects* [online] available from <http://nora.nerc.ac.uk/id/eprint/2959>

Chadwick, R.A., Noy, D.J., and Holloway, S. (2009) 'Flow Processes and Pressure Evolution in Aquifers during the Injection of Supercritical CO2 as a Greenhouse Gas Mitigation Measure'. *Petroleum Geoscience* [online] 15 (1), 59–73. available from <https://doi.org/10.1144/1354-079309-793>

Chadwick, R.A., Zweigel, P., Gregersen, U., and Kirby, G.A. (2004) 'Geological Reservoir Characterization of a CO2 Storage Site: The Utsira Sand, Sleipner, Northern North Sea'. *Energy* [online] 29, 1371–1381. available from <https://doi.org/10.1016/j.energy.2004.03.071>

Chan, M.A., Parry, W.T., and Bowman, J.R. (2000) 'Diagenetic Hematite and Manganese Oxides and Fault-Related Fluid Flow in Jurassic Sandstones, Southeastern Utah 1'. *AAPG bulletin* [online] 9 (9), 1281–1310. available from <https://doi.org/10.1306/A9673E82-1738-11D7-8645000102C1865D>

ChemicaLogic Corporation (2018) *Carbon Dioxide: Temperature - Pressure Diagram* [online] available from <http://www.chemicalogic.com/index.html>

Chiarella, D., Longhitano, S.G., and Tropeano, M. (2017) 'Types of Mixing and Heterogeneities in Siliciclastic-Carbonate Sediments'. *Marine and Petroleum Geology* [online] 88, 617–627. available from <http://dx.doi.org/10.1016/j.marpetgeo.2017.09.010>

Ciais, P., C. Sabine, G. Bala, L. Bopp, V. Brovkin, J. Canadell, A. Chhabra, R. DeFries, J. Galloway, M. Heimann, C. Jones, C. Le Quéré, R.B. Myneni, S.P. and P.T. (2013) 'Carbon and Other Biogeochemical Cycles'. in *Climate Change 2013: The Physical Science Basis. Contribution of Working Group I to the Fifth Assessment Report of the Intergovernmental Panel on Climate Change*. ed. by Stocker, T.F., D. Qin, G.-K. Plattner, M. Tignor, S.K. Allen, J. Boschung, A. Nauels, Y. Xia, V.B. and P.M.M. Cambridge University Press, Cambridge, United Kingdom and New York, NY, USA

CO2CRC (2008) *Storage Capacity Estimation, Site Selection and Characterisation for CO2 Storage Projects*. ed. by in Kaldi, J.G. and Gibson-Poole, C.M. Canbera, Report No.

RPT08-1001.

Crabaugh, M. and Kocurek, G. (1993) 'Entrada Sandstone: An Example of a Wet Aeolian System'. *Geological Society, London, Special Publications* [online] 72 (1), 103–126. available from <https://doi.org/10.1144/GSL.SP.1993.072.01.11>

CSLF (2007) 'Estimation of CO2 Storage Capacity in Geological Media - Phase 2 -'. *Carbon Sequestration Leadership Forum*

Cubasch, U., D. Wuebbles, D. Chen, M.C. Facchini, D. Frame, N. Mahowald, and J.-G.W. (2013) 'Introduction.' in *Climate Change 2013: The Physical Science Basis. Contribution of Working Group I to the Fifth Assessment Report of the Intergovernmental Panel on Climate Change*. ed. by Stocker, T.F., D. Qin, G.-K. Plattner, M. Tignor, S.K. Allen, J. Boschung, A. Nauels, Y. Xia, V.B. and P.M.M. Cambridge University Press, Cambridge, United Kingdom and New York, NY, USA. 119

Dance, T. (2013) 'Assessment and Geological Characterisation of the CO2CRC Otway Project CO2 Storage Demonstration Site: From Prefeasibility to Injection'. *Marine and Petroleum Geology* [online] 46, 251–269. available from <https://doi.org/10.1016/j.marpetgeo.2013.06.008>

Dance, T., Spencer, L., and Xu, J.Q. (2009) 'Geological Characterisation of the Otway Project Pilot Site: What a Difference a Well Makes'. *Energy Procedia* [online] 1 (1), 2871–2878. available from <https://doi.org/10.1016/j.egypro.2009.02.061>

Deng, H., Stauffer, P.H., Dai, Z., Jiao, Z. and Surdam, R.C. (2012) 'Simulation of Industrial-Scale CO2 Storage: Multi-Scale Heterogeneity and Its Impacts on Storage Capacity, Injectivity and Leakage'. *International Journal of Greenhouse Gas Control* [online] 10, 397–418. available from <https://doi.org/10.1016/j.ijggc.2012.07.003>

Dershowitz, B., Lapointe, P., Eiben, T., and Wei, L. (1998) 'Integration of Discrete Feature Network Methods with Conventional Simulator Approaches'. in *SPE Annual Technical Conference and Exhibition* [online] held 1998 at New Orleans, Louisiana. available from <https://doi.org/10.2118/49069-MS>

Deveugle, P.E.K., Jackson, M.D., Hampson, G.J., Farrell, M.E., Sprague, A.R., Stewart, J., and Calvert, C.S. (2011) 'Characterization of Stratigraphic Architecture and Its Impact on Fluid Flow in a Fluvial-Dominated Deltaic Reservoir Analog: Upper Cretaceous Ferron Sandstone Member , Utah'. *AAPG bulletin* [online] 95 (5), 693–727. available from <https://doi.org/10.1306/09271010025%0A>

Dockrill, B. and Shipton, Z.K. (2010) 'Structural Controls on Leakage from a Natural CO2 Geologic Storage Site: Central Utah, U.S.A.' *Journal of Structural Geology* [online] 32 (11), 1768–1782. available from <http://dx.doi.org/10.1016/j.jsg.2010.01.007>

Doelling, H.H. (2001) *Geologic Map of the Moab and Eastern Part of the San Rafael Desert 30' x 60' Quadrangles, Grand and Emery Counties, Utah, and Mesa County, Colorado. Utah Geological Survey, Map 180, 1:100000, Map 180.*

Doherty, B., Vasylkivska, V., Huerta, N.J., and Dilmore, R. (2017) 'Estimating the Leakage along Wells during Geologic CO2 Storage: Application of the Well Leakage Assessment Tool to a Hypothetical Storage Scenario in Natrona County , Wyoming'. *Energy Procedia*

[online] 114 (2016), 5151–5172. available from <http://dx.doi.org/10.1016/j.egypro.2017.03.1669>

Dong, H. and Blunt, M.J. (2009) 'Pore-Network Extraction from Micro-Computerized-Tomography Images'. *Physical review* [online] 80 (3), 1–11. available from <https://doi.org/10.1103/PhysRevE.80.036307>

Doughty, C. (2007) 'Modeling Geologic Storage of Carbon Dioxide: Comparison of Non-Hysteretic and Hysteretic Characteristic Curves'. *Energy Conversion and Management* [online] 48 (6), 1768–1781. available from <https://doi.org/10.1016/j.enconman.2007.01.022>

Downey, M.W. (1984) 'Evaluating Seals for Hydrocarbon Accumulations'. *AAPG bulletin* [online] 68 (11), 1752–1763. available from <https://doi.org/10.1306/AD461994-16F7-11D7-8645000102C1865D>

Dressel, B., Olsen, D., Ibm, N., Usdoe, B.B., Usdoe, P., and Usdoe, J.L. (2010) 'Depositional Environments Being Investigated by the National Energy Technology Laboratory (NETL) for Potential Geologic Storage of CO2'. *SPE Eastern Regional Meeting. Society of Petroleum Engineers* [online] 12–14 Octo. available from <https://doi.org/10.2118/138952-MS>

Eiken, O., Ringrose, P., Hermanrud, C., Nazarian, B., Tore, A.T., and Høier, L. (2011) 'Lessons Learned from 14 Years of CCS Operations: Sleipner, In Salah and Snøhvit'. *Energy Procedia* [online] 4, 5541–5548. available from <https://doi.org/10.1016/j.egypro.2011.02.541>

El-maghraby, R.M. and Blunt, M.J. (2013) 'Residual CO2 Trapping in Indiana Limestone'. *Environmental science & technology* [online] 47 (1), 227–233. available from <https://doi.org/10.1021/es304166u>

Ennis-King, J. and Paterson, L. (2002) 'Engineering Aspects of Geological Sequestration of Carbon Dioxide'. in *SPE Asia Pacific Oil and Gas Conference and Exhibition. Society of Petroleum Engineers.* [online] held 2002 at Melbourne, Australia. available from <https://doi.org/10.2118/77809-MS>

Ennis-King, J. and Paterson, L. (2005) 'Role of Convective Mixing in the Long-Term Storage of Carbon Dioxide in Deep Saline Formations'. *SPE* [online] 10 (03), 349–356. available from <https://doi.org/10.2118/84344-PA%0A>

Espie, T. and Woods, A. (2014) 'Testing Some Common Concepts in CO2 Storage'. *Energy Procedia* [online] 63, 5450–5460. available from <http://dx.doi.org/10.1016/j.egypro.2014.11.576>

Espinoza, D.N., Kim, S.H., and Santamarina, J.C. (2011) 'CO2 Geological Storage − Geotechnical Implications'. *KSCE Journal of Civil Engineering* [online] 15, 707–719. available from <https://doi.org/10.1007/s12205-011-0011-9>

Fachri, M., Rotevatn, A., and Tveranger, J. (2013) 'Fluid Flow in Relay Zones Revisited: Towards an Improved Representation of Small-Scale Structural Heterogeneities in Flow Models'. *Marine and Petroleum Geology* [online] 46, 144–164. available from <http://dx.doi.org/10.1016/j.marpetgeo.2013.05.016>

Falcon-suarez, I., Papageorgiou, G., Chadwick, A., North, L., Best, A.I., and Chapman, M. (2018) 'CO2-Brine Flow-through on an Utsira Sand Core Sample: Experimental and Modelling. Implications for the Sleipner Storage Field'. *International Journal of Greenhouse Gas Control* [online] 68 (2017), 236–246. available from <https://doi.org/10.1016/j.ijggc.2017.11.019>

Faulkner, D.R., Jackson, C.A.L., Lunn, R.J., Schlische, R.W., Shipton, Z.K., Wibberley, C.A.J., and Withjack, M.O. (2010) 'A Review of Recent Developments Concerning the Structure, Mechanics and Fluid Flow Properties of Fault Zones'. *Journal of Structural Geology* [online] 32 (11), 1557–1575. available from <http://dx.doi.org/10.1016/j.jsg.2010.06.009>

Faulkner, D.R., Rutter, E.H., Andrew, S., and Smith, F. (1998) 'The Gas Permeability of Clay-Bearing Fault Gouge at 20°C'. *Geological Society, London, Special Publications* [online] 147 (1), 147–156. available from <https://doi.org/10.1144/GSL.SP.1998.147.01.10>

Fenghour, A., Wakeham, W.A. and Vesovic, V. (1998) 'The Viscosity of Carbon Dioxide'. *Journal of physical and chemical reference data* [online] 27 (1), 31–44. available from <https://doi.org/10.1063/1.556013>

Firoozabadi, A. and Cheng, P. (2010) 'Prospects for Subsurface CO2 Sequestration'. *AIChE Journal* [online] 56 (6), 1398–1405. available from <10.1002/aic.12287>

Fisher, Q.J. and Knipe, R.J. (2001) 'The Permeability of Faults within Siliciclastic Petroleum Reservoirs of the North Sea and Norwegian Continental Shelf'. *Marine and Petroleum Geology* [online] 18 (10), 1063–1081. available from <https://doi.org/10.1016/S0264-8172(01)00042-3>

Flett, M., Brantjes, J., Gurton, R., Mckenna, J., and Tankersley, T. (2009) 'Subsurface Development of CO2 Disposal for the Gorgon Project'. *Energy Procedia* [online] 1 (1), 3031–3038. available from <http://dx.doi.org/10.1016/j.egypro.2009.02.081>

Flett, M., Gurton, R., and Weir, G. (2007) 'Heterogeneous Saline Formations for Carbon Dioxide Disposal: Impact of Varying Heterogeneity on Containment and Trapping'. *Journal of Petroleum Science and Engineering* [online] 57 (1–2), 106–118. available from <https://doi.org/10.1016/j.petrol.2006.08.016>

Fleury, M., Pironon, J., Nindre, Y.M. Le, Bildstein, O., Berne, P., and Lagneau, V. (2011) 'Evaluating Sealing Efficiency of Caprocks for CO2 Storage : An Overview of the Geocarbone Integrity Program and Results .' *Energy Procedia* [online] 4, 5227–5234. available from <http://dx.doi.org/10.1016/j.egypro.2011.02.501>

Fossen, H., Schultz, R.A., Shipton, Z.K. and Mair, K. (2007) 'Deformation Bands in Sandstone: A Review'. *Journal of the Geological Society* [online] 164 (4), 755–769. available from <https://doi.org/10.1144/0016-76492006-036%0A>

Fossen, H., Soliva, R., Ballas, G., Trzaskos, B., Cavalcante, C. and Schultz, R.A. (2017) 'A Review of Deformation Bands in Reservoir Sandstones: Geometries, Mechanisms and Distribution'. *Geological Society, London, Special Publications,* [online] 459 (1), 9–33. available from <https://doi.org/10.1144/SP459.4>

Fossen, H., Zuluaga, L.F., Ballas, G., Soliva, R. and Rotevatn, A. (2015) 'Contractional

Deformation of Porous Sandstone: Insights from the Aztec Sandstone, SE Nevada, USA'. *Journal of Structural Geology* [online] 74, 172–184. available from <https://doi.org/10.1016/j.jsg.2015.02.014>

Fossen, H. and Bale, A. (2007) 'Deformation Bands and Their Influence on Fluid Flow'. *AAPG bulletin* [online] 91 (12), 1685–1700. available from <https://doi.org/10.1306/07300706146%0A>

Fowles, J. and Burley, S. (1994) 'Textural and Permeability Characteristics of Faulted, High Porosity Sandstones Textural and Permeability Characteristics of Faulted, High Porosity Sandstones'. *Marine and Petroleum Geology* [online] 11 (5), 608–623. available from <https://doi.org/10.1016/0264-8172(94)90071-X>

Gabrielsen, R.H. and Koestler, A.G. (1987) 'Description and Structural Implications of Fractures in Late Jurassic Sandstones of the Troll Field, Northern North Sea'. *Norsk Geologisk Tidsskrift* 67 (4), 371–381

Gamboa, D., Williams, J.D.O., Bentham, M., Scho, D.I., and Mitchell, A.C. (2019) 'Application of Three-Dimensional Fault Stress Models for Assessment of Fault Stability for CO2 Storage Sites'. *International Journal of Greenhouse Gas Control* [online] 90, 102820. available from <https://doi.org/10.1016/j.ijggc.2019.102820>

Gao, X., Liu, L., Jiang, Z., Shang, X., and Liu, G. (2013) 'Geoscience Frontiers A Pre-Paleogene Unconformity Surface of the Sikeshu Sag, Junggar Basin: Lithological, Geophysical and Geochemical Implications for the Transportation of Hydrocarbons'. *Geoscience Frontiers* [online] 4 (6), 779–786. available from <http://dx.doi.org/10.1016/j.gsf.2012.12.003>

Gasda, S.E., Nordbotten, J.M., and and Celia, M.A. (2009) 'Vertical Equilibrium with Sub-Scale Analytical Methods for Geological CO2 Sequestration'. *Computational Geosciences* [online] 13 (4), 469–481. available from <https://doi.org/10.1007/s10596-009-9138-x>

Gaus, I. (2010) 'Role and Impact of CO2-Rock Interactions during CO2 Storage in Sedimentary Rocks'. *International Journal of Greenhouse Gas Control* [online] 4 (1), 73–89. available from <https://doi.org/10.1016/j.ijggc.2009.09.015>

Ghanbari, S., Pickup, G.E., Mackay, E., Gozalpour, F., and Todd, A.C. (2006) 'Simulation of CO2 Storage in Saline Aquifers'. *Chemical Engineering Research and Design* 84 (A9), 764–775

Gibson-Poole, C.M., Svendsen, L., Watson, M.N., Daniel, R.F., Ennis-King, J. and Rigg, A.J. (2009) 'Understanding Stratigraphic Heterogeneity: A Methodology to Maximize the Efficiency of the Geological Storage of CO2',. in *Carbon Dioxide Sequestration in Geological Media—State of the Science* [online] ed. by Grobe, M. and J. C. Pashin, and R.L.D. vol. 59. AAPG Studies in Geology, 347–364. available from <doi:10.1306/13171248St593385>

Global CCS Institute (2008) *Aquifer Storage-Development Issues*.

Global CCS Institute (2017) *The Global Status of CCS*. [online] available from <www.globalccsinstitute.com>

Goater, A.L., Bijeljic, B., and Blunt, M.J. (2013) 'Dipping Open Aquifers — The Effect of Top-Surface Topography and Heterogeneity on CO2 Storage Efficiency'. *International Journal of Greenhouse Gas Control* [online] 17, 318–331. available from <http://dx.doi.org/10.1016/j.ijggc.2013.04.015>

Goodman, A., Bromhal, G., Strazisar, B., Rodosta, T., Guthrie, W.F., Allen, D., and Guthrie, G. (2013) 'Comparison of Methods for Geologic Storage of Carbon Dioxide in Saline Formations'. *International Journal of Greenhouse Gas Control* [online] 18, 329–342. available from <http://dx.doi.org/10.1016/j.ijggc.2013.07.016>

Gorecki, C.D., Hamling, J.A., Klapperich, R.J., Steadman, E.N., and Harju, J.A. (2012) 'Integrating CO2EOR and CO2 Storage in the Bell Creek Oil Field'. in *Carbon Management Technology Conference. Carbon Management Technology Conference.* [online] held 2012. 1–12. available from <https://doi.org/10.7122/151476-MS>

Gorecki, C.D., Sorensen, J.A., Bremer, J.M., Knudsen, D.J., and Smith, S.A. (2009) 'Development of Storage Coefficients for Determining the Effective CO2 Storage Resource in Deep Saline Formations'. in *SPE International Conference on CO2 Capture, Storage, and Utilization. Society of Petroleum Engineers.* [online] held 2009. available from <https://doi.org/10.2118/126444-MS>

Green, C., Ennis-king, J., and Pruess, K. (2009) 'Effect of Vertical Heterogeneity on Long-Term Migration of CO2 in Saline Formations'. *Energy Procedia* [online] 1 (1), 1823–1830. available from <http://dx.doi.org/10.1016/j.egypro.2009.01.238>

Griffiths, J., Faulkner, D.R., Edwards, A.P. and Worden, R.H. (2018) 'Deformation Band Development as a Function of Intrinsic Host-Rock Properties in Triassic Sherwood Sandstone'. *geological Society, London, Special Publications,* [online] 435 (1), 161–167. available from <https://doi.org/10.1144/SP435.11>

Grude, S., Landrø, M., and Osdal, B. (2013) 'Time-Lapse Pressure – Saturation Discrimination for CO2 Storage at the Snøhvit Field'. *International Journal of Greenhouse Gas Control* [online] 19, 369–378. available from <http://dx.doi.org/10.1016/j.ijggc.2013.09.014>

Hamling, J.A., Gorecki, C.D., Klapperich, R.J., Saini, D., and Steadman, E.N. (2013) 'Overview of the Bell Creek Combined CO2 Storage and CO2 Enhanced Oil Recovery Project'. *Energy Procedia* [online] 37 (Figure 2), 6402–6411. available from <http://dx.doi.org/10.1016/j.egypro.2013.06.570>

Hampson, G.J., Morris, J.E., and Johnson, H.D. (2014) 'Synthesis of Time-Stratigraphic Relationships and Their Impact on Hydrocarbon Reservoir Distribution and Performance, Bridport Sand Formation, Wessex Basin, UK'. *Geological Society, London, Special Publications* [online] 404 (1), 199–222. available from <https://doi.org/10.1144/SP404.2>

Hansen, O., Gilding, D., Nazarian, B., and Osdal, B. (2013) 'Snøhvit : The History of Injecting and Storing 1 Mt CO2 in the Fluvial Tubåen Fm.' *Energy Procedia* [online] 37, 3565–3573. available from <http://dx.doi.org/10.1016/j.egypro.2013.06.249>

Haszeldine, R.S., Quinn, O., England, G., Wilkinson, M., Shipton, Z.K., Evans, J.P., Heath, J., Crossey, L., Ballentine, C.J., and Graham, C.M. (2005) 'Natural Geochemical Analogues for Carbon Dioxide Storage in Deep Geological Porous Reservoirs, a United Kingdom

Perspective'. *Oil and Gas Science and Technology* [online] 60 (1), 33–49. available from <https://doi.org/10.2516/ogst:2005004>

He, Y., Kerans, C., Zeng, H., Janson, X., and Scott, S.Z. (2019) 'Improving Three-Dimensional Interpretation for Reservoir Model Construction: An Example of Geostatistical and Seismic Forward Modeling of Permian San Andres Shelf – Grayburg Platform Mixed Clastic – Carbonate Strata'. *AAPG Bulletin* [online] 8 (8), 1839–1887. available from <https://doi.org/10.1306/11211817244%0A>

Hellevang, H. (2015) 'Carbon Capture and Storage (CCS)'. in *Petroleum Geoscience: From Sedimentary Environments to Rock Physics*. ed. by Bjørlykke, K. Berlin, Heidelberg.: Springer, 591–602

Hepple, R.P. and Benson, S.M. (2005) 'Geologic Storage of Carbon Dioxide as a Climate Change Mitigation Strategy: Performance Requirements and the Implications of Surface Seepage'. *Environmental Geology* [online] 47 (476–585). available from <https://doi.org/10.1007/s00254-004-1181-2>

Hesse, M.A., Orr, F.M., and Tchelepi, H.A. (2009) 'Gravity Currents with Residual Trapping'. *Energy Procedia* [online] 1 (1), 3275–3281. available from <doi:10.1017/S002211200800219X>

Hester, R.E. and Harrison, R.M. (ed.) (2010) *Carbon Capture: Sequestration and Storage*. Royal Society of Chemistry.

HM Treasury (2020) *Budget 2020: Delivering on Our Promises to the British People* [online] available from <www.gov.uk/official-documents>

Holloway, S. and Savage, D. (1993) 'The Potential for Aquifer Disposal of Carbon Dioxide in the UK'. *Energy Conversion and Management* [online] 34 (9–11), 925–932. available from <https://doi.org/10.1016/0196-8904(93)90038-C>

Holloway, S., Vincent, C.J., Bentham, M.S., and Kirk, K.L. (2006) 'Top-down and Bottom-up Estimates of CO2 Storage Capacity in the United Kingdom Sector of the Southern North Sea Basin'. *Environmental Geosciences* [online] 13 (2), 71–84. available from <https://doi.org/10.1306/eg.11080505015%0A>

Hongjun, Z., Xinwei, L., Yanfang, C., and Xiaoliang, Z. (2010) 'Sensitivity Analysis of CO2 Sequestration in Saline Aquifers'. *Petroleum Science* [online] 7 (3), 372–378. available from <DOI 10.1007/s12182-010-0080-2>

Hovorka, S.D., Doughty, C., Benson, S.M., Pruess, K., and Knox, P.R. (2004) 'The Impact of Geological Heterogeneity on CO2 Storage in Brine Formations: A Case Study from the Texas Gulf Coast'. *Geological Society, London, Special Publications* [online] 233 (1), 147–163. available from <http://sp.lyellcollection.org/lookup/doi/10.1144/GSL.SP.2004.233.01.10>

Hovorka, S.D., Meckel, T.A., Trevino, R.H., Jean-philippe, J.L., Choi, J., Freeman, D., Cook, P., Daley, T.M., Ajo-, J.B., Freifeild, B.M., Doughty, C., Carrigan, C.R., Brecque, D. La, Kharaka, Y.K., Thordsen, J.J., Phelps, T.J., Yang, C., Katherine, D., Zhang, T., Holt, R.M., Lindler, J.S., and Butsch, R.J. (2011) 'Monitoring a Large Volume CO2 Injection: Year Two Results from SECARB Project at Denbury's Cranfield, Mississippi, USA'. *Energy*

Procedia [online] 4, 3478–3485. available from <http://dx.doi.org/10.1016/j.egypro.2011.02.274>

Hovorka, S.D., Sakurai, S., Kharaka, Y.K., Nance, H.S., Benson, S.M., Freifeld, B.M., Trautz, R.C., Phelps, T., and Daley, T.M. (2006) 'Monitoring CO2 Storage in Brine Formations : Lessons Learned from the Frio Field Test One Year Post Injection'. *Gulf coast carbon center publication library, Bookshelf* 1–9

Howell, J.A., Martinus, W.A., and Good, T.R. (2014) 'The Application of Outcrop Analogues in Geological Modelling: A Review, Present Status and Future Outlook'. *Geological Society, London, Special Publications* 387 (1), 1–25

Howell, J.A., Skorstad, A., Macdonald, A., Fordham, A., and Flint, S. (2008) 'Sedimentological Parameterization of Shallow-Marine Reservoirs'. *Petroleum Geoscience* [online] 14 (1), 17–34. available from <https://doi.org/10.1144/1354-079307-787>

Ide, S.T., Jessen, K., and Orr Jr, F.M. (2007) 'Storage of CO2 in Saline Aquifers: Effects of Gravity , Viscous, and Capillary Forces on Amount and Timing of Trapping'. *International journal of greenhouse gas control* [online] 1, 481–491. available from <https://doi.org/10.1016/S1750-5836(07)00091-6>

Iding, M. and Ringrose, P. (2010) 'Evaluating the Impact of Fractures on the Performance of the In Salah CO2 Storage Site'. *International Journal of Greenhouse Gas Control* [online] 4 (2), 242–248. available from <https://doi.org/10.1016/j.ijggc.2009.10.016>

IEA (2011) *Technology Roadmap Carbon Capture and Storage in Industrial Applications*. International Energy Agency, United Nations Industrial Development Organizations.

IEA (2013) *Technology Roadmap: Carbon Capture and Storage*.

IEA (2019) *Word Energy Outlook-Executive Summary*. Paris

IEAGHG (2011) *Caprock Systems for CO2 Geological Storage.* vol. May

Iglauer, S. (2011) *Dissolution Trapping of Carbon Dioxide in Reservoir Formation Brine – A Carbon Storage Mechanism*. ed. by Dr. Hironori Nakajima. INTECH Open Access Publisher

Iglauer, S., Pentland, C.H., and Busch, A. (2014) 'CO2 Wettability of Seal and Reservoir Rocks and the Implications for Carbon Geo-Sequestration'. *Water Resources Research Review* [online] 51 (1), 729–774. available from <https://doi.org/10.1002/2014WR015553>

IPCC: Annex: I (2018) 'Glossary [Matthews, J.B.R. (Ed.)].' in *Global Warming of 1.5°C. An IPCC Special Report on the Impacts of Global Warming of 1.5°C above Pre-Industrial Levels and Related Global Greenhouse Gas Emission Pathways, in the Context of Strengthening the Global Response to the Threat of Climate Change,*. ed. by Masson-Delmotte, V., P. Zhai, H.-O. Pörtner, D. Roberts, J.S., P.R. Shukla, A. Pirani, W. Moufouma-Okia, C. Péan, R. Pidcock, S. Connors, J.B.R. Matthews, Y. Chen, X.Z., and M.I. Gomis, E. Lonnoy, T. Maycock, M. Tignor, and T.W.

IPCC (2005) *IPCC Special Report on Carbon Dioxide Capture and Storage. Prepared by Working Group III of the Intergovernmental Panel on Climate Change [Metz, B., O. Davidson, H. C. de Coninck, M. Loos, and L. A. Meyer* [online] ed. by Metz, B., O.

Davidson, H. C. de Coninck, M. Loos, and L.A.M. vol. 49. United Kingdom and New York, NY, USA: Cambridge University Press, Cambridge. available from <http://www.ncbi.nlm.nih.gov/pubmed/20942501>

IPCC (2013) 'Summary for Policymakers'. in *Climate Change 2013: The Physical Science Basis. Contribution of Working Group I to the Fifth Assessment Report of the Intergovernmental Panel on Climate Change*. ed. by Stocker, T.F., D. Qin, G.-K. Plattner, M. Tignor, S. K. Allen, J. Boschung, A. Nauels, Y. Xia, V.B. and P.M.M. Cambridge University Press, Cambridge, United Kingdom and New York, NY, USA.

IPCC (2018) 'Summary for Policymakers.' in *Global Warming of 1.5°C. An IPCC Special Report on the Impacts of Global Warming of 1.5°C above Pre-Industrial Levels and Related Global Greenhouse Gas Emission Pathways, in the Context of Strengthening the Global Response to the Threat of Climate Change,*. ed. by [Masson-Delmotte, V., P. Zhai, H.-O. Pörtner, D. Roberts, J. Skea, P.R.S., A. Pirani, W. Moufouma-Okia, C. Péan, R. Pidcock, S. Connors, J.B.R. Matthews, Y. Chen, X. Zhou, M.I.G., and E. Lonnoy, T. Maycock, M. Tignor, and T.W.

Islam, A., Chevalier, S., and Sassi, M. (2013) 'Experimental and Numerical Studies of CO2 Injection into Water-Saturated Porous Medium: Capillary to Viscous to Fracture Fingering Phenomenon'. *Energy Procedia* [online] 37, 5511–5519. available from <http://dx.doi.org/10.1016/j.egypro.2013.06.471>

Ivandic, M., Juhlin, C., Lüth, S., Bergmann, P., Kashubin, A., Sopher, D., Ivanova, A., Baumann, G., and Henninges, J. (2015) 'Geophysical Monitoring at the Ketzin Pilot Site for CO2 Storage: New Insights into the Plume Evolution'. *International Journal of Greenhouse Gas Control* [online] 32, 90–105. available from <http://dx.doi.org/10.1016/j.ijggc.2014.10.015>

Jamison, W.R. and Stearns, D.W. (1982) 'Tectonic Deformation of Wingate Sandstone, Colorado National Monument.' *AAPG Bulletin* [online] 66 (12), 2584–2608. available from <https://doi.org/10.1306/03B5AC7D-16D1-11D7-8645000102C1865D%0A>

Jensen, G., Nickel, E., Whittaker, S., and Rostron, B. (2011) 'Site Assessment Update at Weyburn-Midale CO2 Sequestration Project, Saskatchewan, Canada: New Results at an Active CO2 Sequestration Site.' *Energy Procedia* [online] 4, 4777–4784. available from <http://dx.doi.org/10.1016/j.egypro.2011.02.442>

Jiang, X. (2011) 'A Review of Physical Modelling and Numerical Simulation of Long-Term Geological Storage of CO2'. *Applied Energy* [online] 88 (11), 3557–3566. available from <https://doi.org/10.1016/j.apenergy.2011.05.004>

Jin, M., Mackay, E., Quinn, M., Hitchen, K., and Akhurst, M. (2012) 'Evaluation of the CO2 Storage Capacity of the Captain Sandstone Formation'. *In SPE Europec/EAGE Annual Conference. Society of Petroleum Engineers. 4-7 June* [online] available from <https://doi.org/10.2118/154539-MS>

Juanes, R., Spiteri, E.J., Orr, F.M., and Blunt, M.J. (2006) 'Impact of Relative Permeability Hysteresis on Geological CO2 Storage'. *Water Resources Research* [online] 42 (12), 1–13. available from <https://doi.org/10.1029/2005WR004806>

Kampman, N., Bickle, M., Wigley, M., and Dubacq, B. (2014) 'Fluid Flow and CO2-Fluid-

Mineral Interactions during CO2-Storage in Sedimentary Basins'. *Chemical Geology* [online] 369, 22–50. available from <http://dx.doi.org/10.1016/j.chemgeo.2013.11.012>

Kampman, N., Busch, A., Bertier, P., Snippe, J., Hangx, S., Pipich, V., Di, Z., Rother, G., Harrington, J.F., Evans, J.P., Maskell, A., Chapman, H.J., and Bickle, M.J. (2016) 'Observational Evidence Confirms Modelling of the Long-Term Integrity of CO2-Reservoir Caprocks'. *Nature Communications* [online] 7 (1), 1–10. available from <https://doi.org/10.1038/ncomms12268>

Kantorowicz, J.D., Bryant, I.D. and Dawans, J.. (1987) 'Controls on the Geometry and Distribution of Carbonate Cements in Jurassic Sandstones: Bridport Sands, Southern England and Viking Group, Troll Field, Norway'. *Geological Society, London, Special Publications* [online] 36 (1), 103–118. available from <https://doi.org/10.1144/GSL.SP.1987.036.01.09>

Kazemi, H., Merrill Jr, L.S., Porterfield, K.L., and Zeman, P.R. (1976) 'Numerical Simulation of Water-Oil Flow in Naturally Fractured Reservoirs'. *SPE* [online] 16 (6), 317–326. available from <https://doi.org/10.2118/5719-PA>

Kempka, T., Klein, E., Lucia, M. De, Tillner, E., and Kühn, M. (2013) 'Assessment of Long-Term CO2 Trapping Mechanisms at the Ketzin Pilot Site (Germany) by Coupled Numerical Modelling'. *Energy Procedia* [online] 37, 5419–5426. available from <http://dx.doi.org/10.1016/j.egypro.2013.06.460>

Kempka, T., Lucia, M. De, and Kühn, M. (2014) 'Geomechanical Integrity Verification and Mineral Trapping Quantification for the Ketzin CO2 Storage Pilot Site by Coupled Numerical Simulations'. *Energy Procedia* [online] 63, 3330–3338. available from <http://dx.doi.org/10.1016/j.egypro.2014.11.361>

Kopp, A., Class, H., and Helmig, R. (2009) 'Investigations on CO2 Storage Capacity in Saline Aquifers Part 1. Dimensional Analysis of Flow Processes and Reservoir Characteristics'. *International Journal of Greenhouse Gas Control* [online] 3, 263–276. available from <https://doi.org/10.1016/j.ijggc.2008.10.002>

Krevor, S., Blunt, M.J., Benson, S.M., Pentland, C.H., Reynolds, C., Al-menhali, A., and Niu, B. (2015) 'Capillary Trapping for Geologic Carbon Dioxide Storage – From Pore Scale Physics to Field Scale Implications'. *International Journal of Greenhouse Gas Control* [online] 40, 221–237. available from <http://dx.doi.org/10.1016/j.ijggc.2015.04.006>

Krevor, S.C.M., Pini, R., Li, B., and Benson, S.M. (2011) 'Capillary Heterogeneity Trapping of CO2 in a Sandstone Rock at Reservoir Conditions'. *Geophysical Research Letters* [online] 38 (August), 1–5. available from <https://doi.org/10.1029/2011GL048239>

Kumar, A., Noh, M., Pope, G.A., Sepehrnoori, K., Bryant, S., and Lake, L.W. (2004) 'Reservoir Simulation of CO2 Storage in Deep Saline Aquifers'. *Society of Petroleum Engineers Journal* [online] 10 (03), 17–21. available from <https://doi.org/10.2118/89343-PA>

Lafare, A.E.A., Peach, D.W., and Hughes, A.G. (2016) 'Use of Seasonal Trend Decomposition to Understand Groundwater Behaviour in the Permo-Triassic Sandstone Aquifer, Eden Valley, UK'. *Hydrogeology Journal* [online] 24 (1), 141–158. available from <10.1007/s10040-015-1309-3>

Larkin, R.G. (2010) 'Hydrodynamic Trapping of CO2 Geosequestered in Saline Aquifers'. in *SPE Improved Oil Recovery Symposium. Society of Petroleum Engineers* [online] held 2010 at Tulsa, Oklahoma, USA. available from <https://doi.org/10.2118/128205-MS>

Law, D.H. and Bachu, S. (1996) 'Hydrological and Numerical Analysis of CO2 Disposal in Deep Aquifers in the Alberta Sedimentary Basin'. *Energy Conversion & Management* [online] 37 (95), 1167–1174. available from <https://doi.org/10.1016/0196-8904(95)00315-0>

Lei, Q., Latham, J., and Tsang, C. (2017) 'The Use of Discrete Fracture Networks for Modelling Coupled Geomechanical and Hydrological Behaviour of Fractured Rocks'. *Computers and Geotechnics* [online] 85, 151–176. available from <http://dx.doi.org/10.1016/j.compgeo.2016.12.024>

Lengler, U., Lucia, M. De, and Kühn, M. (2010) 'The Impact of Heterogeneity on the Distribution of CO2: Numerical Simulation of CO2 Storage at Ketzin'. *International Journal of Greenhouse Gas Control* [online] 4 (6), 1016–1025. available from <http://dx.doi.org/10.1016/j.ijggc.2010.07.004>

Leung, D.Y.C., Caramanna, G., and Maroto-valer, M.M. (2014) 'An Overview of Current Status of Carbon Dioxide Capture and Storage Technologies'. *Renewable and Sustainable Energy Reviews* [online] 39, 426–443. available from <http://dx.doi.org/10.1016/j.rser.2014.07.093>

Leveille, G.P., Knipe, R., More, C., Ellis, D., Dudley, G., Jones, G., Fisher, Q.J. and Allinson, G. (1997) 'Compartmentalization of Rotliegendes Gas Reservoirs by Sealing Faults, Jupiter Fields Area, Southern North Sea'. *London, Special Publications* [online] 123 (1), 87–104. available from <https://doi.org/10.1144/GSL.SP.1997.123.01.06>

Levorsen, A.I. and and Berry, F.A. (1967) *Geology of Petroleum*. The AAPG Foundation

Lewis, C.L.E., Green, P.F., Carter, A., and Hurford, A.J. (1992) 'Elevated K/T Palaeotemperatures throughout Nortwest England: Three Kilometres of Tertiary Erosion?' *Earth and Planetary Science Letters* [online] 112 (1), 131–145. available from <https://doi.org/10.1016/0012-821X(92)90012-K>

Li, S., Dong, M., Li, Z., Huang, S., Qing, H., and Nickel, E. (2005) 'Gas Breakthrough Pressure for Hydrocarbon Reservoir Seal Rocks : Implications for the Security of Long-Term CO2 Storage in the Weyburn Field'. *Geofluids* [online] 5 (4), 326–334. available from <https://doi.org/10.1111/j.1468-8123.2005.00125.x>

Lindeberg, E. and Bergmo, P. (2003) 'The Long-Term Fate of CO2 Injected into an Aquifer'. in *Greenhouse Gas Control Technologies*. held 2003. pp.489-494

Lindeberg, E., Vuillaume, J., and Ghaderi, A. (2009) 'Determination of the CO2 Storage Capacity of the Utsira Formation'. *Energy Procedia* [online] 1 (1), 2777–2784. available from <http://dx.doi.org/10.1016/j.egypro.2009.02.049>

Løvoll, G., Méheust, Y., Måløy, K.J., Aker, E., and pand Schmittbuhl, J. (2005) 'Competition of Gravity, Capillary and Viscous Forces during Drainage in a Two-Dimensional Porous Medium , a Pore Scale Study'. *Energy* [online] 30 (6), 861–872. available from <https://doi.org/10.1016/j.energy.2004.03.100>

Lu, J., Cook, P.J., Hosseini, S.A., Yang, C., Romanak, K.D., Zhang, T., Freifeld, B.M., Smyth,

R.C., Zeng, H., and Hovorka, S.D. (2012) ‘Complex Fluid Flow Revealed by Monitoring CO2 Injection in a Fluvial Formation’. *Journal of Geophysical Research: Solid Earth* [online] 117, B3. available from <https://doi.org/10.1029/2011JB008939>

Lu, J., Kordi, M., Hovorka, S.D., Meckel, T.A., and Christopher, C.A. (2013) ‘Reservoir Characterization and Complications for Trapping Mechanisms at Cranfield CO2 Injection Site’. *International Journal of Greenhouse Gas Control* [online] 18, 361–374. available from <hhttps://doi.org/10.1016/j.ijggc.2012.10.007>

Måløy, K.J., Feder, J., and Torstein, J. (1985) ‘Viscous Fingering Fractal in Porous Media’. *Physical review letters* [online] 55 (24), 2688. available from <https://link.aps.org/doi/10.1103/PhysRevLett.55.2688>

Manzocchi, T., Walsh, J.J., Nell, P. and Yielding, G. (1999) ‘Fault Transmissibility Multipliers for Flow Simulation Models’. *Petroleum Geoscience* [online] 5 (1), 53–63. available from <https://doi.org/10.1144/petgeo.5.1.53>

Manzocchi, T., Carter, J.N., Skorstad, A., Fjellvoll, B., Stephen, K.D., Howell, J.A., Matthews, J.D., Walsh, J.J., Nepveu, M., Bos, C., Cole, J., Egberts, P., Flint, S., Hern, C., Holden, L., Hovland, H., Jackson, H., Kolbjørnsen, O., and Macdonald, A. (2008) ‘Sensitivity of the Impact of Geological Uncertainty on Production from Faulted and Unfaulted Shallow-Marine Oil Reservoirs : Objectives and Methods’. *Petroleum Geoscience* [online] 14 (1), 3–15. available from <https://doi.org/10.1144/1354-079307-790>

Manzocchi, T., Ringrose, P.S., and Underhill, J.R. (1998) ‘Flow through Fault Systems in High-Porosity Sandstones’. *Geological Society, London, Special Publications* 127 (1), 65–82

Manzocchi, T., Walsh, J.J., Nell, P., and Yielding, G. (2010) ‘Fault Transmissibility Multipliers for Flow Simulation Models’. *Petroleum Geoscience* [online] 5 (1), 53–63. available from <https://doi.org/10.1144/petgeo.5.1.53>

Mathias, S.A., González, G.J., Miguel, M. De, Thatcher, K.E., and Zimmerman, R.W. (2011) ‘Pressure Buildup During CO2 Injection into a Closed Brine Aquifer’. *Transport in Porous Media* [online] 89 (3), 383–397. available from <https://doi.org/10.1007/s11242-011-9776-z>

Matthäi, S.K., Aydin, A., Pollard, D.D. and Roberts, S.G. (1998) ‘Numerical Simulation of Departures from Radial Drawdown in a Faulted Sandstone Reservoir with Joints and Deformation Bands’. *Geological Society, London, Special Publications* 147 (1), 157–191

McNeill, D.F., Cunningham, K.J., Guertin, L.A., and Anselmetti, F.S. (2004) ‘Depositional Themes of Mixed Carbonate-Siliciclastics in the South Florida Neogene: Application to Ancient Deposits’. *AAPG Memoir* (3), 23–43

Menéndez, B., Zhu, W. and Wong, T.F. (1996) ‘Micromechanics of Brittle Faulting and Cataclastic Flow in Berea Sandstone’. *Journal of structural geology* [online] 18 (1), 1–16. available from <https://doi.org/10.1016/0191-8141(95)00076-P>

Meyer, J. and Croskrey, A. (2017) ‘Interpreted Water Quality Calculated from Borehole Resistivity Measurements in the Gulf Coast Aquifer, Lower Rio Grande Valley, Texas, USA.’ *CSEG Recorder* [online] 42 (7), 1–4. available from <Interpreted Water Quality Calculated from Borehole Resistivity Measurements in the Gulf Coast Aquifer, Lower

Rio Grande Valley, Texas, USA>

Michael, K., Golab, A., Shulakova, V., Ennis-King, J., Allinson, G., Sharma, S., and Aiken, T. (2010) 'Geological Storage of CO2 in Saline Aquifers-A Review of the Experience from Existing Storage Operations'. *International Journal of Greenhouse Gas Control* [online] 4 (4), 659–667. available from <https://doi.org/10.1016/j.ijggc.2009.12.011>

Morris, J.E., Hampson, G.J., and Johnson, H.O.W.D. (2006) 'A Sequence Stratigraphic Model for an Intensely Bioturbated Shallow-Marine Sandstone: The Bridport Sand Formation, Wessex Basin , UK'. *Sedimentology* [online] 53, 1229–1263. available from <https://doi.org/10.1111/j.1365-3091.2006.00811.x>

Moss, B., Barson, D., Rakhit, K., Dennis, H., Swarbrick, R., Evans, D., Graham, C., Armour, A. and Bathurst, P. (2003) 'Formation Pore Pressures and Formation Waters. The Millennium Atlas: Petroleum Geology of the Central and Northern North Sea': *Geological Society (London)* 317–329

Mount, J. (1985) 'Mixed Siliciclastic and Carbonate Sediments: A Proposed First-Order Textural and Compositional Classification'. *Sedimentology* 32, 435–442

Newell, A.J., Pourmalek, A., Butcher, A.S., and Shariatipour, S.M. (2019) 'The Importance of Lithofacies Control on Fluid Migration in Heterogeneous Aeolian Formations for Geological CO2 Storage: Lessons from Observational Evidence and Modelling of Bleached Palaeoreservoirs at Salt Wash Graben, Utah'. *International Journal of Greenhouse Gas Control* [online] 91 (December 2018), 1–17. available from <https://doi.org/10.1016/j.ijggc.2019.102841>

Newell, A.J. and Shariatipour, S.M. (2016) 'Linking Outcrop Analogue with Flow Simulation to Reduce Uncertainty in Sub-Surface Carbon Capture and Storage: An Example from the Sherwood Sandstone Group of the Wessex Basin, UK'. *Geological Society, London, Special Publications* [online] 436 (1), 231–246. available from <https://doi.org/10.1144/SP436.2>

Nicol, A., Childs, C., Walsh, J.J., and Schafer, K.W. (2013) 'A Geometric Model for the Formation of Deformation Band Clusters'. *Journal of Structural Geology* [online] 55, 21–33. available from <http://dx.doi.org/10.1016/j.jsg.2013.07.004>

Nilsen, H.M., Lie, K., and Andersen, O. (2015) 'Analysis of CO2 Trapping Capacities and Long-Term Migration for Geological Formations in the Norwegian North Sea Using MRST-Co2lab'. *Computers and Geosciences* [online] 79, 15–26. available from <http://dx.doi.org/10.1016/j.cageo.2015.03.001>

Njiekak, G., Schmitt, D.R., Yam, H., and Kofman, R.S. (2013) 'CO2 Rock Physics as Part of the Weyburn-Midale Geological Storage Project'. *International Journal of Greenhouse Gas Control* [online] 16, S118–S133. available from <https://doi.org/10.1016/j.ijggc.2013.02.007>

NOAA/ESRL (2020) *Image Provided by Earth System Research Laboratories Global Monitoring Laboratory, from Their Website at Https://Www.Esrl.Noaa.Gov/Gmd/Ccgg/Trends/*.

NOAA (2020) *State of the Climate: Global Climate Report for March 2020* [online] available

from <https://www.ncdc.noaa.gov/sotc/global/202003.>

Nordbotten, J.A.N.M., Celia, M.A., and Bachu, S. (2005) 'Injection and Storage of CO2 in Deep Saline Aquifers: Analytical Solution for CO2 Plume Evolution during Injection'. *Transport In Porous Media* [online] 58, 339–360. available from <https://doi.org/10.1007/s11242-004-0670-9>

Nordbotten, J.M. and Celia, M.A. (2006) 'Analysis of Plume Extent Using Analytical Solutions for CO2 Storage'. in *CMWRXVI*. held 2006 at Copenhagen, Denmark. 1–8

North, C.P. and Prosser, D.J. (1993) 'Characterization of Fluvial and Aeolian Reservoirs: Problems and Approaches'. *Geological Society, London, Special Publications* 73 (1), 1–6

North, F. (1985) *Petroleum Geology*. Springer

Noy, D.J., Holloway, S., Chadwick, R.A., Williams, J.D.O., Hannis, S.A., and Lahann, R.W. (2012) 'Modelling Large-Scale Carbon Dioxide Injection into the Bunter Sandstone in the UK Southern North Sea'. *International Journal of Greenhouse Gas Control* [online] 9, 220–233. available from <http://dx.doi.org/10.1016/j.ijggc.2012.03.011>

Nuccio, V.F. and Condon, S.M. (1996) 'Burial and Thermal History of the Paradox Basin, Utah and Colorado, and Petroleum Potential of the Middle Pennsylvanian Paradox Formation'. *U.S geological survey* 57–76

Ogata, K., Senger, K., Braathen, A., and Tveranger, J. (2014) 'Fracture Corridors as Seal-Bypass Systems in Siliciclastic Reservoir-Cap Rock Successions: Field-Based Insights from the Jurassic Entrada Formation (SE Utah, USA)'. *Journal of Structural Geology* [online] 66, 162–187. available from <http://dx.doi.org/10.1016/j.jsg.2014.05.005>

Okwen, R., Yang, F., and Frailey, A. (2014) 'Effect of Geologic Depsoitional Environment on CO2 Storage Efficiency'. *Energy Procedia* [online] 63, 5247–5257. available from <https://doi.org/10.1016/j.egypro.2014.11.556>

Okwen, R.T., Stewart, M.T., and Cunningham, J.A. (2010) 'Analytical Solution for Estimating Storage Efficiency of Geologic Sequestration of CO2'. *International Journal of Greenhouse Gas Control* [online] 4 (1), 102–107. available from <https://doi.org/10.1016/j.ijggc.2009.11.002>

Oldenburg, C.M. (2006) *Migration Mechanisms and Potential Impacts of CO2 Leakage and Seepage Curtis*. [online] 1–32. available from <https://escholarship.org/content/qt015944r2/qt015944r2.pdf>

Olsson, A. (2000) 'Origin of Lüders ' Bands in Deformed Rock'. *Journal of Geophysical Research: Solid Earth* [online] 105 (B3), 5931–5938. available from <https://doi.org/10.1029/1999JB900428>

Onoja, M.U., Ahmadinia, M., Shariatipour, S.M., and Wood, A.M. (2019) 'Characterising the Role of Parametric Functions in the van Genuchten Empirical Model on CO 2 Storage Performance'. *International Journal of Greenhouse Gas Control* [online] 88 (June), 233–250. available from <https://doi.org/10.1016/j.ijggc.2019.06.004>

Onoja, M.U. and Shariatipour, S.M. (2018) 'The Impact of Gradational Contact at the Reservoir-Seal Interface on Geological CO2 Storage Capacity and Security'.

International Journal of Greenhouse Gas Control [online] 72 (March), 1–13. available from <https://doi.org/10.1016/j.ijggc.2018.03.007>

Oostrom, M., White, M.D., Porse, S.L., Krevor, S.C.M. and Mathias, S.A. (2016) 'Comparison of Relative Permeability–saturation–capillary Pressure Models for Simulation of Reservoir CO2 Injection'. *International Journal of Greenhouse Gas Control* [online] 45, 70–85. available from <https://doi.org/10.1016/j.ijggc.2015.12.013>

Orr, F.M. (2009) 'Onshore Geologic Storage of CO2'. *Science* [online] 325 (5948), 1656–1658. available from <10.1126/science.1175677>

Özgur, E. (2006) *Assessment of Diffusive and Convective Mechanisms during Carbon Dioxide Sequestration into Deep Saline Aquifers*. MIDDLE EAST TECHNICAL UNIVERSITY

Parker, J.A. (2013) *Outcrop Analysis of Ooid Grainstones in the Permian Grayburg Formation, Shattuck Escarpment, New Mexico*. The University of Texas at Austin

Pearce, J.M., Kirby, G.A., Lacinska, A., Bateson, L., Wagner, D., Rochelle, C.A., and Cassidy, M. (2011) 'Reservoir-Scale CO2-Fluid Rock Interactions: Preliminary Results from Field Investigations in the Paradox Basin, Southeast Utah'. *Energy Procedia* [online] 4, 5058–5065. available from <http://dx.doi.org/10.1016/j.egypro.2011.02.479>

Pendrigh, N.M. (2005) 'Geological and Geophysical Characterization of the Mississippian Midale Reservoir, Weyburn Field , Saskatchewan'. *Summary of Investigations* 1, 1–16

Pentland, C.H., El-Maghraby, R., Georgiadis, A., Iglauer, S., and Blunt, M.J. (2011) 'Immiscible Displacements and Capillary Trapping in CO2 Storage'. *Energy Procedia* [online] 4, 4969–4976. available from <https://doi.org/10.1016/j.egypro.2011.02.467>

Peters, E., Egberts, P.J.P., Loeve, D., and Hofstee, C. (2015) 'CO2 Dissolution and Its Impact on Reservoir Pressure Behavior'. *International Journal of Greenhouse Gas Control* [online] 43, 115–123. available from <http://dx.doi.org/10.1016/j.ijggc.2015.10.016>

Pittman, E.D. (1981) 'Effect of Fault-Related Granulation on Porosity and Permeability of Quartz Sandstones, Simpson Group (Ordovician), Oklahoma.' *American Association of Petroleum Geologists Bulletin* 65 (11), 2181–2387

Poblet, J. and Mcclay, K. (1996) 'Geometry and Kinematics of Single-Layer Detachment Folds'. *AAPG Bulletin* [online] 80 (7), 1085–1109. available from <https://doi.org/10.1306/64ED8CA0-1724-11D7-8645000102C1865D%0A>

Pourmalek, A., Newell, A.J., Shariatipour, S.M., Butcher, A.S., Milodowski, A.E., Bagheri, M., and Wood, A.M. (2021) 'Deformation Bands in High-Porosity Sandstones :Do They Help or Hinder CO2 Migration and Storage in Geological Formations?' *International Journal of Greenhouse Gas Control* [online] 107 (February), 103292. available from <https://doi.org/10.1016/j.ijggc.2021.103292>

Pourmalek, A., Newell, A.J., Shariatipour, S.M., and Wood, A.M. (2022) 'The Impact of Heterogeneous Mixed Siliciclastic – Carbonate Systems on CO2 Geological Storage'. *Petroleum Geoscience* [online] 28 (1). available from <https://doi.org/10.1144/petgeo2020-086>

Pourmalek, A. and Shariatipour, S.M. (2019) 'Dependence on Temperature and Salinity

Gradients and the Injection Rate of CO2 Storage in Saline Aquifers with an Angular Unconformity'. *Journal of Porous Media* [online] 22 (8), 1065–1078. available from <10.1615/JPorMedia.2019025077>

Preston, C., Monea, M., Jazrawi, W., Brown, K., Whittaker, S., White, D., Law, D., Chalaturnyk, R., and Rostron, B. (2005) 'IEA GHG Weyburn CO2 Monitoring & Storage Project'. *Fuel Processing Technology* [online] 86 (14–15), 1547–1568. available from <https://doi.org/10.1016/j.fuproc.2005.01.019>

Pruess, K. (2006) 'On CO2 Behavior in the Subsurface, Following Leakage from a Geologic Storage Reservoir'. *Lawrence Berkeley National Laboratory*

Qi, R. (2008) *Simulation of Geological Carbon Dioxide Storage*. Imperial College London

Qi, R., Laforce, T.C., and Blunt, M.J. (2009) 'Design of Carbon Dioxide Storage in Aquifers'. *International Journal of Greenhouse Gas Control* [online] 3, 195–205. available from <https://doi.org/10.1016/j.ijggc.2008.08.004>

Qu, D. and Tveranger, J. (2016) 'Incorporation of Deformation Band Fault Damage Zones in Reservoir Models'. *AAPG bulletin* [online] 100 (3), 423–443. available from <https://doi.org/10.1306/12111514166>

Qu, D., Tveranger, J., and Fachri, M. (2017) 'Influence of Deformation-Band Fault Damage Zone on Reservoir Performance'. *Interpretation* [online] 5 (4), 41–56. available from <https://doi.org/10.1190/INT-2016-0229.1%0A>

Ramsay, L.G. (1974) 'Development of Chevron Folds'. *Geological Bulletin, Society of America* [online] 85 (11), 1741–1754. available from <https://doi.org/10.1130/0016-7606(1974)85%3C1741:DOCF%3E2.0.CO;2%0AArticle history%0A Cite >

Ranganathan, P., Farajzadeh, R., Bruining, H., and Zitha, P.L.J. (2012) 'Numerical Simulation of Natural Convection in Heterogeneous Porous Media for CO2 Geological Storage'. *Transport In Porous Media* [online] 95 (1), 25–54. available from <https://doi.org/10.1007/s11242-012-0031-z>

Rasmusson, K., Rasmusson, M., Tsang, Y., and Niemi, A. (2016) 'A Simulation Study of the Effect of Trapping Model, Geological Heterogeneity and Injection Strategies on CO2 Trapping'. *International Journal of Greenhouse Gas Control* [online] 52, 52–72. available from <http://dx.doi.org/10.1016/j.ijggc.2016.06.020>

Rawling, G.C. and Goodwin, L.B. (2003) 'Cataclasis and Particulate Flow in Faulted, Poorly Lithified Sediment'. *Journal of Structural Geology* [online] 25 (3), 317–331. available from <https://doi.org/10.1016/S0191-8141(02)00041-X>

Reading, H.G. (1980) *Characteristics and Recognition of Strike-Slip Fault Systems*. International Association of Sedimentologists

Riaz, A., Hesse, M., Tchelepi, H.A., and ORR JR, F.M. (2006) 'Onset of Convection in a Gravitationally Unstable Diffusive Boundary Layer in Porous Media'. *Journal of Fluid Mechanics* [online] 548, 87–111. available from <doi:10.1017/S0022112005007494>

Ringrose, P. and Bentley, M. (2015) *Reservoir Model Design* [online] Berlin: Springer. available from <http://link.springer.com/10.1007/978-94-007-5497-3>

Ringrose, P.S., Mathieson, A.S., Wright, I.W., Selama, F., Hansen, O., Bissell, R., Saoula, N., and Midgley, J. (2013) 'The In Salah CO2 Storage Project: Lessons Learned and Knowledge Transfer'. *Energy Procedia* [online] 37, 6226–6236. available from <https://doi.org/10.1016/j.egypro.2013.06.551>

Rittenhouse, G. (1972) 'Stratigraphic-Trap Classification: Geologic Exploration Methods.' *AAPG Memoir*

Robert J. Bodnar (2003) 'Introduction to Aqueous-Electrolyte Fluid Inclusions'. in *Fluid Inclusions: Analysis and Interpretation*. vol. 32. 81–100

Rotevatn, A. and Fossen, H. (2012) 'Soft Faults with Hard Tips: Magnitude-Order Displacement Gradient Variations Controlled by Strain Softening versus Hardening; Implications for Fault Scaling'. *Journal of the Geological Society* [online] 169 (2), 123–126. available from <https://doi.org/10.1144/0016-76492011-108>

Rotevatn, A., Buckley, S.J., and Howell, J.A. (2009) 'Overlapping Faults and Their Effect on Fluid Flow in Different Reservoir Types: A LIDAR-Based Outcrop Modeling and Flow Simulation Study'. *AAPG Bulletin* [online] 93 (3), 407–427. available from <https://doi.org/10.1306/09300807092%0A>

Rotevatn, A. and Fossen, H. (2011) 'Simulating the Effect of Subseismic Fault Tails and Process Zones in a Siliciclastic Reservoir Analogue: Implications for Aquifer Support and Trap Definition'. *Marine and Petroleum Geology* [online] 28 (9), 1648–1662. available from <http://dx.doi.org/10.1016/j.marpetgeo.2011.07.005>

Rotevatn, A., Fossmark, H.S., Bastesen, E., Thorsheim, E., and Torabi, A. (2017) 'Do Deformation Bands Matter for Flow? Insights from Permeability Measurements and Flow Simulations in Porous Carbonate Rocks'. *Petroleum Geoscience* [online] 23 (1), 104–119. available from <https://doi.org/10.1144/petgeo2016-038>

Rotevatn, A., Sandve, T.H., Keilegavlen, E., Kolyukhin, D., and Fossen, H. (2013) 'Deformation Bands and Their Impact on Fluid Flow in Sandstone Reservoirs: The Role of Natural Thickness Variations'. *Geofluids* 13 (3), 359–371

Rotevatn, A., Torabi, A., Fossen, H., and Braathen, A. (2008) 'Slipped Deformation Bands: A New Type of Cataclastic Deformation Bands in Western Sinai, Suez Rift, Egypt'. *Journal of Structural Geology* [online] 30 (11), 1317–1331. available from <https://doi.org/10.1016/j.jsg.2008.06.010>

Rotevatn, A., Tveranger, J., Howell, J.A., and Fossen, H. (2009) 'Dynamic Investigation of the Effect of a Relay Ramp on Simulated Fluid Flow: Geocellular Modelling of the Delicate Arch Ramp, Utah'. *Petroleum Geoscience,* [online] 15 (1), 45–58. available from <https://doi.org/10.1144/1354-079309-779%0AAdd to Cart ($35)>

Rutqvist, J., Birkholzer, J.T., and Tsang, C.-F. (2008) 'Coupled Reservoir–geomechanical Analysis of the Potential for Tensile and Shear Failure Associated with CO2 Injection in Multilayered Reservoir–caprock Systems'. *International Journal of Rock Mechanics and Mining Sciences* [online] 45 (2), 132–143. available from <https://doi.org/10.1016/j.ijrmms.2007.04.006>

Rutqvist, J. and Tsang, C. (2002) 'A Study of Caprock Hydromechanical Changes Associated

with CO2 -Injection into a Brine Formation'. *Environmental Geology,* [online] 42 (2–3), 296–305. available from <https://doi.org/10.1007/s00254-001-0499-2>

Saillet, E. and Wibberley, C.A.J. (2010) 'Evolution of Cataclastic Faulting in High-Porosity Sandstone, Bassin Du Sud-Est'. *Journal of Structural Geology* [online] 32 (11), 1590–1608. available from <http://dx.doi.org/10.1016/j.jsg.2010.02.007>

Schueller, S., Braathen, A., Fossen, H., and Tveranger, J. (2013) 'Spatial Distribution of Deformation Bands in Damage Zones of Extensional Faults in Porous Sandstones: Statistical Analysis of Field Data'. *Journal of Structural Geology* [online] 52, 148–162. available from <https://doi.org/10.1016/j.jsg.2013.03.013>

Scott, V., Gilfillan, S., Markusson, N., Chalmers, H., and Haszeldine, R.S. (2012) 'Last Chance for Carbon Capture and Storage'. *Nature Climate Change* [online] 3 (2), 105–111. available from <http://dx.doi.org/10.1038/nclimate1695>

Seers, T.D. and Hodgetts, D. (2016) 'Extraction of Three-Dimensional Fracture Trace Maps from Calibrated Image Sequences'. *Geosphere* [online] 12 (4), 1323–1340. available from <https://doi.org/10.1130/GES01276.1%0A>

Shariatipour, S.M., Pickup, G.E., and Mackay, E.J. (2014) 'The Effect of Aquifer / Caprock Interface on Geological Storage of CO2'. *Energy Procedia* [online] 63, 5544–5555. available from <http://dx.doi.org/10.1016/j.egypro.2014.11.588>

Shariatipour, S.M., Pickup, G.E., and Mackay, E.J. (2016) 'Investigation of CO2 Storage in a Saline Formation with an Angular Unconformity at the Caprock Interface'. *Petroleum Geoscience* [online] 22 (2), 203–210. available from <https://doi.org/10.1144/petgeo2015-039>

ShellCanada (2019) *Quest Carbon Capture and Storage Project 2018 Annual Status Report*. Calgary, Alberta

Shipton, Z.K., Evans, J.P., Robeson, K.R., Forster, C.B. and Snelgrove, S. (2002) 'Structural Heterogeneity and Permeability in Faulted Eolian Sandstone: Implications for Subsurface Modeling of Faults.' *AAPG Bulletin* [online] 86 (5), 863–883. available from <https://doi.org/10.1306/61EEDBC0-173E-11D7-8645000102C1865D>

Shipton, Z.K., Evans, J.P., Kirchner, D., Kolesar, P.T., Williams, A.P., and Heath, J. (2004) 'Analysis of CO2 Leakage through "Low-Permeability" Faults from Natural Reservoirs in the Colorado Plateau, Southern Utah'. *Geological Storage of Carbon Dioxide* [online] 233 (1), 43–58. available from <https://doi.org/10.1144/GSL.SP.2004.233.01.05>

Sifuentes, W., Blunt, M.J., and Giddins, M.A. (2009) 'Modeling CO2 Storage in Aquifers: Assessing the Key Contributors to Uncertainty'. *spe in Offshore Europe. Society of Petroleum Engineers.* (8–11 September)

De Silva, G.P.D., Ranjith, P. and Perera, M.S.A. (2015) 'Geochemical Aspects of CO2 Sequestration in Deep Saline Aquifers: A Review'. *Fuel* [online] 155 (April), 128–143. available from <http://dx.doi.org/10.1016/j.fuel.2015.03.045>

Slatt, R.M. (2013) *Basic Principles and Applications of Reservoir Characterization*. Elsevier

Slob, S. and Hack, R. (2004) '3D Terrestrial Laser Scanning as a New Field Measurement and

Monitoring Technique 30 Terrestrial Laser Scanning as a New Field'. in *Engineering Geology for Infrastructure Planning in Europe* [online] Berlin: Springer, 179–189. available from <https://doi.org/10.1007/978-3-540-39918-6_22>

Soliva, R., Schultz, R.A., Ballas, G., Taboada, A., Wibberley, C., Saillet, E., and Benedicto, A. (2013) 'A Model of Strain Localization in Porous Sandstone as a Function of Tectonic Setting, Burial and Material Properties; New Insight from Provence (Southern France)'. *Journal of Structural Geology* [online] 49, 50–63. available from <http://dx.doi.org/10.1016/j.jsg.2012.11.011>

Solum, J.G., Brandenburg, J.P., Naruk, S.J., Kostenko, O. V, Wilkins, S.J., Schultz, R.A., Solum, J.G., and International, S. (2010) 'Characterization of Deformation Bands Associated with Normal and Reverse Stress States in the Navajo Sandstone, Utah'. *AAPG bulletin* [online] 9 (9), 1453–1475. available from <https://doi.org/10.1306/01051009137%0A>

Song, J. and Zhang, D. (2013) 'Comprehensive Review of Caprock-Sealing Mechanisms for Geologic Carbon Sequestration'. *Environmental science & technology* [online] 47 (1), 9–22. available from <https://doi.org/10.1021/es301610p>

SPE (2017) 'CO2 Storage Resources Management System'. *Society of Petroleum Engineers Journal* (July)

Spycher, N., Pruess, K. and Ennis-King, J. (2003) 'CO2-H2O Mixtures in the Geological Sequestration of CO2. I. Assessment and Calculation of Mutual Solubilities from 12 to 100 °C and up to 600 Bar'. *Geochimica et Cosmochimica Acta* [online] 67 (16), 3015–3031. available from <https://doi.org/10.1016/S0016-7037(03)00273-4>

Spycher, N. and Pruess, K. (2005) 'CO2-H2O Mixtures in the Geological Sequestration of CO2. I . Assessment and Calculation of Mutual Solubilities from 12 to 100 °C and up to 600 Bar'. *Geochimica et Cosmochimica Acta,* [online] 69 (13), 3309–3320. available from <https://doi.org/10.1016/j.gca.2005.01.015>

Spycher, N. and Pruess, K. (2009) 'A Phase-Partitioning Model for CO2 – Brine Mixtures at Elevated Temperatures and Pressures: Application to CO2 -Enhanced Geothermal Systems'. *Transport in Porous Media* [online] 82 (1), 173–196. available from <https://doi.org/10.1007/s11242-009-9425-y>

Sternlof, K.R., Pollard, D.D., and Durlofsky, L.J. (2006) 'Flow and Transport Effects of Compaction Bands in Sandstone at Scales Relevant to Aquifer and Reservoir Management'. *Water Resources Research* [online] 42, 1–16. available from <https://doi.org/10.1029/2005WR004664>

Stow, D.A.V., Reading, H.G. and Collinson, J.D. (1996) *Sedimentary Environments: Process, Facies and Stratigraphy*.

Sundal, A., Petter, J., Dypvik, H., Miri, R., and Aagaard, P. (2013) 'Effects of Geological Heterogeneity on CO2 Distribution and Migration - A Case Study from the Johansen Formation , Norway'. *Energy Procedia* [online] 37 (1876), 5046–5054. available from <http://dx.doi.org/10.1016/j.egypro.2013.06.418>

Suppe, B.J. and Medwedeff, D.A. (1990) 'Geometry and Kinematics of Fault-Propagation Folding'. *Eclogae Geologicae Helvetiae* 83 (3), 409–454

Suppe, J. (1983) ‘Geometry and Kinematics of Fault-Bend Folding’. *American Journal of science* 283 (7), 684–721

Szulczewski, M.L., Macminn, C.W., Herzog, H.J., and Juanes, R. (2012) ‘Lifetime of Carbon Capture and Storage as a Climate-Change Mitigation Technology’. *Proceedings of the National Academy of Sciences* [online] 109 (14), 5185–5189. available from <https://doi.org/10.1073/pnas.1115347109>

Tawiah, P., Duer, J., Bryant, S.L., Larter, S., Brien, S.O., and Dong, M. (2020) ‘CO2 Injectivity Behaviour under Non-Isothermal Conditions – Field Observations and Assessments from the Quest CCS Operation’. *International Journal of Greenhouse Gas Control* [online] 92 (August 2019), 102843. available from <https://doi.org/10.1016/j.ijggc.2019.102843>

The Climate Change Committee (2019) *Net Zero: The UK’s Contribution to Stopping Global Warming*.

Thrana, C. and Talbot, M.R. (2006) ‘High-Frequency Carbonate-Siliciclastic Cycles in the Miocene of the Lorca Basin (Western Mediterranean, SE Spain)’. *Geologica Acta* [online] 4, 343–354. available from <Available online at www.geologica-acta.com%0D>

Tindall, S.E. (2006) ‘Jointed Deformation Bands May Not Compartmentalize Reservoirs’. *AAPG Bulletin* 90 (2), 177–192

Tondi, E., Antonellini, M., Aydin, A., Marchegiani, L., and Cello, G. (2006) ‘The Role of Deformation Bands, Stylolites and Sheared Stylolites in Fault Development in Carbonate Grainstones of Majella Mountain, Italy’. *Journal of Structural Geology* [online] 28 (3), 376–391. available from <https://doi.org/10.1016/j.jsg.2005.12.001>

Torabi, A. and Fossen, H. (2009) ‘Spatial Variation of Microstructure and Petrophysical Properties along Deformation Bands in Reservoir Sandstones’. *AAPG bulletin* [online] 93 (7), 919–938. available from <https://doi.org/10.1306/03270908161>

Torabi, A., Fossen, H., and Alaei, B. (2008) ‘Application of Spatial Correlation Functions in Permeability Estimation of Deformation Bands in Porous Rocks’. *Journal of Geophysical Research: Solid Earth* [online] 113 (February), 1–10. available from <https://doi.org/10.1029/2007JB005455>

Torabi, A., Fossen, H., and Braathen, A. (2013) ‘Insight into Petrophysical Properties of Deformed Sandstone Reservoirs’. *AAPG bulletin* [online] 97 (4), 619–637. available from <https://doi.org/10.1306/10031212040%0A>

Tucker, M. and Wright, V. (2009) *Carbonate Sedimentology*.

Tucker, M.E. (2003) ‘Mixed Clastic – Carbonate Cycles and Sequences: Quaternary of Egypt and Carboniferous of England’. *Geologia Croatica* [online] 56 (1), 19–38. available from <https://hrcak.srce.hr/3789>

Tucker, M.E. (2009) *Sedimentary Petrology: An Introduction to the Origin of Sedimentary Rocks*. John Wiley & Sons.

Turner, P., Burley, S.D., Rey, D., and Prosser, J. (1995) ‘Burial History of the Penrith Sandstone (Lower Permian) Deduced from the Combined Study of Fluid Inclusion and

Palaeomagnetic Data'. *Geological Society, London, Special Publications* [online] 98 (1), 43–78. available from <https://doi.org/10.1144/GSL.SP.1995.098.01.04>

Twiss, R.J and Moores, E.M. (1992) *Structural Geology*. Macmillan

Underhill, J.R. and Woodcock, N.H. (1987) 'Faulting Mechanisms in High-Porosity Sandstones; New Red Sandstone, Arran, Scotland'. *Geological Society Special Publication* [online] 29 (1), 91–105. available from <https://doi.org/10.1144/GSL.SP.1987.029.01.09>

Underschultz, J., Boreham, C., Dance, T., Stalker, L., Freifeld, B., Kirste, D., and Ennis-King, J. (2011) 'CO2 Storage in a Depleted Gas Field: An Overview of the CO2CRC Otway Project and Initial Results'. *International Journal of Greenhouse Gas Control* [online] 5 (4), 922–932. available from <https://doi.org/10.1016/j.ijggc.2011.02.009>

UNFCCC (1992) *United Nation*. New York

USDOE (2010) *Carbon Sequestration Atlas of the United States and Canada*.

USEPA (1994) *Determination of Maximum Injection Pressure for Class I Wells*.

Vesovic, V., Wakeham, W.A., Olchowy, G.A., Sengers, J.V., Watson, J.T.R. and Millat, J. (1990) 'The Transport Properties of Carbon Dioxide'. *Journal of physical and chemical reference data* [online] 19 (3), 763–808. available from <https://doi.org/10.1063/1.555875>

Victor D. G., D. Zhou, E. H. M. Ahmed, P. K. Dadhich, J. G. J. Olivier, H-H. Rogner, K. Sheikho, and M. Yamaguchi, 2014: (2014) 'Introductory Chapter'. in *Climate Change 2014: Mitigation of Climate Change. Contribution of Working Group III to the Fifth Assessment Report of the Intergovernmental Panel on Climate Change*. ed. by Edenhofer, O., R. Pichs-Madruga, Y. Sokona, E. Farahani, S. Kadner, K. Seyboth, A. Adler, I. Baum, S. Brunner, P. Eickemeier, B. Kriemann, J. Savolainen, S. Schlömer, C. von Stechow, T.Z. and J.C.M. Cambridge University Press, Cambridge, United Kingdom and New York, NY, USA.

Vidal-Gilbert, S., Tenthorey, E., Dewhurst, D., Ennis-king, J., Ruth, P. Van, and Hillis, R. (2010) 'Geomechanical Analysis of the Naylor Field , Otway Basin , Australia : Implications for CO2 Injection and Storage'. *International Journal of Greenhouse Gas Control* [online] 4 (5), 827–839. available from <http://dx.doi.org/10.1016/j.ijggc.2010.06.001>

Vuuren, D.P. Van, Edmonds, J., Kainuma, M., Riahi, K., Nakicenovic, N., Smith, S.J., and Rose, S.K. (2011) 'The Representative Concentration Pathways: An Overview'. *Climate Change* [online] 109 (1–2), 5–31. available from <https://doi.org/10.1007/s10584-011-0148-z>

Wang, Y., Zhang, K., and Wu, N. (2013) 'Numerical Investigation of the Storage Efficiency Factor for CO2 Geological Sequestration in Saline Formations'. *Energy Procedia* [online] 37, 5267–5274. available from <http://dx.doi.org/10.1016/j.egypro.2013.06.443>

White, J.A., Chiaramonte, L., Ezzedine, S., Foxall, W., Hao, Y., and Ramirez, A. (2014) 'Geomechanical Behavior of the Reservoir and Caprock System at the In Salah CO2 Storage Project'. *Proceedings of the National Academy of Sciences* [online] 111 (24), 8747–8752. available from <https://doi.org/10.1073/pnas.1316465111>

Wigley, M., Dubacq, B., Kampman, N., and Bickle, M. (2013) 'Controls of Sluggish, CO2-Promoted, Hematite and K-Feldspar Dissolution Kinetics in Sandstones'. *Earth and Planetary Science Letters* [online] 362, 76–87. available from <https://doi.org/10.1016/j.epsl.2012.11.045>

Wigley, M., Kampman, N., Dubacq, B., and Bickle, M. (2012) 'Fluid-Mineral Reactions and Trace Metal Mobilization in an Exhumed Natural CO2 Reservoir, Green River, Utah'. *Geology* [online] 40 (6), 555–558. available from <https://doi.org/10.1130/G32946.1>

Wilkinson, M., S. V. M. Gilfillan, R. S. Haszeldine, and C.J.B. (2008) 'Plumbing the Depths: Testing Natural Tracers of Subsurface CO2 Origin and Migration, Utah'. in *Carbon Dioxide Sequestration in Geological Media—State of the Science* [online] ed. by M. Grobe, J. C. Pashin, and R.L.D. AAPG Studies 59, 1–16. available from <doi:10.1306/13171266St591353>

Williams, J.D.O., Bentham, M., Jin, M., Pickup, G., Mackay, E., and Gammer, D. (2013) 'The Effect of Geological Structure and Heterogeneity on CO2 Storage in Simple 4-Way Dip Structures ; a Modeling Study from the UK Southern North Sea'. *Energy Procedia* [online] 37, 3980–3988. available from <http://dx.doi.org/10.1016/j.egypro.2013.06.297>

Williams, J.D.O., Fellgett, M.W., and Quinn, M.F. (2016) 'Carbon Dioxide Storage in the Captain Sandstone Aquifer: Determination of in Situ Stresses and Fault-Stability Analysis'. *Petroleum Geoscience* [online] 22 (3), 211–222. available from <https://doi.org/10.1144/petgeo2016-036>

Wilson, C.E., Aydin, A., Durlofsky, L.J., Sagy, A., Emily, E., Kreylos, O., and Kellogg, L.H. (2011) 'From Outcrop to Flow Simulation: Constructing Discrete Fracture Models from a LIDAR Survey'. *AAPG Bulletin* [online] 11 (11), 1883–1905. available from <https://doi.org/10.1306/03071110122>

Wollenweber, J., Alles, S., Busch, A., Krooss, B.M., Stanjek, H., and Littke, R. (2010) 'Experimental Investigation of the CO2 Sealing Efficiency of Caprocks'. *International Journal of Greenhouse Gas Control* [online] 4 (2), 231–241. available from <http://dx.doi.org/10.1016/j.ijggc.2010.01.003>

Xu, T., Kharaka, Y.K., Doughty, C., Freifeld, B.M., and Daley, T.M. (2010) 'Reactive Transport Modeling to Study Changes in Water Chemistry Induced by CO2 Injection at the Frio-I Brine Pilot'. *Chemical Geology* [online] 271 (3–4), 153–164. available from <https://doi.org/10.1016/j.chemgeo.2010.01.006>

Zahasky, C. and Krevor, S. (2020) 'Environmental Science Climate Change Mitigation Scenarios'. *Energy & Environmental Science* [online] 13, 1561–1567. available from <10.1039/D0EE00674B>

Zecchin, M. and Catuneanu, O. (2017) 'High-Resolution Sequence Stratigraphy of Clastic Shelves VI: Mixed Siliciclastic-Carbonate Systems'. *Marine and Petroleum Geology* [online] 88, 712–723. available from <https://doi.org/10.1016/j.marpetgeo.2017.09.012>

Zhang, C., Oostrom, M., Wietsma, T.W., Grate, J.W., and Warner, M.G. (2011) 'Influence of Viscous and Capillary Forces on Immiscible Fluid Displacement: Pore-Scale

Experimental Study in a Water-Wet Micromodel Demonstrating Viscous and Capillary Fingering'. *Energy & fuels* [online] 25 (8), 3493–3505. available from <https://doi.org/10.1021/ef101732k>

Zhou, D., Fayers, F.J., and Orr Jr, F.M. (1997) 'Scaling of Multiphase Flow in Simple Heterogeneous Porous Media'. *SPE Reservoir Engineering* [online] 12 (03), 173–178. available from <https://doi.org/10.2118/27833-PA>

Zhou, Q., Birkholzer, J.T., Tsang, C., and Rutqvist, J. (2008) 'A Method for Quick Assessment of CO2 Storage Capacity in Closed and Semi-Closed Saline Formations'. *International Journal of Greenhouse Gas Control* [online] 2 (4), 626–639. available from <https://doi.org/10.1016/j.ijggc.2008.02.004>

Zhu, C., Zhang, G., Lu, P., Meng, L., and Ji, X. (2015) 'Seismic Data for the Uppermost Layer and Model Sensitivity Analysis'. *International Journal of Greenhouse Gas Control* [online] 43, 233–246. available from <http://dx.doi.org/10.1016/j.ijggc.2014.12.016>

Zuluaga, L.F., Rotevatn, A., Keilegavlen, E., and Fossen, H. (2016) 'The Effect of Deformation Bands on Simulated Fluid Flow within Fault-Propagation Fold Trap Types: Lessons from the San Rafael Monocline, Utah'. *AAPG bulletin* [online] 100 (10), 1523–1540. available from <https://doi.org/10.1306/04151614153>

Zweigel, P., Arts, R., Lothe, A.E., and Lindeberg, E.B. (2004) 'Reservoir Geology of the Utsira Formation at the First Industrial-Scale Underground CO2 Storage Site (Sleipner Area, North Sea)'. *Geological Society, London, Special Publications* [online] 233 (1), 165–180. available from <https://doi.org/10.1144/GSL.SP.2004.233.01.11>

Zweigel, P., Hamborg, M., Arts, R., Lothe, A., Sylta, Ø., and Tømmerås, A. (2000) 'Prediction of Migration of CO2 Injected into an Underground Depository: Reservoir Geology and Migration Modelling in the Sleipner Case (North Sea)'. in *International Conference on Greenhouse Gas Control Technologies, Cairns (Australia)*. held 2000 at Cairns (Australia)

Ahr, W.M. (2011) *Geology of Carbonate: The Identification, Description, and Characterization of Hydrocarbon Reservoirs in Carbonate Rocks.* John Wiley & Sons.

Alcalde, J., Flude, S., Wilkinson, M., Johnson, G., Edlmann, K., Bond, C.E., Scott, V., Gil, S.M. V, Ogaya, X., and Haszeldine, R.S. (2018) 'Estimating Geological CO2 Storage Security to Deliver on Climate Mitigation'. *Nature Communications* [online] 1 (9), 1–13. available from <https://doi.org/10.1038/s41467-018-04423-1>

Alghalandis, Y.F. (2017) 'ADFNE: Open Source Software for Discrete Fracture Network Engineering, Two and Three Dimensional Applications'. *Computers and Geosciences* [online] 102 (September 2016), 1–11. available from <http://dx.doi.org/10.1016/j.cageo.2017.02.002>

Allis, R., Chidsey, T., Gwynn, W., Morgan, C., White, S., Adams, M., and Moore, J. (2001) 'Natural CO2 Reservoirs on the Colorado Plateau – Candidates for CO2 Sequestration'. *Proceedings of the First National Conference on Carbon Sequestration* 14–17

Ambrose, W.A., Lakshminarasimhan, S., Holtz, M.H., Núñez-López, V., Hovorka, S.D., and Duncan, I. (2008) 'Geologic Factors Controlling CO2 Storage Capacity and Permanence: Case Studies Based on Experience with Heterogeneity in Oil and Gas Reservoirs Applied

to CO2 Storage'. *Environmental Geology* [online] 54 (8), 1619–1633. available from <https://doi.org/10.1007/s00254-007-0940-2>

Andre, L., Audigane, P., Azaroual, M., and Menjoz, A. (2007) 'Numerical Modeling of Fluid – Rock Chemical Interactions at the Supercritical CO2 – Liquid Interface during CO2 Injection into a Carbonate Reservoir, the Dogger Aquifer (Paris Basin, France)'. *Energy Conversion and Management* [online] 48 (6), 1782–1797. available from <https://doi.org/10.1016/j.enconman.2007.01.006>

Antonellini, M. and Aydin, A. (1994) 'Effect of Faulting on Fluid Flow in Porous Sandstones: Petrophysical Properties'. *AAPG bulletin* [online] 78 (3), 355–377. available from <https://doi.org/10.1306/BDFF90AA-1718-11D7-8645000102C1865D>

Antonellini, M., Cilona, A., Tondi, E., and Zambrano, M. (2014) 'Fluid Flow Numerical Experiments of Faulted Porous Carbonates, Northwest Sicily (Italy)'. *Marine and Petroleum Geology* [online] 55, 186–201. available from <http://dx.doi.org/10.1016/j.marpetgeo.2013.12.003>

Arthurton, R.S. and Wadge, A.J. (1981) *Geology of the Country around Penrith: Memoir for 1:50,000 Geological Sheet 24*.

Aydin, A. and Johnson, A.M. (1983) 'Analysis of Faulting in Porous Sandstones'. *Journal of Structural Geology,* [online] 5 (1), 19–31. available from <https://doi.org/10.1016/0191-8141(83)90004-4>

Aydin, A. (1978) 'Small Faults Formed as Deformation Bands in Sandstone'. in *Rock Friction and Earthquake Prediction*. Birkhäuser, Basel, 913–930

Aydin, A., Borja, R.I., and Eichhubl, P. (2006) 'Geological and Mathematical Framework for Failure Modes in Granular Rock'. *Journal of structural geology* [online] 28 (1), 83–98. available from <https://doi.org/10.1016/j.jsg.2005.07.008>

Bachu, S., Bonijoly, D., Bradshaw, J., Burruss, R., Holloway, S., Christensen, N.P. and Mathiassen, O.M. (2007) 'CO2 Storage Capacity Estimation: Methodology and Gaps'. *International Journal of Greenhouse Gas Control* [online] 1 (4), 430–443. available from <https://doi.org/10.1016/S1750-5836(07)00086-2>

Bachu, S., Gunter, W.D. and Perkins, E.H. (1994) 'Aquifer Disposal of CO2: Hydrodynamic and Mineral Trapping'. *Energy Conversion & Management* [online] 35 (4), 269–279. available from <https://doi.org/10.1016/0196-8904(94)90060-4>

Bachu, S. (2000) 'Sequestration of CO2 in Geological Media: Criteria and Approach for Site Selection in Response to Climate Change'. *Energy Conversion & Management* [online] 41 (9), 953–970. available from <https://doi.org/10.1016/S0196-8904(99)00149-1>

Bachu, S. (2003) 'Screening and Ranking Sedimentary Basins for Sequestration of CO2 in Geological Media in Response to Climate Change'. *Environmental Geology* 44 (3), 277–289

Bachu, S. (2008) 'CO2 Storage in Geological Media: Role, Means, Status and Barriers to Deployment'. *Progress in energy and combustion science* [online] 34 (2), 254–273. available from <https://doi.org/10.1016/j.pecs.2007.10.001>

Bachu, S. (2015) ‘Review of CO2 Storage Efficiency in Deep Saline Aquifers’. *International Journal of Greenhouse Gas Control* [online] 40 (September 2015), 188–202. available from <http://dx.doi.org/10.1016/j.ijggc.2015.01.007>

Bachu, S. and Adams, J.J. (2003) ‘Sequestration of CO2 in Geological Media in Response to Climate Change: Capacity of Deep Saline Aquifers to Sequester CO2 in Solution’. *Energy Conversion and management* [online] 44 (20), 3151–3175. available from <https://doi.org/10.1016/S0196-8904(03)00101-8>

Bachu, S. and Stewart, S. (2002) ‘Geological Sequestration of Anthropogenic Carbon Dioxide in the Western Canada Sedimentary Basin: Suitability Analysis’. *Journal of Canadian Petroleum Technology* [online] 41 (02). available from <https://doi.org/10.2118/02-02-01>

Bagheri, M., Shariatipour, S.M., and Ganjian, E. (2018) ‘A Review of Oil Well Cement Alteration in CO2-Rich Environments’. *Construction and Building Materials* [online] 186, 946–968. available from <https://doi.org/10.1016/j.conbuildmat.2018.07.250>

Bagheri, M., Shariatipour, S.M., and Ganjian, E. (2019) ‘Prediction of the Lifespan of Cement at a Specific Depth Based on the Coupling of Geomechanical and Geochemical Processes for CO2 Storage’. *International Journal of Greenhouse Gas Control* [online] 86 (September 2018), 43–65. available from <https://doi.org/10.1016/j.ijggc.2019.04.016>

Ballas, G., Fossen, H., and Soliva, R. (2015) ‘Factors Controlling Permeability of Cataclastic Deformation Bands and Faults in Porous Sandstone Reservoirs’. *Journal of Structural Geology* [online] 76, 1–21. available from <http://dx.doi.org/10.1016/j.jsg.2015.03.013>

Barnaby R.J and Ward W. B (2007) ‘Outcrop Analog for Mixed Siliciclastic – Carbonate Ramp Reservoirs — Stratigraphic Hierarchy, Facies Architecture, and Geologic Heterogeneity: Grayburg Formation’. *Journal of Sedimentary Research* [online] 77 (1), 34–58. available from <https://doi.org/10.2110/jsr.2007.007%0A>

Beitler, B., Chan, M.A., and Parry, W.T. (2003) ‘Bleaching of Jurassic Navajo Sandstone on Colorado Plateau Laramide Highs: Evidence of Exhumed Hydrocarbon Supergiants?’ *Geology* [online] 31 (12), 1041–1044. available from <https://doi.org/10.1130/G19794.1%0A>

Bennion, B. and Bachu, S. (2005) ‘Relative Permeability Characteristics for Supercritical CO2 Displacing Water in a Variety of Potential Sequestration Zones in the Western Canada Sedimentary Basin’. *SPE Annual Technical Conference and Exhibition. Society of Petroleum Engineers. 9-12 October* [online] (9–12 October). available from <https://doi.org/10.2118/95547-MS>

Bennion, D.B. and Bachu, S. (2006a) ‘Dependence on Temperature, Pressure, and Salinity of the IFT and Relative Permeability Displacement Characteristics of CO2 Injected in Deep Saline Aquifers’. *SPE Annual Technical Conference and Exhibition. Society of Petroleum Engineers.* [online] (24–27 September). available from <https://doi.org/10.2118/102138-MS>

Bennion, D.B. and Bachu, S. (2006b) ‘Supercritical CO2 and H2S — Brine Drainage and Imbibition Relative Permeability Relationships for Intergranular Sandstone and

Carbonate Formations'. *SPE Europec/EAGE Annual Conference and Exhibition.* [online] (12–15 June). available from <https://doi.org/10.2118/99326-MS>

Bennion, D.B. and Bachu, S. (2006c) 'The Impact of Interfacial Tension and Pore - Size Distribution / Capillary Pressure Character on CO2 Relative Permeability at Reservoir Conditions in CO2-Brine Systems'. *SPE/DOE Symposium on Improved Oil Recovery. Society of Petroleum Engineers.* [online] (22–26 April). available from <https://doi.org/10.2118/99325-MS>

Bennion, D.B. and Bachu, S. (2008) 'Drainage and Imbibition Relative Permeability Relationships for Supercritical CO2 / Brine and H2S / Brine Systems in Intergranular Sandstone, Carbonate, Shale, and Anhydrite Rocks'. in *SPE Reservoir Evaluation & Engineering*. held 2008. 487–496

Bennion, D.B. and S Bachu (2010) 'Drainage and Imbibition CO2 / Brine Relative Permeability Curves at Reservoir Conditions for Carbonate Formations'. *SPE Annual Technical Conference and Exhibition. Society of Petroleum Engineers.* [online] (12–15 June), 1–18. available from <https://doi.org/10.2118/134028-MS>

Bentham, M. and Kirby, G. (2005) 'CO2 Storage in Saline Aquifers'. *Oil & gas science and technology* [online] 60 (3), 559–567. available from <https://doi.org/10.2516/ogst:2005038>

Bentley, M. and Ringrose, P. (2018) 'Future Directions in Reservoir Modelling: New Tools and "Fit-for-Purpose" Workflows'. *Geological Society, London, Petroleum Geology Conference series* [online] 8 (1), 537–546. available from <http://pgc.lyellcollection.org/lookup/doi/10.1144/PGC8.40>

Berg, S., Oedai, S., and Ott, H. (2013) 'Displacement and Mass Transfer between Saturated and Unsaturated CO2 – Brine Systems in Sandstone'. *International Journal of Greenhouse Gas Control* [online] 12, 478–492. available from <http://dx.doi.org/10.1016/j.ijggc.2011.04.005>

Bergman, P.D. and Winter, E.M. (1995) 'Disposal of Carbon Dioxide in Aquifers in the US'. *Energy Conversion and Management* [online] 36 (6–9), 523–526. available from <https://doi.org/10.1016/0196-8904(95)00058-L>

Du Bernard, X., Labaume, P., Darcel, C., Davy, P. and Bour, O. (2002) 'Cataclastic Slip Band Distribution in Normal Fault Damage Zones, Nubian Sandstones, Suez Rift'. *Journal of Geophysical Research: Solid Earth* 107 (B7), ETG-6

Du Bernard, X., Eichhubl, P., and Aydin, A. (2002) 'Dilation Bands: A New Form of Localized Failure in Granular Media'. *Geophysical Research Letters* 29 (24), 1–4

Bernstein, L., Bosch, P., Canziani, O., Chen, Z., Christ, R., Davidson, O., Hare, W., Karoly, D., Kattsov, V., Kundzewicz, Z., Liu, J., Lohmann, U., Manning, M., Matsuno, T., Menne, B., Metz, B., Mirza, M., Nicholls, N., Nurse, L., Pachauri, R., Palutikof, J., Qin, D., Ravindranath, N., Reisinger, A., Ren, J., Riahi, K., Rosenzweig, C., Schneider, S., Sokona, Y., Solomon, S., Stott, P., Stouffer, R., Sugiyama, T., Swart, R., Tirpak, D., Vogel, C., and Yohe, G. (2008) *Climate Change 2007: Synthesis Report Summary for Policymakers*. 12–17

Bickle, M., Kampman, N. and Wigley, M. (2013) 'Natural Analogues'. in *Reviews in Mineralogy and Geochemistry* [online] vol. 77. 15–71. available from <https://doi.org/10.2138/rmg.2013.77.2>

Bickle, M., Chadwick, A., Huppert, H.E., Hallworth, M., and Lyle, S. (2007) 'Modelling Carbon Dioxide Accumulation at Sleipner: Implications for Underground Carbon Storage'. *Earth and Planetary Science Letters* [online] 255 (1–2), 164–176. available from <https://doi.org/10.1016/j.epsl.2006.12.013>

Bickle, M. and Kampman, N. (2013) 'Lessons in Carbon Storage from Geological Analogues'. *Geology* [online] 41 (4), 525–526. available from <https://doi.org/10.1130/focus0420132.1>

Bickle, M., Kampman, N., Chapman, H., Ballentine, C., Dubacq, B., Galy, A., Sirikitputtisak, T., Warr, O., Wigley, M., and Zhou, Z. (2017) 'Rapid Reactions between CO2 , Brine and Silicate Minerals during Geological Carbon Storage: Modelling Based on a Field CO2 Injection Experiment'. *Chemical Geology* [online] 468 (December 2016), 17–31. available from <http://dx.doi.org/10.1016/j.chemgeo.2017.07.031>

Biddle, K.T. and Wielchowsky, C.C. (1994) 'Hydrocarbon Traps'. in *The Petroleum System-from Source to Trap*. vol. 60. AAPG Memoir, 219–235

Birkholzer, J.T., Zhou, Q., and Tsang, C. (2009) 'Large-Scale Impact of CO2 Storage in Deep Saline Aquifers: A Sensitivity Study on Pressure Response in Stratified Systems'. *International Journal of Greenhouse Gas Controlas control,* [online] 3 (2), 181–194. available from <https://doi.org/10.1016/j.ijggc.2008.08.002>

Boggs Jr, S. (2014) *Principles of Sedimentology and Stratigraphy*. Pearson Education

BP Energy Outlook (2019) *2019 Edition*. London, United kingdom

Bradshaw, J., Bachu, S., Bonijoly, D., Burruss, R., Holloway, S., Peter, N., and Magne, O. (2007) 'CO2 Storage Capacity Estimation: Issues and Development of Standards'. *International Journal of Greenhouse Gas Control* [online] 1 (1), 62–68. available from <https://doi.org/10.1016/S1750-5836(07)00027-8>

Brandsæter, I., Mcilroy, D., Lia, O., Ringrose, P., and Næss, A. (2005) 'Reservoir Modelling and Simulation of Lajas Formation Outcrops (Argentina) to Constrain Tidal Reservoirs of the Halten Terrace (Norway)'. *Petroleum Geoscience* [online] 11 (1), 37–46. available from <https://doi.org/10.1144/1354-079303-611>

Breckels, I.M. and van Eekelen, H.A.M. (1982) 'Relationship between Horizontal Stress and Depth in Sedimentary Basins'. *Journal of Petroleum Technology* [online] 34 (09), 2191–2199. available from <http://www.onepetro.org/doi/10.2118/10336-PA>

Brown, K., Whittaker, S., Wilson, M., Srisang, W., Smithson, H., and Tontiwachwuthikul, P. (2017) 'The History and Development of the IEA GHG Weyburn-Midale CO2 Monitoring and Storage Project in Saskatchewan, Canada (the World Largest CO2 for EOR and CCS Program)'. *Petroleum* [online] 3 (1), 3–9. available from <http://dx.doi.org/10.1016/j.petlm.2016.12.002>

Brown, L.T. (2002) *Integration of Rock Physics and Reservoir Simulation for the Interpretation of Time-Lapse Seismic Data at Weyburn Field, Saskatchewa*. Doctoral

dissertation, Colorado School of Mines. Arthur Lakes Library

Bryant, D., Kantorowicz, J.D., and Love, C.F. (1988) 'The Origin and Recognition of Laterally Continuous Carbonate-Cemented Horizons in the Upper Lias Sands of Southern England'. *Marine and Petroleum Geology* [online] 5 (2), 108–133. available from <https://doi.org/10.1016/0264-8172(88)90018-9>

Buckley, S.J., Enge, H.D., Carlsson, C. and Howell, J.A. (2010) 'Terrestrial Laser Scanning for Use in Virtual Outcrop Geology'. *The Photogrammetric Record* [online] 25 (131), 225–239. available from <https://doi.org/10.1111/j.1477-9730.2010.00585.x>

Burchette, T.P. (2012) 'Carbonate Rocks and Petroleum Reservoirs: A Geological Perspective from the Industry'. *Geological Society, London, Special Publications* [online] 370 (1), 17–37. available from <https://doi.org/10.1144/SP370.14>

Burnside, N.M. and Naylor, M. (2014) 'Review and Implications of Relative Permeability of CO2/Brine Systems and Residual Trapping of CO2'. *International Journal of Greenhouse Gas Control* [online] 23, 1–11. available from <http://dx.doi.org/10.1016/j.ijggc.2014.01.013>

Burnside, N.M., Shipton, Z.K., Dockrill, B., and Ellam, R.M. (2013) 'Man-Made versus Natural CO2 Leakage: A 400 k.y. History of an Analogue for Engineered Geological Storage of CO2'. *Geology* [online] 41 (4), 471–474. available from <https://doi.org/10.1130/G33738.1>

Busch, A., Amann-Hildenbrand, A., Bertier, P., Waschbuesch, M., and Krooss, B.M. (2010) 'The Significance of Caprock Sealing Integrity for CO2 Storage'. *SPE International Conference on CO2 Capture, Storage, and Utilization. Society of Petroleum Engineers.* [online] (10–12 November). available from <https://doi.org/10.2118/139588-MS>

Catuneanu, O., Galloway, W.E., Kendall, C.G.S.C., Miall, A.D., Posamentier, H.W., Strasser, A., and Tucker, M.E. (2011) 'Sequence Stratigraphy: Methodology and Nomenclature'. *Newsletters on Stratigraphy* [online] 44 (3), 173–245. available from <http://dx.doi.org/10.1127/0078-0421/2011/0011>

Cavanagh, A.J. and Haszeldine, R.S. (2014) 'The Sleipner Storage Site: Capillary Flow Modeling of a Layered CO2 Plume Requires Fractured Shale Barriers within the Utsira Formation'. *International Journal of Greenhouse Gas Control* [online] 21 (2014), 101–112. available from <http://dx.doi.org/10.1016/j.ijggc.2013.11.017>

Celia, M.A., Bachu, S., Nordbotten, J.M. and Bandilla, K.W. (2015) 'Status of CO2 Storage in Deep Saline Aquifers with Emphasis on Modeling Approaches and Practical Simulations'. *Water Resources Research* 51 (9), 6846–6892

Chadwick, A., Arts, R., Bernstone, C., May, F., Thibeau, S., and Zweigel, P. (2008) *Best Practice for the Storage of CO2 in Saline Aquifers - Observations and Guidelines from the SACS and CO2STORE Projects* [online] available from <http://nora.nerc.ac.uk/id/eprint/2959>

Chadwick, R.A., Noy, D.J., and Holloway, S. (2009) 'Flow Processes and Pressure Evolution in Aquifers during the Injection of Supercritical CO2 as a Greenhouse Gas Mitigation Measure'. *Petroleum Geoscience* [online] 15 (1), 59–73. available from

<https://doi.org/10.1144/1354-079309-793>

Chadwick, R.A., Zweigel, P., Gregersen, U., and Kirby, G.A. (2004) 'Geological Reservoir Characterization of a CO2 Storage Site: The Utsira Sand, Sleipner, Northern North Sea'. *Energy* [online] 29, 1371–1381. available from <https://doi.org/10.1016/j.energy.2004.03.071>

Chan, M.A., Parry, W.T., and Bowman, J.R. (2000) 'Diagenetic Hematite and Manganese Oxides and Fault-Related Fluid Flow in Jurassic Sandstones, Southeastern Utah 1'. *AAPG bulletin* [online] 9 (9), 1281–1310. available from <https://doi.org/10.1306/A9673E82-1738-11D7-8645000102C1865D>

ChemicaLogic Corporation (2018) *Carbon Dioxide: Temperature - Pressure Diagram* [online] available from <http://www.chemicalogic.com/index.html>

Chiarella, D., Longhitano, S.G., and Tropeano, M. (2017) 'Types of Mixing and Heterogeneities in Siliciclastic-Carbonate Sediments'. *Marine and Petroleum Geology* [online] 88, 617–627. available from <http://dx.doi.org/10.1016/j.marpetgeo.2017.09.010>

Ciais, P., C. Sabine, G. Bala, L. Bopp, V. Brovkin, J. Canadell, A. Chhabra, R. DeFries, J. Galloway, M. Heimann, C. Jones, C. Le Quéré, R.B. Myneni, S.P. and P.T. (2013) 'Carbon and Other Biogeochemical Cycles'. in *Climate Change 2013: The Physical Science Basis. Contribution of Working Group I to the Fifth Assessment Report of the Intergovernmental Panel on Climate Change*. ed. by Stocker, T.F., D. Qin, G.-K. Plattner, M. Tignor, S.K. Allen, J. Boschung, A. Nauels, Y. Xia, V.B. and P.M.M. Cambridge University Press, Cambridge, United Kingdom and New York, NY, USA

CO2CRC (2008) *Storage Capacity Estimation, Site Selection and Characterisation for CO2 Storage Projects*. ed. by in Kaldi, J.G. and Gibson-Poole, C.M. Canbera, Report No. RPT08-1001.

Crabaugh, M. and Kocurek, G. (1993) 'Entrada Sandstone: An Example of a Wet Aeolian System'. *Geological Society, London, Special Publications* [online] 72 (1), 103–126. available from <https://doi.org/10.1144/GSL.SP.1993.072.01.11>

CSLF (2007) 'Estimation of CO2 Storage Capacity in Geological Media - Phase 2 -'. *Carbon Sequestration Leadership Forum*

Cubasch, U., D. Wuebbles, D. Chen, M.C. Facchini, D. Frame, N. Mahowald, and J.-G.W. (2013) 'Introduction.' in *Climate Change 2013: The Physical Science Basis. Contribution of Working Group I to the Fifth Assessment Report of the Intergovernmental Panel on Climate Change*. ed. by Stocker, T.F., D. Qin, G.-K. Plattner, M. Tignor, S.K. Allen, J. Boschung, A. Nauels, Y. Xia, V.B. and P.M.M. Cambridge University Press, Cambridge, United Kingdom and New York, NY, USA. 119

Dance, T. (2013) 'Assessment and Geological Characterisation of the CO2CRC Otway Project CO2 Storage Demonstration Site: From Prefeasibility to Injection'. *Marine and Petroleum Geology* [online] 46, 251–269. available from <https://doi.org/10.1016/j.marpetgeo.2013.06.008>

Dance, T., Spencer, L., and Xu, J.Q. (2009) 'Geological Characterisation of the Otway Project

Pilot Site: What a Difference a Well Makes'. *Energy Procedia* [online] 1 (1), 2871–2878. available from <https://doi.org/10.1016/j.egypro.2009.02.061>

Deng, H., Stauffer, P.H., Dai, Z., Jiao, Z. and Surdam, R.C. (2012) 'Simulation of Industrial-Scale CO2 Storage: Multi-Scale Heterogeneity and Its Impacts on Storage Capacity, Injectivity and Leakage'. *International Journal of Greenhouse Gas Control* [online] 10, 397–418. available from <https://doi.org/10.1016/j.ijggc.2012.07.003>

Dershowitz, B., Lapointe, P., Eiben, T., and Wei, L. (1998) 'Integration of Discrete Feature Network Methods with Conventional Simulator Approaches'. in *SPE Annual Technical Conference and Exhibition* [online] held 1998 at New Orleans, Louisiana. available from <https://doi.org/10.2118/49069-MS>

Deveugle, P.E.K., Jackson, M.D., Hampson, G.J., Farrell, M.E., Sprague, A.R., Stewart, J., and Calvert, C.S. (2011) 'Characterization of Stratigraphic Architecture and Its Impact on Fluid Flow in a Fluvial-Dominated Deltaic Reservoir Analog: Upper Cretaceous Ferron Sandstone Member , Utah'. *AAPG bulletin* [online] 95 (5), 693–727. available from <https://doi.org/10.1306/09271010025%0A>

Dockrill, B. and Shipton, Z.K. (2010) 'Structural Controls on Leakage from a Natural CO2 Geologic Storage Site: Central Utah, U.S.A.' *Journal of Structural Geology* [online] 32 (11), 1768–1782. available from <http://dx.doi.org/10.1016/j.jsg.2010.01.007>

Doelling, H.H. (2001) *Geologic Map of the Moab and Eastern Part of the San Rafael Desert 30' x 60' Quadrangles, Grand and Emery Counties, Utah, and Mesa County, Colorado. Utah Geological Survey, Map 180, 1:100000, Map 180.*

Doherty, B., Vasylkivska, V., Huerta, N.J., and Dilmore, R. (2017) 'Estimating the Leakage along Wells during Geologic CO2 Storage: Application of the Well Leakage Assessment Tool to a Hypothetical Storage Scenario in Natrona County , Wyoming'. *Energy Procedia* [online] 114 (2016), 5151–5172. available from <http://dx.doi.org/10.1016/j.egypro.2017.03.1669>

Dong, H. and Blunt, M.J. (2009) 'Pore-Network Extraction from Micro-Computerized-Tomography Images'. *Physical review* [online] 80 (3), 1–11. available from <https://doi.org/10.1103/PhysRevE.80.036307>

Doughty, C. (2007) 'Modeling Geologic Storage of Carbon Dioxide: Comparison of Non-Hysteretic and Hysteretic Characteristic Curves'. *Energy Conversion and Management* [online] 48 (6), 1768–1781. available from <https://doi.org/10.1016/j.enconman.2007.01.022>

Downey, M.W. (1984) 'Evaluating Seals for Hydrocarbon Accumulations'. *AAPG bulletin* [online] 68 (11), 1752–1763. available from <https://doi.org/10.1306/AD461994-16F7-11D7-8645000102C1865D>

Dressel, B., Olsen, D., Ibm, N., Usdoe, B.B., Usdoe, P., and Usdoe, J.L. (2010) 'Depositional Environments Being Investigated by the National Energy Technology Laboratory (NETL) for Potential Geologic Storage of CO2'. *SPE Eastern Regional Meeting. Society of Petroleum Engineers* [online] 12–14 Octo. available from <https://doi.org/10.2118/138952-MS>

Eiken, O., Ringrose, P., Hermanrud, C., Nazarian, B., Tore, A.T., and Høier, L. (2011) 'Lessons Learned from 14 Years of CCS Operations: Sleipner, In Salah and Snøhvit'. *Energy Procedia* [online] 4, 5541–5548. available from <https://doi.org/10.1016/j.egypro.2011.02.541>

El-maghraby, R.M. and Blunt, M.J. (2013) 'Residual CO2 Trapping in Indiana Limestone'. *Environmental science & technology* [online] 47 (1), 227–233. available from <https://doi.org/10.1021/es304166u>

Ennis-King, J. and Paterson, L. (2002) 'Engineering Aspects of Geological Sequestration of Carbon Dioxide'. in *SPE Asia Pacific Oil and Gas Conference and Exhibition. Society of Petroleum Engineers.* [online] held 2002 at Melbourne, Australia. available from <https://doi.org/10.2118/77809-MS>

Ennis-King, J. and Paterson, L. (2005) 'Role of Convective Mixing in the Long-Term Storage of Carbon Dioxide in Deep Saline Formations'. *SPE* [online] 10 (03), 349–356. available from <https://doi.org/10.2118/84344-PA%0A>

Espie, T. and Woods, A. (2014) 'Testing Some Common Concepts in CO2 Storage'. *Energy Procedia* [online] 63, 5450–5460. available from <http://dx.doi.org/10.1016/j.egypro.2014.11.576>

Espinoza, D.N., Kim, S.H., and Santamarina, J.C. (2011) 'CO2 Geological Storage − Geotechnical Implications'. *KSCE Journal of Civil Engineering* [online] 15, 707–719. available from <https://doi.org/10.1007/s12205-011-0011-9>

Fachri, M., Rotevatn, A., and Tveranger, J. (2013) 'Fluid Flow in Relay Zones Revisited: Towards an Improved Representation of Small-Scale Structural Heterogeneities in Flow Models'. *Marine and Petroleum Geology* [online] 46, 144–164. available from <http://dx.doi.org/10.1016/j.marpetgeo.2013.05.016>

Falcon-suarez, I., Papageorgiou, G., Chadwick, A., North, L., Best, A.I., and Chapman, M. (2018) 'CO2-Brine Flow-through on an Utsira Sand Core Sample: Experimental and Modelling. Implications for the Sleipner Storage Field'. *International Journal of Greenhouse Gas Control* [online] 68 (2017), 236–246. available from <https://doi.org/10.1016/j.ijggc.2017.11.019>

Faulkner, D.R., Jackson, C.A.L., Lunn, R.J., Schlische, R.W., Shipton, Z.K., Wibberley, C.A.J., and Withjack, M.O. (2010) 'A Review of Recent Developments Concerning the Structure, Mechanics and Fluid Flow Properties of Fault Zones'. *Journal of Structural Geology* [online] 32 (11), 1557–1575. available from <http://dx.doi.org/10.1016/j.jsg.2010.06.009>

Faulkner, D.R., Rutter, E.H., Andrew, S., and Smith, F. (1998) 'The Gas Permeability of Clay-Bearing Fault Gouge at 20°C'. *Geological Society, London, Special Publications* [online] 147 (1), 147–156. available from <https://doi.org/10.1144/GSL.SP.1998.147.01.10>

Fenghour, A., Wakeham, W.A. and Vesovic, V. (1998) 'The Viscosity of Carbon Dioxide'. *Journal of physical and chemical reference data* [online] 27 (1), 31–44. available from <https://doi.org/10.1063/1.556013>

Firoozabadi, A. and Cheng, P. (2010) 'Prospects for Subsurface CO2 Sequestration'. *AIChE*

Journal [online] 56 (6), 1398–1405. available from <10.1002/aic.12287>

Fisher, Q.J. and Knipe, R.J. (2001) 'The Permeability of Faults within Siliciclastic Petroleum Reservoirs of the North Sea and Norwegian Continental Shelf'. *Marine and Petroleum Geology* [online] 18 (10), 1063–1081. available from <https://doi.org/10.1016/S0264-8172(01)00042-3>

Flett, M., Brantjes, J., Gurton, R., Mckenna, J., and Tankersley, T. (2009) 'Subsurface Development of CO2 Disposal for the Gorgon Project'. *Energy Procedia* [online] 1 (1), 3031–3038. available from <http://dx.doi.org/10.1016/j.egypro.2009.02.081>

Flett, M., Gurton, R., and Weir, G. (2007) 'Heterogeneous Saline Formations for Carbon Dioxide Disposal: Impact of Varying Heterogeneity on Containment and Trapping'. *Journal of Petroleum Science and Engineering* [online] 57 (1–2), 106–118. available from <https://doi.org/10.1016/j.petrol.2006.08.016>

Fleury, M., Pironon, J., Nindre, Y.M. Le, Bildstein, O., Berne, P., and Lagneau, V. (2011) 'Evaluating Sealing Efficiency of Caprocks for CO2 Storage : An Overview of the Geocarbone Integrity Program and Results .' *Energy Procedia* [online] 4, 5227–5234. available from <http://dx.doi.org/10.1016/j.egypro.2011.02.501>

Fossen, H., Schultz, R.A., Shipton, Z.K. and Mair, K. (2007) 'Deformation Bands in Sandstone: A Review'. *Journal of the Geological Society* [online] 164 (4), 755–769. available from <https://doi.org/10.1144/0016-76492006-036%0A>

Fossen, H., Soliva, R., Ballas, G., Trzaskos, B., Cavalcante, C. and Schultz, R.A. (2017) 'A Review of Deformation Bands in Reservoir Sandstones: Geometries, Mechanisms and Distribution'. *Geological Society, London, Special Publications,* [online] 459 (1), 9–33. available from <https://doi.org/10.1144/SP459.4>

Fossen, H., Zuluaga, L.F., Ballas, G., Soliva, R. and Rotevatn, A. (2015) 'Contractional Deformation of Porous Sandstone: Insights from the Aztec Sandstone, SE Nevada, USA'. *Journal of Structural Geology* [online] 74, 172–184. available from <https://doi.org/10.1016/j.jsg.2015.02.014>

Fossen, H. and Bale, A. (2007) 'Deformation Bands and Their Influence on Fluid Flow'. *AAPG bulletin* [online] 91 (12), 1685–1700. available from <https://doi.org/10.1306/07300706146%0A>

Fowles, J. and Burley, S. (1994) 'Textural and Permeability Characteristics of Faulted, High Porosity Sandstones Textural and Permeability Characteristics of Faulted, High Porosity Sandstones'. *Marine and Petroleum Geology* [online] 11 (5), 608–623. available from <https://doi.org/10.1016/0264-8172(94)90071-X>

Gabrielsen, R.H. and Koestler, A.G. (1987) 'Description and Structural Implications of Fractures in Late Jurassic Sandstones of the Troll Field, Northern North Sea'. *Norsk Geologisk Tidsskrift* 67 (4), 371–381

Gamboa, D., Williams, J.D.O., Bentham, M., Scho, D.I., and Mitchell, A.C. (2019) 'Application of Three-Dimensional Fault Stress Models for Assessment of Fault Stability for CO2 Storage Sites'. *International Journal of Greenhouse Gas Control* [online] 90, 102820. available from <https://doi.org/10.1016/j.ijggc.2019.102820>

Gao, X., Liu, L., Jiang, Z., Shang, X., and Liu, G. (2013) 'Geoscience Frontiers A Pre-Paleogene Unconformity Surface of the Sikeshu Sag, Junggar Basin: Lithological, Geophysical and Geochemical Implications for the Transportation of Hydrocarbons'. *Geoscience Frontiers* [online] 4 (6), 779–786. available from <http://dx.doi.org/10.1016/j.gsf.2012.12.003>

Gasda, S.E., Nordbotten, J.M., and and Celia, M.A. (2009) 'Vertical Equilibrium with Sub-Scale Analytical Methods for Geological CO2 Sequestration'. *Computational Geosciences* [online] 13 (4), 469–481. available from <https://doi.org/10.1007/s10596-009-9138-x>

Gaus, I. (2010) 'Role and Impact of CO2-Rock Interactions during CO2 Storage in Sedimentary Rocks'. *International Journal of Greenhouse Gas Control* [online] 4 (1), 73–89. available from <https://doi.org/10.1016/j.ijggc.2009.09.015>

Ghanbari, S., Pickup, G.E., Mackay, E., Gozalpour, F., and Todd, A.C. (2006) 'Simulation of CO2 Storage in Saline Aquifers'. *Chemical Engineering Research and Design* 84 (A9), 764–775

Gibson-Poole, C.M., Svendsen, L., Watson, M.N., Daniel, R.F., Ennis-King, J. and Rigg, A.J. (2009) 'Understanding Stratigraphic Heterogeneity: A Methodology to Maximize the Efficiency of the Geological Storage of CO2',. in *Carbon Dioxide Sequestration in Geological Media—State of the Science* [online] ed. by Grobe, M. and J. C. Pashin, and R.L.D. vol. 59. AAPG Studies in Geology, 347–364. available from <doi:10.1306/13171248St593385>

Global CCS Institute (2008) *Aquifer Storage-Development Issues*.

Global CCS Institute (2017) *The Global Status of CCS*. [online] available from <www.globalccsinstitute.com>

Goater, A.L., Bijeljic, B., and Blunt, M.J. (2013) 'Dipping Open Aquifers — The Effect of Top-Surface Topography and Heterogeneity on CO2 Storage Efficiency'. *International Journal of Greenhouse Gas Control* [online] 17, 318–331. available from <http://dx.doi.org/10.1016/j.ijggc.2013.04.015>

Goodman, A., Bromhal, G., Strazisar, B., Rodosta, T., Guthrie, W.F., Allen, D., and Guthrie, G. (2013) 'Comparison of Methods for Geologic Storage of Carbon Dioxide in Saline Formations'. *International Journal of Greenhouse Gas Control* [online] 18, 329–342. available from <http://dx.doi.org/10.1016/j.ijggc.2013.07.016>

Gorecki, C.D., Hamling, J.A., Klapperich, R.J., Steadman, E.N., and Harju, J.A. (2012) 'Integrating CO2EOR and CO2 Storage in the Bell Creek Oil Field'. in *Carbon Management Technology Conference. Carbon Management Technology Conference.* [online] held 2012. 1–12. available from <https://doi.org/10.7122/151476-MS>

Gorecki, C.D., Sorensen, J.A., Bremer, J.M., Knudsen, D.J., and Smith, S.A. (2009) 'Development of Storage Coefficients for Determining the Effective CO2 Storage Resource in Deep Saline Formations'. in *SPE International Conference on CO2 Capture, Storage, and Utilization. Society of Petroleum Engineers.* [online] held 2009. available from <https://doi.org/10.2118/126444-MS>

Green, C., Ennis-king, J., and Pruess, K. (2009) 'Effect of Vertical Heterogeneity on Long-Term Migration of CO2 in Saline Formations'. *Energy Procedia* [online] 1 (1), 1823–1830. available from <http://dx.doi.org/10.1016/j.egypro.2009.01.238>

Griffiths, J., Faulkner, D.R., Edwards, A.P. and Worden, R.H. (2018) 'Deformation Band Development as a Function of Intrinsic Host-Rock Properties in Triassic Sherwood Sandstone'. *geological Society, London, Special Publications,* [online] 435 (1), 161–167. available from <https://doi.org/10.1144/SP435.11>

Grude, S., Landrø, M., and Osdal, B. (2013) 'Time-Lapse Pressure – Saturation Discrimination for CO2 Storage at the Snøhvit Field'. *International Journal of Greenhouse Gas Control* [online] 19, 369–378. available from <http://dx.doi.org/10.1016/j.ijggc.2013.09.014>

Hamling, J.A., Gorecki, C.D., Klapperich, R.J., Saini, D., and Steadman, E.N. (2013) 'Overview of the Bell Creek Combined CO2 Storage and CO2 Enhanced Oil Recovery Project'. *Energy Procedia* [online] 37 (Figure 2), 6402–6411. available from <http://dx.doi.org/10.1016/j.egypro.2013.06.570>

Hampson, G.J., Morris, J.E., and Johnson, H.D. (2014) 'Synthesis of Time-Stratigraphic Relationships and Their Impact on Hydrocarbon Reservoir Distribution and Performance, Bridport Sand Formation, Wessex Basin, UK'. *Geological Society, London, Special Publications* [online] 404 (1), 199–222. available from <https://doi.org/10.1144/SP404.2>

Hansen, O., Gilding, D., Nazarian, B., and Osdal, B. (2013) 'Snøhvit : The History of Injecting and Storing 1 Mt CO2 in the Fluvial Tubåen Fm.' *Energy Procedia* [online] 37, 3565–3573. available from <http://dx.doi.org/10.1016/j.egypro.2013.06.249>

Haszeldine, R.S., Quinn, O., England, G., Wilkinson, M., Shipton, Z.K., Evans, J.P., Heath, J., Crossey, L., Ballentine, C.J., and Graham, C.M. (2005) 'Natural Geochemical Analogues for Carbon Dioxide Storage in Deep Geological Porous Reservoirs, a United Kingdom Perspective'. *Oil and Gas Science and Technology* [online] 60 (1), 33–49. available from <https://doi.org/10.2516/ogst:2005004>

He, Y., Kerans, C., Zeng, H., Janson, X., and Scott, S.Z. (2019) 'Improving Three-Dimensional Interpretation for Reservoir Model Construction: An Example of Geostatistical and Seismic Forward Modeling of Permian San Andres Shelf – Grayburg Platform Mixed Clastic – Carbonate Strata'. *AAPG Bulletin* [online] 8 (8), 1839–1887. available from <https://doi.org/10.1306/11211817244%0A>

Hellevang, H. (2015) 'Carbon Capture and Storage (CCS)'. in *Petroleum Geoscience: From Sedimentary Environments to Rock Physics*. ed. by Bjørlykke, K. Berlin, Heidelberg.: Springer, 591–602

Hepple, R.P. and Benson, S.M. (2005) 'Geologic Storage of Carbon Dioxide as a Climate Change Mitigation Strategy: Performance Requirements and the Implications of Surface Seepage'. *Environmental Geology* [online] 47 (476–585). available from <https://doi.org/10.1007/s00254-004-1181-2>

Hesse, M.A., Orr, F.M., and Tchelepi, H.A. (2009) 'Gravity Currents with Residual Trapping'. *Energy Procedia* [online] 1 (1), 3275–3281. available from <doi:10.1017/S002211200800219X>

Hester, R.E. and Harrison, R.M. (ed.) (2010) *Carbon Capture: Sequestration and Storage*. Royal Society of Chemistry.

HM Treasury (2020) *Budget 2020: Delivering on Our Promises to the British People* [online] available from <www.gov.uk/official-documents>

Holloway, S. and Savage, D. (1993) 'The Potential for Aquifer Disposal of Carbon Dioxide in the UK'. *Energy Conversion and Management* [online] 34 (9–11), 925–932. available from <https://doi.org/10.1016/0196-8904(93)90038-C>

Holloway, S., Vincent, C.J., Bentham, M.S., and Kirk, K.L. (2006) 'Top-down and Bottom-up Estimates of CO2 Storage Capacity in the United Kingdom Sector of the Southern North Sea Basin'. *Environmental Geosciences* [online] 13 (2), 71–84. available from <https://doi.org/10.1306/eg.11080505015%0A>

Hongjun, Z., Xinwei, L., Yanfang, C., and Xiaoliang, Z. (2010) 'Sensitivity Analysis of CO2 Sequestration in Saline Aquifers'. *Petroleum Science* [online] 7 (3), 372–378. available from <DOI 10.1007/s12182-010-0080-2>

Hovorka, S.D., Doughty, C., Benson, S.M., Pruess, K., and Knox, P.R. (2004) 'The Impact of Geological Heterogeneity on CO2 Storage in Brine Formations: A Case Study from the Texas Gulf Coast'. *Geological Society, London, Special Publications* [online] 233 (1), 147–163. available from <http://sp.lyellcollection.org/lookup/doi/10.1144/GSL.SP.2004.233.01.10>

Hovorka, S.D., Meckel, T.A., Trevino, R.H., Jean-philippe, J.L., Choi, J., Freeman, D., Cook, P., Daley, T.M., Ajo-, J.B., Freifeild, B.M., Doughty, C., Carrigan, C.R., Brecque, D. La, Kharaka, Y.K., Thordsen, J.J., Phelps, T.J., Yang, C., Katherine, D., Zhang, T., Holt, R.M., Lindler, J.S., and Butsch, R.J. (2011) 'Monitoring a Large Volume CO2 Injection: Year Two Results from SECARB Project at Denbury's Cranfield, Mississippi, USA'. *Energy Procedia* [online] 4, 3478–3485. available from <http://dx.doi.org/10.1016/j.egypro.2011.02.274>

Hovorka, S.D., Sakurai, S., Kharaka, Y.K., Nance, H.S., Benson, S.M., Freifeld, B.M., Trautz, R.C., Phelps, T., and Daley, T.M. (2006) 'Monitoring CO2 Storage in Brine Formations : Lessons Learned from the Frio Field Test One Year Post Injection'. *Gulf coast carbon center publication library, Bookshelf* 1–9

Howell, J.A., Martinus, W.A., and Good, T.R. (2014) 'The Application of Outcrop Analogues in Geological Modelling: A Review, Present Status and Future Outlook'. *Geological Society, London, Special Publications* 387 (1), 1–25

Howell, J.A., Skorstad, A., Macdonald, A., Fordham, A., and Flint, S. (2008) 'Sedimentological Parameterization of Shallow-Marine Reservoirs'. *Petroleum Geoscience* [online] 14 (1), 17–34. available from <https://doi.org/10.1144/1354-079307-787>

Ide, S.T., Jessen, K., and Orr Jr, F.M. (2007) 'Storage of CO2 in Saline Aquifers: Effects of Gravity , Viscous, and Capillary Forces on Amount and Timing of Trapping'. *International journal of greenhouse gas control* [online] 1, 481–491. available from <https://doi.org/10.1016/S1750-5836(07)00091-6>

Iding, M. and Ringrose, P. (2010) 'Evaluating the Impact of Fractures on the Performance of

the In Salah CO2 Storage Site'. *International Journal of Greenhouse Gas Control* [online] 4 (2), 242–248. available from <https://doi.org/10.1016/j.ijggc.2009.10.016>

IEA (2011) *Technology Roadmap Carbon Capture and Storage in Industrial Applications*. International Energy Agency, United Nations Industrial Development Organizations.

IEA (2013) *Technology Roadmap: Carbon Capture and Storage*.

IEA (2019) *Word Energy Outlook-Executive Summary*. Paris

IEAGHG (2011) *Caprock Systems for CO2 Geological Storage.* vol. May

Iglauer, S. (2011) *Dissolution Trapping of Carbon Dioxide in Reservoir Formation Brine – A Carbon Storage Mechanism*. ed. by Dr. Hironori Nakajima. INTECH Open Access Publisher

Iglauer, S., Pentland, C.H., and Busch, A. (2014) 'CO2 Wettability of Seal and Reservoir Rocks and the Implications for Carbon Geo-Sequestration'. *Water Resources Research Review* [online] 51 (1), 729–774. available from <https://doi.org/10.1002/2014WR015553>

IPCC: Annex: I (2018) 'Glossary [Matthews, J.B.R. (Ed.)].' in *Global Warming of 1.5°C. An IPCC Special Report on the Impacts of Global Warming of 1.5°C above Pre-Industrial Levels and Related Global Greenhouse Gas Emission Pathways, in the Context of Strengthening the Global Response to the Threat of Climate Change,*. ed. by Masson-Delmotte, V., P. Zhai, H.-O. Pörtner, D. Roberts, J.S., P.R. Shukla, A. Pirani, W. Moufouma-Okia, C. Péan, R. Pidcock, S. Connors, J.B.R. Matthews, Y. Chen, X.Z., and M.I. Gomis, E. Lonnoy, T. Maycock, M. Tignor, and T.W.

IPCC (2005) *IPCC Special Report on Carbon Dioxide Capture and Storage. Prepared by Working Group III of the Intergovernmental Panel on Climate Change [Metz, B., O. Davidson, H. C. de Coninck, M. Loos, and L. A. Meyer* [online] ed. by Metz, B., O. Davidson, H. C. de Coninck, M. Loos, and L.A.M. vol. 49. United Kingdom and New York, NY, USA: Cambridge University Press, Cambridge. available from <http://www.ncbi.nlm.nih.gov/pubmed/20942501>

IPCC (2013) 'Summary for Policymakers'. in *Climate Change 2013: The Physical Science Basis. Contribution of Working Group I to the Fifth Assessment Report of the Intergovernmental Panel on Climate Change*. ed. by Stocker, T.F., D. Qin, G.-K. Plattner, M. Tignor, S. K. Allen, J. Boschung, A. Nauels, Y. Xia, V.B. and P.M.M. Cambridge University Press, Cambridge, United Kingdom and New York, NY, USA.

IPCC (2018) 'Summary for Policymakers.' in *Global Warming of 1.5°C. An IPCC Special Report on the Impacts of Global Warming of 1.5°C above Pre-Industrial Levels and Related Global Greenhouse Gas Emission Pathways, in the Context of Strengthening the Global Response to the Threat of Climate Change,*. ed. by [Masson-Delmotte, V., P. Zhai, H.-O. Pörtner, D. Roberts, J. Skea, P.R.S., A. Pirani, W. Moufouma-Okia, C. Péan, R. Pidcock, S. Connors, J.B.R. Matthews, Y. Chen, X. Zhou, M.I.G., and E. Lonnoy, T. Maycock, M. Tignor, and T.W.

Islam, A., Chevalier, S., and Sassi, M. (2013) 'Experimental and Numerical Studies of CO2 Injection into Water-Saturated Porous Medium: Capillary to Viscous to Fracture Fingering Phenomenon'. *Energy Procedia* [online] 37, 5511–5519. available from

<http://dx.doi.org/10.1016/j.egypro.2013.06.471>

Ivandic, M., Juhlin, C., Lüth, S., Bergmann, P., Kashubin, A., Sopher, D., Ivanova, A., Baumann, G., and Henninges, J. (2015) 'Geophysical Monitoring at the Ketzin Pilot Site for CO2 Storage: New Insights into the Plume Evolution'. *International Journal of Greenhouse Gas Control* [online] 32, 90–105. available from <http://dx.doi.org/10.1016/j.ijggc.2014.10.015>

Jamison, W.R. and Stearns, D.W. (1982) 'Tectonic Deformation of Wingate Sandstone, Colorado National Monument.' *AAPG Bulletin* [online] 66 (12), 2584–2608. available from <https://doi.org/10.1306/03B5AC7D-16D1-11D7-8645000102C1865D%0A>

Jensen, G., Nickel, E., Whittaker, S., and Rostron, B. (2011) 'Site Assessment Update at Weyburn-Midale CO2 Sequestration Project, Saskatchewan, Canada: New Results at an Active CO2 Sequestration Site.' *Energy Procedia* [online] 4, 4777–4784. available from <http://dx.doi.org/10.1016/j.egypro.2011.02.442>

Jiang, X. (2011) 'A Review of Physical Modelling and Numerical Simulation of Long-Term Geological Storage of CO2'. *Applied Energy* [online] 88 (11), 3557–3566. available from <https://doi.org/10.1016/j.apenergy.2011.05.004>

Jin, M., Mackay, E., Quinn, M., Hitchen, K., and Akhurst, M. (2012) 'Evaluation of the CO2 Storage Capacity of the Captain Sandstone Formation'. *In SPE Europec/EAGE Annual Conference. Society of Petroleum Engineers. 4-7 June* [online] available from <https://doi.org/10.2118/154539-MS>

Juanes, R., Spiteri, E.J., Orr, F.M., and Blunt, M.J. (2006) 'Impact of Relative Permeability Hysteresis on Geological CO2 Storage'. *Water Resources Research* [online] 42 (12), 1–13. available from <https://doi.org/10.1029/2005WR004806>

Kampman, N., Bickle, M., Wigley, M., and Dubacq, B. (2014) 'Fluid Flow and CO2-Fluid-Mineral Interactions during CO2-Storage in Sedimentary Basins'. *Chemical Geology* [online] 369, 22–50. available from <http://dx.doi.org/10.1016/j.chemgeo.2013.11.012>

Kampman, N., Busch, A., Bertier, P., Snippe, J., Hangx, S., Pipich, V., Di, Z., Rother, G., Harrington, J.F., Evans, J.P., Maskell, A., Chapman, H.J., and Bickle, M.J. (2016) 'Observational Evidence Confirms Modelling of the Long-Term Integrity of CO2-Reservoir Caprocks'. *Nature Communications* [online] 7 (1), 1–10. available from <https://doi.org/10.1038/ncomms12268>

Kantorowicz, J.D., Bryant, I.D. and Dawans, J.. (1987) 'Controls on the Geometry and Distribution of Carbonate Cements in Jurassic Sandstones: Bridport Sands, Southern England and Viking Group, Troll Field, Norway'. *Geological Society, London, Special Publications* [online] 36 (1), 103–118. available from <https://doi.org/10.1144/GSL.SP.1987.036.01.09>

Kazemi, H., Merrill Jr, L.S., Porterfield, K.L., and Zeman, P.R. (1976) 'Numerical Simulation of Water-Oil Flow in Naturally Fractured Reservoirs'. *SPE* [online] 16 (6), 317–326. available from <https://doi.org/10.2118/5719-PA>

Kempka, T., Klein, E., Lucia, M. De, Tillner, E., and Kühn, M. (2013) 'Assessment of Long-Term

CO2 Trapping Mechanisms at the Ketzin Pilot Site (Germany) by Coupled Numerical Modelling'. *Energy Procedia* [online] 37, 5419–5426. available from <http://dx.doi.org/10.1016/j.egypro.2013.06.460>

Kempka, T., Lucia, M. De, and Kühn, M. (2014) 'Geomechanical Integrity Verification and Mineral Trapping Quantification for the Ketzin CO2 Storage Pilot Site by Coupled Numerical Simulations'. *Energy Procedia* [online] 63, 3330–3338. available from <http://dx.doi.org/10.1016/j.egypro.2014.11.361>

Kopp, A., Class, H., and Helmig, R. (2009) 'Investigations on CO2 Storage Capacity in Saline Aquifers Part 1. Dimensional Analysis of Flow Processes and Reservoir Characteristics'. *International Journal of Greenhouse Gas Control* [online] 3, 263–276. available from <https://doi.org/10.1016/j.ijggc.2008.10.002>

Krevor, S., Blunt, M.J., Benson, S.M., Pentland, C.H., Reynolds, C., Al-menhali, A., and Niu, B. (2015) 'Capillary Trapping for Geologic Carbon Dioxide Storage – From Pore Scale Physics to Field Scale Implications'. *International Journal of Greenhouse Gas Control* [online] 40, 221–237. available from <http://dx.doi.org/10.1016/j.ijggc.2015.04.006>

Krevor, S.C.M., Pini, R., Li, B., and Benson, S.M. (2011) 'Capillary Heterogeneity Trapping of CO2 in a Sandstone Rock at Reservoir Conditions'. *Geophysical Research Letters* [online] 38 (August), 1–5. available from <https://doi.org/10.1029/2011GL048239>

Kumar, A., Noh, M., Pope, G.A., Sepehrnoori, K., Bryant, S., and Lake, L.W. (2004) 'Reservoir Simulation of CO2 Storage in Deep Saline Aquifers'. *Society of Petroleum Engineers Journal* [online] 10 (03), 17–21. available from <https://doi.org/10.2118/89343-PA>

Lafare, A.E.A., Peach, D.W., and Hughes, A.G. (2016) 'Use of Seasonal Trend Decomposition to Understand Groundwater Behaviour in the Permo-Triassic Sandstone Aquifer, Eden Valley, UK'. *Hydrogeology Journal* [online] 24 (1), 141–158. available from <10.1007/s10040-015-1309-3>

Larkin, R.G. (2010) 'Hydrodynamic Trapping of CO2 Geosequestered in Saline Aquifers'. in *SPE Improved Oil Recovery Symposium. Society of Petroleum Engineers* [online] held 2010 at Tulsa, Oklahoma, USA. available from <https://doi.org/10.2118/128205-MS>

Law, D.H. and Bachu, S. (1996) 'Hydrological and Numerical Analysis of CO2 Disposal in Deep Aquifers in the Alberta Sedimentary Basin'. *Energy Conversion & Management* [online] 37 (95), 1167–1174. available from <https://doi.org/10.1016/0196-8904(95)00315-0>

Lei, Q., Latham, J., and Tsang, C. (2017) 'The Use of Discrete Fracture Networks for Modelling Coupled Geomechanical and Hydrological Behaviour of Fractured Rocks'. *Computers and Geotechnics* [online] 85, 151–176. available from <http://dx.doi.org/10.1016/j.compgeo.2016.12.024>

Lengler, U., Lucia, M. De, and Kühn, M. (2010) 'The Impact of Heterogeneity on the Distribution of CO2: Numerical Simulation of CO2 Storage at Ketzin'. *International Journal of Greenhouse Gas Control* [online] 4 (6), 1016–1025. available from <http://dx.doi.org/10.1016/j.ijggc.2010.07.004>

Leung, D.Y.C., Caramanna, G., and Maroto-valer, M.M. (2014) 'An Overview of Current Status of Carbon Dioxide Capture and Storage Technologies'. *Renewable and*

Sustainable Energy Reviews [online] 39, 426–443. available from <http://dx.doi.org/10.1016/j.rser.2014.07.093>

Leveille, G.P., Knipe, R., More, C., Ellis, D., Dudley, G., Jones, G., Fisher, Q.J. and Allinson, G. (1997) 'Compartmentalization of Rotliegendes Gas Reservoirs by Sealing Faults, Jupiter Fields Area, Southern North Sea'. *London, Special Publications* [online] 123 (1), 87–104. available from <https://doi.org/10.1144/GSL.SP.1997.123.01.06>

Levorsen, A.I. and and Berry, F.A. (1967) *Geology of Petroleum*. The AAPG Foundation

Lewis, C.L.E., Green, P.F., Carter, A., and Hurford, A.J. (1992) 'Elevated K/T Palaeotemperatures throughout Nortwest England: Three Kilometres of Tertiary Erosion?' *Earth and Planetary Science Letters* [online] 112 (1), 131–145. available from <https://doi.org/10.1016/0012-821X(92)90012-K>

Li, S., Dong, M., Li, Z., Huang, S., Qing, H., and Nickel, E. (2005) 'Gas Breakthrough Pressure for Hydrocarbon Reservoir Seal Rocks : Implications for the Security of Long-Term CO2 Storage in the Weyburn Field'. *Geofluids* [online] 5 (4), 326–334. available from <https://doi.org/10.1111/j.1468-8123.2005.00125.x>

Lindeberg, E. and Bergmo, P. (2003) 'The Long-Term Fate of CO2 Injected into an Aquifer'. in *Greenhouse Gas Control Technologies*. held 2003. pp.489-494

Lindeberg, E., Vuillaume, J., and Ghaderi, A. (2009) 'Determination of the CO2 Storage Capacity of the Utsira Formation'. *Energy Procedia* [online] 1 (1), 2777–2784. available from <http://dx.doi.org/10.1016/j.egypro.2009.02.049>

Løvoll, G., Méheust, Y., Måløy, K.J., Aker, E., and pand Schmittbuhl, J. (2005) 'Competition of Gravity, Capillary and Viscous Forces during Drainage in a Two-Dimensional Porous Medium , a Pore Scale Study'. *Energy* [online] 30 (6), 861–872. available from <https://doi.org/10.1016/j.energy.2004.03.100>

Lu, J., Cook, P.J., Hosseini, S.A., Yang, C., Romanak, K.D., Zhang, T., Freifeld, B.M., Smyth, R.C., Zeng, H., and Hovorka, S.D. (2012) 'Complex Fluid Flow Revealed by Monitoring CO2 Injection in a Fluvial Formation'. *Journal of Geophysical Research: Solid Earth* [online] 117, B3. available from <https://doi.org/10.1029/2011JB008939>

Lu, J., Kordi, M., Hovorka, S.D., Meckel, T.A., and Christopher, C.A. (2013) 'Reservoir Characterization and Complications for Trapping Mechanisms at Cranfield CO2 Injection Site'. *International Journal of Greenhouse Gas Control* [online] 18, 361–374. available from <hhttps://doi.org/10.1016/j.ijggc.2012.10.007>

Måløy, K.J., Feder, J., and Torstein, J. (1985) 'Viscous Fingering Fractal in Porous Media'. *Physical review letters* [online] 55 (24), 2688. available from <https://link.aps.org/doi/10.1103/PhysRevLett.55.2688>

Manzocchi, T., Walsh, J.J., Nell, P. and Yielding, G. (1999) 'Fault Transmissibility Multipliers for Flow Simulation Models'. *Petroleum Geoscience* [online] 5 (1), 53–63. available from <https://doi.org/10.1144/petgeo.5.1.53>

Manzocchi, T., Carter, J.N., Skorstad, A., Fjellvoll, B., Stephen, K.D., Howell, J.A., Matthews, J.D., Walsh, J.J., Nepveu, M., Bos, C., Cole, J., Egberts, P., Flint, S., Hern, C., Holden, L., Hovland, H., Jackson, H., Kolbjørnsen, O., and Macdonald, A. (2008) 'Sensitivity of the

Impact of Geological Uncertainty on Production from Faulted and Unfaulted Shallow-Marine Oil Reservoirs : Objectives and Methods'. *Petroleum Geoscience* [online] 14 (1), 3–15. available from <https://doi.org/10.1144/1354-079307-790>

Manzocchi, T., Ringrose, P.S., and Underhill, J.R. (1998) 'Flow through Fault Systems in High-Porosity Sandstones'. *Geological Society, London, Special Publications* 127 (1), 65–82

Manzocchi, T., Walsh, J.J., Nell, P., and Yielding, G. (2010) 'Fault Transmissibility Multipliers for Flow Simulation Models'. *Petroleum Geoscience* [online] 5 (1), 53–63. available from <https://doi.org/10.1144/petgeo.5.1.53>

Mathias, S.A., González, G.J., Miguel, M. De, Thatcher, K.E., and Zimmerman, R.W. (2011) 'Pressure Buildup During CO2 Injection into a Closed Brine Aquifer'. *Transport in Porous Media* [online] 89 (3), 383–397. available from <https://doi.org/10.1007/s11242-011-9776-z>

Matthäi, S.K., Aydin, A., Pollard, D.D. and Roberts, S.G. (1998) 'Numerical Simulation of Departures from Radial Drawdown in a Faulted Sandstone Reservoir with Joints and Deformation Bands'. *Geological Society, London, Special Publications* 147 (1), 157–191

McNeill, D.F., Cunningham, K.J., Guertin, L.A., and Anselmetti, F.S. (2004) 'Depositional Themes of Mixed Carbonate-Siliciclastics in the South Florida Neogene: Application to Ancient Deposits'. *AAPG Memoir* (3), 23–43

Menéndez, B., Zhu, W. and Wong, T.F. (1996) 'Micromechanics of Brittle Faulting and Cataclastic Flow in Berea Sandstone'. *Journal of structural geology* [online] 18 (1), 1–16. available from <https://doi.org/10.1016/0191-8141(95)00076-P>

Meyer, J. and Croskrey, A. (2017) 'Interpreted Water Quality Calculated from Borehole Resistivity Measurements in the Gulf Coast Aquifer, Lower Rio Grande Valley, Texas, USA.' *CSEG Recorder* [online] 42 (7), 1–4. available from <Interpreted Water Quality Calculated from Borehole Resistivity Measurements in the Gulf Coast Aquifer, Lower Rio Grande Valley, Texas, USA>

Michael, K., Golab, A., Shulakova, V., Ennis-King, J., Allinson, G., Sharma, S., and Aiken, T. (2010) 'Geological Storage of CO2 in Saline Aquifers-A Review of the Experience from Existing Storage Operations'. *International Journal of Greenhouse Gas Control* [online] 4 (4), 659–667. available from <https://doi.org/10.1016/j.ijggc.2009.12.011>

Morris, J.E., Hampson, G.J., and Johnson, H.O.W.D. (2006) 'A Sequence Stratigraphic Model for an Intensely Bioturbated Shallow-Marine Sandstone: The Bridport Sand Formation, Wessex Basin , UK'. *Sedimentology* [online] 53, 1229–1263. available from <https://doi.org/10.1111/j.1365-3091.2006.00811.x>

Moss, B., Barson, D., Rakhit, K., Dennis, H., Swarbrick, R., Evans, D., Graham, C., Armour, A. and Bathurst, P. (2003) 'Formation Pore Pressures and Formation Waters. The Millennium Atlas: Petroleum Geology of the Central and Northern North Sea': *Geological Society (London)* 317–329

Mount, J. (1985) 'Mixed Siliciclastic and Carbonate Sediments: A Proposed First-Order Textural and Compositional Classification'. *Sedimentology* 32, 435–442

Newell, A.J., Pourmalek, A., Butcher, A.S., and Shariatipour, S.M. (2019) 'The Importance of

Lithofacies Control on Fluid Migration in Heterogeneous Aeolian Formations for Geological CO2 Storage: Lessons from Observational Evidence and Modelling of Bleached Palaeoreservoirs at Salt Wash Graben, Utah'. *International Journal of Greenhouse Gas Control* [online] 91 (December 2018), 1–17. available from <https://doi.org/10.1016/j.ijggc.2019.102841>

Newell, A.J. and Shariatipour, S.M. (2016) 'Linking Outcrop Analogue with Flow Simulation to Reduce Uncertainty in Sub-Surface Carbon Capture and Storage: An Example from the Sherwood Sandstone Group of the Wessex Basin, UK'. *Geological Society, London, Special Publications* [online] 436 (1), 231–246. available from <https://doi.org/10.1144/SP436.2>

Nicol, A., Childs, C., Walsh, J.J., and Schafer, K.W. (2013) 'A Geometric Model for the Formation of Deformation Band Clusters'. *Journal of Structural Geology* [online] 55, 21–33. available from <http://dx.doi.org/10.1016/j.jsg.2013.07.004>

Nilsen, H.M., Lie, K., and Andersen, O. (2015) 'Analysis of CO2 Trapping Capacities and Long-Term Migration for Geological Formations in the Norwegian North Sea Using MRST-Co2lab'. *Computers and Geosciences* [online] 79, 15–26. available from <http://dx.doi.org/10.1016/j.cageo.2015.03.001>

Njiekak, G., Schmitt, D.R., Yam, H., and Kofman, R.S. (2013) 'CO2 Rock Physics as Part of the Weyburn-Midale Geological Storage Project'. *International Journal of Greenhouse Gas Control* [online] 16, S118–S133. available from <https://doi.org/10.1016/j.ijggc.2013.02.007>

NOAA/ESRL (2020) *Image Provided by Earth System Research Laboratories Global Monitoring Laboratory, from Their Website at Https://Www.Esrl.Noaa.Gov/Gmd/Ccgg/Trends/*.

NOAA (2020) *State of the Climate: Global Climate Report for March 2020* [online] available from <https://www.ncdc.noaa.gov/sotc/global/202003.>

Nordbotten, J.A.N.M., Celia, M.A., and Bachu, S. (2005) 'Injection and Storage of CO2 in Deep Saline Aquifers: Analytical Solution for CO2 Plume Evolution during Injection'. *Transport In Porous Media* [online] 58, 339–360. available from <https://doi.org/10.1007/s11242-004-0670-9>

Nordbotten, J.M. and Celia, M.A. (2006) 'Analysis of Plume Extent Using Analytical Solutions for CO2 Storage'. in *CMWRXVI*. held 2006 at Copenhagen, Denmark. 1–8

North, C.P. and Prosser, D.J. (1993) 'Characterization of Fluvial and Aeolian Reservoirs: Problems and Approaches'. *Geological Society, London, Special Publications* 73 (1), 1–6

North, F. (1985) *Petroleum Geology*. Springer

Noy, D.J., Holloway, S., Chadwick, R.A., Williams, J.D.O., Hannis, S.A., and Lahann, R.W. (2012) 'Modelling Large-Scale Carbon Dioxide Injection into the Bunter Sandstone in the UK Southern North Sea'. *International Journal of Greenhouse Gas Control* [online] 9, 220–233. available from <http://dx.doi.org/10.1016/j.ijggc.2012.03.011>

Nuccio, V.F. and Condon, S.M. (1996) 'Burial and Thermal History of the Paradox Basin, Utah and Colorado, and Petroleum Potential of the Middle Pennsylvanian Paradox

Formation'. *U.S geological survey* 57–76

Ogata, K., Senger, K., Braathen, A., and Tveranger, J. (2014) 'Fracture Corridors as Seal-Bypass Systems in Siliciclastic Reservoir-Cap Rock Successions: Field-Based Insights from the Jurassic Entrada Formation (SE Utah, USA)'. *Journal of Structural Geology* [online] 66, 162–187. available from <http://dx.doi.org/10.1016/j.jsg.2014.05.005>

Okwen, R., Yang, F., and Frailey, A. (2014) 'Effect of Geologic Depsoitional Environment on CO2 Storage Efficiency'. *Energy Procedia* [online] 63, 5247–5257. available from <https://doi.org/10.1016/j.egypro.2014.11.556>

Okwen, R.T., Stewart, M.T., and Cunningham, J.A. (2010) 'Analytical Solution for Estimating Storage Efficiency of Geologic Sequestration of CO2'. *International Journal of Greenhouse Gas Control* [online] 4 (1), 102–107. available from <https://doi.org/10.1016/j.ijggc.2009.11.002>

Oldenburg, C.M. (2006) *Migration Mechanisms and Potential Impacts of CO2 Leakage and Seepage Curtis*. [online] 1–32. available from <https://escholarship.org/content/qt015944r2/qt015944r2.pdf>

Olsson, A. (2000) 'Origin of Lüders ' Bands in Deformed Rock'. *Journal of Geophysical Research: Solid Earth* [online] 105 (B3), 5931–5938. available from <https://doi.org/10.1029/1999JB900428>

Onoja, M.U., Ahmadinia, M., Shariatipour, S.M., and Wood, A.M. (2019) 'Characterising the Role of Parametric Functions in the van Genuchten Empirical Model on CO 2 Storage Performance'. *International Journal of Greenhouse Gas Control* [online] 88 (June), 233–250. available from <https://doi.org/10.1016/j.ijggc.2019.06.004>

Onoja, M.U. and Shariatipour, S.M. (2018) 'The Impact of Gradational Contact at the Reservoir-Seal Interface on Geological CO2 Storage Capacity and Security'. *International Journal of Greenhouse Gas Control* [online] 72 (March), 1–13. available from <https://doi.org/10.1016/j.ijggc.2018.03.007>

Oostrom, M., White, M.D., Porse, S.L., Krevor, S.C.M. and Mathias, S.A. (2016) 'Comparison of Relative Permeability–saturation–capillary Pressure Models for Simulation of Reservoir CO2 Injection'. *International Journal of Greenhouse Gas Control* [online] 45, 70–85. available from <https://doi.org/10.1016/j.ijggc.2015.12.013>

Orr, F.M. (2009) 'Onshore Geologic Storage of CO2'. *Science* [online] 325 (5948), 1656–1658. available from <10.1126/science.1175677>

Özgur, E. (2006) *Assessment of Diffusive and Convective Mechanisms during Carbon Dioxide Sequestration into Deep Saline Aquifers*. MIDDLE EAST TECHNICAL UNIVERSITY

Parker, J.A. (2013) *Outcrop Analysis of Ooid Grainstones in the Permian Grayburg Formation, Shattuck Escarpment, New Mexico*. The University of Texas at Austin

Pearce, J.M., Kirby, G.A., Lacinska, A., Bateson, L., Wagner, D., Rochelle, C.A., and Cassidy, M. (2011) 'Reservoir-Scale CO2-Fluid Rock Interactions: Preliminary Results from Field Investigations in the Paradox Basin, Southeast Utah'. *Energy Procedia* [online] 4, 5058–5065. available from <http://dx.doi.org/10.1016/j.egypro.2011.02.479>

Pendrigh, N.M. (2005) ‘Geological and Geophysical Characterization of the Mississippian Midale Reservoir, Weyburn Field , Saskatchewan’. *Summary of Investigations* 1, 1–16

Pentland, C.H., El-Maghraby, R., Georgiadis, A., Iglauer, S., and Blunt, M.J. (2011) ‘Immiscible Displacements and Capillary Trapping in CO2 Storage’. *Energy Procedia* [online] 4, 4969–4976. available from <https://doi.org/10.1016/j.egypro.2011.02.467>

Peters, E., Egberts, P.J.P., Loeve, D., and Hofstee, C. (2015) ‘CO2 Dissolution and Its Impact on Reservoir Pressure Behavior’. *International Journal of Greenhouse Gas Control* [online] 43, 115–123. available from <http://dx.doi.org/10.1016/j.ijggc.2015.10.016>

Pittman, E.D. (1981) ‘Effect of Fault-Related Granulation on Porosity and Permeability of Quartz Sandstones, Simpson Group (Ordovician), Oklahoma.’ *American Association of Petroleum Geologists Bulletin* 65 (11), 2181–2387

Poblet, J. and Mcclay, K. (1996) ‘Geometry and Kinematics of Single-Layer Detachment Folds’. *AAPG Bulletin* [online] 80 (7), 1085–1109. available from <https://doi.org/10.1306/64ED8CA0-1724-11D7-8645000102C1865D%0A>

Pourmalek, A., Newell, A.J., Shariatipour, S.M., Butcher, A.S., Milodowski, A.E., Bagheri, M., and Wood, A.M. (2021) ‘Deformation Bands in High-Porosity Sandstones :Do They Help or Hinder CO2 Migration and Storage in Geological Formations?’ *International Journal of Greenhouse Gas Control* [online] 107 (February), 103292. available from <https://doi.org/10.1016/j.ijggc.2021.103292>

Pourmalek, A., Newell, A.J., Shariatipour, S.M., and Wood, A.M. (2022) ‘The Impact of Heterogeneous Mixed Siliciclastic – Carbonate Systems on CO2 Geological Storage’. *Petroleum Geoscience* [online] 28 (1). available from <https://doi.org/10.1144/petgeo2020-086>

Pourmalek, A. and Shariatipour, S.M. (2019) ‘Dependence on Temperature and Salinity Gradients and the Injection Rate of CO2 Storage in Saline Aquifers with an Angular Unconformity’. *Journal of Porous Media* [online] 22 (8), 1065–1078. available from <10.1615/JPorMedia.2019025077>

Preston, C., Monea, M., Jazrawi, W., Brown, K., Whittaker, S., White, D., Law, D., Chalaturnyk, R., and Rostron, B. (2005) ‘IEA GHG Weyburn CO2 Monitoring & Storage Project’. *Fuel Processing Technology* [online] 86 (14–15), 1547–1568. available from <https://doi.org/10.1016/j.fuproc.2005.01.019>

Pruess, K. (2006) ‘On CO2 Behavior in the Subsurface, Following Leakage from a Geologic Storage Reservoir’. *Lawrence Berkeley National Laboratory*

Qi, R. (2008) *Simulation of Geological Carbon Dioxide Storage*. Imperial College London

Qi, R., Laforce, T.C., and Blunt, M.J. (2009) ‘Design of Carbon Dioxide Storage in Aquifers’. *International Journal of Greenhouse Gas Control* [online] 3, 195–205. available from <https://doi.org/10.1016/j.ijggc.2008.08.004>

Qu, D. and Tveranger, J. (2016) ‘Incorporation of Deformation Band Fault Damage Zones in Reservoir Models’. *AAPG bulletin* [online] 100 (3), 423–443. available from <https://doi.org/10.1306/12111514166>

Qu, D., Tveranger, J., and Fachri, M. (2017) 'Influence of Deformation-Band Fault Damage Zone on Reservoir Performance'. *Interpretation* [online] 5 (4), 41–56. available from <https://doi.org/10.1190/INT-2016-0229.1%0A>

Ramsay, L.G. (1974) 'Development of Chevron Folds'. *Geological Bulletin, Society of America* [online] 85 (11), 1741–1754. available from <https://doi.org/10.1130/0016-7606(1974)85%3C1741:DOCF%3E2.0.CO;2%0AArticle history%0A Cite >

Ranganathan, P., Farajzadeh, R., Bruining, H., and Zitha, P.L.J. (2012) 'Numerical Simulation of Natural Convection in Heterogeneous Porous Media for CO2 Geological Storage'. *Transport In Porous Media* [online] 95 (1), 25–54. available from <https://doi.org/10.1007/s11242-012-0031-z>

Rasmusson, K., Rasmusson, M., Tsang, Y., and Niemi, A. (2016) 'A Simulation Study of the Effect of Trapping Model, Geological Heterogeneity and Injection Strategies on CO2 Trapping'. *International Journal of Greenhouse Gas Control* [online] 52, 52–72. available from <http://dx.doi.org/10.1016/j.ijggc.2016.06.020>

Rawling, G.C. and Goodwin, L.B. (2003) 'Cataclasis and Particulate Flow in Faulted, Poorly Lithified Sediment'. *Journal of Structural Geology* [online] 25 (3), 317–331. available from <https://doi.org/10.1016/S0191-8141(02)00041-X>

Reading, H.G. (1980) *Characteristics and Recognition of Strike-Slip Fault Systems*. International Association of Sedimentologists

Riaz, A., Hesse, M., Tchelepi, H.A., and ORR JR, F.M. (2006) 'Onset of Convection in a Gravitationally Unstable Diffusive Boundary Layer in Porous Media'. *Journal of Fluid Mechanics* [online] 548, 87–111. available from <doi:10.1017/S0022112005007494>

Ringrose, P. and Bentley, M. (2015) *Reservoir Model Design* [online] Berlin: Springer. available from <http://link.springer.com/10.1007/978-94-007-5497-3>

Ringrose, P.S., Mathieson, A.S., Wright, I.W., Selama, F., Hansen, O., Bissell, R., Saoula, N., and Midgley, J. (2013) 'The In Salah CO2 Storage Project: Lessons Learned and Knowledge Transfer'. *Energy Procedia* [online] 37, 6226–6236. available from <https://doi.org/10.1016/j.egypro.2013.06.551>

Rittenhouse, G. (1972) 'Stratigraphic-Trap Classification: Geologic Exploration Methods.' *AAPG Memoir*

Robert J. Bodnar (2003) 'Introduction to Aqueous-Electrolyte Fluid Inclusions'. in *Fluid Inclusions: Analysis and Interpretation*. vol. 32. 81–100

Rotevatn, A. and Fossen, H. (2012) 'Soft Faults with Hard Tips: Magnitude-Order Displacement Gradient Variations Controlled by Strain Softening versus Hardening; Implications for Fault Scaling'. *Journal of the Geological Society* [online] 169 (2), 123–126. available from <https://doi.org/10.1144/0016-76492011-108>

Rotevatn, A., Buckley, S.J., and Howell, J.A. (2009) 'Overlapping Faults and Their Effect on Fluid Flow in Different Reservoir Types: A LIDAR-Based Outcrop Modeling and Flow Simulation Study'. *AAPG Bulletin* [online] 93 (3), 407–427. available from <https://doi.org/10.1306/09300807092%0A>

Rotevatn, A. and Fossen, H. (2011) 'Simulating the Effect of Subseismic Fault Tails and Process Zones in a Siliciclastic Reservoir Analogue: Implications for Aquifer Support and Trap Definition'. *Marine and Petroleum Geology* [online] 28 (9), 1648–1662. available from <http://dx.doi.org/10.1016/j.marpetgeo.2011.07.005>

Rotevatn, A., Fossmark, H.S., Bastesen, E., Thorsheim, E., and Torabi, A. (2017) 'Do Deformation Bands Matter for Flow? Insights from Permeability Measurements and Flow Simulations in Porous Carbonate Rocks'. *Petroleum Geoscience* [online] 23 (1), 104–119. available from <https://doi.org/10.1144/petgeo2016-038>

Rotevatn, A., Sandve, T.H., Keilegavlen, E., Kolyukhin, D., and Fossen, H. (2013) 'Deformation Bands and Their Impact on Fluid Flow in Sandstone Reservoirs: The Role of Natural Thickness Variations'. *Geofluids* 13 (3), 359–371

Rotevatn, A., Torabi, A., Fossen, H., and Braathen, A. (2008) 'Slipped Deformation Bands: A New Type of Cataclastic Deformation Bands in Western Sinai, Suez Rift, Egypt'. *Journal of Structural Geology* [online] 30 (11), 1317–1331. available from <https://doi.org/10.1016/j.jsg.2008.06.010>

Rotevatn, A., Tveranger, J., Howell, J.A., and Fossen, H. (2009) 'Dynamic Investigation of the Effect of a Relay Ramp on Simulated Fluid Flow: Geocellular Modelling of the Delicate Arch Ramp, Utah'. *Petroleum Geoscience,* [online] 15 (1), 45–58. available from <https://doi.org/10.1144/1354-079309-779%0AAdd to Cart ($35)>

Rutqvist, J., Birkholzer, J.T., and Tsang, C.-F. (2008) 'Coupled Reservoir–geomechanical Analysis of the Potential for Tensile and Shear Failure Associated with CO2 Injection in Multilayered Reservoir–caprock Systems'. *International Journal of Rock Mechanics and Mining Sciences* [online] 45 (2), 132–143. available from <https://doi.org/10.1016/j.ijrmms.2007.04.006>

Rutqvist, J. and Tsang, C. (2002) 'A Study of Caprock Hydromechanical Changes Associated with CO2 -Injection into a Brine Formation'. *Environmental Geology,* [online] 42 (2–3), 296–305. available from <https://doi.org/10.1007/s00254-001-0499-2>

Saillet, E. and Wibberley, C.A.J. (2010) 'Evolution of Cataclastic Faulting in High-Porosity Sandstone, Bassin Du Sud-Est'. *Journal of Structural Geology* [online] 32 (11), 1590–1608. available from <http://dx.doi.org/10.1016/j.jsg.2010.02.007>

Schueller, S., Braathen, A., Fossen, H., and Tveranger, J. (2013) 'Spatial Distribution of Deformation Bands in Damage Zones of Extensional Faults in Porous Sandstones: Statistical Analysis of Field Data'. *Journal of Structural Geology* [online] 52, 148–162. available from <https://doi.org/10.1016/j.jsg.2013.03.013>

Scott, V., Gilfillan, S., Markusson, N., Chalmers, H., and Haszeldine, R.S. (2012) 'Last Chance for Carbon Capture and Storage'. *Nature Climate Change* [online] 3 (2), 105–111. available from <http://dx.doi.org/10.1038/nclimate1695>

Seers, T.D. and Hodgetts, D. (2016) 'Extraction of Three-Dimensional Fracture Trace Maps from Calibrated Image Sequences'. *Geosphere* [online] 12 (4), 1323–1340. available from <https://doi.org/10.1130/GES01276.1%0A>

Shariatipour, S.M., Pickup, G.E., and Mackay, E.J. (2014) 'The Effect of Aquifer / Caprock

Interface on Geological Storage of CO2'. *Energy Procedia* [online] 63, 5544–5555. available from <http://dx.doi.org/10.1016/j.egypro.2014.11.588>

Shariatipour, S.M., Pickup, G.E., and Mackay, E.J. (2016) 'Investigation of CO2 Storage in a Saline Formation with an Angular Unconformity at the Caprock Interface'. *Petroleum Geoscience* [online] 22 (2), 203–210. available from <https://doi.org/10.1144/petgeo2015-039>

ShellCanada (2019) *Quest Carbon Capture and Storage Project 2018 Annual Status Report*. Calgary, Alberta

Shipton, Z.K., Evans, J.P., Robeson, K.R., Forster, C.B. and Snelgrove, S. (2002) 'Structural Heterogeneity and Permeability in Faulted Eolian Sandstone: Implications for Subsurface Modeling of Faults.' *AAPG Bulletin* [online] 86 (5), 863–883. available from <https://doi.org/10.1306/61EEDBC0-173E-11D7-8645000102C1865D>

Shipton, Z.K., Evans, J.P., Kirchner, D., Kolesar, P.T., Williams, A.P., and Heath, J. (2004) 'Analysis of CO2 Leakage through "Low-Permeability" Faults from Natural Reservoirs in the Colorado Plateau, Southern Utah'. *Geological Storage of Carbon Dioxide* [online] 233 (1), 43–58. available from <https://doi.org/10.1144/GSL.SP.2004.233.01.05>

Sifuentes, W., Blunt, M.J., and Giddins, M.A. (2009) 'Modeling CO2 Storage in Aquifers: Assessing the Key Contributors to Uncertainty'. *spe in Offshore Europe. Society of Petroleum Engineers.* (8–11 September)

De Silva, G.P.D., Ranjith, P. and Perera, M.S.A. (2015) 'Geochemical Aspects of CO2 Sequestration in Deep Saline Aquifers: A Review'. *Fuel* [online] 155 (April), 128–143. available from <http://dx.doi.org/10.1016/j.fuel.2015.03.045>

Slatt, R.M. (2013) *Basic Principles and Applications of Reservoir Characterization*. Elsevier

Slob, S. and Hack, R. (2004) '3D Terrestrial Laser Scanning as a New Field Measurement and Monitoring Technique 30 Terrestrial Laser Scanning as a New Field'. in *Engineering Geology for Infrastructure Planning in Europe* [online] Berlin: Springer, 179–189. available from <https://doi.org/10.1007/978-3-540-39918-6_22>

Soliva, R., Schultz, R.A., Ballas, G., Taboada, A., Wibberley, C., Saillet, E., and Benedicto, A. (2013) 'A Model of Strain Localization in Porous Sandstone as a Function of Tectonic Setting, Burial and Material Properties; New Insight from Provence (Southern France)'. *Journal of Structural Geology* [online] 49, 50–63. available from <http://dx.doi.org/10.1016/j.jsg.2012.11.011>

Solum, J.G., Brandenburg, J.P., Naruk, S.J., Kostenko, O. V, Wilkins, S.J., Schultz, R.A., Solum, J.G., and International, S. (2010) 'Characterization of Deformation Bands Associated with Normal and Reverse Stress States in the Navajo Sandstone, Utah'. *AAPG bulletin* [online] 9 (9), 1453–1475. available from <https://doi.org/10.1306/01051009137%0A>

Song, J. and Zhang, D. (2013) 'Comprehensive Review of Caprock-Sealing Mechanisms for Geologic Carbon Sequestration'. *Environmental science & technology* [online] 47 (1), 9–22. available from <https://doi.org/10.1021/es301610p>

SPE (2017) 'CO2 Storage Resources Management System'. *Society of Petroleum Engineers Journal* (July)

Spycher, N., Pruess, K. and Ennis-King, J. (2003) 'CO2-H2O Mixtures in the Geological Sequestration of CO2. I. Assessment and Calculation of Mutual Solubilities from 12 to 100 °C and up to 600 Bar'. *Geochimica et Cosmochimica Acta* [online] 67 (16), 3015–3031. available from <https://doi.org/10.1016/S0016-7037(03)00273-4>

Spycher, N. and Pruess, K. (2005) 'CO2-H2O Mixtures in the Geological Sequestration of CO2. I . Assessment and Calculation of Mutual Solubilities from 12 to 100 °C and up to 600 Bar'. *Geochimica et Cosmochimica Acta,* [online] 69 (13), 3309–3320. available from <https://doi.org/10.1016/j.gca.2005.01.015>

Spycher, N. and Pruess, K. (2009) 'A Phase-Partitioning Model for CO2 – Brine Mixtures at Elevated Temperatures and Pressures: Application to CO2 -Enhanced Geothermal Systems'. *Transport in Porous Media* [online] 82 (1), 173–196. available from <https://doi.org/10.1007/s11242-009-9425-y>

Sternlof, K.R., Pollard, D.D., and Durlofsky, L.J. (2006) 'Flow and Transport Effects of Compaction Bands in Sandstone at Scales Relevant to Aquifer and Reservoir Management'. *Water Resources Research* [online] 42, 1–16. available from <https://doi.org/10.1029/2005WR004664>

Stow, D.A.V., Reading, H.G. and Collinson, J.D. (1996) *Sedimentary Environments: Process, Facies and Stratigraphy*.

Sundal, A., Petter, J., Dypvik, H., Miri, R., and Aagaard, P. (2013) 'Effects of Geological Heterogeneity on CO2 Distribution and Migration - A Case Study from the Johansen Formation , Norway'. *Energy Procedia* [online] 37 (1876), 5046–5054. available from <http://dx.doi.org/10.1016/j.egypro.2013.06.418>

Suppe, B.J. and Medwedeff, D.A. (1990) 'Geometry and Kinematics of Fault-Propagation Folding'. *Eclogae Geologicae Helvetiae* 83 (3), 409–454

Suppe, J. (1983) 'Geometry and Kinematics of Fault-Bend Folding'. *American Journal of science* 283 (7), 684–721

Szulczewski, M.L., Macminn, C.W., Herzog, H.J., and Juanes, R. (2012) 'Lifetime of Carbon Capture and Storage as a Climate-Change Mitigation Technology'. *Proceedings of the National Academy of Sciences* [online] 109 (14), 5185–5189. available from <https://doi.org/10.1073/pnas.1115347109>

Tawiah, P., Duer, J., Bryant, S.L., Larter, S., Brien, S.O., and Dong, M. (2020) 'CO2 Injectivity Behaviour under Non-Isothermal Conditions – Field Observations and Assessments from the Quest CCS Operation'. *International Journal of Greenhouse Gas Control* [online] 92 (August 2019), 102843. available from <https://doi.org/10.1016/j.ijggc.2019.102843>

The Climate Change Committee (2019) *Net Zero: The UK's Contribution to Stopping Global Warming*.

Thrana, C. and Talbot, M.R. (2006) 'High-Frequency Carbonate-Siliciclastic Cycles in the Miocene of the Lorca Basin (Western Mediterranean, SE Spain)'. *Geologica Acta* [online] 4, 343–354. available from <Available online at www.geologica-acta.com%0D>

Tindall, S.E. (2006) 'Jointed Deformation Bands May Not Compartmentalize Reservoirs'.

AAPG Bulletin 90 (2), 177–192

Tondi, E., Antonellini, M., Aydin, A., Marchegiani, L., and Cello, G. (2006) 'The Role of Deformation Bands, Stylolites and Sheared Stylolites in Fault Development in Carbonate Grainstones of Majella Mountain, Italy'. *Journal of Structural Geology* [online] 28 (3), 376–391. available from <https://doi.org/10.1016/j.jsg.2005.12.001>

Torabi, A. and Fossen, H. (2009) 'Spatial Variation of Microstructure and Petrophysical Properties along Deformation Bands in Reservoir Sandstones'. *AAPG bulletin* [online] 93 (7), 919–938. available from <https://doi.org/10.1306/03270908161>

Torabi, A., Fossen, H., and Alaei, B. (2008) 'Application of Spatial Correlation Functions in Permeability Estimation of Deformation Bands in Porous Rocks'. *Journal of Geophysical Research: Solid Earth* [online] 113 (February), 1–10. available from <https://doi.org/10.1029/2007JB005455>

Torabi, A., Fossen, H., and Braathen, A. (2013) 'Insight into Petrophysical Properties of Deformed Sandstone Reservoirs'. *AAPG bulletin* [online] 97 (4), 619–637. available from <https://doi.org/10.1306/10031212040%0A>

Tucker, M. and Wright, V. (2009) *Carbonate Sedimentology*.

Tucker, M.E. (2003) 'Mixed Clastic – Carbonate Cycles and Sequences: Quaternary of Egypt and Carboniferous of England'. *Geologia Croatica* [online] 56 (1), 19–38. available from <https://hrcak.srce.hr/3789>

Tucker, M.E. (2009) *Sedimentary Petrology: An Introduction to the Origin of Sedimentary Rocks*. John Wiley & Sons.

Turner, P., Burley, S.D., Rey, D., and Prosser, J. (1995) 'Burial History of the Penrith Sandstone (Lower Permian) Deduced from the Combined Study of Fluid Inclusion and Palaeomagnetic Data'. *Geological Society, London, Special Publications* [online] 98 (1), 43–78. available from <https://doi.org/10.1144/GSL.SP.1995.098.01.04>

Twiss, R.J and Moores, E.M. (1992) *Structural Geology*. Macmillan

Underhill, J.R. and Woodcock, N.H. (1987) 'Faulting Mechanisms in High-Porosity Sandstones; New Red Sandstone, Arran, Scotland'. *Geological Society Special Publication* [online] 29 (1), 91–105. available from <https://doi.org/10.1144/GSL.SP.1987.029.01.09>

Underschultz, J., Boreham, C., Dance, T., Stalker, L., Freifeld, B., Kirste, D., and Ennis-King, J. (2011) 'CO2 Storage in a Depleted Gas Field: An Overview of the CO2CRC Otway Project and Initial Results'. *International Journal of Greenhouse Gas Control* [online] 5 (4), 922–932. available from <https://doi.org/10.1016/j.ijggc.2011.02.009>

UNFCCC (1992) *United Nation*. New York

USDOE (2010) *Carbon Sequestration Atlas of the United States and Canada*.

USEPA (1994) *Determination of Maximum Injection Pressure for Class I Wells*.

Vesovic, V., Wakeham, W.A., Olchowy, G.A., Sengers, J.V., Watson, J.T.R. and Millat, J. (1990) 'The Transport Properties of Carbon Dioxide'. *Journal of physical and chemical*

reference data [online] 19 (3), 763–808. available from <https://doi.org/10.1063/1.555875>

Victor D. G., D. Zhou, E. H. M. Ahmed, P. K. Dadhich, J. G. J. Olivier, H-H. Rogner, K. Sheikho, and M. Yamaguchi, 2014: (2014) 'Introductory Chapter'. in *Climate Change 2014: Mitigation of Climate Change. Contribution of Working Group III to the Fifth Assessment Report of the Intergovernmental Panel on Climate Change*. ed. by Edenhofer, O., R. Pichs-Madruga, Y. Sokona, E. Farahani, S. Kadner, K. Seyboth, A. Adler, I. Baum, S. Brunner, P. Eickemeier, B. Kriemann, J. Savolainen, S. Schlömer, C. von Stechow, T.Z. and J.C.M. Cambridge University Press, Cambridge, United Kingdom and New York, NY, USA.

Vidal-Gilbert, S., Tenthorey, E., Dewhurst, D., Ennis-king, J., Ruth, P. Van, and Hillis, R. (2010) 'Geomechanical Analysis of the Naylor Field , Otway Basin , Australia : Implications for CO2 Injection and Storage'. *International Journal of Greenhouse Gas Control* [online] 4 (5), 827–839. available from <http://dx.doi.org/10.1016/j.ijggc.2010.06.001>

Vuuren, D.P. Van, Edmonds, J., Kainuma, M., Riahi, K., Nakicenovic, N., Smith, S.J., and Rose, S.K. (2011) 'The Representative Concentration Pathways: An Overview'. *Climate Change* [online] 109 (1–2), 5–31. available from <https://doi.org/10.1007/s10584-011-0148-z>

Wang, Y., Zhang, K., and Wu, N. (2013) 'Numerical Investigation of the Storage Efficiency Factor for CO2 Geological Sequestration in Saline Formations'. *Energy Procedia* [online] 37, 5267–5274. available from <http://dx.doi.org/10.1016/j.egypro.2013.06.443>

White, J.A., Chiaramonte, L., Ezzedine, S., Foxall, W., Hao, Y., and Ramirez, A. (2014) 'Geomechanical Behavior of the Reservoir and Caprock System at the In Salah CO2 Storage Project'. *Proceedings of the National Academy of Sciences* [online] 111 (24), 8747–8752. available from <https://doi.org/10.1073/pnas.1316465111>

Wigley, M., Dubacq, B., Kampman, N., and Bickle, M. (2013) 'Controls of Sluggish, CO2-Promoted, Hematite and K-Feldspar Dissolution Kinetics in Sandstones'. *Earth and Planetary Science Letters* [online] 362, 76–87. available from <https://doi.org/10.1016/j.epsl.2012.11.045>

Wigley, M., Kampman, N., Dubacq, B., and Bickle, M. (2012) 'Fluid-Mineral Reactions and Trace Metal Mobilization in an Exhumed Natural CO2 Reservoir, Green River, Utah'. *Geology* [online] 40 (6), 555–558. available from <https://doi.org/10.1130/G32946.1>

Wilkinson, M., S. V. M. Gilfillan, R. S. Haszeldine, and C.J.B. (2008) 'Plumbing the Depths: Testing Natural Tracers of Subsurface CO2 Origin and Migration, Utah'. in *Carbon Dioxide Sequestration in Geological Media—State of the Science* [online] ed. by M. Grobe, J. C. Pashin, and R.L.D. AAPG Studies 59, 1–16. available from <doi:10.1306/13171266St591353>

Williams, J.D.O., Bentham, M., Jin, M., Pickup, G., Mackay, E., and Gammer, D. (2013) 'The Effect of Geological Structure and Heterogeneity on CO2 Storage in Simple 4-Way Dip Structures ; a Modeling Study from the UK Southern North Sea'. *Energy Procedia* [online] 37, 3980–3988. available from <http://dx.doi.org/10.1016/j.egypro.2013.06.297>

Williams, J.D.O., Fellgett, M.W., and Quinn, M.F. (2016) 'Carbon Dioxide Storage in the Captain Sandstone Aquifer: Determination of in Situ Stresses and Fault-Stability Analysis'. *Petroleum Geoscience* [online] 22 (3), 211–222. available from <https://doi.org/10.1144/petgeo2016-036>

Wilson, C.E., Aydin, A., Durlofsky, L.J., Sagy, A., Emily, E., Kreylos, O., and Kellogg, L.H. (2011) 'From Outcrop to Flow Simulation: Constructing Discrete Fracture Models from a LIDAR Survey'. *AAPG Bulletin* [online] 11 (11), 1883–1905. available from <https://doi.org/10.1306/03071110122>

Wollenweber, J., Alles, S., Busch, A., Krooss, B.M., Stanjek, H., and Littke, R. (2010) 'Experimental Investigation of the CO2 Sealing Efficiency of Caprocks'. *International Journal of Greenhouse Gas Control* [online] 4 (2), 231–241. available from <http://dx.doi.org/10.1016/j.ijggc.2010.01.003>

Xu, T., Kharaka, Y.K., Doughty, C., Freifeld, B.M., and Daley, T.M. (2010) 'Reactive Transport Modeling to Study Changes in Water Chemistry Induced by CO2 Injection at the Frio-I Brine Pilot'. *Chemical Geology* [online] 271 (3–4), 153–164. available from <https://doi.org/10.1016/j.chemgeo.2010.01.006>

Zahasky, C. and Krevor, S. (2020) 'Environmental Science Climate Change Mitigation Scenarios'. *Energy & Environmental Science* [online] 13, 1561–1567. available from <10.1039/D0EE00674B>

Zecchin, M. and Catuneanu, O. (2017) 'High-Resolution Sequence Stratigraphy of Clastic Shelves VI: Mixed Siliciclastic-Carbonate Systems'. *Marine and Petroleum Geology* [online] 88, 712–723. available from <https://doi.org/10.1016/j.marpetgeo.2017.09.012>

Zhang, C., Oostrom, M., Wietsma, T.W., Grate, J.W., and Warner, M.G. (2011) 'Influence of Viscous and Capillary Forces on Immiscible Fluid Displacement: Pore-Scale Experimental Study in a Water-Wet Micromodel Demonstrating Viscous and Capillary Fingering'. *Energy & fuels* [online] 25 (8), 3493–3505. available from <https://doi.org/10.1021/ef101732k>

Zhou, D., Fayers, F.J., and Orr Jr, F.M. (1997) 'Scaling of Multiphase Flow in Simple Heterogeneous Porous Media'. *SPE Reservoir Engineering* [online] 12 (03), 173–178. available from <https://doi.org/10.2118/27833-PA>

Zhou, Q., Birkholzer, J.T., Tsang, C., and Rutqvist, J. (2008) 'A Method for Quick Assessment of CO2 Storage Capacity in Closed and Semi-Closed Saline Formations'. *International Journal of Greenhouse Gas Control* [online] 2 (4), 626–639. available from <https://doi.org/10.1016/j.ijggc.2008.02.004>

Zhu, C., Zhang, G., Lu, P., Meng, L., and Ji, X. (2015) 'Seismic Data for the Uppermost Layer and Model Sensitivity Analysis'. *International Journal of Greenhouse Gas Control* [online] 43, 233–246. available from <http://dx.doi.org/10.1016/j.ijggc.2014.12.016>

Zuluaga, L.F., Rotevatn, A., Keilegavlen, E., and Fossen, H. (2016) 'The Effect of Deformation Bands on Simulated Fluid Flow within Fault-Propagation Fold Trap Types: Lessons from the San Rafael Monocline, Utah'. *AAPG bulletin* [online] 100 (10), 1523–1540. available from <https://doi.org/10.1306/04151614153>

Zweigel, P., Arts, R., Lothe, A.E., and Lindeberg, E.B. (2004) 'Reservoir Geology of the Utsira Formation at the First Industrial-Scale Underground CO2 Storage Site (Sleipner Area, North Sea)'. *Geological Society, London, Special Publications* [online] 233 (1), 165–180. available from <https://doi.org/10.1144/GSL.SP.2004.233.01.11>

Zweigel, P., Hamborg, M., Arts, R., Lothe, A., Sylta, Ø., and Tømmerås, A. (2000) 'Prediction of Migration of CO2 Injected into an Underground Depository: Reservoir Geology and Migration Modelling in the Sleipner Case (North Sea)'. in *International Conference on Greenhouse Gas Control Technologies, Cairns (Australia)*. held 2000 at Cairns (Australia)